Managed Aquifer Recharge with Marginal Water for Irrigation and Contaminant Attenuation

Darrell Tang

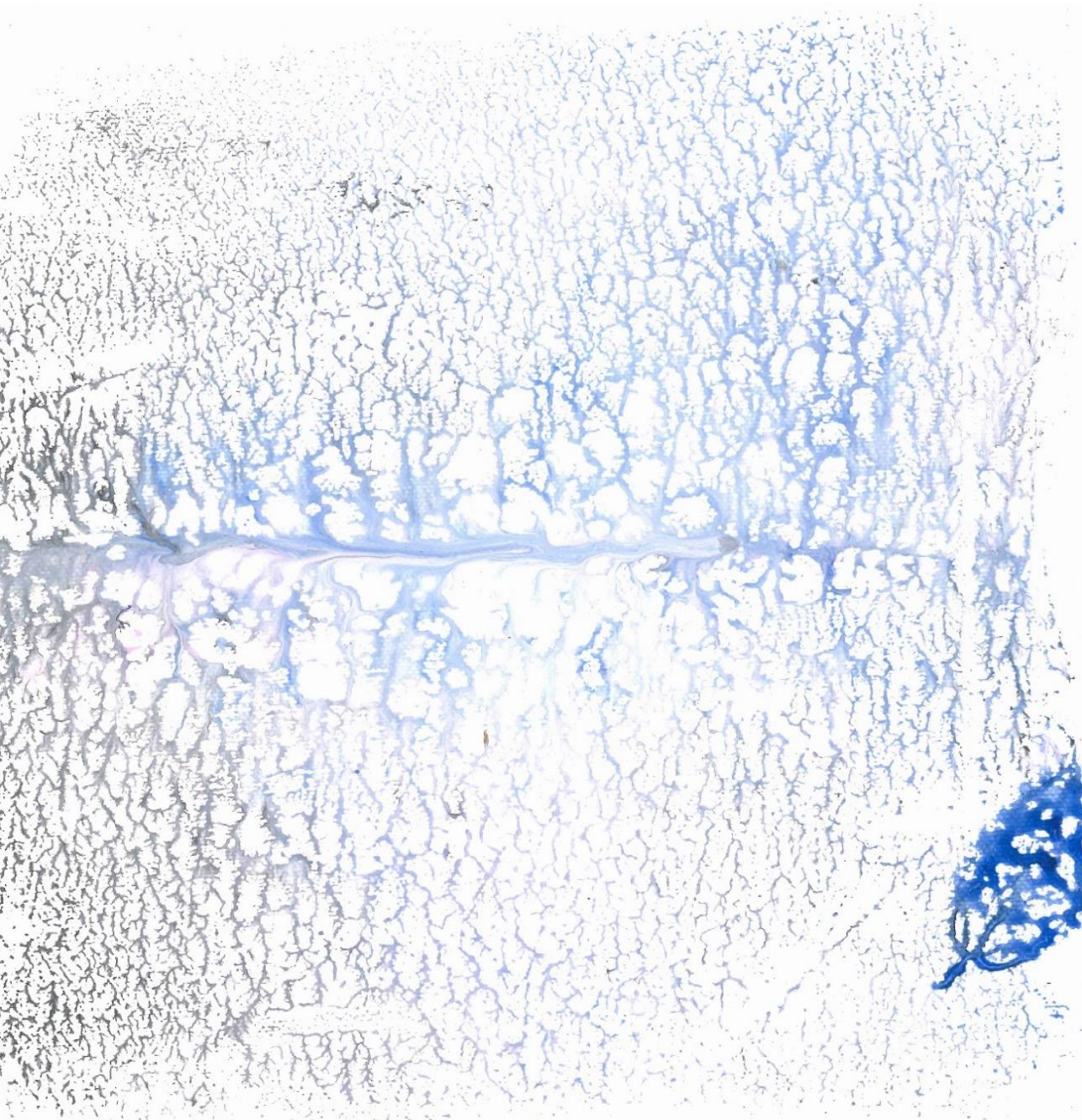

Propositions

1. The use of marginal water in agricultural irrigation does not necessarily lead to crop or environmental contamination.
   (this thesis)

2. The effectiveness of various managed aquifer recharge systems scales with system size and operational history in most but not all cases.
   (this thesis)

3. Sustainable agriculture is an oxymoron.

4. The arbitrary demarcation between economics and ecology is yen and bananas.

5. The philosophy of science is incomplete without existentialism.

6. All phenomena are emergent phenomena.

7. Freedom is an illusion under the shadow of big data.

8. Communicating ideas is easier than facts.

Propositions belonging to the thesis, entitled

Managed Aquifer Recharge with Marginal Water for Irrigation and Contaminant Attenuation

Darrell Tang
Wageningen, 4 July 2022

Managed Aquifer Recharge with Marginal Water for Irrigation and Contaminant Attenuation

Darrell W S Tang

Thesis committee

Promotor
Prof. Dr S.E.A.T.M. van der Zee
Emeritus Personal Chair of Ecohydrology
Wageningen University & Research

Co-promotors
Prof. Dr A. Leijnse
Emeritus Professor of Groundwater Quality
Wageningen University & Research

Dr R.P. Bartholomeus
Principal Scientist in Ecohydrology
KWR Water Research Institute

Other members
Prof. Dr H.H.M. Rijnaarts, Wageningen University & Research
Prof. Dr S.C. Dekker, Utrecht University
Prof. Dr S.M. Hassanizadeh, Utrecht University
Prof. Dr S. Garré, Flanders Research Institute for Agriculture, Fisheries and Food, Belgium

This research was conducted under the auspices of the Research School for Socio-Economic and Natural Sciences of the Environment (SENSE)

Managed Aquifer Recharge with Marginal Water for Irrigation and Contaminant Attenuation

Darrell W S Tang

Thesis

submitted in fulfillment of the requirements for the degree of doctor
at Wageningen University
by the authority of the Rector Magnificus
Prof. Dr A.P.J. Mol
in the presence of the
Thesis Committee appointed by the Academic Board
to be defended in public
on Monday 04 July 2022
at 11 a.m. in the Omnia Auditorium.

Darrell Tang
Managed Aquifer Recharge with Marginal Water for Irrigation and Contaminant Attenuation,
188 pages.

PhD thesis, Wageningen University, Wageningen, the Netherlands (2022)
With references, with summary in English

ISBN 978-94-6447-251-6
DOI https://doi.org/10.18174/570696

Table of Contents

Chapter 1

General Introduction

1.1 Water scarcity and marginal water in agriculture

History progresses through the adaptation of new technologies and practices. The agricultural revolution, which was an important factor in the emergence of organized society, brought about stability and consistency in the provision of food, one of the most fundamental needs of society. Due in part to large and growing human populations, the demand for water across many sectors of societal function such as industry, transport, and agriculture is increasing. Hence, we now live in an era where water scarcity poses an ever larger risk to the sustainability of society and the environment. As water stress exacerbates across the world, it has become a matter of dire urgency to allocate available water resources more efficiently. To ensure that supplies of freshwater never fall below the amount necessary for human consumption and essential industrial applications, it is paramount that methods of utilizing alternative sources of water are developed where possible. Presently, the single largest global consumer of freshwater resources is agricultural irrigation (Valipour and Singh, 2016). It is therefore important to reduce the freshwater usage of agriculture.

Even in humid temperate regions, seasonal variabilities in freshwater availability frequently lead to agricultural soils that are too dry for optimal crop growth in the summer, due to excess evaporation or equivalently, insufficient precipitation, even though such shortages do not occur when considered on an annual scale (Klijn et al., 2011). This is most severe during dry years, but poses a problem even on an 'average' year, possibly drying out the root zone and lowering the groundwater table during the summer, leading to a deterioration in crop quality or yields (Klijn et al., 2011). Hence, it is necessary to irrigate the fields during such dry periods. In coastal areas, which are agriculturally important in the Netherlands, this issue is further exacerbated by saltwater intrusion, resulting in severe decline in soil quality (Vermue et al., 2013) and causing as much as five hundred million euros in crop damage on an especially dry year (Klijn et al., 2011). In the future, variability in soil moisture content is expected to increase as a result of climate change, bringing about more periods of both extreme wet and dry conditions, in effect amplifying variations in soil moisture conditions, and negatively affecting crop yields (Knapp et al., 2008). To tackle these challenges, legislators, regulators, researchers and stakeholders in agriculture and water management will have to devise methods to use and allocate water resources more efficiently.

One route towards efficient water resource allocation is to use less freshwater and more recycled water where possible, bearing in mind that recycled water tends to be of marginal quality. The use of marginal water for irrigation is by itself not new; crops have been irrigated with marginal water through traditional surface irrigation methods, often improperly in hindsight with regards to health and environmental risks, by the ancient Greeks as early as the Bronze Age (Jaramillo and Restrepo, 2017). Treated domestic and industrial wastewater is a potentially abundant source of marginal water that may satisfy a significant proportion of agricultural water demand in certain regions (Narain-Ford et al., 2021; Pronk et al., 2021). The treated wastewater is not sufficiently pure to be used for all purposes requiring freshwater, but it may possibly be used for agricultural irrigation.

1.2 Contaminants of emerging concern

Treated wastewater contains contaminants that were not fully eliminated by the treatment process, including contaminants of emerging concern (CECs), which refer to a list of substances with adverse environmental and health effects whose toxicity and ecotoxicity are not yet well understood. Such substances include pharmaceuticals and industrial solvents. Benefits of treated wastewater reuse in irrigation in general include a decrease in the stress on freshwater resources, avoiding the cost of extracting groundwater resources, savings on fertilizer due to nutrients naturally present in wastewater, reducing the cost of fresh water going towards human consumption.

Ensuring that crops and agricultural workers are not directly exposed to the treated wastewater is important. Wastewater, including treated wastewater, contains biological (bacteria, viruses, protozoans) and chemical (sewage, hydrocarbons, heavy metals) pollutants, including CECs (pharmaceuticals, antibiotics, hormones), which contemporary treatment technologies are unable to completely eliminate. Their toxicological effects, especially on humans, are yet to be fully understood (Jaramillo and Restrepo, 2017; Moermond et al., 2016; Loos et al., 2013; Loos et al., 2009). CEC toxicity, ecotoxicity, and behavior in the soil, water, and overall environment are largely unknown for reasons such as novelty and rarity. What is known is that CECs have shown to produce immunological and endocrine disruption effects on various aquatic organisms, and lead to the proliferation of antibiotic resistant microorganisms in water bodies (Jaramillo and Restrepo, 2017). Hence, preventing crops from taking up CECs is highly important, as it would be difficult to evaluate the public health implications of CEC exposure through the food chain.

Accordingly, although the use of marginal water in irrigation is not novel, it has not been popular due to the possible contamination of crops with toxic substances, and adverse health effects on agricultural workers, who may be directly exposed to the marginal water. Therefore, marginal water tends to be used in irrigation only in poorer regions, where freshwater may be costly or inaccessible due to high demand and inadequate infrastructure. The development and implementation of a system of marginal water irrigation that is able to avoid or minimize exposing crops and agricultural workers to the contaminants contained within the marginal water would enable freshwater to be diverted to more pressing uses, such as drinking water. This would also allow farmers who are unable to afford freshwater for irrigation to apply low cost marginal water to their fields, without compromising their safety and crop quality. With subsurface irrigation, which may be more efficient per unit of water used and per unit area of arable land depending on the application method and regional hydrogeology (Dastorani et al., 2010), these advantages could be magnified. The relative water inefficiency of surface irrigation implies that much of the irrigated water is lost to evaporation or runoff, meaning that the contaminants contained within the irrigated water end up either in the root zone of soils (Al-Nakshabandi et al., 1997) or in nearby surface water bodies (Pedersen et al., 2005), polluting the environment and contaminating crops.

1.3 Subsurface irrigation with treated wastewater

Treated wastewater irrigation with minimal risks of crop and human exposure may be accomplished by subsurface irrigation through pipes buried some distance beneath the root zone. Conveniently, such pipes are already present beneath many agricultural fields for drainage purposes. Many such drainage systems have already been implemented in humid regions such as the Netherlands, in order to drain away excess water in the soil before it causes any damage to crops. As the pipes in these systems are usually buried far beneath the root zone of agricultural crops, this system allows for the possibility of fulfilling (part of) the agricultural water demand by applying marginal water resources, such as treated wastewater of industrial or domestic origin, to the soil through these pipes, without directly exposing crop roots to the contaminants possibly contained within the effluent. This is because the subsurface irrigation system does not directly inject effluent into the root zone; instead, as they are buried deeper in the soil, the irrigation system maintains soil moisture levels in the root zone during dry periods by maintaining higher phreatic groundwater levels, which translate to higher hydraulic heads in the root zone (Figure 1.1). The existing drainage capabilities of these drainage systems can be complemented with irrigation capabilities easily by applying water to them at a pressure higher than that of the soil matrix. Since such a subsurface irrigation system would often make use of existing pipes, and since the water to be applied would be of marginal quality and hence low cost, the system is financially accessible as it requires low initial investment costs and low operational costs.

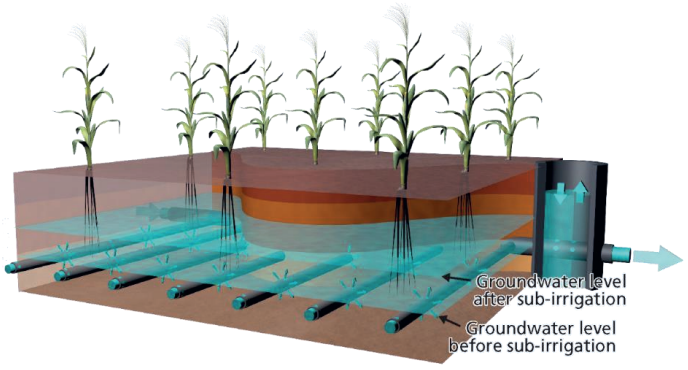

Figure 1.1: An illustration of the subsurface irrigation and drainage system (Narain-Ford et al., 2020).

The subsurface irrigation and drainage system described above is a new method of irrigation, that differs significantly from other existing types of subsurface irrigation systems, such as subsurface drip irrigation, in which water is injected directly into root zone soil. With the use of treated wastewater, the new system has the potential to significantly reduce the agricultural usage of freshwater resources such as groundwater. However, it also poses risks to crops and the environment, due to the spreading of CECs in the subsurface. Aside from the possible public health implications of crop contamination, it is also possible that the CECs pollute deep groundwater and surface water bodies at the outlet of the groundwater shed. The deep groundwater aquifers and surface water bodies that are at risk of contamination may be bodies of freshwater, and the contamination of these waters would defeat the freshwater-saving purpose of subirrigation with treated wastewater. Therefore, it is necessary to better understand the risks and benefits of such a subirrigation system.

With subsurface irrigation, much of the CECs contained in the treated wastewater could instead be degraded or transformed in the subsurface through chemical (Mueller et al., 1992) or biological (Jenks et al., 1998) processes, collectively known as natural attenuation (Röling et al., 2002), or at the very least, be immobilized in the soil matrix through mechanisms such as adsorption and filtration (Grassi et al., 2012). Furthermore, the potential of the soil to eliminate CECs introduced into it by subsurface irrigation or otherwise can be enhanced by altering the physical (Tratnyek et al., 2006), chemical (Amos et al., 2005), or biological (Thomas and Ward, 1989) properties of the soil system to favour the elimination processes. Since natural attenuation allows the spread of CECs in the soil to become more manageable under subsurface irrigation than under traditional irrigation management methods such as surface spray irrigation and drip irrigation, the subsurface irrigation and drainage system proposed here may provide a feasible means by which treated wastewater may be reused in agriculture. Therefore, it is important to study the extent to which natural attenuation can make the use of subsurface irrigation with treated wastewater attractive from the perspective of public health, environmental concerns and economic benefit.

As treated wastewater is typically discharged into rivers and other surface channels, which ultimately flow to the sea, subsurface irrigation with treated wastewater may reduce environmental water pollution, as more wastewater used for agriculture implies less wastewater directly discharged into surface water bodies (Jaramillo and Restrepo, 2017). Monitoring analyses in the European Union have shown that there are no fewer than 125 CECs present in wastewater treatment plant effluents (Loos et al., 2013) that are deliberately released into surface water bodies for the purpose of waste disposal, resulting in the contamination of around 90% of rivers (Loos et al., 2009). With subsurface irrigation, some of the CECs

would be naturally attenuated in the soil before the irrigated treated wastewater enters surface water at the end of the groundwater aquifer, thereby achieving superior environmental outcomes compared to directly discharging the treated wastewater to surface water. Simulations of direct CEC emission to surface water (Coppens et al., 2015) have reaffirmed their adverse environmental effects, while models of sub-surface natural attenuation have produced encouraging results (Bertelkamp et al., 2016; Laws et al., 2011). Nevertheless, given the current novelty of the system, subsurface irrigation with treated effluent has to be approached with caution, especially over long time periods that cannot yet be experimentally investigated, because some CECs may be highly persistent in the sub-surface environment (Hamann et al., 2016). Promisingly, however, studies have shown that most CECs present in the effluent do not readily disperse in the soil (Nham et al., 2015; Ternes et al., 2007), reaching neither the root zone nor deep groundwater in significant quantities even when considering relatively mobile substances such as metformin (Bartholomeus et al., 2016).

Currently, detailed models that characterize the effects of subsurface irrigation with treated wastewater on agriculture and the environment, and that pay heed to spatio-temporal heterogeneity, seasonality and other dynamic processes are not yet available in the literature. Furthermore, although the ambition is to eventually be able to evaluate subsurface irrigation with treated wastewater for large scale regional use, empirical investigations can at the moment only be conducted at the laboratory or single field scale. It is therefore important to fill this gap by constructing generalizable models that are able to widely characterize such subsurface irrigation systems, so as to overcome the perceived risks and uncertainties that currently preclude widespread adoption of this innovative agricultural technology. Accordingly, the analysis of a pilot experimental implementation, and the construction of numerical and analytical models characterizing the subsurface irrigation and drainage system and the associated risks of crop and environmental contamination, is one of the goals of this thesis. To this end, the system is currently being tested and evaluated in an experimental agricultural field in the Netherlands; data and findings from the experimental site will be used in this thesis to support the analyses and models constructed in this thesis. Furthermore, widespread adaptation of subsurface irrigation and drainage with treated wastewater is necessary for the new method of irrigation to have an appreciable impact on water scarcity worldwide. Hence, to evaluate the feasibility of implementing similar systems in regions with geographic and hydrogeological characteristics different from the experimental site, it is also necessary to perform sensitivity analyses on these models.

Various fates are possible for the irrigated CECs, which for example may be taken up by crops, biodegraded in the soil, recovered by the subsurface irrigation and drainage system, leached to deeper groundwater aquifers, or discharged to surface water at the end of the groundwater aquifer. While all of the outcomes listed here are studied to some extent in this thesis, special attention is paid to in-situ biodegradation, and recovery by the drains, as these two outcomes may be the most desirable amongst the listed possibilities. Unlike the other listed possibilities, the CECs cease to exist upon transformation, whereas they are merely transported to various locations under the other possibilities. Furthermore, the water recovered by the drainage system would contain a smaller concentration of CECs that are more biodegradable, compared to the irrigated effluent, because CECs that are more biodegradable would have been attenuated to a larger extent in the soil. The recovered water, with its lower biodegradable CEC load, can then be more easily and safely subjected to further treatment or disposal, compared to the originally irrigated effluent. Hence, recovery by the drainage system is an important means by which the environmental impact of non-biodegradable CECs contained within the treated wastewater may be limited. Therefore, insight into such subsurface irrigation and drainage with treated wastewater may be obtained from other engineering applications in groundwater aquifers that involve the injection and subsequent recovery of water, which are collectively known as managed aquifer recharge and have a much longer history of research compared to subsurface irrigation and drainage.

1.4 Managed aquifer recharge

Managed aquifer recharge (MAR) refers to the intentional recharge of groundwater aquifers either to achieve certain environmental objectives, or to store water of a certain quality for later extraction and use whilst ensuring that the water quality either improves or retains its quality over time (Zhang et al., 2020). Subsurface irrigation and drainage with treated wastewater is a form of managed aquifer recharge, as it fulfils both purposes: the maintenance of relatively high phreatic groundwater levels to ensure that sufficient moisture is delivered to the root zone through capillary rise, and attenuation of the contaminants possibly contained within the treated wastewater. Several other forms of MAR exist, an example being aquifer thermal energy storage (ATES), in which for example warm or hot water is pumped into aquifers for storage during the summer and later pumped out during the winter to be used for indoor heating. An example in the context of water scarcity is aquifer storage and recovery (ASR), where freshwater is stored in groundwater aquifers to preserve its quality over time and later extracted for purposes such as irrigation (Maliva et al., 2006). Managed aquifer recharge has also been used as a method of water treatment, by using groundwater aquifers as bioreactors, in which degraded water is transformed by microorganisms present within the subsurface (Istok et al., 2004). In addition to research on the crop and environmental risks of the subsurface irrigation and drainage system, this thesis also studies abstracted and generalized representations of MAR systems, so as to advance the general theory that can be applied to all types of MAR systems.

MAR systems may be implemented for multiple purposes: for example, ASR systems in coastal areas may serve the dual purpose of freshwater storage and the reduction of saltwater intrusion. The larger hydraulic heads in the aquifers due to the injection of freshwater slows down the rate at which saltwater intrudes inland. However, the dual purpose may complicate the design and operation of the ASR system, as it is also necessary to ensure that the stored freshwater does not become too brackish for its intended use through salt dispersion from the intruding saltwater. Hence, ASR in coastal aquifers is a rewarding yet technically challenging problem that has received a significant amount of attention in the literature (Maliva et al., 2020).

As discussed in section 1.3, subsurface irrigation and drainage with treated wastewater serves a dual purpose. A balance has to be struck between the target groundwater level and the spread of the effluent, when determining the volume and rate of irrigation. The larger the irrigated volume, the higher the groundwater level maintained, enabling a larger amount of moisture to reach the root zone. Furthermore, the larger the irrigated volume, the more CECs may be transformed in the soil. However, a larger irrigated volume also implies that more effluent is irrigated into the subsurface, and that the CECs in the effluent would spread further from the pipes towards the crops and the wider environment. Aside from extracting water from the soil when the groundwater level is too high, the presence of drainage capabilities in the irrigation and drainage system also allows for previously injected but yet to be attenuated CECs to be subsequently recovered from the subsurface either after the crop has been harvested, or on particularly wet days during the crop season. Hence, the drainage capabilities of the subsurface irrigation and drainage system are also integral in managing the balance between maintaining optimal groundwater levels and the spreading of CECs in the subsurface.

A key performance metric of a managed aquifer recharge system in general is the recovery efficiency, which is the fraction of the injected freshwater (ASR) or thermal mass (ATES) that can be subsequently extracted from the aquifer. It is not possible to recover all of the injected freshwater or thermal mass, as the injected water interacts with the surrounding groundwater due to various dispersion processes. For example, stored hot water loses its heat to the surrounding groundwater due to mechanical dispersion and thermal diffusion, while contaminants or salt from the surrounding groundwater disperses into the stored freshwater due to mechanical dispersion and molecular diffusion. In the case of subsurface

irrigation and drainage, the recovery efficiency quantifies how much of the injected (non-biodegraded) CECs are subsequently recovered during drainage, and how much is lost to the environment due to factors such as dispersion, which has implications on the spreading of CECs to crops and the environment.

The various solute dispersion processes, such as mechanical dispersion, molecular diffusion, and macrodispersion, have magnitudes that are dependent to different extents on the flow velocity of water, which is in turn affected by other factors in the design and operation of the MAR system, such as the flow path geometry, spatial heterogeneity, the injection rate, the injection duration, and the injected volume. In most analytical studies on the performance of MAR systems currently available in the literature, the effects of one of either mechanical dispersion or molecular diffusion on the recovery efficiency, concentration, or temperature are studied. The most crucial difference between these dispersion processes is the extent to which they depend on the velocity of water flow. One of the aims of this thesis is thus to investigate how the velocity dependence of a dispersion process itself affects the performance of MAR systems, so that future analyses will not be limited to one of the above dispersion processes, which may both occur simultaneously. If the velocity-dependence of a dispersion process can be linked directly to the performance of a MAR system, then this will yield a general theory that is similarly applicable to all commonly studied dispersion processes, meaning that future studies will be less limited to the investigation of the effects of one specific dispersion process.

In aquifers with spatially heterogeneous physical properties such as the hydraulic conductivity, groundwater flow paths may become spatially heterogeneous, splitting up into fast and slow flow zones, such that macrodispersion becomes an important determinant of the spreading and fate of the injected water. Macrodispersion is a complex dispersion process whose velocity-dependence may vary nonlinearly with the flow velocity, unlike mechanical dispersion, whose velocity-dependence is generally accepted to be linear, and unlike molecular diffusion, which is thought to have no velocity dependence. In addition, the velocity dependence and strength of macrodispersion is related to the extent and type of spatial heterogeneity, the distance travelled by the contaminant plume, and the geometry of the streamlines advecting the contaminant plume (Indelman, 2004). These complexities in the determination of the strength and velocity-dependence of macrodispersion imply that it is a much more complex phenomena than the aforementioned dispersion processes with simpler velocity-dependence. Another aim of this thesis is thus to provide a clearer link between the complex velocity-dependence of the magnitude of macrodispersion and the recovery efficiency of MAR systems.

1.5 Biodegradation and fate of CECs under complex transport phenomena

In light of the above discussion, how CECs disperse and attenuate after being injected into the subsurface, and to what extent they can be recovered, is an important topic of research. The key to a better understanding of the environmental and crop contamination risks of the subsurface irrigation and drainage system is to better understand the processes that affect the transport, attenuation, and fate of the CECs. Although many simple models of solute spreading in the subsurface make use of models with spatially homogeneous soil and aquifer properties subject to steady-state flow, in reality soils and aquifers may be highly spatially heterogeneous and subject to transient flow. As previously mentioned, spatial heterogeneity substantially affects the various dispersion processes and groundwater flow paths, which in turn have large impacts on the quantity and reach of the irrigated solutes. Temporal heterogeneity in flow, due to transient flow stemming from the occurrence of rainfall events, the physiological requirements of crop root water uptake, and irrigation water influx, also determine the fate of the irrigated CECs.

Aside from the complexities that spatial heterogeneity or transient flow alone bring to the characterization of solute fate, they also interact to give rise to higher-order complexities. In unsaturated zone soils with spatially heterogeneous physical properties, which may be encountered in agricultural soils, the spatial distribution of fast and slow flow zones depends on the average flow velocity. With a small average flow velocity, high conductivity zones permitting relatively fast flow tend to be located in fine-textured regions of the soil, and with a large average flow velocity, high conductivity zones permitting relatively fast flow zones tend to be located in coarse-textured regions of the soil. This is because the relationship between the hydraulic conductivity and matric head vary with soil texture (Roth, 1995). Hence, under transient flow, the positions and fluxes of fast and slow flow zones may change dynamically over time in response to changing weather conditions or irrigation input. The effects of transient flow on CEC transport are therefore especially important in the vadose zone, where soil physical properties are dynamically dependent on flow characteristics.

In addition to the effects of the above complex transport phenomena on the spreading of CECs in the soil, they also affect attenuation processes in the soil such as CEC biodegradation. Biodegradation is a primary consideration in the implementation of subsurface irrigation and drainage systems, as it is directly related to the two goals of the system: 1) irrigation with treated wastewater without adverse environmental effects, and 2) further attenuation of the CECs contained within the treated wastewater. Biodegradation of organic contaminants in the soil often requires soil microbes to metabolize the contaminants in the presence of electron acceptors such as oxygen. In other words, the rate of CEC attenuation might depend on the concentrations of the various components of the biodegradation reaction: CECs, microbes, and electron acceptors. Hence, in determining the fate of CECs in the subsurface, it is not only important to be able to characterize the transport of CECs, but also how and where they mix with other substances that may be present in the soil or groundwater. The spatially and temporally heterogeneous flow paths present in unsaturated heterogeneous soils subject to transient infiltration rates therefore render the dispersion, spreading and mixing of the various reaction components, and the biodegradation process itself, highly complex phenomena. As few studies so far have studied the biodegradation of contaminants governed by multicomponent reaction kinetics in soils subject to spatio-temporally varying flow fields, this will be one of the issues studied in this thesis.

1.6 General outline

In order to better evaluate the risks and benefits of the subsurface irrigation and drainage system, this thesis reports on and discusses research that has been conducted on an experimental implementation of the system that has been in operation in the Netherlands since 2015 (chapters 2 and 3). As the experimental subsurface irrigation and drainage system is a form of managed aquifer recharge, the above research is complemented by general theoretical research on the dispersion and recovery of solutes in MAR systems (chapters 4 and 5). Due to the importance of contaminant biodegradation in determining the fate of the irrigated CECs, and the sensitivity of the biodegradation process to spatio-temporal heterogeneity, contaminant biodegradation in the subsurface subject to spatio-temporal flow heterogeneity is also studied (chapter 6). The main methods of investigation throughout this thesis is the numerical modelling and mathematical analysis of abstract and general representations of the subsurface irrigation and drainage system and other MAR systems, as the goal is to obtain results that are general and widely applicable to MAR applications beyond the field experiment discussed in chapter 2.

In chapter 2, the risks to crops and the environment of the experimental subsurface irrigation and drainage system, are modelled, analyzed, and validated with data from the field experiment. This provides a general theoretical overview and analysis of how such a system is expected to behave, and how a system like the experimental system might perform in the long-term, with regard to the risks of environmental and crop contamination due to CECs. In chapter 3, an extensive sensitivity analysis is

performed on the model of the subsurface irrigation and drainage system. The sensitivity analysis investigates the effects of variations and heterogeneity in the hydrogeological parameters of the subsurface, climate parameters of the agricultural plot, biogeochemical parameters of the irrigated contaminants, and irrigation parameters such as the injection pressure and irrigation drain placement. Thus, chapter 3 extends the findings of chapter 2 by providing insight into how the subsurface irrigation and drainage system might perform if it were to be implemented in a region characterized by different marginal water quality and type, hydrogeological parameters, climates, and extent of hydrogeological and climactic variability across space and time. Furthermore, the sensitivity analysis of the irrigation parameters will elucidate how and to what extent it is possible to make up for suboptimality in hydrogeological and climactic factors with optimized irrigation system design and management. Altogether, the aims of chapters 2 and 3 are to characterize the theoretical underpinnings, risks, optimization, and wider adaptation potential of the subsurface irrigation and drainage system when fed with water of marginal quality, in the context of crop and environmental contamination.

In chapter 4, theoretical aspects of managed aquifer recharge governing the dispersion and recovery of injected water are derived and discussed for simple homogeneous aquifers, and validated with numerical models. The aspects of managed aquifer recharge studied in chapter 4 include how the recovery efficiency varies with the injection-extraction flux rate, the period of the injection-extraction cycle, the injected volume of water, the number of injection-extraction cycles, the geometry of flow paths in the aquifer when the system is in operation, and the type of solute dispersion processes (e.g. mechanical dispersion and molecular diffusion) that occur. The geometry of the flow paths under forcing from the injection-extraction wells differ, depending on the geometry of the wells (e.g. fully-penetrating well, or point-source), and on the geometry of the aquifer. Thus, this general theoretical analysis of chapter 4 enable the recovery efficiency of managed aquifer recharge systems to be analytically determined for simple systems under a wide range of scenarios, whereas this previously required the use of numerical models, whose results cannot easily be generalized.

The results of chapter 4 are extended to aquifers with spatially heterogeneous physical properties in chapter 5 using mathematical analyses and numerical modelling, with a focus on the effects of heterogeneity-induced macrodispersion on solute dispersion. Chapter 5 also elaborates on how the wells and theoretical considerations used for managed aquifer recharge may be used to perform push-pull tests, which yield recovery efficiency data that allow hydrogeological properties of the aquifer to be characterized. Performing aquifer characterization prior to subsurface irrigation will allow practitioners to better determine whether a specific subsurface is hydrogeologically suitable for a MAR or subsurface irrigation and drainage system, and whether there is a significant risk of injected contaminants spreading beyond the agricultural plot untransformed.

Chapter 6 employs numerical simulations to study how spatial heterogeneity in soil physical properties in the unsaturated zone may interact with complexities that often arise in agricultural settings. These are namely transient flow, and multicomponent reactions whose reaction rates depend on the electron acceptor concentration and microbial biomass density, in determining the effectiveness of the soil as a bioreactor for contaminant attenuation. The soil microbial biomass density is spatially heterogeneously distributed, and changes over time due to biomass growth that occurs when the contaminants and other organic compounds in the soil are metabolized by the microorganisms. Through numerical simulations, the influences of various parameters such as the initial contaminant concentration, initial microbial biomass density, and transient flow regime on contaminant biodegradation outcomes are investigated. At the moment, the fate of biodegradable contaminants in such problems can only be characterized numerically, not analytically, and the spatio-temporal complexity of the problem implies that large computational times are necessary to solve a single scenario. Therefore, another goal of this chapter is to uncover whether it is possible for certain aspects of the complexity, such as spatial heterogeneity or

transient flow, to be omitted from numerical or analytical treatments of the problem in certain regions of parameter space. For example, if the biodegradation rate is highly unsensitive to the electron acceptor concentration and the microbial biomass density, then the biodegradation outcomes may be characterized with simpler models that invoke monocomponent decay kinetics, whose responses to transient flow or spatial heterogeneity have been widely studied in the past. The main results and implications of this thesis are summarized and discussed in chapter 7, and recommendations are provided for the direction of future scientific research and policymaking regarding managed aquifer recharge in general, and the specific example of subsurface irrigation and drainage with treated wastewater.

Chapter 2

Managed Aquifer Recharge for Irrigation and Marginal Water Treatment

Based on:

Tang, D. W. S., van der Zee, S. E. A. T. M., Narain-Ford, D. M., van den Eertwegh., G. A. P. H., Bartholomeus, R. P. Managed Aquifer Recharge for Irrigation and Marginal Water Treatment. *To be submitted to Environmental Science and Technology*.

Abstract

Managed aquifer recharge with marginal water allows for contaminants of emerging concern (CECs) to be attenuated in-situ, and for water to be more efficiently used. In phreatic aquifers underlying agricultural fields, this also increases water availability for crops. Existing drainage systems may be adapted for both injection (subirrigation) and extraction (drainage). We address subirrigation with treated domestic wastewater by considering numerical simulations and an experimental field site implemented as a proof-of-concept. The transport, adsorption, and biodegradation of tracers, and relatively mobile and persistent CECs (using carbamazepine as an example), are analyzed. For this scenario, almost all non-biodegraded solutes irrigated into the soil are advected laterally towards surface water channels by regional groundwater flow. During the crop season, tracers may rise to the root zone, but only directly above irrigation drains. Accordingly, although up to 10% of tracers irrigated over four years are passively taken up by crops, this is concentrated in the plants situated directly above irrigation drains. No significant spreading of carbamazepine to the root zone occurs, and <1% of the total irrigated amount is taken up by crops after four years. Due to the annual precipitation surplus, solutes that are not very mobile are unlikely to enter the root zone even after decades of irrigation, because the length of the short-term precipitation shortage (crop season) is insufficient for them to rise to the root zone. Furthermore, carbamazepine biodegrades almost completely before being advected any significant distance from the drains. As carbamazepine is a relatively mobile and persistent CEC, the risks of crop, soil and surface water contamination by most other CECs is even smaller. The fraction of the irrigated CEC mass that seeps into surface water channels from the phreatic aquifer decreases exponentially with the distance between the agricultural plot and the channel, and increases exponentially with the agricultural plot width. Thus, the studied subsurface wastewater irrigation system reduces the environmental impacts of marginal water discharge and agricultural water use, with minimal risk of crop and environmental contamination.

2.1. Introduction

Even in temperate humid regions, periodic shortages of fresh water resources may constrain irrigation. Use of treated wastewater for irrigation may be an effective strategy to balance regional fresh water supply and agricultural water demand (Dingemans et al., 2021, Pronk et al., 2021, Narain-Ford et. al 2021). Water stress caused by climate change exacerbates the need to re-use treated wastewater (Elliott et al., 2014). Moreover, the treated wastewater may contain nutrients, which enriches the soil (Lubello et al., 2004). However, wastewater treatment does not remove all impurities from the water, such as pharmaceuticals, pathogens, and other contaminants of emerging concern (CECs) (Yang et al., 2017; Richardson and Ternes, 2018). Surface irrigation with treated wastewater may cause adverse health effects amongst farm workers and the general public through direct exposure or crop contamination (Qadir et al., 2010; Devaux et al., 2001). It may also adversely affect soil fertility because it induces nutrient leaching (Dole et al., 1994) and alters the pH and composition of root zone water (Mohammad and Mazahreh, 2003). Meanwhile, treated industrial and domestic wastewater is often discharged via surface water channels towards the sea, spreading contaminants along these discharge paths (Beard et al., 2019). Accordingly, utilizing treated wastewater in subsurface irrigation may reduce these risks (Narain-Ford et al., 2020). In the Netherlands, it is logistically plausible for 78% to 84% of all treated wastewater to be used in subirrigation, which would reduce freshwater demand in agriculture by 17% to 24% (Narain-Ford et al., 2021).

Managed aquifer recharge refers to the intentional recharge of aquifers to maintain or enhance groundwater levels or quality, such as river bank filtration (Dillon et al., 2019) and aquifer storage and recovery (ASR) (Hartog and Stuyfzand, 2017). Subsurface irrigation and drainage of phreatic aquifers using marginal water as water supply, is a new method of managed aquifer recharge that allows for treated wastewater to undergo further in-situ filtration and remediation in the soil, while simultaneously ameliorating crop water stress. In such a subirrigation system, the subirrigation pipes are buried in the phreatic zone some distance below the root zone, thereby preventing direct exposure of crop roots to CECs (Bern et al., 2013a). Subirrigation is applied using controlled drainage systems, which can drain excess water (prevent waterlogging) and recharge the phreatic aquifer (subirrigation) when necessary (Figure 2.1). Water is fed into the soil to raise the groundwater level and thereby increase capillary fluxes towards the root zone, and vice-versa when the soil moisture content exceeds optimal levels. Controlled drainage may also reduce nutrient losses from the root zone caused by high groundwater levels (Bonaiti and Borin, 2010; Peng et al., 2015; Borin et al., 2001; Borin et al., 1998), and reduce the spreading of the CECs contained in the effluent. Buried drains that are already present in agricultural fields for the purpose of drainage may be modified to work as subirrigation systems, making this a flexible and widely adaptable option.

Many CECs, being organic compounds, are biodegradable by soil microbes (Greskowiak et al., 2017). Subsurface irrigation with treated wastewater enables effluent CECs to be biodegraded in the subsurface while avoiding direct crop exposure. This concept uses the soil, groundwater, and rainwater between the drains and root zone as a biofilter or buffer zone for biodegradation and adsorption, similar to river bank filtration, managed aquifer recharge, and constructed wetlands (Narain-Ford et al., 2020). Due to biodegradation and adsorption, the soil also functions as a bioreactor: water recovered by the drains will be of higher quality than the injected effluent as it would contain lower concentrations of CECs, because of biodegradation, adsorption, and dilution. Still, CECs may enter the root zone through dispersion and capillary rise, or be advected further into the environment by regional groundwater flow. In this system, the exposure of crops to CECs is indirect, while the groundwater is directly exposed, which is opposite to traditional surface irrigation systems. Therefore, it is important to investigate the risks of both crop and environmental contamination specific to subirrigation systems.

In this paper we construct a numerical model to investigate effluent transport in the subsurface and the risks of crop and environmental contamination with CECs in subirrigation systems. We build upon a controlled drainage and subsurface irrigation system fed with treated domestic wastewater in the Netherlands that has been monitored from 2015 onwards. The field site is briefly described, including the data that are used to obtain realistic boundary conditions for the model (e.g. realistic values for solute concentrations in effluent). We emphasize however, that the numerical model constructed here is not meant to closely recreate the field site, but rather, meant to illustrate the fate of CECs in a generic controlled drainage-subirrigation system that represents a simplified form of the field site.

The processes that affect the fate of solutes contained within the effluent (tracers and geochemically reactive CECs that undergo adsorption and biodegradation) are characterized. The solute transport model is validated against CEC concentration data from soil water samples obtained from the field site. With the model, we quantify solute mass balances, breakthrough curves, and plume transport. The solute mass balance considered is split between crop solute uptake, advection in the phreatic groundwater, leaching to deeper groundwater, biodegradation, soil water, and drainage by the drainage system. The partitioning of the irrigated solutes in the mass balance ultimately determines the extent of crop and environmental contamination. Furthermore, we also use the model to investigate the potential of the subirrigation system to lead to adverse environmental effects in the long-term, such as long-term accumulation of CECs in the soil.

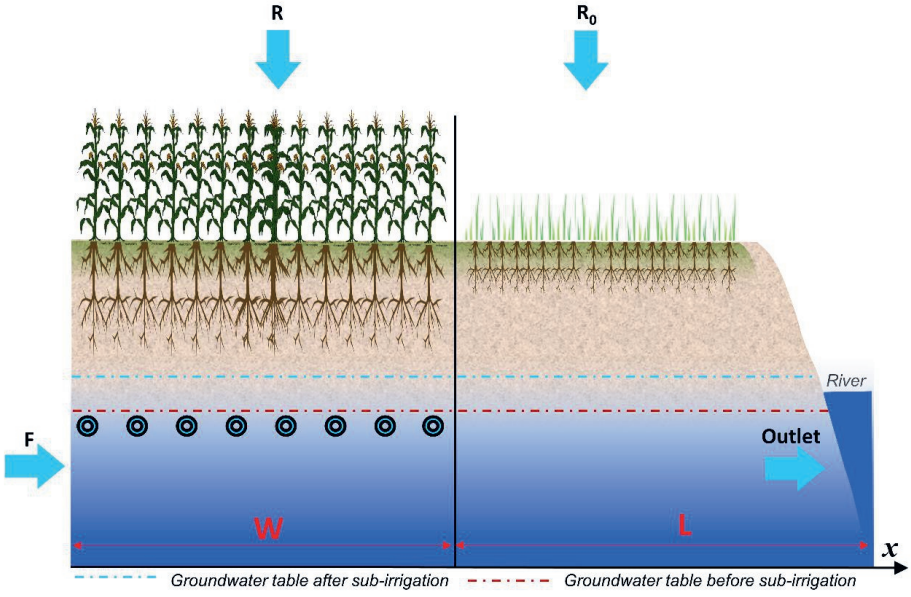

Figure 2.1: Schematic of the subsurface irrigation system and the downstream environment, including an adjacent grass field and body of surface water, considered in the model and subsequent analysis.

2.2 Methods: Field experiment and numerical model

The subsurface irrigation and drainage system we use as an example is implemented in a 58500 m^2 field site in Haaksbergen, the Netherlands, and is the only such system in operation as far as we are aware. Maize grain destined to be livestock fodder is grown. Treated wastewater from the Haaksbergen

municipal wastewater treatment plant, which processes domestic waste from residential sewerage, is fed into the subsurface irrigation system. The experimental system has been in operation since May 2015. Samples of soil water were taken at the observations points three to four times per year during the crop season, and just before the start and during subirrigation, and analyzed for Cl:Br levels, electrical conductivity (EC) and carbamazepine concentrations. We assume that Cl:Br (Davis et al., 1998) and EC (Chaali et al., 2013; Scott et al., 2020) behave as tracers of the effluent, and carbamazepine as a reactive solute that undergoes instantaneous equilibrium adsorption and first-order biodegradation (Durán-Álvarez et al., 2012; Williams et al., 2014; Williams et al., 2006).

The subsurface irrigation/drainage system was numerically modeled with HYDRUS-2D (Šimůnek et al., 2016). Many studies in the literature have shown that HYDRUS-2D is suitable for simulating subirrigation (Cai et al., 2019; Saefuddin et al., 2019; Siyal et al., 2013) and drainage (Kacimov and Obnosov, 2021) systems. The simulation period of the model is four years, starting from the crop season of 2016. Additional details on the field site, the numerical model, and validation and calibration of the model, are provided in the supplementary material.

2.3. Results and discussion

2.3.1 Cl:Br and EC

The results presented in sections 2.3.1 and 2.3.2 refer to the base model with a regional head gradient of 0.0014m/m. The simulated breakthrough curves (Figure 2.2) for the base model show that the solute concentrations in the root zone (0.6m depth and above) resets to nearly background levels before the start of every crop season, with no evidence of accumulation over time, due to the large excess precipitation that occurs outside the crop season. Hence, long term simulations spanning multiple years are not necessary to determine the root zone effluent concentration and the extent of root solute uptake.

During the crop season, the effluent plume moves upwards due to capillary rise when crop water requirements are not fulfilled by atmospheric fluxes. Therefore, the upper part of the effluent plume rises in the summer to above drain level, then sinks back to drain level during the drainage season, and may be partially drained away. For EC, where we assumed that the maximum root uptake concentration is the rainwater level, the root zone concentration may significantly exceed the effluent concentration during the crop season. This is because the ions that contribute to EC are left behind in the soil when water is absorbed by crops, increasing the EC of the remaining soil water, as was also previously observed by Siyal et al (2013) and Fujimaki et al (2006). In our simulations, this is observed only in the soil directly above a drain, and not in the root zone soil midway between drains (Figure 2.2a), because little effluent reaches the root zone midway between drains, even while the roots there have access to sufficient water due to the presence of freshwater (rainwater and ambient groundwater) pushed upwards by the effluent injection. Therefore, if the effluent is very saline, there is a possibility that the irrigation system causes crops directly above drains to experience salinity stress during dry years (Heidarpour et al., 2007), even though it reduces the chance of water stress. Such large EC levels will decrease to ambient levels by the start of the following crop season, and thus should not result in long-term salt accumulation, though long-term issues related to sodicity may occur (van de Craats et al., 2020; Assadian et al., 2005). This implies that any crop contamination that might occur during any one irrigation period would not carry over to the following years, regardless of whether they accumulate in the root zone (EC) or not (Cl:Br).

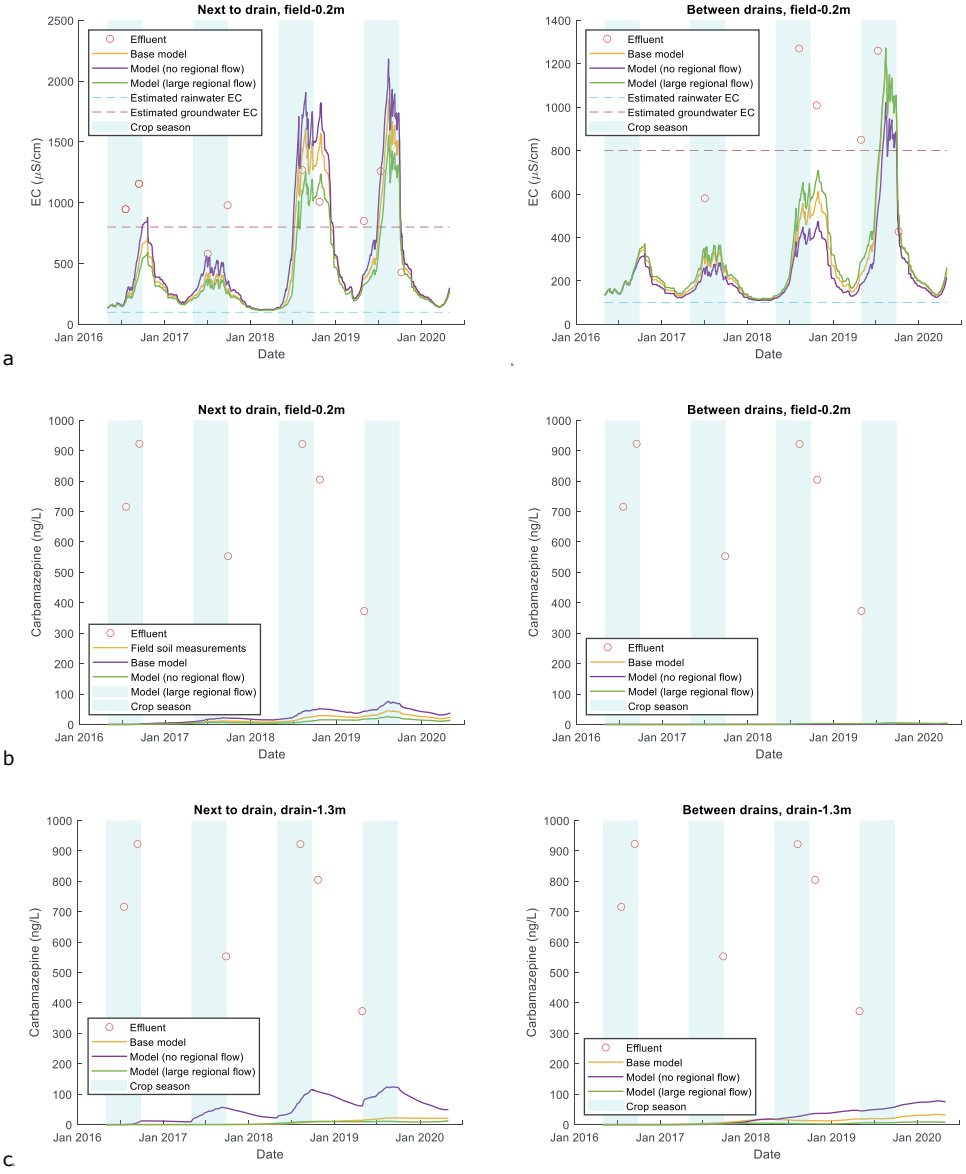

Figure 2.2: Simulation data for

(a) EC at the shallowest observation points (left) directly above drains and (right) midway between drains.

(b) Carbamazepine concentrations at the shallowest observation points (left) directly above drains and (right) midway between drains.

(c) Carbamazepine concentrations at the deepest observation points (left) directly below drains and (right) midway between drains.

2.3.2 Carbamazepine

We compare carbamazepine against a generic tracer (with identical effluent concentration timeseries) to illustrate the effect of adsorption and biodegradation on solute transport; their detailed mass balances are presented in the supplementary material (Table 2S.2). No downwards vertical discharge of carbamazepine from the model domain occurs, due to the effects of adsorption and biodegradation. For the generic tracer, the amount of downwards vertical solute discharge from the domain is finite but essentially negligible. Furthermore, less than 10% of the generic tracer and 1% of carbamazepine are taken up by the crop. Hence, we emphasize that most of the subirrigated solutes, whether tracers or carbamazepine, is advected laterally out of the domain along with regional groundwater flow.

Small amounts carbamazepine spread through capillary rise to the soil directly above (Figure 2.2b) within four years, while comparatively much smaller amounts of carbamazepine spread to the soil midway between drains at identical depths. At the deepest observation points simulated, the opposite applies: the carbamazepine concentrations are higher midway between drains than directly below drains (Figure 2.2c), except in the simulation with zero regional head gradient, because of lateral advection in the saturated zone. The mass influx of the generic tracer and carbamazepine at the drains varies between 0mg to 10^{-2}mg per day during subirrigation. The generic tracer mass flux at the downstream lateral boundary reaches 10^{-3}mg per day by the first crop season, and remains above that level for most of the rest of the simulation. However, carbamazepine mass fluxes at the downstream lateral boundary never exceeds 10^{-3}mg per day, and only reaches 10^{-4}mg per day during the second crop season. No significant levels of the generic tracer nor carbamazepine reaches the bottom boundary even after four years. In the phreatic groundwater, carbamazepine spreads less than 3m from the drains after four years. Hence, the transport of carbamazepine is highly limited compared to that of the tracer.

When drainage occurs during the crop season, the concentrations of tracer and carbamazepine in the drained water are similar. When drainage occurs outside the crop season, the concentration of carbamazepine drained is larger than the tracer, despite carbamazepine undergoing biodegradation, because adsorption keeps the carbamazepine plume close to the drains. This explains why 30% more carbamazepine than tracer is drained in total, even though carbamazepine biodegrades in the soil but not the tracer.

Differences in the mobility of the tracer and carbamazepine results in different spatial distributions of root solute uptake: the root zone directly above drains receives the most solutes due to capillary rise. The relative amounts of total root solute uptake differs with the horizontal position and depth of the roots. For the tracer, the roots at the nodes at 0.2m depth take up roughly four times as much tracer as the roots at 0.6m depth, even though solute concentrations are 10% higher at 0.6m depth, because the root density is four times larger at 0.2m depth. The roots directly above drains take up roughly four times as much tracer as the roots midway between drains, because solute concentrations directly above drains are two to four times larger. These patterns are also observed for carbamazepine. Carbamazepine uptake directly above drains is over ten times that midway between drains, because adsorption arrests the spreading of carbamazepine. Therefore, most root uptake of tracer and carbamazepine occurs directly above drains, and this spatial heterogeneity in root solute uptake is stronger for less mobile and less persistent solutes.

Unlike the tracer, for which appreciable levels of root solute uptake (11%), horizontal discharge (78%) and vertical discharge (<1%) were observed (89% in total), very little carbamazepine had been taken up by crops (<1%) or discharged from the domain horizontally (9%) or vertically (0%) by the end of the simulation (10% in total), while 67% was biodegraded. Solute concentrations in the root zone essentially

reset on an annual basis due to the annual precipitation surplus, which means that the crop solute uptake of carbamazepine is not expected to increase with the number of years of operation of the subirrigation system. Since less than 1% of the irrigated carbamazepine is taken up by crops, and since most crop solute uptake of carbamazepine is concentrated in roots directly above the drains, carbamazepine levels in crops is likely negligible everywhere except directly above drains. However, this also implies that the system studied here might not be suitable for irrigation in a climate with an annual precipitation shortage.

Field data from the experimental site are in agreement with the results of the model presented above, and will be briefly presented here. Further details will be made available in Narain-Ford et al (in prep.). Of the 55 CECs found in the wastewater effluent but not in the control field beside the experimental plot, the fraction of CECs classified as mobile and persistent (MP CECs) is 19/55. In the surface water stream located 1m from the end of the agricultural plot, and in deep groundwater under the agricultural plot, the average detected concentrations of MP CECs as a fraction of the effluent concentrations was smaller than 0.01 in deep groundwater and in the surface water stream on all sampling occasions. An exception was that in the middle of the crop season during the drought of 2018, somewhat elevated levels (average relative concentration of 0.5) of MP CECs were detected at the surface water stream, but not in deeper groundwater. When correcting for the effect of dilution by precipitation, groundwater and surface water, less than 1% of MP CECs reaches deeper groundwater in the field site, which is in agreement with our model. In addition, from the field data we observe that the concentrations of all CECs in the root zone, regardless of mobility or persistence, reset to background levels by the start of the following year's crop season, except if there is a period of severe drought such as that of the summer of 2018.

2.3.3 Regional groundwater flow

Despite the large effect of the regional head gradient on the breakthrough curves, varying the regional head gradient had little effect on the relative partitioning of solute mass balances. Most importantly, in the simulations with high and zero regional head gradients, the main findings of the base model continue to apply: Crop solute uptake is around 10% for tracers and 1% for carbamazepine, little tracer mass seeps to deeper aquifers, no carbamazepine seeps to deeper aquifers, little solute mass is drained by the drainage system, and the rest of the irrigated solute mass is discharged horizontally out of the simulated domain. Therefore, uncertainty in the regional head gradient does not undermine the findings of the study. In fact, we have shown that while the regional head gradient may affect the rate at which CECs are laterally advected, it does not significantly change our conclusions relating to the overall mass balance of the CECs. Since there is an annual precipitation surplus, the average annual transport direction of the CECs can only be laterally downstream and/or vertically downwards, even when the regional groundwater head gradient is zero. Since the calibrated lateral flow resistance is effectively much lower than the downwards flow resistance, the transport of CECs is primarily lateral even in the absence of regional flow. This explains why the solute mass balance partitioning is not sensitive to the regional head gradient.

When the regional head gradient is low, the natural groundwater level is lower, therefore requiring a higher irrigation flux to maintain target water table levels. In the base model (0.0014m/m head gradient), 16.3mg of carbamazepine was irrigated over the four year simulation period. The corresponding values in the model with no regional flow (0 m/m) and high regional flow (0.0022m/m) were 25.4mg and 10.9mg respectively, which implies that even such a large uncertainty in regional head gradient would translate only to a 50% difference in the irrigated solute mass. Nevertheless, in practice it is easy to monitor the absolute volume of water used by the irrigation system. Therefore, knowledge of the solute mass balance partitioning, which is not sensitive to the regional head gradient, is sufficient to evaluate the fate of the irrigated CECs.

2.3.4 Environmental impact beyond the agricultural plot

The fact that most of the effluent leaves the crop field by lateral advection enables a simple analysis of the main implications for the longer term environmental impact. For this analysis, we approximate the aquifer as a one-dimensional horizontal flow domain, where all flow occurs along the x-axis illustrated in Figure 2.1. Regional groundwater flow of flux F_{in} enters the unconfined aquifer of height H and porosity θ underneath a subirrigated field of length W, which experiences a net recharge (precipitation plus irrigation, minus evapotranspiration, drainage, and leaching) flux equal to R. Downstream of the subirrigated crop field is an unirrigated grass field of length L with a net recharge of R_0. An outlet, representing for example a surface water body such as a stream or river, lies at the lateral downstream extremity of this aquifer. Parameter values used for the following analysis are $\theta = 0.41, H = 3m, W = 500m, L = 1000m, F_{in} = 0.0019m, R = 0.000767m, R_0 = 0.0001m$ unless otherwise specified. The parameter L=1000m used in this example is meant to illustrate a generic scenario, and does not approximate the experimental field site, as it represents a trivial case of L=1m.

Neglecting dispersion, the travel time of effluent solute particles to the outlet may be calculated according to Leray et al (2019). The flow rate at position x is

$$F(x \le W) = \int_0^x R(u)\,du = F_{in} + Rx$$

$$F(x \ge W) = F_{in} + RW + R_0 x. \tag{2.1}$$

For solutes entering the soil at position x, the travel time t_1 to the end of the subirrigated field, and the travel time t_2 of solutes from the end of the subirrigated field to the outlet, are respectively

$$t_1(x) = \theta H \int_x^W \frac{1}{F(u)}\,du = \frac{\theta H}{R}\ln\left(\frac{F_{in} + RW}{F_{in} + Rx}\right), \tag{2.2}$$

$$t_2 = \frac{\theta H}{R_0}\left(\frac{\ln[F_{in} + RW + R_0 L]}{\ln[F_{in} + RW]}\right). \tag{2.3}$$

where u is a dummy variable for integration. The total travel time of solutes from position x to the outlet is

$$t(x) = t_1(x) + t_2. \tag{2.4}$$

As L increases, the travel time t increases (Figure 2.3a). As W increases from zero, $t(x)$ first decreases to a minimum at around $W = 1000$, then increases as W increases further (Figure 2.3b). This non-monotonicity occurs because increasing W increases two competing factors: the travel distance from x to the outlet, and the groundwater flow velocity.

Denote the shortest and largest possible travel times, which are $t(x = W)$ and $t(x = 0)$ respectively, by t_a and t_b respectively. To compute the effluent travel time distribution $\pi(t)$, we invert the travel time expression, yielding

$$x(t) = \frac{F_{in} + RW}{R \cdot \exp\left[\frac{R}{\theta H}t - \frac{R}{R_0}\left(\frac{\ln[F_{in} + RW + R_0 L]}{\ln[F_{in} + RW]}\right)\right]} - \frac{F_{in}}{R}, \qquad (t_a \le t \le t_b) \tag{2.5}$$

which may be used to compute the tracer travel time distribution $\pi^*(t)$

$$\pi^*(t) = \pi(x)\left|\frac{dx}{dt}\right| = \frac{F_{in} + RW}{W\theta H}\exp\left[\frac{R}{R_0}\left(\frac{\ln[F_{in} + RW + R_0 L]}{\ln[F_{in} + RW]}\right) - \frac{R}{\theta H}t\right]. \qquad (t_a \le t \le t_b) \tag{2.6}$$

Here, $\pi(x)$ is the probability of a solute particle entering the soil at position x, and is equal to 1/W at $0 \leq x \leq W$ and 0 everywhere else, since we have assumed uniform irrigation rates across the entire crop field. For solutes with biodegradation rate constant μ, where μ is defined as the inverse of the biodegradation half-life, the probability that a particle reaches the outlet without being biodegraded can be expressed as a function of the particle's travel time to the outlet

$$\pi_{out}(t) = \exp(-\mu \ln(2)\, t)\,. \tag{2.7}$$

The travel time distribution $\pi(t)$ of biodegradable solute particles that arrive at the outlet is thus

$$\pi(t) = \pi_{out}(t)\pi^*(t) = \frac{F_{in} + RW}{W\theta H} \exp\left[\frac{R}{R_0}\left(\frac{\ln[F_{in} + RW + R_0 L]}{\ln[F_{in} + RW]}\right) - \left(\frac{R}{\theta H} + \mu \ln(2)\right) t\right]. \qquad (t_a \leq t \leq t_b) \tag{2.8}$$

The normalized cumulative travel time distribution $\Pi(t)$ of particles arriving at the outlet is

$$\Pi(t) = \frac{\int_{t_a}^{t} \pi(t)dt}{\int_{t_a}^{t_b} \pi(t)dt} = \frac{1 - \exp\left[\left(\frac{R}{\theta H} + \mu \ln(2)\right)(t_a - t)\right]}{1 - \exp\left[\left(\frac{R}{\theta H} + \mu \ln(2)\right)(t_a - t_b)\right]}. \qquad (t_a \leq t \leq t_b) \tag{2.9}$$

Figure 2.3c and Figure 2.3d illustrate $\pi(t)$ and $\Pi(t)$ respectively, and shows that as μ increases, only the contaminant particles that have shorter travel times reach the outlet.

Effluent will first reach the outlet at time t_a after the onset of subirrigation, and the solute flux at the outlet will reach steady-state at time t_b. Given that the orders of magnitude of R and $\theta H \ln(2)$ do not deviate significantly from 0.001 and 1 respectively in this problem, whereas μ of CECs span a range of 0 to 10 (Nham et al., 2015), the travel time distribution of CEC particles arriving at the outlet is predominantly determined by μ. At steady-state, for conservative solutes, the solute flux at the outlet equals the total irrigated solute flux. For biodegradable CECs, the fraction f of the total irrigated solute mass that arrives unbiodegraded at the outlet is

$$f = \frac{\int_{t_a}^{t_b} \pi(t)dt}{\int_{t_a}^{t_b} \pi^*(t)dt} = \frac{\exp\left[-\left(\frac{R}{\theta H} + \mu \ln(2)\right) t_a\right] - \exp\left[-\left(\frac{R}{\theta H} + \mu \ln(2)\right) t_b\right]}{\exp\left[-\frac{R}{\theta H} t_a\right] - \exp\left[-\frac{R}{\theta H} t_b\right]}. \tag{2.10}$$

Figure 2.3e shows that as L increases, f decreases because the travel distance becomes larger, and that this decrease is more rapid for larger μ. Figure 2.3f shows that as W increases, f increases meaning that less biodegradation occurs overall, because the groundwater velocity increases as the crop field lengthens. These figures show that the fraction of the irrigated CEC mass that seeps into surface water channels from the phreatic aquifer decreases exponentially with the distance between the agricultural plot and the channel, and increases exponentially with the agricultural plot width. The distance between the crop field and outlet has a stronger effect on the fate of solutes with higher biodegradation rates. For the parameter values used, f only varies meaningfully (i.e. between 0.01 and 0.9) within one order of magnitude of μ, namely $0.0001 \leq \mu \leq 0.001$. Hence, any solute with a smaller biodegradation rate than this range may be assumed to behave conservatively, while any solute with a larger biodegradation rate may be assumed to be fully biodegraded by the time it reaches the outlet. In the case of carbamazepine, for which $\mu = 0.008\ day^{-1}$, no significant levels will be detected at the outlet.

We have shown the that significant levels of crop, soil and groundwater contamination due to carbamazepine was unlikely, and that carbamazepine is unlikely to contaminate the surface water channel downstream of the aquifer. Therefore, even for an outlet located a relatively short distance (1000m) from the subirrigated field, only CECs significantly more persistent than carbamazepine will seep into the surface environment. If the expected CEC content of the wastewater to be used for irrigation, and its biodegradability in soil, is known in advance, then the distance between the agricultural plot and the downstream outlet L can be a parameter in the design of such subirrigation systems.

In Ternes et al's (2007) study of 54 CECs present in treated domestic wastewater in Germany, carbamazepine was found to be one of the most persistent and mobile CECs in the soil. Therefore, the spreading of other CECs in the environment is likely to be even more limited than what we have observed for carbamazepine. Since the effluent would have likely been directly discharged into surface water in the absence of the subirrigation system, the subirrigation system therefore ultimately reduces the adverse environmental impacts associated with treated wastewater discharge, thereby leading to better surface water quality in the vicinity of the treatment plant. However this might also lead to an increase in metabolites which may be more toxic than the parent CEC (Murrell et al., 2021).

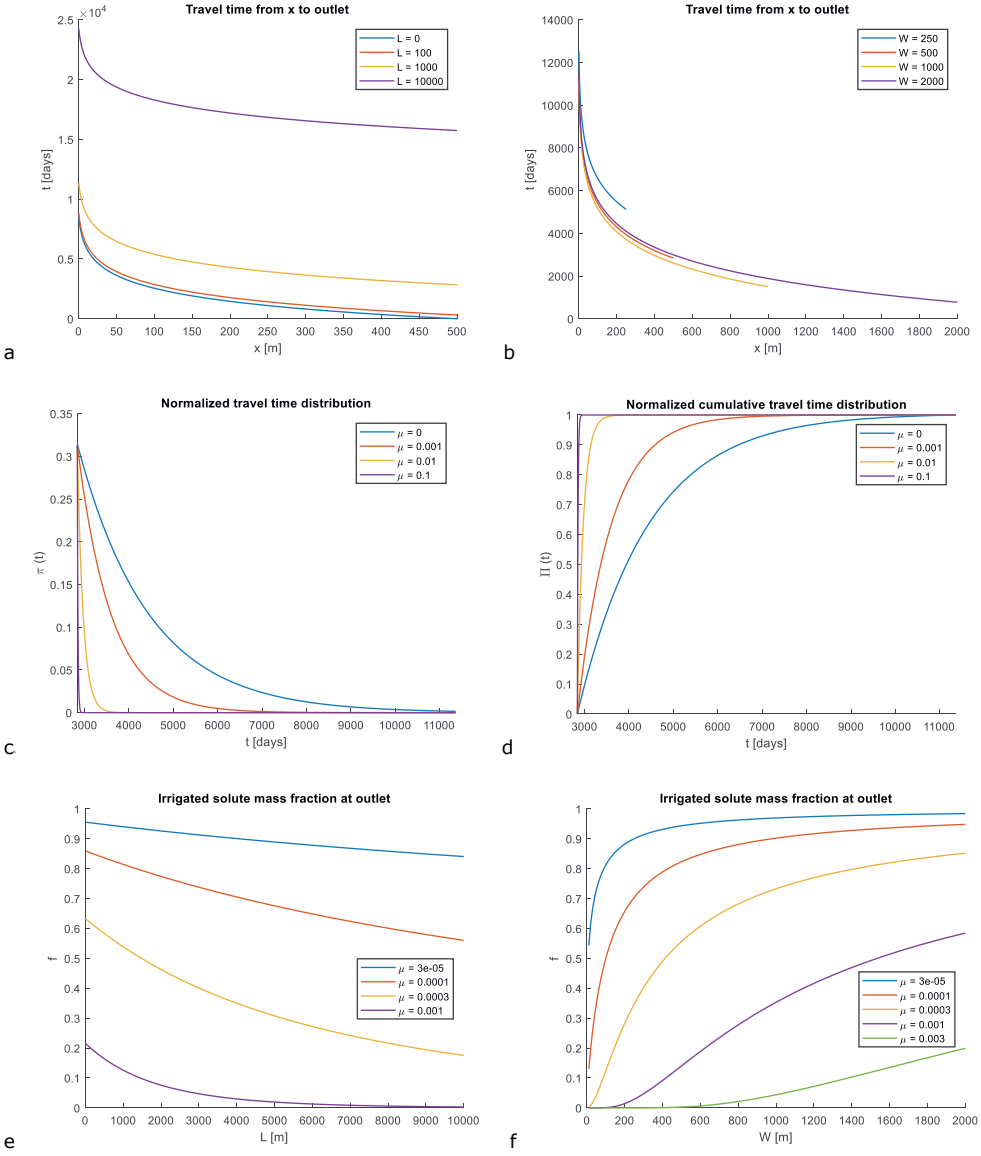

Figure 2.3: Solute particle travel time as a function of entry location, for various values of (a) L and (b) W. (c) Travel time distribution and (d) cumulative travel time distribution of solute particles that arrive at the outlet, for various values of μ. Irrigated solute mass fraction that arrives at the outlet, for various values of μ, as a function of (e) L and (f) W.

2.4 Conclusion and outlook

The results and analyses of the model have provided additional understanding of how effluent is transported and how CEC concentrations in the subsurface develop over time and space under subsurface irrigation and drainage in phreatic aquifers, a new method of managed aquifer recharge. The soil water Cl:Br ratio and EC were studied as tracers of the effluent, while carbamazepine was studied as an example of a relatively mobile and persistent CEC. In the long term, effluent contamination in both the root zone and the phreatic zone within the agricultural plot becomes periodically steady-state, with large concentrations during the crop season and low concentrations during the drainage season. The long term severity of contamination within the agricultural plot depends mainly on the efficiency with which the annual net recharge and regional flow pushes the contaminants downstream in the aquifer, and the mobility and degradability of the contaminants.

For the modelled case study, transport of contaminants from the phreatic zone to deeper groundwater accounts for a negligible portion of the solute mass balance. As around 90% of the effluent tracer leaves the simulated domain along with lateral advection by regional groundwater flow, most of the effluent would end up discharged to the surface water body at the end of the aquifer if not biodegraded or leached to deeper groundwater along the way. A brief analysis of solute travel times in the phreatic groundwater revealed that CECs that are equally or less persistent than carbamazepine, which is considered mobile and persistent, would be fully biodegraded before travelling a relatively small distance from the confines of the agricultural plot. Hence, when the phreatic groundwater is eventually discharged to surface water, much of the CECs contained within the treated wastewater leaving the treatment plant would no longer be present, due to biodegradation and adsorption in the soil. Furthermore, no long-term accumulation of CECs in the root zone occurs under an annual precipitation surplus.

The subirrigation and drainage system is effective in preventing crop damage from insufficient or excess moisture, by maintaining the groundwater level within a narrow range suitable for capillary-fed evapotranspiration. Without the system, or if the supply of treated wastewater becomes insufficient to meet demands, the groundwater level drops to deeper levels, with drought damage as a result. Conversely, excessive precipitation may lead to waterlogging in the absence of the drainage system. While drainage is effective at preventing excessive soil moisture, it does not remove significant amounts of CECs from the soil. There is some risk that CECs, especially tracer-like CECs, will be absorbed by crop roots during particularly dry crop seasons, or that particularly saline effluent would cause the crops to experience salinity stress. Concentrations of carbamazepine in the entire root zone remained low throughout the simulated period. Accordingly, less than 10% of total irrigated tracer mass and 1% of carbamazepine was taken up by crop roots over four years, and this appears to not be significantly dependent on the regional groundwater flow rate. Despite the possibility of crop contamination by mobile CECs, most of the crop solute uptake occurred for crops located directly above drains, whereas crops located midway between drains are barely exposed even to irrigated tracers. Hence, it may be prudent to consider diverting crops located directly above drains to non-food uses, or to plant non-food crops there. Regardless of crop contamination during any particular crop season, tracer levels in the root zone decrease to nearly zero before the start of every subsequent crop season due to the precipitation surpluses that occur during the rest of the year, possibly unless extreme precipitation shortages occur. Therefore, long-term accumulation of CECs in the subsurface over a time scale exceeding one year will not occur, perhaps except for CECs that are significantly more immobile and persistent than carbamazepine, and even then these CECs will not rise to the root zone unless prolonged droughts occur. The above model results are supported by data from the experimental field site.

Using the treated wastewater in subsurface irrigation therefore leads ultimately to superior environmental outcomes in surface water, compared to the alternative of direct discharge of the treated

wastewater into rivers and canals. Furthermore, such a system of subsurface irrigation with treated wastewater may be implemented using existing subsurface drainage pipes, while also allowing less freshwater to be used in agriculture. Hence, this system has the potential to significantly reduce anthropogenic environmental damage associated with agriculture and biological waste at a low difficulty and initial investment cost. Despite the initial investment costs, the reduction in freshwater usage, improvements in the quality of the surrounding environment, and increased crop yields and quality due to improved crop access to water, may lead to financial returns in the long term.

2S Supplementary material

2S.1 Field site description

Here we provide only the details most pertinent to the construction of the two-dimensional numerical model, which will be described below. Further descriptions of the experimental implementation are available in Bartholomeus et al (2016), Bartholomeus et al (2017) and Stofberg et al (2021). The primary soil types in the root zone and phreatic zone are sandy soils with slight loam content. The perforated polyethylene subsurface drains have an outer diameter of 6cm and are installed 1.2m beneath the soil surface, with a 6m drain spacing.

Field measurements of water balances, soil pressure heads, and solute concentrations in both effluent and soil water were collected during the four crop seasons (May to September) from 2016 till 2019. There are 51 sampling points present at various depths in the experimental plot, some directly above or beneath drains, and some located midway between two drains. Thus far, no effluent has been detected at the 21 sampling points (minifilters) located 4m beneath the surface or deeper, based on measurements of the chloride-bromide ion ratio Cl:Br, which behaves as a tracer (Davis et al., 1998). Therefore, we validate our model with data from the 30 shallower sampling points: MacroRhizons at 0.2m, 0.6m, and 1.0m beneath the soil surface (three locations per depth), and minifilters at 0.25m, 0.8m, and 1.3m beneath drain level (seven locations per depth). Some of the shallower sampling points might lack data on certain sampling dates because the soil was too dry for any water to be extracted.

The greatest determinant and the largest source of uncertainty regarding solute fate is arguably the adsorption coefficient and the biodegradation rate, as they span multiple orders of magnitude, are highly uncertain in the field, and vary not only with CEC identity but also environmental parameters. The effect of these parameters is studied by comparing the transport of Cl:Br, EC, and carbamazepine. However, aside from these biogeochemical parameters, the regional groundwater head gradient has a large and direct effect on solute breakthrough curves, especially at the observation points located at a larger distance from the drains. This is caused by the direct impact of regional groundwater head on the lateral advection velocity, and because it is responsible for a much larger proportion of the flux passing through the simulated domain than any other flux source or sink. Since detailed information on the regional head gradient over the measurement period is unavailable, the regional head gradient also has a significant contribution to uncertainty in the model parameterization. The combination of relatively large uncertainty in a relatively impactful parameter might manifest as uncertainty in the simulation results. To identify the extent to which uncertainty in the regional head gradient would affect the accuracy of the simulation results, we briefly investigate the effect of varying the regional head gradient on the simulated breakthrough curves. In the base model, a single constant value of the regional head gradient (0.0014m/m) was used. We repeated the numerical simulations with two other regional flow scenarios, namely zero head gradient (0 m/m) and high regional head gradient (0.0022m/m).

2S.2 Numerical model setup

An overview of the parameter values can be found in Table 2S.1. The 13m by 4m model domain (Figure 2S.1) represents the subsurface to a depth of 4m from the soil surface, with a root zone of the maize crop that reaches a depth of 0.6m, and two drainage/irrigation pipes buried 1.2m beneath the surface spaced 6m apart. We insert breakthrough curve observation points at the same approximate locations as in the field experiment (0.2m, 0.6m, 1.0m beneath the soil surface, and 0.25m, 0.8m, 1.3m beneath drain level), with one column of observation points directly above and below the downstream irrigation drain, and one column midway between the two drains, for a total of twelve points. Three indicators of effluent spreading are analyzed for model validation: the Cl:Br ratio, solution EC, and concentrations of the antiepileptic pharmaceutical carbamazepine.

For all substances except EC, we assume that all solutes in soil water are taken up by crop roots along with the water regardless of concentration; this is reasonable for CECs, which are present in trace amounts. As Cl:Br is a ratio of trace elements, not a concentration, it is reasonable that root uptake does not affect levels in the soil water. Since root salt uptake rates increase linearly with soil salinity up to some physiological threshold (Moya et al., 1999), we assume for simplicity that the maximum root uptake concentration of the ions that contribute to EC is the rainwater concentration. The rainwater ionic content is small compared to groundwater and effluent, thus our implementation is in principle similar but slightly more realistic than other studies in the literature (e.g. Siyal et al., 2013) that assume no ions are taken up by roots. In the simulations, excess ionic content in the soil water beyond the rainwater concentration is left behind in the soil water, where it accumulates and increases the EC.

The top boundary for water flow is an atmospheric boundary that represents precipitation; excess precipitation beyond the soil's infiltration capacity is lost to runoff (Šimůnek et al., 2016). Daily precipitation and reference evapotranspiration data (calculated according to Makkink, 1957) were obtained from the Dutch meteorological institute (KNMI). The daily potential evapotranspiration of the root zone during the crop season was calculated by multiplying the reference evapotranspiration with a weekly crop factor for Dutch grain maize crops (LAGO, 1984). Outside of the crop season, the reference evapotranspiration was used as the potential evapotranspiration.

The root zone is modelled with an exponentially decreasing root density from the surface to the bottom of the root zone. The potential evapotranspiration rate is partitioned across each node in the root zone proportionally to the root density at each node (Šimůnek and Hopmans, 2009). The actual root water uptake flux is then determined with the pressure head reduction function of Feddes et al (1978), with the parameters for corn (Wesseling et al, 1991) that are pre-programmed into Hydrus 2D. Crop solute uptake is assumed completely passive for all species except EC, as previously described.

The bottom boundary is a deep drainage boundary condition: an imposed flux boundary whose magnitude depends on the groundwater level (Hopmans and Stricker, 1989). The left (upstream) boundary for water flow is an imposed head gradient boundary representing the regional head gradient. The right (downstream) boundary is a Cauchy boundary condition whose parameter values were obtained by calibrating the simulated groundwater levels (simulated without irrigation and crops) against field data obtained from a grassfield 1km Northeast of the experimental plot, with a post-calibration Nash-Sutcliffe efficiency of 0.61, which is considered good (Moriasi et al., 2007).

Each irrigation drain is modelled as a circular opening with a 4cm internal diameter and 8cm external diameter. The crop season in the model lasts for 150 days every year starting from the first of May, while the drainage season occurs the rest of the time. The irrigation drains have imposed pressure head boundaries during the crop season, and 'seepage face' boundary conditions (Liu et al., 2021) outside the crop season.

Concentration flux boundary conditions were applied for solute transport at all boundaries. Daily effluent Cl:Br ratio, EC, and carbamazepine concentrations from the field site were interpolated from the two to four effluent samples measured per year and used as realistic input values for the model analysis. Daily effluent EC values became available after June 2018, and were incorporated into the simulations. The Cl:Br ratio of rainwater is estimated at 100 from samples taken from the shallow soil in 2016, and agrees roughly with the literature (e.g. Davis et al, 1998). The EC of rainwater is estimated at 100 µS/cm from

early shallow soil samples, and also agrees in general with the literature (e.g. Zdeb et al (2018)). Groundwater Cl:Br (300) and EC (800 µS/cm) were estimated from field samples obtained from 4m beneath the soil surface or deeper, as they both are uniformly and constantly measured at these respective values over the entire subsurface profile deeper than 4m, during the measurement period. These values are also in approximate agreement with various studies in the literature on ambient Cl:Br and EC values (e.g. Alcalá and Custodio, 2008; Van den Brink et al., 2007). Groundwater and rainwater carbamazepine concentrations are assumed to be zero.

The initial conditions for water flow were set to hydrostatic equilibrium relative to a water table depth of 1m, corresponding to measurement data from the unirrigated field on the day before the crop season of 2016 began. Initial conditions for solutes were set as the rainwater concentration at the top boundary, the groundwater concentration at the bottom boundary, and a linear distribution with depth within the model domain.

Test simulations with a generic tracer with a constant input concentration during the irrigation season show that the tracer reaches the root zone within the first crop season (Figure 2S.2a), and achieves an annual periodic steady-state at the end of the drainage season in terms of effluent plume shape, location, size (Figure 2S.2b), solute concentrations, and solute mass balances within four years. A test simulation with a larger model domain suggests that the plume would maintain the same shape and linear direction of movement indefinitely if it does not encounter a boundary condition. Therefore, the size of the model domain and a simulation period of four years is sufficient for long-term analyses of the system, regardless of the extent of solute mobility or persistence.

2S.3 Model comparison with field data

The field data and simulated breakthrough curves, for Cl:Br and EC show good agreement in general (Figure 2S.3 – 2S.8). The fit between simulation data and field measurements appears slightly better for Cl:Br than for the EC, especially at the measuring points midway between drains. This is consistent with Cl:Br being likely a more reliable tracer than EC, because Cl:Br is more conservative (Davis et al., 1998) than EC (Pellerin et al., 2008).

Adsorption coefficients and biodegradation rates of carbamazepine available in the literature vary over orders of magnitude, depending on environmental factors and in-situ physical and biochemical conditions (Durán-Álvarez et al., 2012; Williams et al., 2014; Williams et al., 2006). Therefore, we calibrated these biochemical parameters so that the simulated breakthrough curves match the observed field data. This resulted in a half-life of 125 days (biodegradation rate coefficient of 0.008 day^{-1}) and an adsorption coefficient of 1 L/kg, implying a retardation factor of 2.5, falling well within the range provided in the literature. With these parameters, the simulated breakthrough curves for carbamazepine generally agree with the field data.

The measurement points located 0.8m and 1.3m beneath drain level, directly below the drains, are among the deepest measurement points where effluent has been detected in the field site. For these two measurement points, the base model consistently and significantly underestimates concentrations of Cl:Br, EC, and carbamazepine. Concentrations of carbamazepine at the measurement points 0.8m and 1.3m directly below a drain display significantly larger concentrations than the simulations predict. These measured concentrations are almost identical to effluent concentrations, which implies that carbamazepine did not experience adsorption as it was transported from the irrigation drains to those points, despite showing signs of retardation across the rest of the domain. The fast downwards transport

of solutes described above is consistent with solute transport in large macropores or fractures, which have small surface-area-to-volume ratios and hence less adsorption sites, thereby causing effluent to travel vertically downwards much faster than simulated. Therefore, a likely explanation for the elevated levels of carbamazepine, Cl:Br, and EC at 0.8m and 1.3m beneath drains is the presence of vertical preferential flow in the field. In addition, note that on many sampling dates, there are large spreads in measured levels of effluent observed at different sampling points located at the same depths and same position relative to drains. This suggests a significant presence of spatial heterogeneity in soil hydraulic properties in the field. Core samples show that low conductivity loam layers are present at depths of 3m to 4m in some parts of our experimental plot, which may contribute to the absence of effluent at sampling points deeper than 4m. Such structural heterogeneity may greatly affect wetting patterns, water fluxes, and effluent fates. Since the large disagreement occurs only for two observation points out of twelve, and since these two points are located at the same direction from the drains suggesting a common unknown cause, we conclude that the model mimics the field data well in general.

Despite the complications arising from possible aquifer heterogeneity, the base model agrees well, but not perfectly, with the field data. It is also possible that other complexities unaccounted for in the simulations are present in the field, such temporal heterogeneity in environmental conditions, and slight differences in subirrigation periods and pressures applied in the field. Another possible explanation is that in the field site, the angle between the length of the drains and the regional flow vector is not perfectly perpendicular. Nevertheless, the model successfully captures the general flow and solute transport patterns observed in the field, as will be further elaborated upon in the results and discussion section. Therefore, further analyses of the system is possible with the model.

2S.4 Effects of the regional head gradient on model validation

The breakthrough curves from the base model has overall the best fit with the field data. The simulations with a high regional head gradient result in breakthrough curves that are not highly different from those of the base model, but at all observation points the field data fits better with the base model than with the high head gradient simulations. The simulations with no regional head gradient result in breakthrough curves that deviate more significantly from the base model, especially at observation points between drains.

In general, the simulations with no head gradient lead to poorer fits with experimental data compared to the base model. However, at the two observation points where the base model tends to fit poorly with the experimental data (directly beneath drains, 0.8m and 1.3m below drain level), the simulations with no regional head gradient have better fits with the experimental data than the base model. Since the base model has better fits with the data when considering all other observation points, and since even the extremely unrealistic situation of a regional head gradient of 0 does not lead to a good fit at the two observation points in question, it is unlikely that overestimation of the regional head gradient is responsible for the base model's poor fitting at 0.8m and 1.3m directly beneath drains. This reinforces the hypothesis that other mechanisms, such as aquifer heterogeneity, are more likely to be the cause of the rapid increase in effluent concentrations 0.8m and 1.3m directly beneath drains during the crop season.

Table 2S.1: Parameters used in the simulations. Soil 1 is present from field level to 0.2m depth. Soil 2 is present from 0.2m to 0.6m depth. Soil 3 makes up the bulk of the aquifer. Sources of parameter values: 1) Heinen et al (2020); 2) Dutch geological survey (TNO); 3) Ernst and Feddes (1979); 4) Calibrated to experimental data; 5) Estimates

Parameter	Value	Source
θr (soil 1,2,3)	0.01	1
θs (soil 1,2,3)	0.42	1
α (soil 1,2,3) [1/m]	2	1
n (soil 1,2,3)	1.5	1
Ks (soil 1) [m/day]	0.5	1
Ks (soil 2) [m/day]	2	1
Ks (soil 3) [m/day]	5	1
L (all soils)	0.5	1
Regional head gradient	0.0014	2
Reference depth [m]*	0	3
A [m/day]*	0.0025	3
B [1/m]*	-1.250	3
Water table depth at downstream boundary [m]	1.6	4
Conductivity of downstream boundary [m/day]	0.02	4
Irrigation drain conductivity [m/day]	0.025	4
Irrigation pressure [m]	0.3	4
Drainage backpressure [m]	0.3	4
Longitudinal dispersivity D_l [m]	0.2	5
Transverse dispersivity D_t [m]	0.02	5
Soil bulk density ρ [kg/L]	1.5	5

*Deep drainage boundary parameter

Table 2S.2: Water and solute mass balances over the duration of the model scenarios used for model validation against field data. Water balances are expressed in millimeters for comparison with rainfall volumes. Since each observation node is a zero-dimensional object with no volume, the crop solute uptake at each node is dimensionless. Therefore, the crop solute uptake values per observation node are normalized (separately for each solute) to observation point at 0.2m depth directly above a drain.

Water balances	**Irrigated water (mm)**	**Drained water (mm)**	**Crop water uptake (mm)**	**Rainfall (mm)**	**Lateral flow in (mm)**	**Lateral flow out (mm)**	**Vertical flow out (mm)**
Field data	1828	280	–	3150	–	–	–
Base model	1895	269	1916	3150	2785	4041	1004
Solute mass balances	**Irrigated solute (mg)**	**Drained solute (mg)**	**Crop solute uptake (mg)**	**Crop solute uptake fraction**	**Horizontal solute discharge (mg)**	**Vertical solute discharge (mg)**	**Biodegraded solute fraction**
Base model (generic tracer)	16.3	0.520	1.75	0.107	12.7	0.0330	0
Base model (Carbamazepine)	16.3	0.689	0.136	0.00833	1.46	0	0.666
Total root solute uptake at observation node	**Directly above drain**		**Midway between drains**				
	0.2m depth	**0.6m depth**	**0.2m depth**	**0.6m depth**			
Base model (generic tracer)	1	0.291	0.281	0.0818			
Base model (Carbamazepine)	1	0.663	0.0566	0.0487			

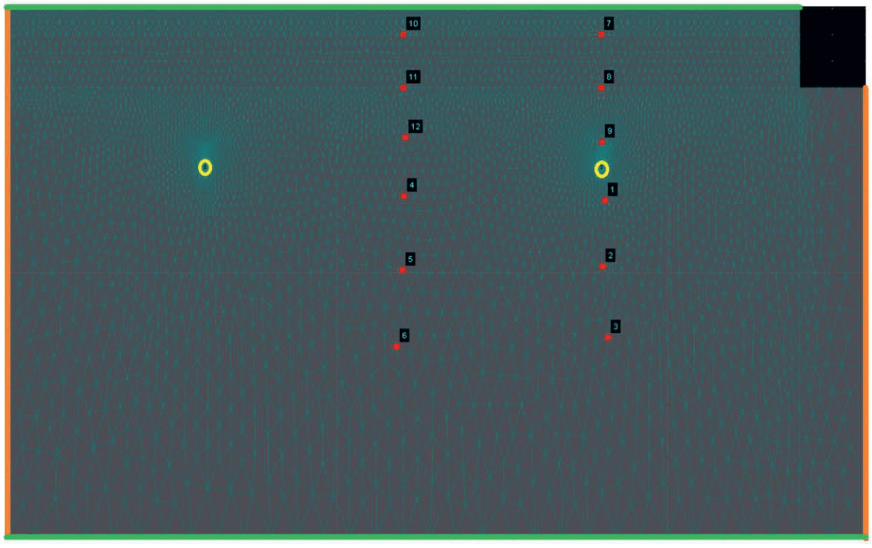

Figure 2S.1: (b) Cross-section of the numerical model domain showing the locations of sampling points (red points), the drains (yellow circles), and the four boundary conditions (orange and green lines). Regional groundwater flow flows from left to right.

a

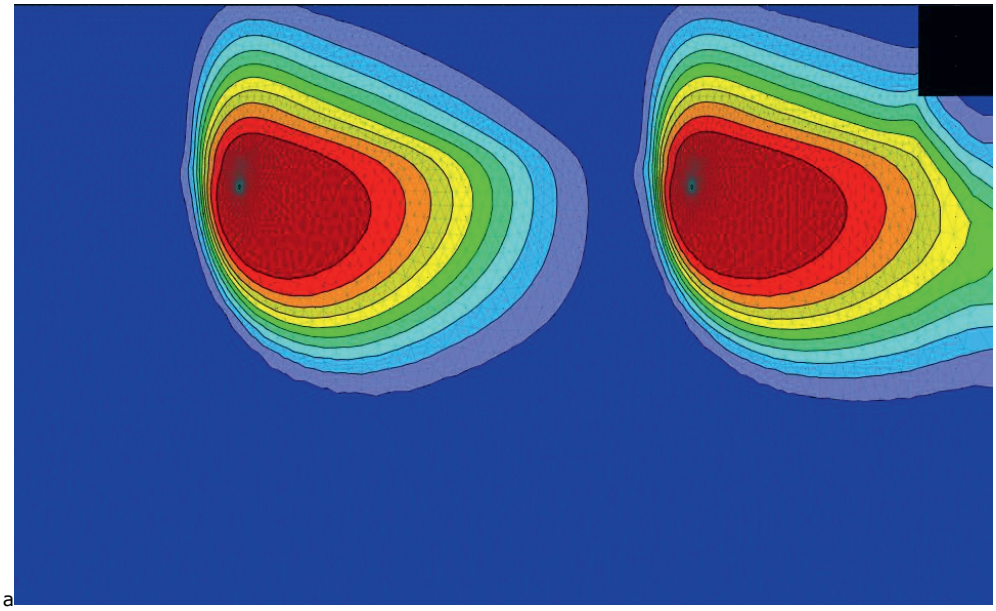

b

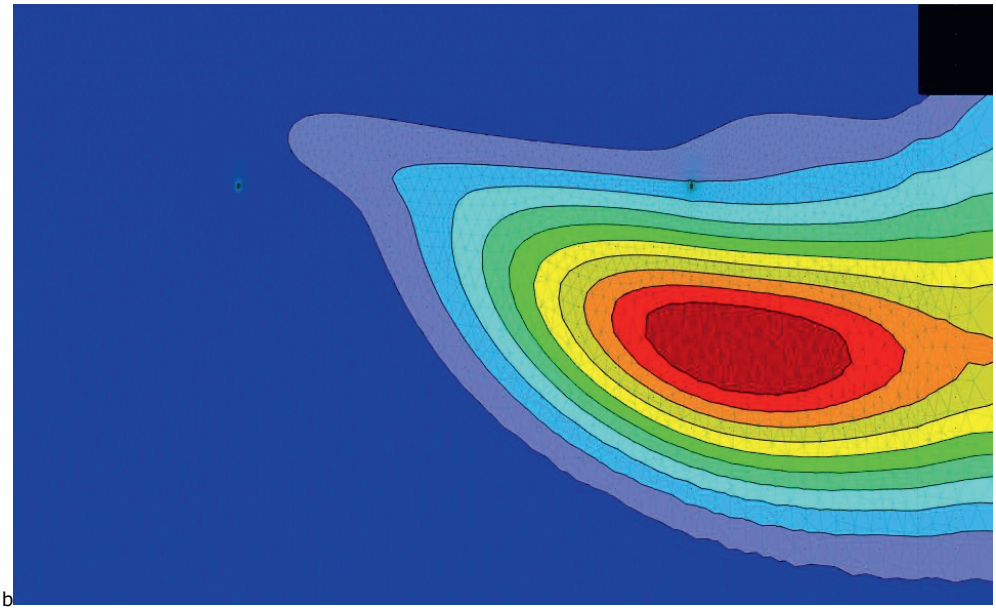

Figure 2S.2: (a) Tracer plume in the base model at the end of the first crop season. (b) Periodic steady-state tracer plume at the end of the fourth drainage season, for the base model. Red represents a relative concentration of 1 (relative to the input concentration), blue a relative concentration of 0, and the intermediate colors represent intermediate relative concentrations.

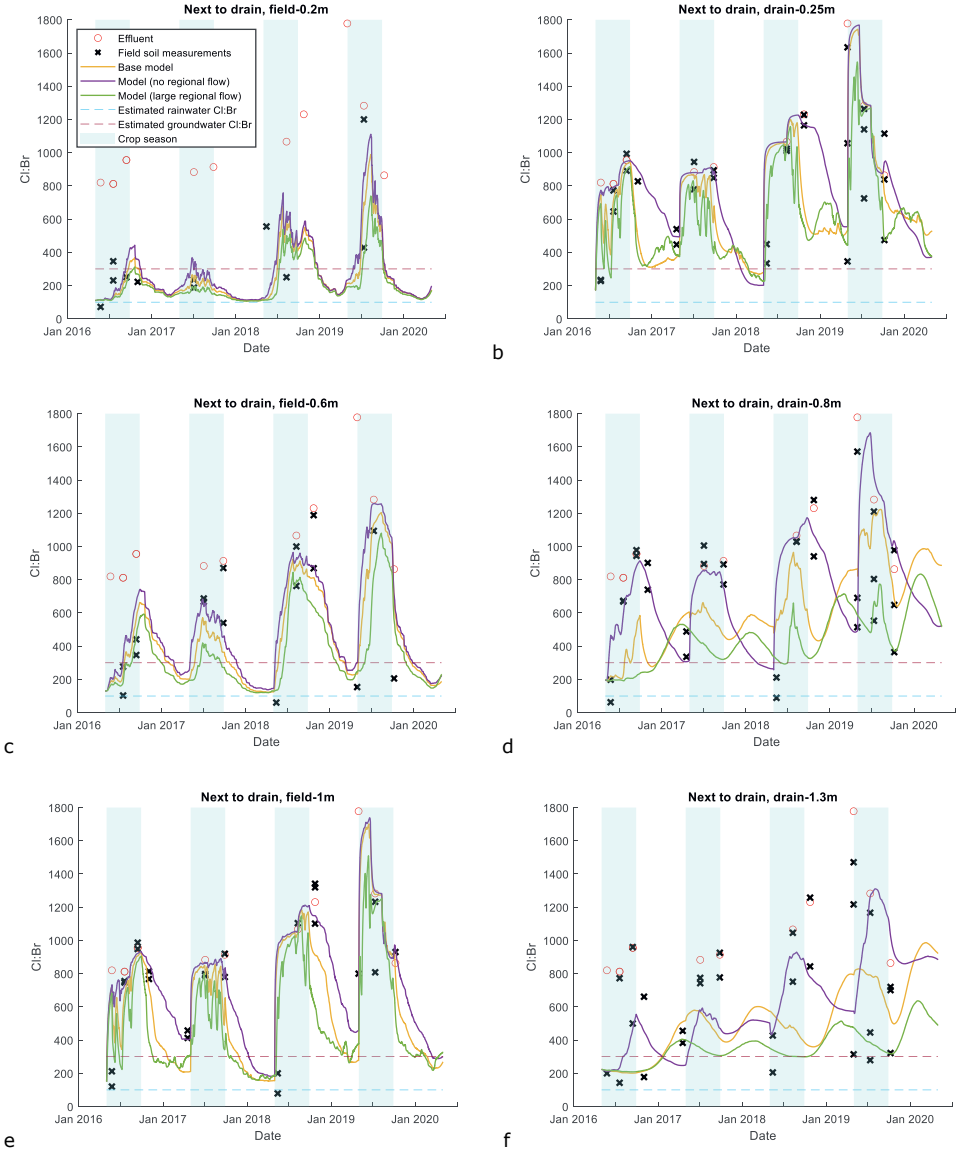

Figure 2S.3: Field data and simulation data for Cl:Br at observation points by drains.

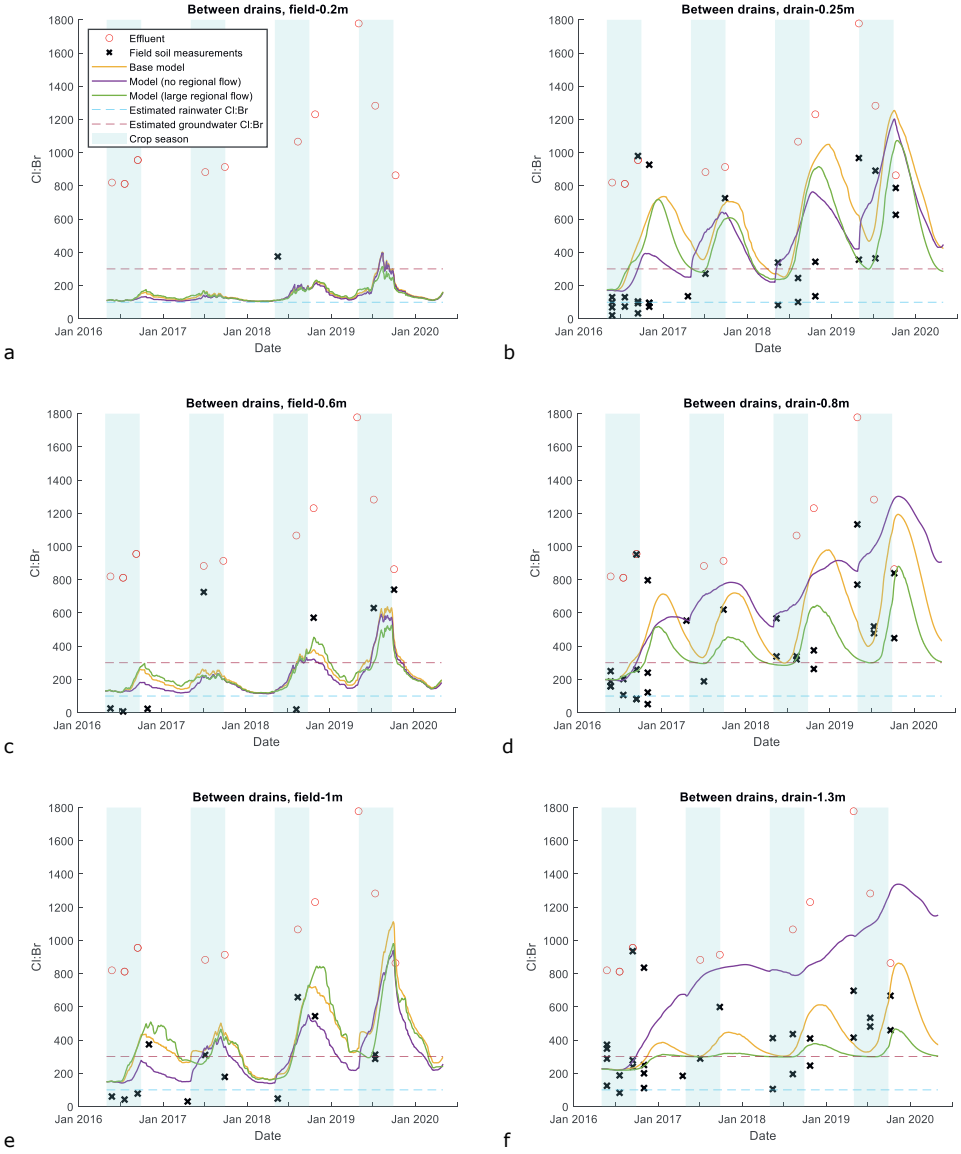

Figure 2S.4: Field data and simulation data for Cl:Br at observation points between drains.

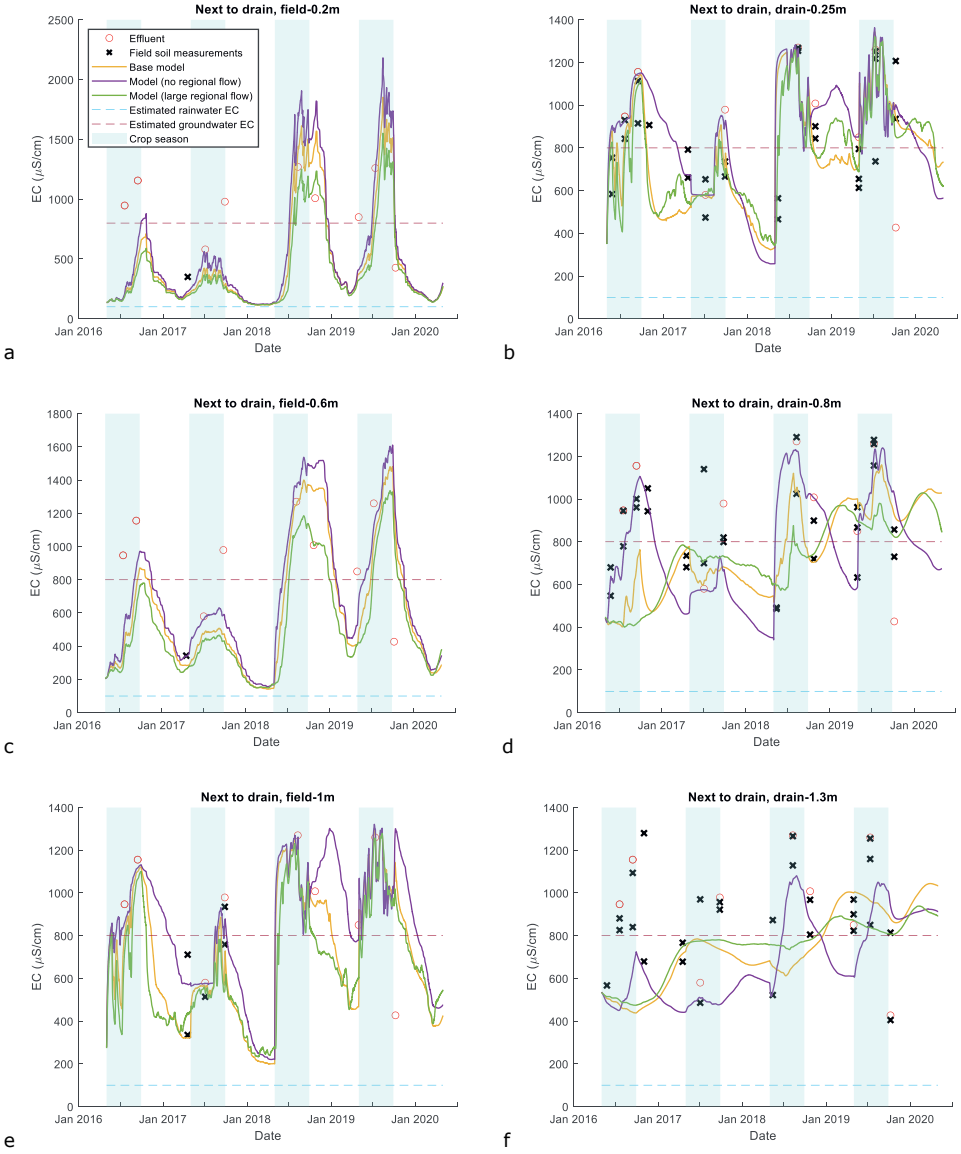

Figure 2S.5: Field data and simulation data for EC at observation points by drains.

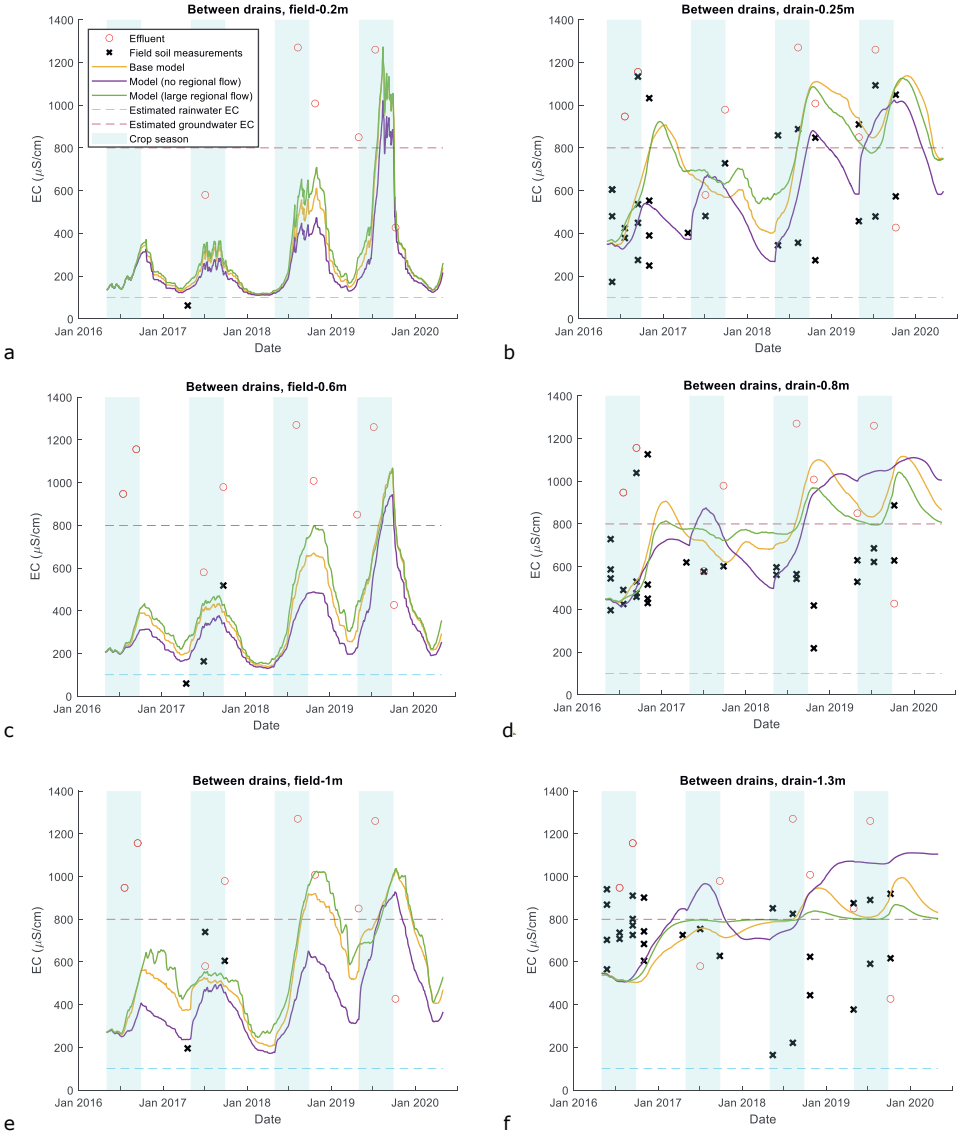

Figure 2S.6: Field data and simulation data for EC at observation points between drains.

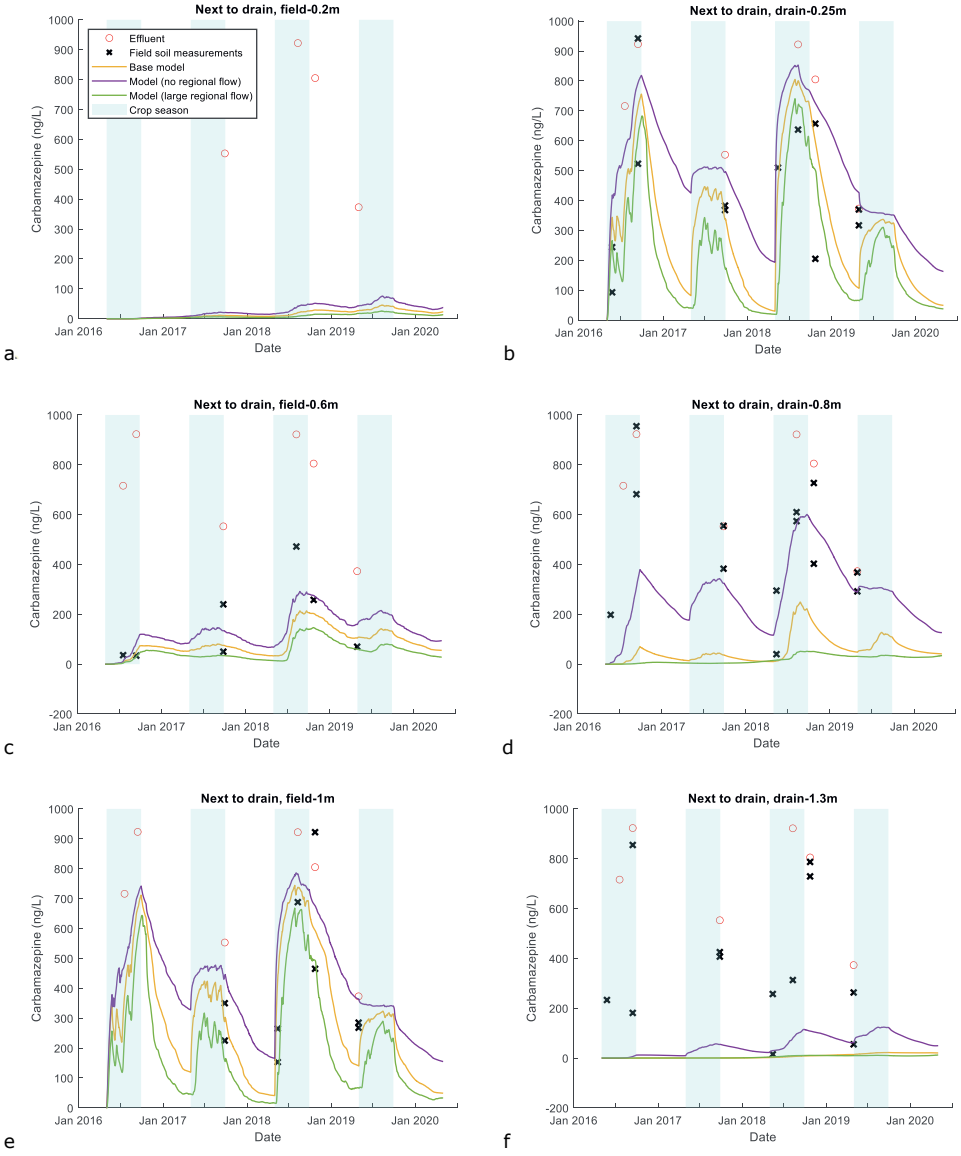

Figure 2S.7: Field data and simulation data for carbamazepine at observation points by drains.

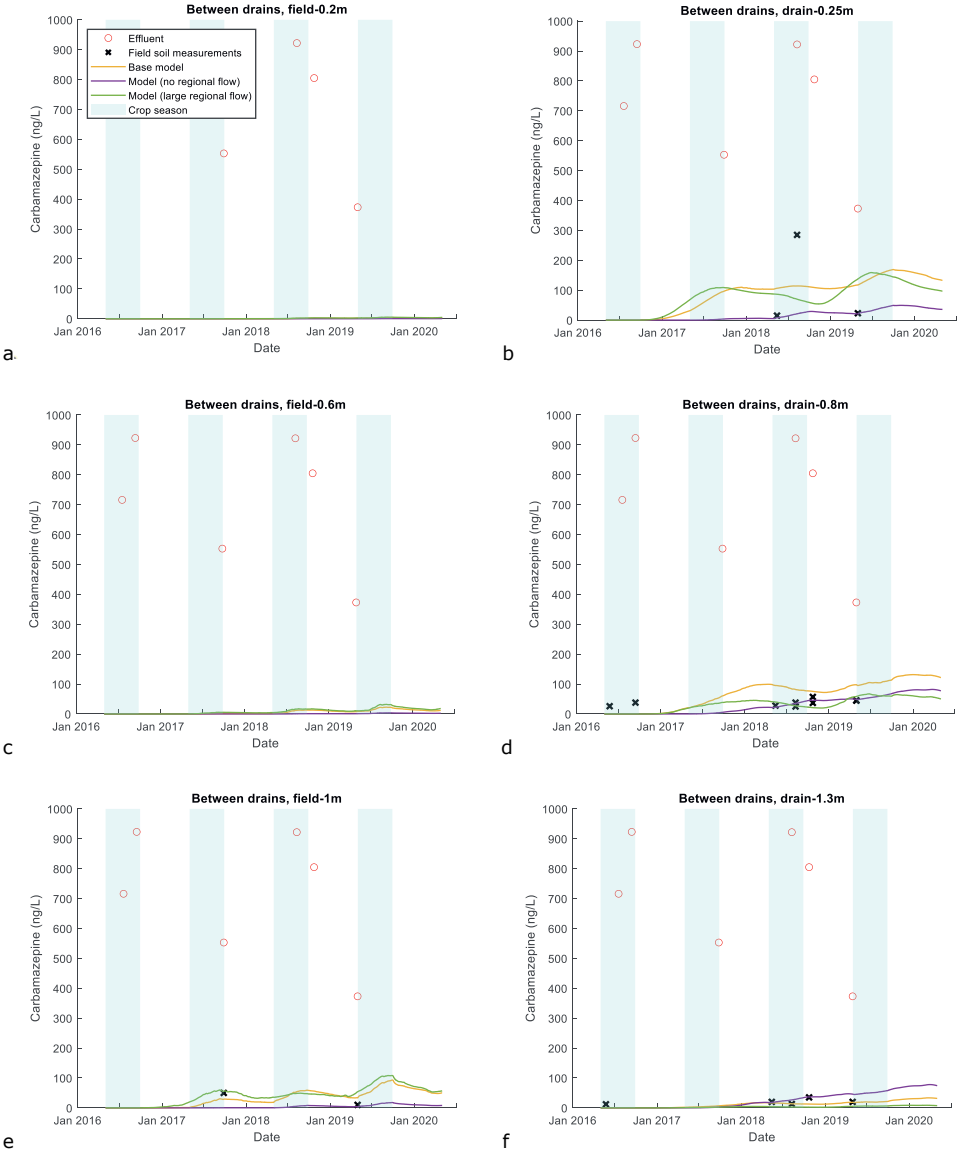

Figure 2S.8: Field data and simulation data for carbamazepine at observation points between drains.

Chapter 3

Sensitivity Analysis of Subsurface Irrigation with Marginal Water

Based on:

Tang, D. W. S., van der Zee, S. E. A. T. M., Bartholomeus, R. P. Sensitivity Analysis of Subsurface Irrigation with Marginal Water. *To be submitted to Journal of Hydrology.*

Abstract

Reuse of treated wastewater in irrigation allows for scarce freshwater to be conserved. Deep subsurface irrigation and drainage systems allow marginal water to be used in irrigation, without directly exposing crops to soluble contaminants of emerging concern (CECs), though CECs gradually disperse towards the crops over time. Through numerical modelling, we perform analyses on the fate of irrigated effluent solutes. We investigate how variations and heterogeneities in physical hydrogeological parameters (soil and aquifer properties, and environmental fluxes), irrigation parameters, and CEC biogeochemical properties, affect the fate and mass balances of the CECs. These determine the effect on crops and the environment, of using effluent for subirrigation. In general, the CEC mass discharged into the saturated zone varied more greatly across scenarios than the crop CEC uptake. CEC biogeochemical parameters most greatly affected the solute mass balances, followed by physical parameters. Amongst the physical parameters, those that most strongly affect groundwater flow (regional head gradient, aquifer conductivity, and aquifer boundary resistances) have the greatest impact. Aquifer heterogeneity increased solute discharge in the saturated zone, to a greater extent under stronger heterogeneity, but had no effect on average on crop solute uptake. Atmospheric flux balances have moderate impacts, while irrigation parameters have the smallest impact on solute mass balances. Therefore, the viability of effluent subirrigation is primarily determined by geography: unfavorable hydrogeological conditions and effluent types, which are specific to regional geography, cannot be offset by optimizing the irrigation parameters.

3.1. Introduction

Deep subsurface irrigation and drainage is increasingly receiving attention as a method of agricultural water management and managed aquifer recharge, that prevents crop water stress caused by insufficient and excessive soil moisture. In a deep subirrigation system, porous drains are laid some distance below the root zone, in contrast to subsurface drip irrigation. During dry periods, water is fed into the soil through the drains to maintain the water table at levels high enough for capillary rise fluxes to compensate for any inadequacy in rainfall. The system is climate-adaptive, thus during extremely wet periods, water is drained away to prevent waterlogging of crops. It allows for the use of treated wastewater for irrigation while minimizing the risks of crop and environmental contamination that might otherwise occur with methods such as sprinkler or drip irrigation (Narain-Ford et al., 2021). The soil between the drains and the root zone, and the background groundwater naturally present in the subsurface, act as a buffer separating the crops from the effluent. Many contaminants in the effluent are organic contaminants of emerging concern (CEC) that would undergo adsorption and microbe-induced biodegradation within this buffer zone (Narain-Ford et al., 2020). After the crop season, the drains remove soil water during wet periods, which prevents CECs and other contaminants present in the groundwater from moving to root zone soil. As some CECs biodegrade in the soil, the irrigated effluent gradually contains an increasingly larger proportion of non-biodegradable contaminants such as salts and heavy metals than it initially did. Subsequent drainage thus reduces the accumulation of persistent contaminants in the soil.

If not used for subirrigation, the treated wastewater would have likely been directly discharged towards rivers. When used for subirrigation, biodegradation due to soil microbes would have reduced the contaminant load by the time the effluent is transported to an ecotoxicologically important location, such as the root zone, deep groundwater aquifers, or surface water. Hence, using treated wastewater for deep subsurface irrigation and drainage may ultimately lead to superior environmental outcomes than the current practice of discharging to surface water. As deep subsurface irrigation and drainage, using marginal water, is a relatively new method of irrigation, there are neither existing guidelines for its design and operation, nor studies on hydrogeologically and climactically suitable conditions for implementation. Hence, it is important to be able to systematically characterize the fate of CECs under such a system, provide physical explanations for these behaviors, and describe how variations in environmental conditions may affect outcomes. Such knowledge is also instrumental for understanding the viability of future adaptation of such subirrigation systems to agricultural settings with different climates, hydrogeological conditions, and effluent origins. Additionally, understanding the risks of subsurface irrigation using marginal water is needed in order to define risk management plans, as necessitated by the EU regulations (Alcade-Sanz & Gawlik, 2017) regarding water reuse for agriculture.

In chapter 2, we described an experimental plot of the system in the Netherlands, that was irrigated with treated domestic wastewater. We constructed a numerical model to characterize the system, validated the model against the experiment, and described the fate of some tracers and solutes that the effluent contains. The subirrigation system is illustrated in Figure 3.1. A key finding was that most irrigated solutes were laterally advected away from the agricultural plot along with regional groundwater flow. Through an analysis of contaminant fate in the phreatic groundwater, based on realistic estimates of regional groundwater fluxes and groundwater recharge rates, we found that CECs that are not highly persistent would be almost fully biodegraded before traveling more than several hundred meters laterally from the agricultural plot. Hence, upon reaching the outlet of the aquifer, much of the CECs in the effluent would have been attenuated. Less than 10% of irrigated tracer mass and less than 1% of a relatively mobile and persistent CEC (carbamazepine) were passively taken up by crop roots. Even in homogeneous soils, crop solute uptake was mostly concentrated in the roots situated directly above irrigation drains, whereas crop solute uptake was insignificant for roots midway between drains. Overall,

the risks of crop and environmental contamination, both in the long and short term, are significant only for extremely persistent contaminants that biodegrade very slowly or not at all.

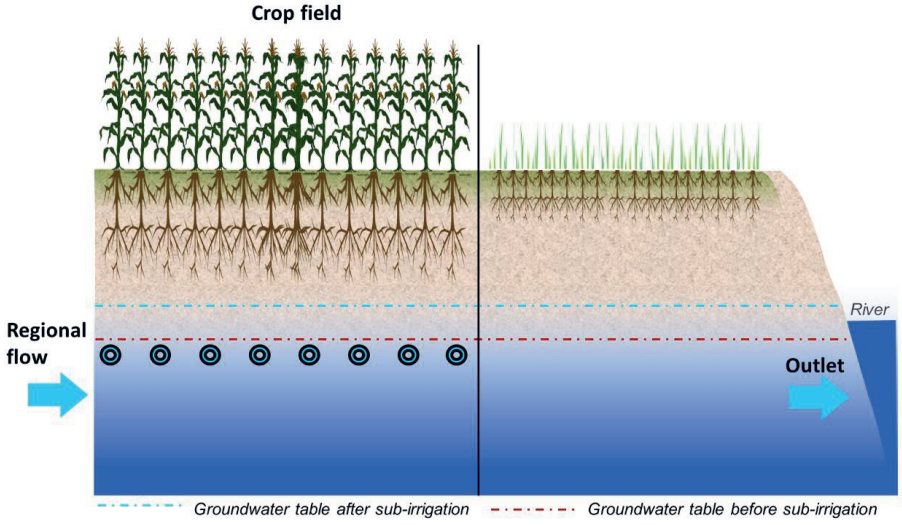

Figure 3.1: Illustration of the subirrigation system and the subsurface.

The objective of this paper is to perform a sensitivity analysis of effluent solute fate using the model described and validated in chapter 2, which quantitatively characterizes a climate adaptive subsurface irrigation and drainage system implemented in the Netherlands. The analysis involves soil and hydrogeological parameters, environmental fluxes, boundary resistances, irrigation parameters, CEC biogeochemical parameters, and also an analysis of random soil heterogeneity. The range of soil types, hydrogeological parameters, environmental fluxes, and biogeochemical parameters investigated span a wide and realistic range that represents diverse geographic and climactic conditions. The outcomes considered in the analysis include the solute mass balance (root solute uptake, effluent drainage with the drains, effluent discharge in the saturated zone), solute transport direction, irrigation water use, root zone solute concentrations, and breakthrough curves.

While many studies on solute leaching, crop contamination, and environmental risks in agricultural contexts exist in the literature (e.g. Cheviron and Coquet, 2009; Spurlock et al., 2013; van den Berg et al., 2008; Gärdenäs et al, 2005; Cornelissen et al., 2021), none of them specifically study a deep subsurface irrigation and drainage system. Currently, in regulatory frameworks such as the EU regulation, subsurface application of marginal water is not explicitly considered. Therefore, it is important to gain knowledge on risks and benefits of the system, which has many peculiarities that are absent from other forms of irrigation, so that the potential for future implementation can be better determined. For subirrigation systems that have previously been studied extensively, such as drip irrigation, irrigated water enters the unsaturated root zone directly, and crops are immediately exposed to contaminants contained within the irrigated water, regardless of persistence or mobility. However, with deep subirrigation and drainage, the irrigated water is instead delivered through capillary rise from the

phreatic zone. Furthermore, deep irrigation and drainage involves two-dimensional flow fields, and frequently fluctuating water and solute flux directions both in the unsaturated and saturated zones, along both the horizontal and vertical axes. Thus, the spreading and distribution of CECs in the subsurface, and its sensitivity to environmental conditions, would differ greatly from that of other irrigation methods.

3.2 Methods

3.2.1 Numerical model

The model of the subsurface irrigation system was created with HYDRUS-2D (Šimůnek et al., 2016). The model domain, and the parameter values used in the base configuration of the model, are identical to that in chapter 2. The base model is calibrated and validated against field observations made at an experimental plot in Haaksbergen, the Netherlands, as described in chapter 2. The base model, and the field data it was validated against, corresponds to the four years spanning 2016 to 2020. The base model characterizes essentially the subirrigation of a sandy-loamy soil under a temperate climate with an annual precipitation excess but temporary precipitation shortage during the crop season, with moderate regional groundwater fluxes. Details (boundary and initial conditions) on the model are available in the original study, and will not be reproduced here.

In addition to the solute mass balances, concentrations, and breakthrough curves, which were considered in chapter 2, in this study the travel direction of the effluent is characterized with a proxy indicator, the ratio of total horizontal to vertical solute discharge (H/V ratio) from the model domain. A scenario with a larger H/V ratio has a plume that travels in a more horizontal direction, and a scenario with a smaller H/V ratio has a plume that travels in a more vertical direction.

3.2.2 Sensitivity analyses

The sensitivity analyses performed are listed in Table 3.1. In the sensitivity analyses where two or three parameters are simultaneously varied, all possible combinations are simulated, except for root zone soils, where certain combinations typical of very coarse sands caused numerical instabilities associated with extremely sharp wetting fronts. Nevertheless, all common soil textures were represented in the parameter analysis, including soils associated with moderately sharp wetting fronts. The analyses on soil and aquifer hydraulic properties, on regional groundwater flow, and on hydrodynamic dispersion, involve broad realistic parameter ranges that encompass a wide range of soil types, geological compositions, and hydrogeological situations.

Table 3.1: List of sensitivity analyses.

Analysis of:	**Parameters varied:**	**Range**
Atmospheric fluxes	Precipitation and evapotranspiration [mm/day]	Daily timeseries from 1990 to 2020.
Lateral inwards flux	Regional head gradient [m]	0 – 0.0035
Irrigation pressure	Irrigation pressure [m]	0.1 – 0.6
Drainage backpressure	Drainage backpressure [m]	0 – 0.5
Irrigation pipe conductivity	Irrigation pipe conductivity [m/day]	(0.005 0.025 0.125 0.625 3.125 15.625)
Right boundary conductivity	K_s [m/day]	(0.005 0.01 0.02 0.04 0.08 0.16 0.32 0.64 1.25 2.5 5 10)
Vertical water discharge	A [m/day]	(-0.00125, -0.0025, -0.005)
	B [1/m]	(-1, -1.25, -2, -5)
Root zone soil hydraulic properties	K_s [m/day]	Between 0.05 and 5
	α [1/m]	Between 0.5 and 4
	n [–]	Between 1 and 2.5
Aquifer hydraulic properties	K_s [m/day]	(1, 5, 25)
	α [1/m]	(0.5, 1, 2, 3)
Solute dispersivity	D_l [m]	(0.02, 0.2, 2)
	D_t [m]	(0.002, 0.02, 0.2, 2)
Biogeochemical parameters (λ_a=0)	K_d [L/kg]	10^(-2, -1, 0, 1, 2, 3)
	λ_s [1/day]	10^(-3.5, -3, -2.5, -2, -1.5, -1)
Biogeochemical parameters (λ_a= λ_s)	K_d [L/kg]	10^(-2, -1, 0, 1, 2, 3)
	λ_s [1/day]	10^(-3.5, -3, -2.5, -2, -1.5, -1)
Random soil heterogeneity	Standard deviation of log10(m)	(0.25, 0.75)
	Horizontal correlation length [m]	2
	Vertical correlation length [m]	0.5

For the analyses on atmospheric fluxes, daily precipitation and reference evapotranspiration data are available from the Dutch meteorological institute (KNMI) for 1990 till 2020. Since such subsurface irrigation systems are capital-intensive, meaning that they are expected to be used for many years after installation, and since the base model achieves periodic steady-state after four years chapter 2, most of the variation in outcomes arising from operating the system is expected to materialize during the four-year start-up phase. Hence, we simulate every possible period of four years (i.e. four crop – drainage cycles) that occurs between 1990 to 2020, for a total of 27 simulations.

The range of adsorption coefficients K_d and solute phase biodegradation rates λ_s used in the analysis on biogeochemical parameters are realistic values representative of a wide variety of CECs (Williams et al., 2009; Kodesova et al 2016; Nham et al., 2015). However, the ability for biodegradation to occur in the adsorbed phase (Poeton et al., 1999; Gamerdinger et al., 1997; Scow and Johnson, 1996; Woo et al., 2001) are uncertain for many substances. Therefore, we perform the analysis of biogeochemical

parameters in two separate sets of simulations: one without and one with adsorbed phase biodegradation, setting the adsorbed phase biodegradation rate to $\lambda_a = \lambda_s$.

In addition to the analyses of irrigation parameters listed in Table 3.1, the 27 simulations with different atmospheric flux time series were repeated for irrigation drains placed at a depth of 1.8m, which is 0.6m lower than in the base model, and separately, also for drains spaced 12m apart, which is double the spacing of the base model.

Roth (1995) found that the spatial structures of soil hydraulic properties (water retention, pressure head, and flow velocity) became highly sensitive to random heterogeneity in the scaling factor m if the standard deviation of $\log10(m)$, σ_m, is larger than 0.7. Therefore, we perform simulations with random soil heterogeneity, based on Miller-Miller similitude (Miller and Miller, 1956). To simulate mild random spatial heterogeneity, we simulate the base model with 30 random fields of the scaling factor m, with $\sigma_m = 0.25$, and horizontal and vertical autocorrelation lengths of 2m and 0.5m respectively. The simulations with mild heterogeneity are contrasted against simulations with strong heterogeneity, with $\sigma_m = 0.75$.

3.3. Results

3.3.1 Environmental fluxes

3.3.1.1 Atmospheric fluxes

Across the 27 simulations with different atmospheric flux timeseries, root solute uptake is strongly positively correlated (Pearson correlation) with the net solute mass injected (total injected minus drained) (Figure 3.2a) and strongly negatively correlated with the excess precipitation (rainfall minus evapotranspiration for each four year period) (Figure 3.2b). This is because the net solute mass injected is strongly negatively correlated with the excess precipitation. Note that the total solute mass injected scales proportionally with the irrigation water use, because the effluent solute concentration is constant. Hence, scenarios with large solute mass influxes also have large irrigation water usage, which translates into a low water use efficiency if target crop yields are to be fixed. Figure 3.2c shows that since the solute mass drained away is a very small fraction of the total solute influx, the total and net solute mass injected are very similar in all simulations. This close relationship between solute mass injected and root solute uptake enables the prediction of relative crop contamination risks from irrigation volume data.

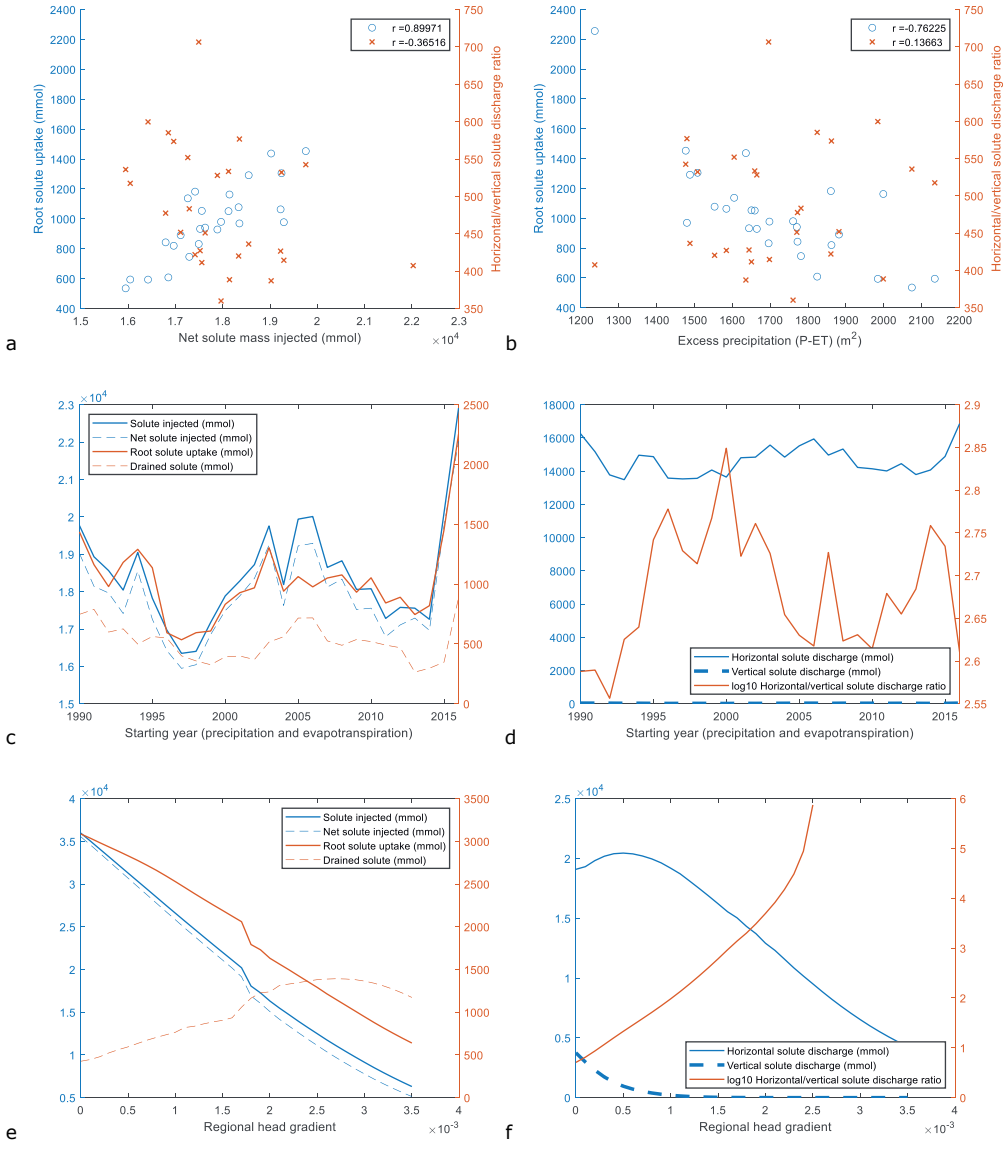

Figure 3.2: Scatter plot of root solute uptake and the H/V ratio against the (a) net solute mass injected and (b) excess precipitation, in the sensitivity analysis of atmospheric fluxes. (c) Root solute uptake and drainage, and (d) saturated zone solute discharge outcomes as a function of the starting year of the atmospheric flux timeseries. (e) Root solute uptake and drainage, and (f) saturated zone solute discharge outcomes as a function of the regional head gradient.

Unlike the root solute uptake, the H/V ratio is weakly correlated with the solute mass injected, and essentially uncorrelated with the excess precipitation implying that wetter conditions increase the horizontal and vertical solute discharge in the saturated zone by similar extents. Figure 3.2d shows that the horizontal and vertical solute discharges in the saturated zone, and the H/V ratio, are relatively

insensitive to the atmospheric flux timeseries. The horizontal solute discharge remained within 5% of the mean of around 15000mmol in all 27 four-year simulations, while little vertical solute discharge occurred in all cases. We note that the peak in solute injected and root solute uptake in Figure 2c in the simulation beginning in 2016 reflects the effects of the extreme dry years 2018-2020.

A correlation matrix of the outcomes concerning water balances and solute fate, concerning the 27 starting years, is presented in Figure 3.3. The drained solute mass is positively correlated with the irrigated solute mass: more solute is available to be drained away if more solute is irrigated. Indeed, the drained solute mass increases more than linearly in proportion to the increase in irrigated solute mass (see Tang and van der Zee, 2021). It is noteworthy that in contrast, the drained water volume is uncorrelated with the irrigated water volume, because the irrigated water volume accounts for a small proportion of the overall water balance of the system.

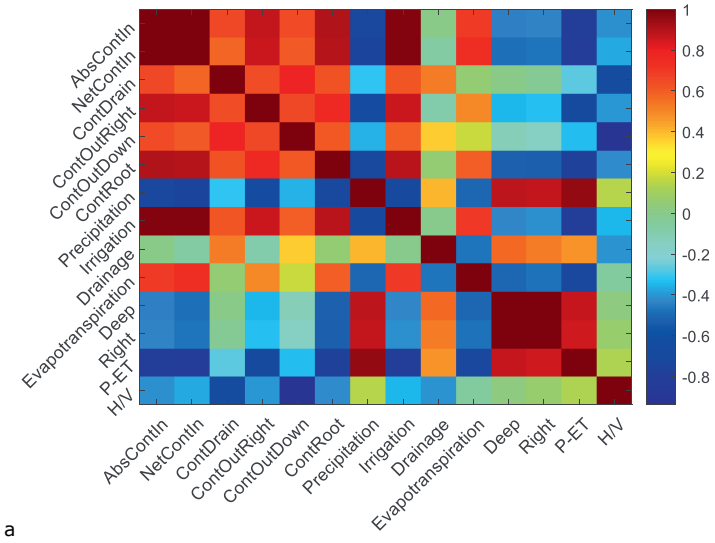

a

Figure 3.3: Correlation matrix of simulation outcomes for the sensitivity analyses over 66 different four year periods. AbsContIn = absolute injected solute mass; NetContIn = net injected solute mass (injected – drained), ContDrain = drained solute mass, ContOutRight = horizontal solute discharge, ContOutDown = vertical solute discharge, ContRoot = total root solute uptake, Precipitation = total rainfall volume, Irrigation = total irrigation volume, Drainage = total drainage volume, Evapotranspiration = total evapotranspiration volume, Deep = vertical water discharge, Right = horizontal water discharge, P-ET = excess precipitation, H/V = H/V ratio (ContOutRight/ContOutDown).

The correlation matrix also shows that the root solute uptake and lateral solute discharge is strongly positively correlated to the irrigation volume and negatively correlated to the excess precipitation, while the solute mass drained is positively correlated with the volume of water drained. Hence, these important solute fate outcomes are strongly correlated to easily measurable quantities. However, the vertical solute discharge and H/V ratio are not strongly correlated to any easily observable or calculable quantities. The H/V ratio has a strong correlation with only the vertical solute discharge mass, but it is neither easily observable nor calculable in the field. Since the denominator of the H/V ratio varies across a larger relative range (19 to 42 mmol) than the numerator (13500 to 17000 mmol), it is the vertical

solute discharge that ultimately controls the H/V ratio. The H/V ratio and vertical solute discharge are moderately correlated with the solute mass drained, but not with the amount of water drained. Hence, it may be possible to estimate the H/V ratio by monitoring the solute mass drained through a readily monitorable tracer, such as electrical conductivity (EC) or temperature (Cox et al., 2007). Nevertheless, it is the lateral solute discharge that comprises the bulk of the absolute solute mass balance. More discussion on the fate of CECs that are horizontally discharged in the phreatic aquifer is analyzed to greater detail in chapter 2.

Since this parameter analysis concerns the precipitation and evapotranspiration timeseries, and since the H/V ratio and vertical solute discharge have little correlation with the total precipitation, evapotranspiration, or excess precipitation volumes, it follows that these outcomes must be primarily affected by the actual sequences, magnitudes, and variances of individual rainfall events within those timeseries. This is also a logical consequence of the fact that the H/V ratio is determined primarily by the vertical solute discharge, and that the vertical discharge of water and solutes is a nonlinear function of the groundwater level.

The strong dependence of irrigation fluxes and root solute uptake, and weak dependence of saturated zone solute discharge, on atmospheric fluxes, can also be seen from the simulated breakthrough curves. The variance between the breakthrough curves is large in the root zone (Figure 3.4a,3.5a), but small in the saturated zone (Figure 3.4b,3.5b). This is because pressure heads, water fluxes and moisture contents are most sensitive to varying weather conditions at the topsoil, and become less sensitive with depth (Salvucci and Entekhabi, 1994). The breakthrough curve variance is also, in general, larger the closer the observation point is to an irrigation drain, because the fluxes there are more significantly affected by the frequently alternating flux velocities and directions at the drain.

In addition to varying the rainfall timeseries as previously discussed, we also simulated the base model with the extreme situation of zero precipitation over the entire simulated period. The solute mass balance of the base model corresponds to the results for starting year 2016 in Figure 3.2c and Figure 3.2d. With zero precipitation, the water and solute mass injected was 50% higher and the root solute uptake was seven times that of the base model, but the horizontal solute discharge was a quarter less and the vertical solute discharge was unchanged. Less saturated zone solute discharge occurs than in the base model, because a much larger portion of all irrigated effluent moves up towards the root zone. An outcome unique to this scenario is that large quantities of solutes accumulate in the topsoil over time because large amounts are transported to the root zone but not volatilized when soil water evaporates. After four years, the tracer concentration in topsoil water reached 7.5 times the irrigated concentration. Therefore, care should be taken if the subirrigation system is used in regions or periods with long-term precipitation shortages.

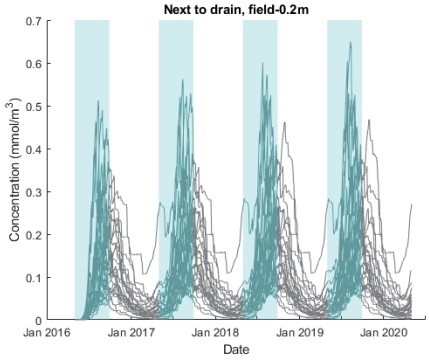
Next to drain, field-0.2m
Concentration (mmol/m3)
Jan 2016
Jan 2017
Jan 2018
Jan 2019
Jan 2020
Date

a

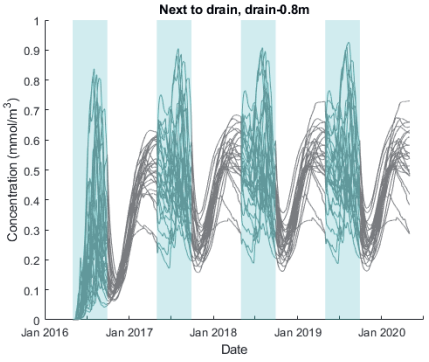
Next to drain, drain-0.8m
Concentration (mmol/m3)
Jan 2016
Jan 2017
Jan 2018
Jan 2019
Jan 2020
Date

b

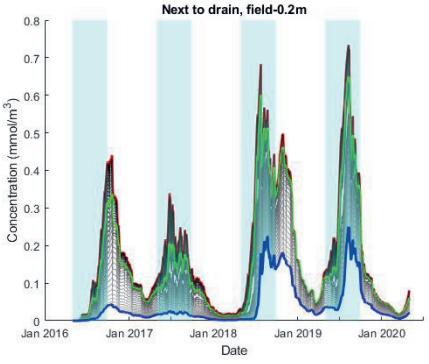
Next to drain, field-0.2m
Concentration (mmol/m3)
Jan 2016
Jan 2017
Jan 2018
Jan 2019
Jan 2020
Date

c

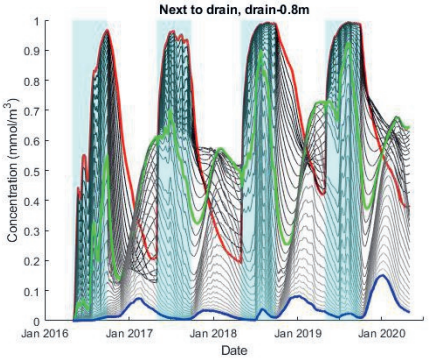
Next to drain, drain-0.8m
Concentration (mmol/m3)
Jan 2016
Jan 2017
Jan 2018
Jan 2019
Jan 2020
Date

d

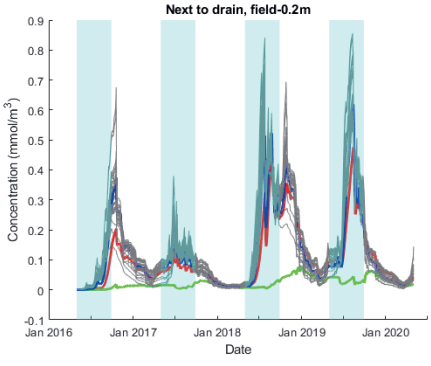
Next to drain, field-0.2m
Concentration (mmol/m3)
Jan 2016
Jan 2017
Jan 2018
Jan 2019
Jan 2020
Date

e

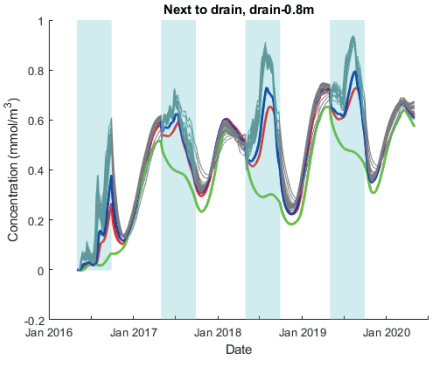
Next to drain, drain-0.8m
Concentration (mmol/m3)
Jan 2016
Jan 2017
Jan 2018
Jan 2019
Jan 2020
Date

f.

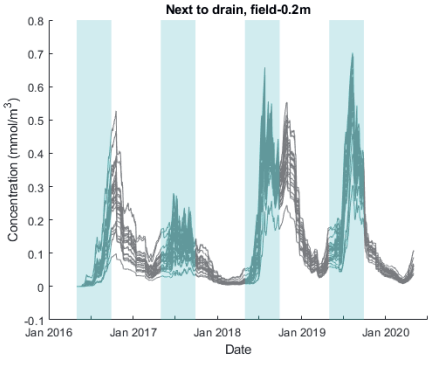
Next to drain, field-0.2m
Concentration (mmol/m3)
Jan 2016
Jan 2017
Jan 2018
Jan 2019
Jan 2020
Date

g

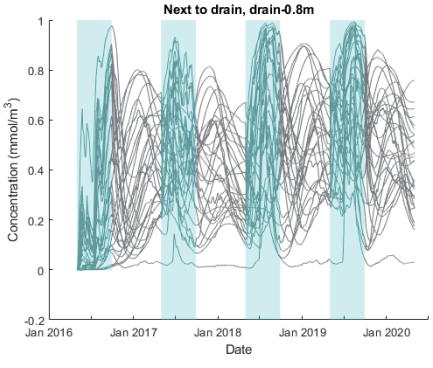
Next to drain, drain-0.8m
Concentration (mmol/m3)
Jan 2016
Jan 2017
Jan 2018
Jan 2019
Jan 2020
Date

h.

Figure 3.4: Breakthrough curves at observation points directly above and below drains, in the sensitivity analysis of (a,b) environmental fluxes, (c,d) regional head gradient (The red curve is for zero regional head gradient, the green curve is for the base model with regional head gradient of 0.0014, and the blue curve is for the highest regional head gradient of 0.0035.), (e,f) root zone soil parameters. (The colored lines refer to the outlier soil types.), and (g,h) mild spatial heterogeneity. Each line represents an individual simulation.

3.3.1.2 Regional head gradient

Increasing the regional head gradient decreases the volume of water and solute mass injected (Figure 3.2e). It also increases the mass of solutes recovered, except at very high regional head gradient where injected solutes are immediately advected away from the drains. Although it might be expected that a larger regional head gradient predominantly leads to a smaller recovered solute fraction due to solutes being displaced horizontally away from the drains, the larger regional head gradient also raises the water table higher, thereby pushing effluent upwards. Therefore, the effluent may be more easily intercepted by the drains as it subsequently moves downwards due to gravity and excess precipitation, thereby increasing the recovery fraction. Thus, the solute fraction taken up by crop roots and drained away is higher with high regional head gradient, but the absolute mass of root solute uptake is higher with low regional head gradient, because the total irrigation volume is much larger with a low regional head gradient.

The lateral and horizontal solute discharge both decrease as the regional head gradient increase, because less effluent is irrigated. As the regional head gradient increases, the vertical solute discharge decreases faster than the lateral solute discharge, causing the H/V ratio to greatly increase (Figure 3.2f). Comparing Figure 3.2c with Figure 3.2e, and Figure 3.2d with Figure 3.2f, it is evident that root solute uptake is similarly sensitive to the simulated ranges of atmospheric fluxes and regional head gradient, but solute fate in the saturated zone is much more sensitive to the regional head gradient than to atmospheric fluxes.

Unlike for the atmospheric fluxes, the breakthrough curves are highly sensitive to the regional head gradient at all observation points, regardless of depth or distance from the drains (Figure 3.4c,3.4d; Figure 3.5c,3.5d). It is interesting to note that in general, the breakthrough curves under zero regional head gradient (red lines) and under the highest regional head gradient (blue lines) do not bound the breakthrough curves for the intermediate head gradients. This is because regional flow occurs primarily along only one dimension, whereas the breakthrough curves depend on the transient two-dimensional flow originating from the interactions between regional fluxes, atmospheric fluxes, and irrigation and drainage.

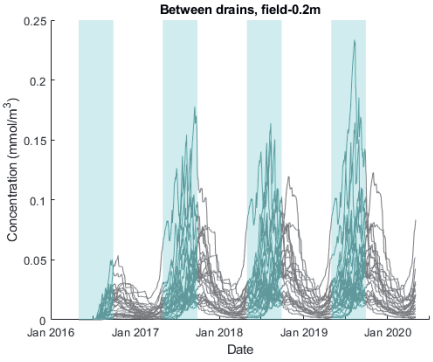
Between drains, field-0.2m
Concentration (mmol/m3)
Jan 2016
Jan 2017
Jan 2018
Jan 2019
Jan 2020
Date

a

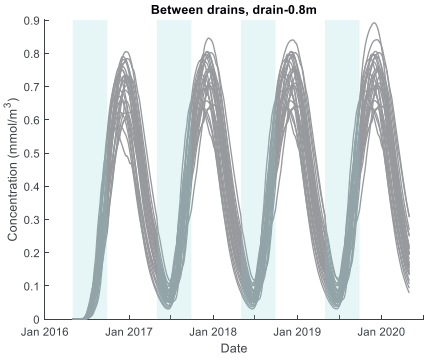
Between drains, drain-0.8m
Concentration (mmol/m3)
Jan 2016
Jan 2017
Jan 2018
Jan 2019
Jan 2020
Date

b

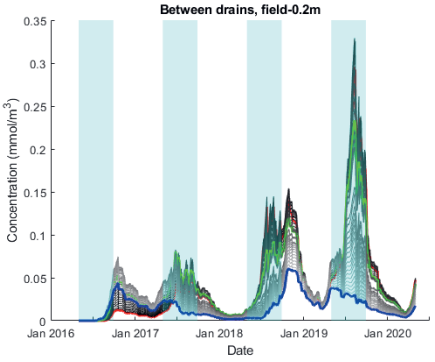
Between drains, field-0.2m
Concentration (mmol/m3)
Jan 2016
Jan 2017
Jan 2018
Jan 2019
Jan 2020
Date

c

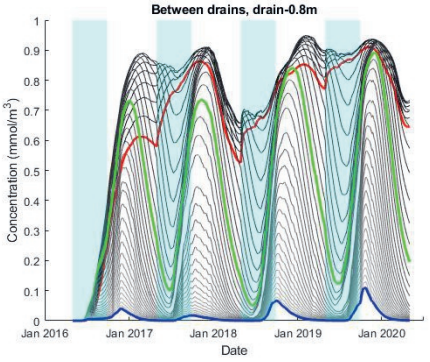
Between drains, drain-0.8m
Concentration (mmol/m3)
Jan 2016
Jan 2017
Jan 2018
Jan 2019
Jan 2020
Date

d

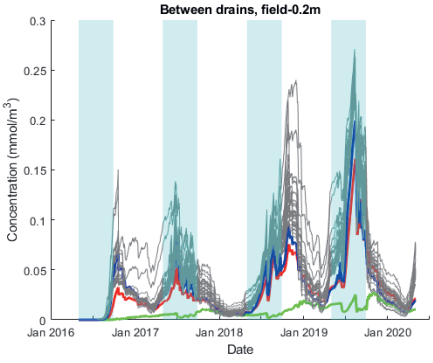
Between drains, field-0.2m
Concentration (mmol/m3)
Jan 2016
Jan 2017
Jan 2018
Jan 2019
Jan 2020
Date

e

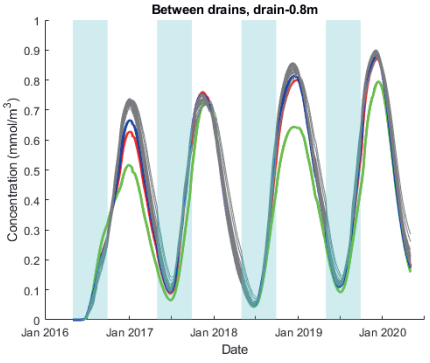
Between drains, drain-0.8m
Concentration (mmol/m3)
Jan 2016
Jan 2017
Jan 2018
Jan 2019
Jan 2020
Date

f

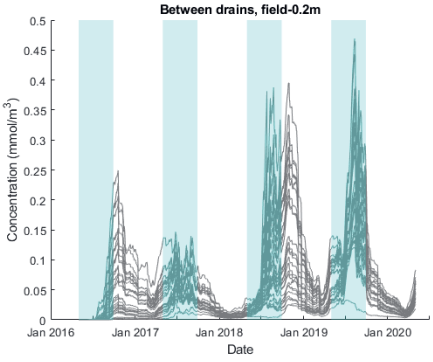
Between drains, field-0.2m
Concentration (mmol/m3)
Jan 2016
Jan 2017
Jan 2018
Jan 2019
Jan 2020
Date

g

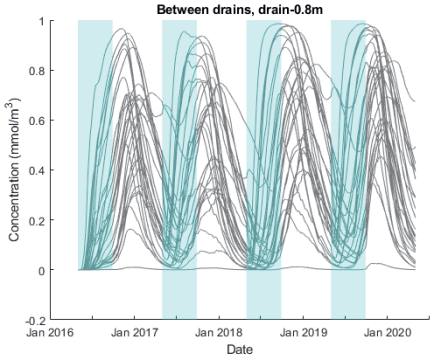
Between drains, drain-0.8m
Concentration (mmol/m3)
Jan 2016
Jan 2017
Jan 2018
Jan 2019
Jan 2020
Date

h

Figure 3.5: Breakthrough curves at observation points midway between drains, in the sensitivity analysis of (a,b) environmental fluxes, (c,d) regional head gradient, (e,f) root zone soil parameters, and (g,h) mild spatial heterogeneity. See Figure 4 for explanation of colors.

f

3.3.2 Irrigation and drainage parameters

3.3.2.1 Irrigation pressure

As the irrigation pressure (i.e. the head difference between the SSI tank and the soil) increases, the injected water, injected solute mass, drained solute mass, and root solute uptake increases (Figure 3.6a). As the irrigation pressure increases, the horizontal and vertical saturated zone solute discharge increase and the H/V ratio decreases (Figure 3.6b). Thus, as more water is irrigated, the fraction of water that sinks downwards increases, compared to water that is advected laterally.

3.3.2.2 Drainage backpressure

Imposing a higher drainage backpressure (by lowering the drainage crest in the SSI system) greatly reduces the amount of solutes drained, thereby greatly increasing the net injected solutes. While the drained solute mass decreases from 3600mmol to 400mmol when the drainage backpressure increases from 0m to 0.5m, the root solute uptake increases by merely 250mmol or 10% (Figure 3.6c). The drainage backpressure hardly affects root solute uptake because most of the solutes that come within the capture zone of the drains do so during the drainage season, on their way downwards from the soil above drain level. Hence, the decrease in solutes drained due to higher drainage backpressures is mostly compensated by the increase in saturated zone solute discharge (Figure 3.6d). The H/V ratio appears to be independent of the drainage backpressure (note scale), because the drainage volume is in all scenarios an order of magnitude smaller than the environmental flow or irrigation volumes.

3.3.2.3 Drain conductivity

At low drain conductivities, an increase in drain conductivity increases root solute uptake because more effluent is injected. However, at high drain conductivities, an increase in drain conductivity does not cause more effluent to be injected because lower drain conductivities are already sufficient to maintain the target groundwater level (Figure 3.6e). At higher drain conductivities, further increasing drain conductivity decreases root solute uptake. When the excess precipitation is large, highly conductive drains quickly remove large volumes of effluent from the root zone, thus effluent residence times in the root zone become shorter. As drain conductivity increases, the saturated zone horizontal and vertical solute discharges also increase (Figure 3.6f).

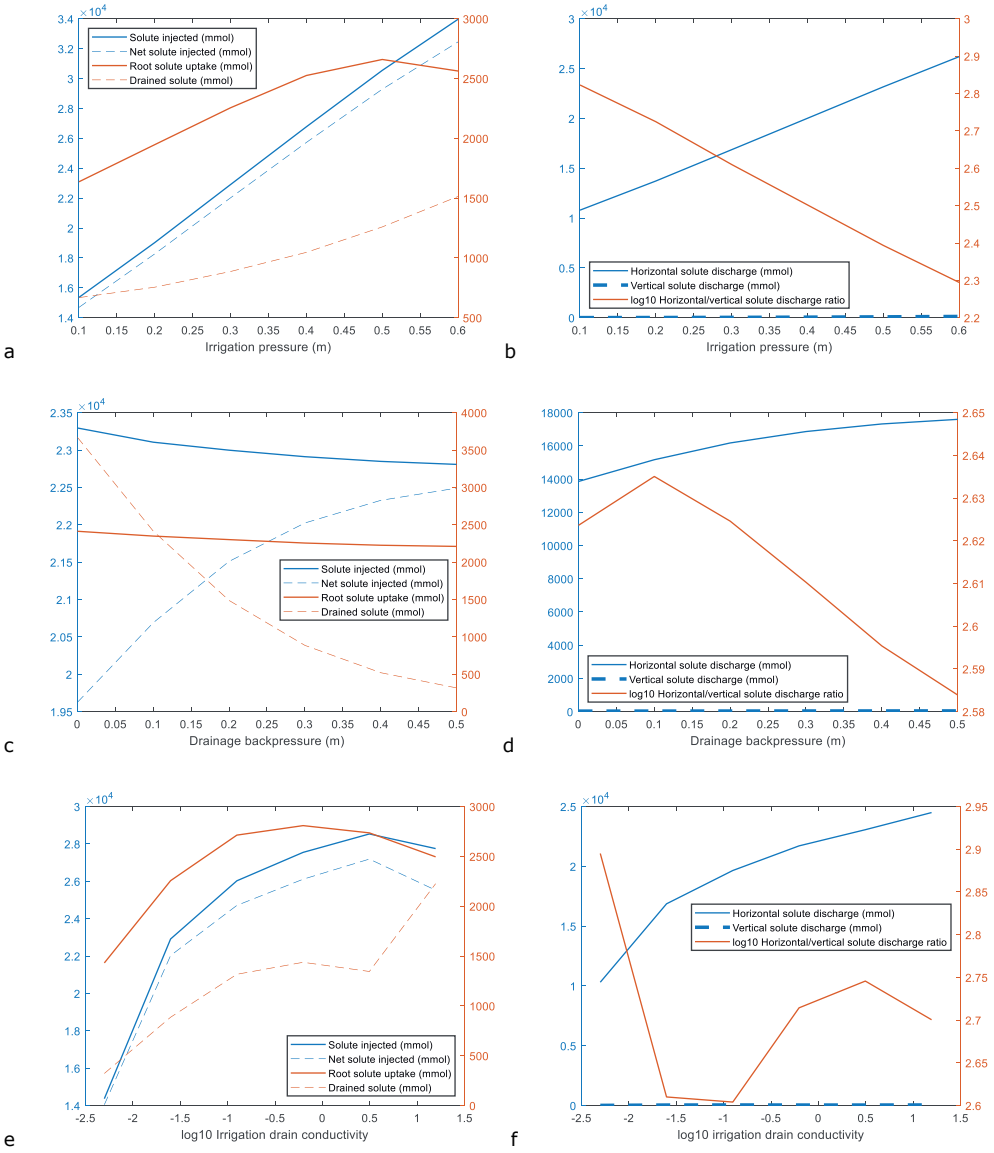

Figure 3.6: Root solute uptake and drainage as a function of (a) irrigation pressure, (c) drainage backpressure, and (e) irrigation drain conductivity. Saturated zone solute discharge outcomes as a function of (b) irrigation pressure, (d) drainage backpressure, and (f) irrigation drain conductivity.

3.3.2.4 Drain depth

With drains located deeper than in the base model, the maintained groundwater level, and the amount of water and solute irrigated and drained remain similar to the base model. Root solute uptake is approximately halved, but as a tradeoff, the amount of vertical solute discharge in the saturated zone increased by about 10%. The optimal drain depth is therefore determined by the relative subjective hazard posed by root solute uptake and solute discharge to deeper aquifers. Note that we modelled biodegradation as a spatially homogeneous first-order process here. In practice, the biodegradation rate

may sometimes be smaller with depth because microbial populations tend to be concentrated near the topsoil (Hickman and Novak, 1989). Thus, to maximize the biodegradation of CECs in effluent with high organic matter content (e.g. domestic wastewater), it might be advantageous to place the irrigation drains shallower in the soil. On the contrary, effluent with primarily non-biodegradable contaminants such as metal ions (e.g. industrial wastewater) might be better irrigated from deeper depths, to minimize crop contamination and salinity stress.

3.3.2.5 Drain spacing

With doubly wide spacing between drains, the amount of water and solute irrigated per unit area of the agricultural plot is about 25% smaller than in the base model, because the irrigation flux at each drain is limited by the drain conductivity. This causes the maintained groundwater level to be lower than in the base model. Hence, when reducing the number of drains, one must be careful to ensure that the reduced irrigation capacity can provide sufficient moisture for the crops. The optimal drain spacing thus depends on the drain conductivity, and also the soil conductivity, which determines the extent of capillary rise. Therefore, the drain spacing must be calibrated for each agricultural plot. The amount of root solute uptake per unit field area decreased by 30% to 50%, depending on the starting year of the atmospheric flux timeseries. Similarly to the base model, most root solute uptake occurs immediately above the irrigation drains, whereas the root zone midway between drains has low effluent concentrations throughout the crop season. Accordingly, since there are fewer drains per unit length of the agricultural field than in the base model, the decrease in root solute uptake is comparatively larger than the decrease in effluent influx.

In the case of the base model with 6m spacing between drains, the effluent plume from the upstream irrigation drain is in-phase with effluent plume originating from the downstream drain during the following crop season. Hence, the old plume from the upstream drain merges with the new plume from the downstream drain, and the effluent is more concentrated. Conversely, with 12m between drains, the effluent plumes of the upstream and downstream drains are out of phase, and do not merge, causing the effluent in the subsurface to be more diluted. Whether effluent plumes from each drain are in-phase or out of phase with the plumes from adjacent drains depends on the (non-integer) number of drain spacings that the effluent plume horizontally traverses every year. Therefore, effluent solute concentrations in the groundwater, and the spatial heterogeneity of these concentrations, depend on the groundwater flow rate, distance between drains, and mobility of the solutes.

3.3.3 Boundary parameters

3.3.3.1 Lateral discharge resistance

Increasing the conductivity of the Cauchy boundary condition at the right boundary greatly increases the amount of solutes injected, root solute uptake (Figure 3.7a), and the amount of horizontal and vertical solute discharge (Figure 3.7b). This is because higher irrigation fluxes are necessary to maintain the groundwater level at the target position, as the high boundary conductivity causes irrigated water to be quickly removed from the domain. When the right boundary conductivity is large, further increases do not increase the amount of solute injected and discharged any further, because then solute injection is limited by the irrigation drain’s conductivity.

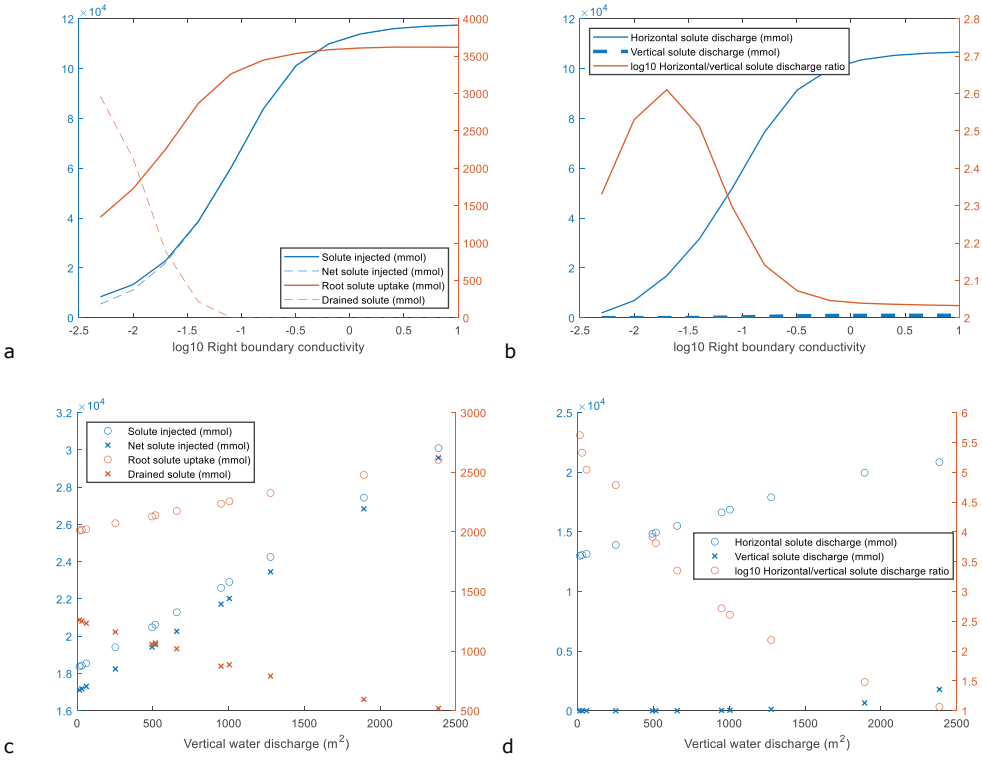

Figure 3.7: (a) Root solute uptake and drainage, and (b) saturated zone solute discharge outcomes as a function of the right boundary conductivity. (c) Root solute uptake and drainage, and (d) saturated zone solute discharge outcomes as a function of the vertical water discharge (due to variations in the deep drainage boundary parameters).

3.3.3.2 Vertical discharge resistance

As the two deep drainage boundary parameters are varied, the amount of vertical water discharge changes. Figure 3.7c and Figure 3.7d are scatterplots of simulation outcomes with respect to the total vertical water discharge of the simulation. The most direct effect of increasing the vertical water discharge is that the vertical solute discharge increases, while the H/V ratio decreases. Furthermore, the solute mass injected and root solute uptake increases because more irrigation is required to maintain the groundwater level at its target position. However, the amount of solutes drained decreases, because the natural equilibrium groundwater level decreases, resulting in less water drained, and also causing solutes to sink downwards more quickly.

3.3.4 Hydrogeological parameters

3.3.4.1 Root zone soil hydraulic properties

Root zone soil hydraulic parameters were found to weakly affect outcomes. A distinct trend in increasing vertical solute discharge is observed as the soil texture moves from clayey to loamy to sandy. This trend is associated with increasing horizontal water discharge, decreasing drained solute mass, and slightly increasing root solute uptake (Figure 3.8a; Figure 3.8b). This is because sandy soils are less water

retentive, thereby allowing quicker downwards discharge of water from the root zone, consequently requiring more irrigation.

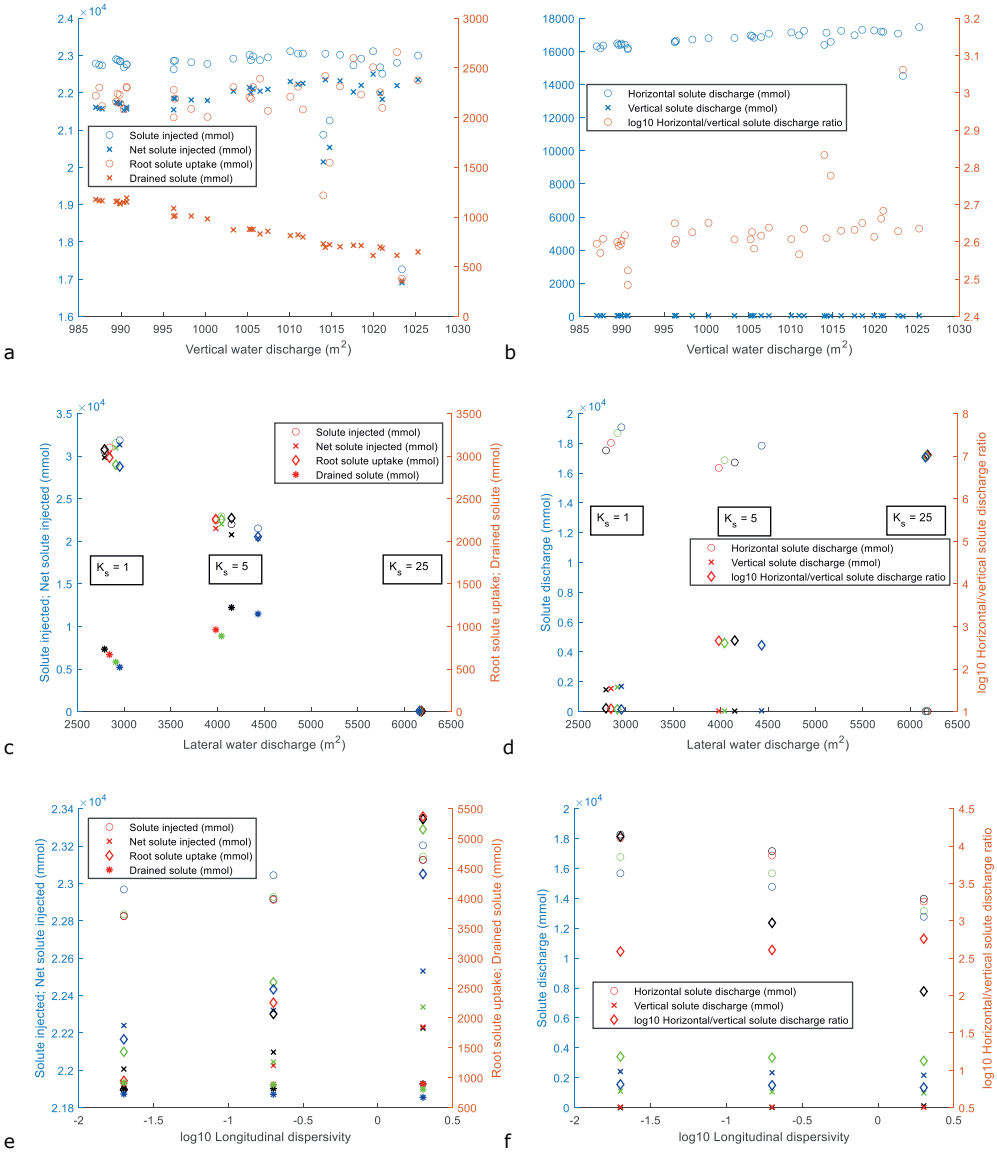

Figure 3.8: (a) Root solute uptake and drainage, and (b) saturated zone solute discharge outcomes as a function of the vertical water discharge (due to variations in the root zone soil hydraulic parameters). (c) Root solute uptake and drainage, and (d) saturated zone solute discharge outcomes as a function of the horizontal water discharge (due to variations in the aquifer hydraulic properties) [Colors black, red, green, blue correspond to α = 0.5, 1, 2, 3 respectively]. (e) Root solute uptake and drainage, and (f) saturated zone solute discharge outcomes as a function of the mechanical dispersivity [Colors black, red, green, blue correspond to D_t = 0.002, 0.02, 0.2, 2 respectively].

Three outlier soil types are visible in the data: these are soils with large α, large n, and low K_s. The van Genuchten parameter α is an increasing function of the modal pore size, while n is related to the pore size distribution variance (Ghezzehei et al., 2007). These outlier soils have hydraulic properties that are characteristic of hydrophobic coarse sandy soils (e.g. Lamparter et al., 2006). Very little capillary rise occurs in these soils, which reduces actual evapotranspiration (i.e. crop yield), and consequently also reduces crop solute uptake. The large reduction of actual evapotranspiration decreases the total volume of water and solute mass injected and taken up by crops. As actual evapotranspiration is reduced, the average downwards vertical velocity increasing, thereby decreasing the vertical solute discharge and increasing the H/V ratio.

Aside from the outlier root zone soils mentioned above, the breakthrough curves under all simulations are almost identical (Figure 3.4e,3.4f; Figure 3.5e,3.5f), even in the root zone. Therefore, the effect of root zone soil properties on solute fate appears to be a discrete, threshold-like function of soil texture. Only when the aforementioned low conductivity coarse soils are present in the root zone, do the breakthrough curves throughout the entire domain deviate significantly from the other simulations, including deep in the saturated zone.

3.3.4.2 Aquifer hydraulic properties

As the hydraulic conductivity of the aquifer increases, the natural groundwater level rises because the incoming regional flow flux from the imposed head gradient boundary increases. Therefore, as the aquifer hydraulic conductivity increases, the amount of solute injected and root solute uptake decreases significantly (Figure 3.8c). The vertical solute discharge decreases while the H/V ratio increases as the conductivity increases (Figure 3.8d), because more horizontal groundwater flow occurs. The downwards flux however is not significantly affected due to the deep drainage (i.e. head-dependent imposed flux) bottom boundary. At a conductivity of 25 m/day, the natural groundwater level is high enough that no irrigation flux occurs for most of the simulated period, resulting in negligible solute injection.

Varying the aquifer hydraulic parameter α has minimal effect on the model outcomes. It affects the water retention curve and maximum capillary rise height of the groundwater, but not the saturated conductivity. Therefore it has negligible effects on the fluxes at the left and right boundaries: only the part of the aquifer above the water table and below the root zone is affected by α. Hence, the saturated conductivity is by far the most important hydraulic property for parts of the subsurface beneath the target water table.

3.3.4.3 Mechanical dispersivity

Capillary fluxes bring irrigated effluent upwards to the root zone, alternating with periods where precipitation excesses push root zone effluent downwards in a largely one-dimensional manner. Therefore, an increase in longitudinal dispersivity significantly increases solute dispersion to the root zone and hence root solute uptake (Figure 3.8e). In contrast, the effect of transverse dispersivity is a small, higher-order effect that does not have a significant impact on solute fate.

An increase in longitudinal dispersivity decreases the horizontal solute discharge but appears to have little effect on the vertical solute discharge (Figure 3.8f). Note that the decrease in horizontal solute discharge resulting from an increase in longitudinal dispersivity is of a similar magnitude as the resulting increase in crop solute uptake. Since the advection velocity is relatively large in the saturated zone

compared to the unsaturated zone, the magnitudes of the mechanical dispersivities have relatively little effect on where solutes in the saturated zone are discharged to. This means that the decrease in horizontal solute discharge is just a mass balancing result of the increase in crop solute uptake.

Generally, increasing the transverse dispersivity decreases the horizontal solute discharge but increases the vertical solute discharge, thereby decreasing the H/V ratio. This is because the primary direction of advection in the saturated zone is horizontal. The solute mass injected increases very slightly as either of the dispersivities increase, because of the concentration-flux solute boundary condition at the irrigation drains that allow solutes to not only be advected, but also be dispersed from the drains into the soil.

3.3.5 Spatial heterogeneity

Summary statistics boxplots of the simulations with mild random heterogeneity (Figure 3.9a) show that the medians and means of the outcomes are very close to the homogeneous base model. The simulated heterogeneity is responsible for less than a half-order of magnitude variation in outcomes. At most one outlier occurred for each of the outcomes. Hence, in an heterogeneous agricultural plot that is large enough to be ergodic relative to the autocorrelation lengths, crop solute uptake and saturated zone discharge should on average be similar to that of a homogeneous soil, except that breakthrough curves and contaminated crops will be more unevenly spatially distributed in the heterogeneous soil. However, spatially uneven distribution of crop solute uptake is already a feature of the subsurface irrigation system even in homogeneous soils, as most crop solute uptake occurs directly above the individual drains, whereas crops located midway between drains take up little solute (chapter 2).

Strong heterogeneity, on the other hand, led to significantly worse outcomes compared to the base model (Figure 3.9b). On average, about twice as much effluent had to be irrigated into the system to maintain the target groundwater levels. More saturated zone solute discharge occurred, while less solute was drained away. However, the total root solute uptake, and solute discharge direction (i.e. H/V ratio), were similar as in homogeneous soils. Thus, most of the additional irrigated effluent caused by soil heterogeneity is discharged into the saturated zone through high conductivity channels. Consequently, effluent in the saturated zone has a farther reach and larger mass, which may render subirrigation unfeasible in strongly heterogeneous soils. It is also noteworthy that of all the key simulation outcomes, root solute uptake had the lowest variance across realizations, for both mild and strong heterogeneity. Therefore, even though spatial heterogeneity was present both in the root zone and beneath the root zone, most of its effects were concentrated in the saturated zone.

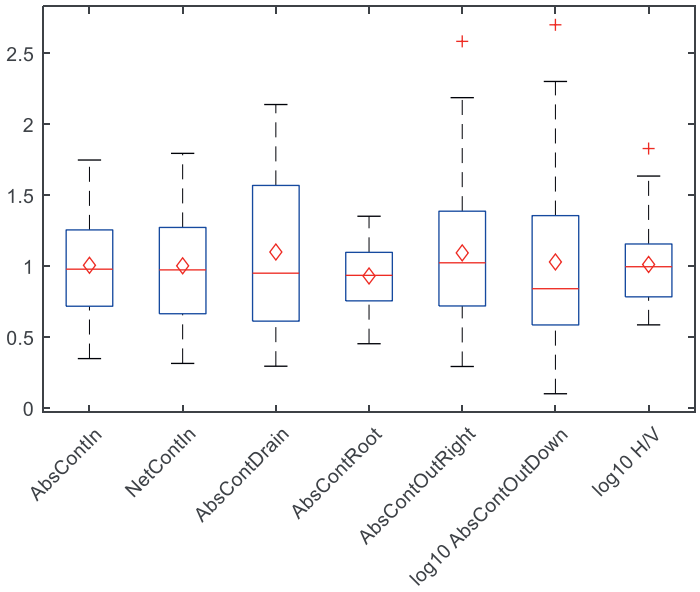

a

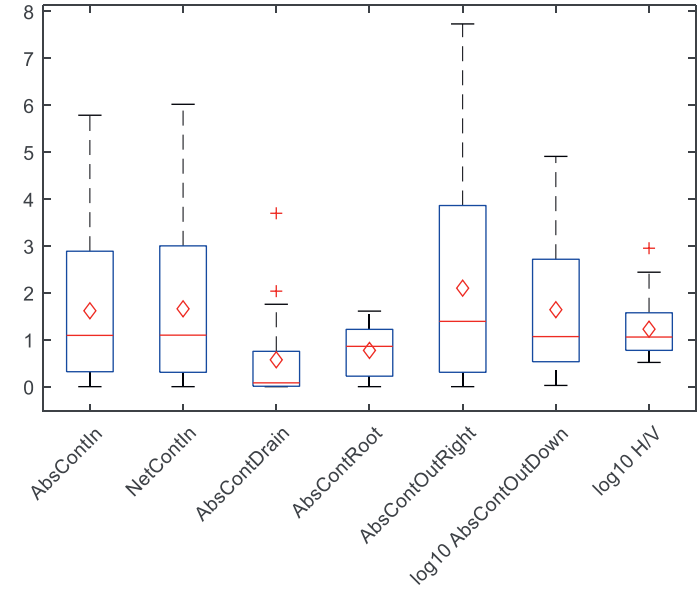

b

Figure 3.9: Summary statistics boxplots of the 30 simulations with (a) mild and (b) strong spatial heterogeneity, normalized against the values of the homogeneous base model. The boxes represent the interquartile range, whiskers represent 1.5x interquartile range, the plusses are outliers, the red lines are the medians, and the diamonds are means. See Figure 3 for an explanation of variable names.

For both mild and strong random heterogeneity, breakthrough concentrations and times varied significantly across random realizations, especially at observation points midway between drains (Figure 3.5g, Figure 3.5h). At observation points in the saturated zone (Figure 3.4h, Figure 3.5h), the breakthrough curves varied both in shape and amplitude. However, breakthrough curves in the root zone varied mostly in amplitude, and not in shape (Figure 3.4g, Figure 3.5g). This suggests that capillary rise is less sensitive to heterogeneity than advective flow in the saturated zone, which is congruent with root solute uptake having the lowest variance across realizations.

3.3.6 Biogeochemical parameters

Solute fate is highly sensitive to the biogeochemical parameters, regardless of whether the solute is able to biodegrade in the adsorbed phase. The fraction of injected solute drained by the irrigation drains is a non-monotonic function of the adsorption coefficient, with a maximum around K_d=10 (Figure 3.10a, 3.10b). When K_d increases from 0.01 to 10, the drained fraction increases because the effluent plume remains closer to the irrigation drains, such that solute-rich water is preferentially drained whenever drainage occurs. When K_d increases beyond 10, the drained water contains very little contaminant, as most of the contaminant although situated near the drains are in the adsorbed phase, thereby decreasing the drained solute fraction.

Root solute uptake is a monotonically decreasing function of both K_d and λ_s (Figure 3.10c, 3.10d), which is a straightforward consequence of the fact that less mobility and increased biodegradability decreases the solute mass reaching the root zone. The H/V ratio is also a monotonically decreasing function of both K_d and λ_s (Figure 3.10e, 3.10f). The H/V ratio increases as λ_s increases because the contaminant travel time from the drains to the right boundary is shorter than the travel time to the bottom boundary, hence solute particles moving downwards have more time to biodegrade.

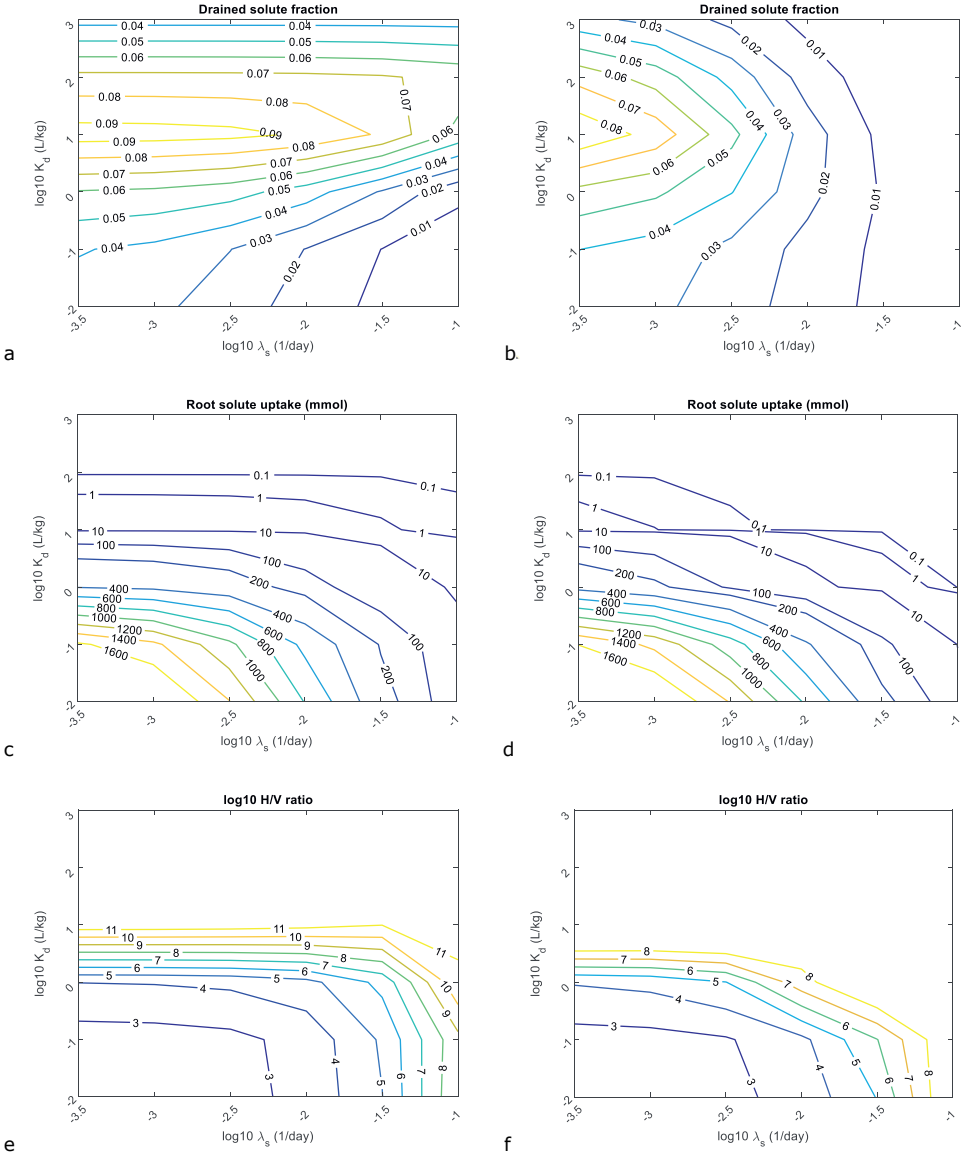

Figure 3.10: Contour plots of the (a) drained solute fraction, (c) root solute uptake, and (e) H/V ratio as a function of the biodegradation rate and adsorption coefficient, for scenarios with biodegradation only in the solute phase. The same is illustrated in (b,d,f) for scenarios with biodegradation in the solute and adsorbed phases.

The H/V ratio increases as K_d increases partly because solute retardation magnifies the aforementioned travel time difference between rightwards and downwards travelling solute particles, therefore giving solutes moving downwards more time to biodegrade. However, the same pattern is observed in test simulations with no biodegradation, which warrants an additional explanation. Increased solute residence times due to adsorption causes a higher order effect that further increases solute residence times. During the drainage season, water and solutes in the subsurface generally travel downwards due to low

potential evapotranspiration rates. If injected solute has not exited the domain by the start of the following year's crop season, then the water and solutes within the subsurface begin to move upwards again, due to large precipitation shortages that result in net upwards flow. This causes the position of the solute plume to oscillate up and down, thereby significantly reducing downwards solute discharge. Conversely, the solute plume's direction of travel along the horizontal axis is always rightwards along with regional flow. In summary, retardation causes an increase in solute residence times, during which its average downwards velocity decreases more significantly than its average rightwards velocity, thereby increasing the H/V ratio.

The ability of solutes to biodegrade in the adsorbed phase leads to more biodegradation, less solute drainage, less root solute uptake, and a higher H/V ratio. The increase in total biodegradation due to adsorbed phase biodegradation is largest for large K_d, because more contaminant exists in the adsorbed phase, and small λ_s, because the biodegraded mass as a function of time spent biodegrading has diminishing returns. Root solute uptake and the drained solute mass are reduced by biodegradation in the adsorbed phase, especially for large K_d and large λ_s, relative to the scenario with no adsorbed phase biodegradation. The H/V ratio is increased by adsorbed phase biodegradation, especially for large K_d and large λ_s, because the additional biodegradation amplifies the reduction in vertical solute discharge discussed in the previous two paragraphs.

As also noted in chapter 2, biodegradation decreases breakthrough concentrations, while adsorption causes breakthrough curves to be smoother and vary less rapidly over time. This is because solute in the adsorbed phase acts as a buffer for solute in the solution phase, hence any change in solute phase concentrations due to unsteady flow caused by sudden fluctuations in atmospheric fluxes are dampened by desorbing solutes. Therefore, under erratic weather conditions, immobile solutes may better reflect the true long-term travel direction of the effluent plume and act as a better 'tracer' than a true tracer, assuming that the adsorption parameters are known. This is especially relevant for subsurface irrigation and drainage systems, where the predominant water flux direction switches often, with varying frequencies of oscillation, across multiple boundary conditions.

3.4 Discussion

3.4.1 Solute mass balances

Across the simulated range of adsorption coefficients and biodegradation rates, both have similarly large effects on solute mass balances in the simulations, spanning multiple orders of magnitude. However, if considering the ultimate fate of solutes in the overall environment, then the biodegradation rate is arguably a more important factor than the adsorption coefficient. This is because biodegradation transforms contaminants into potentially harmless compounds, whereas adsorption merely delays transport from one point to another. Adsorption, however, plays an important role in reducing the overall extent of CEC dispersion into the environment, if biodegradation can occur in the adsorbed phase.

The analyses, which were conducted with realistic ranges of model parameters, may be summarized to classify the parameters that important outcomes are more sensitive to. Typically, solute fate was sensitive to model parameters in the following order: 1) biogeochemical parameters, 2) physical parameters (hydrogeological parameters and environmental fluxes) and mechanical dispersivity, and 3) irrigation parameters, as evident in figure 3.11. Therefore, biogeochemical parameters are the primary determinant of solute fate. Uncertainties arising in the field also follow this hierarchy: the biogeochemical parameters of individual solutes may be uncertain by orders of magnitude (Nham et al., 2015), while those of aquifer properties and environmental fluxes tend to be known somewhat more accurately.

Uncertainties in irrigation parameters are the smallest, as they are directly controlled variables. Hence, the parameters that solute fate are more sensitive to, are also parameters that are more uncertain in the field. This means that understanding the effluent to be used in irrigation is of utmost importance.

The physical parameters that have the greatest effects on solute mass balances notably belong to the hydrogeological parameters: the regional head gradient, aquifer conductivity, and right boundary conductivity (Figure 3.11). Amongst the solutes that have been advected away from the agricultural plot by regional flow, accounting for around 90% of the total irrigated solute mass, the extent of groundwater mobility is also the main determinant of solute fate chapter 2. Hence, it can be concluded that the extent of groundwater mobility in the subsurface is by far the most impactful physical parameter on the fate pf irrigated solutes, both inside and outside the agricultural plot. These findings contrast with those for surface irrigation and shallow drip irrigation, where amongst the physical parameters, the atmospheric flux timeseries and root zone soil properties are the primary determinants of solute fate: residence times in the root zone, root solute uptake, and leaching to groundwater (Schotanus et al., 2013; van der Zee and Boesten, 1991). Since the key factors influencing the viability of deep subsurface irrigation are different from those of other irrigation methods, deep subsurface irrigation may be a good alternative in areas where other irrigation methods are unsuitable.

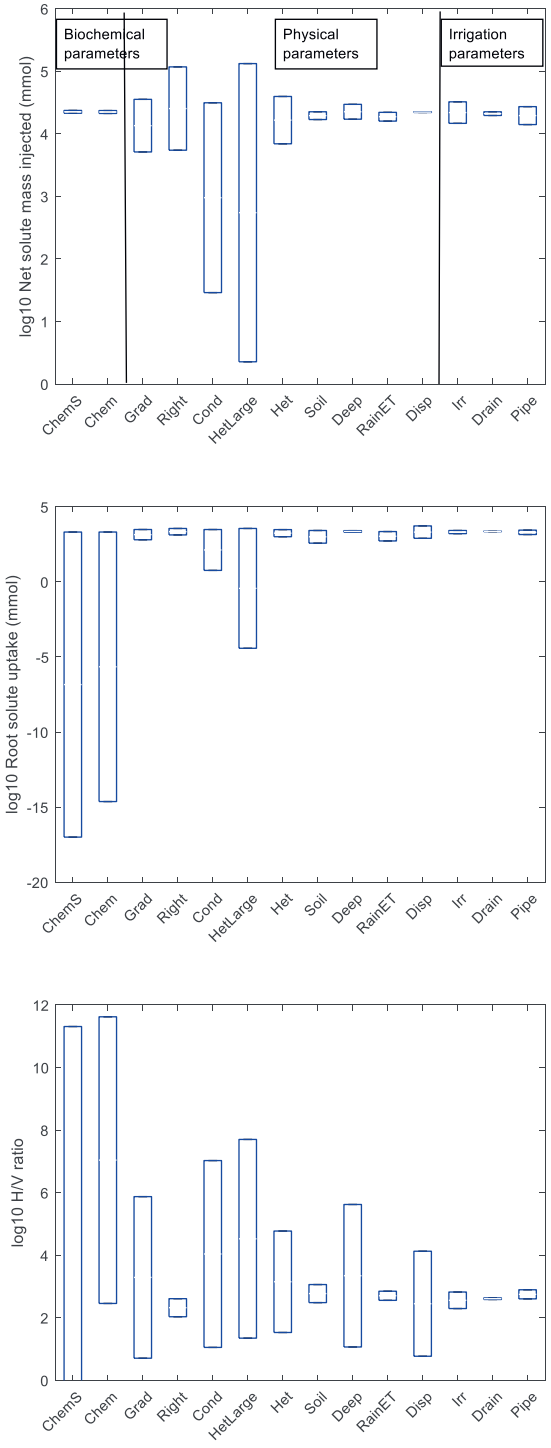

Figure 3.11: Range of outcomes for (a) net contaminant injected, (b) root solute uptake, and (c) the H/V ratio for each individual parameter analysis.

3.4.2 Groundwater mobility

Denote the relaxation time of the system as the time required for fluxes to equilibrate and for the water table to reach its new equilibrium position whenever changes in boundary fluxes occur, such as precipitation and evapotranspiration. This relaxation time is controlled by the wetting pattern of the subsurface irrigation and drainage system. The wetting pattern in turn is controlled by the various hydrogeological parameters, such as the hydraulic conductivity and water retention of the soil, the resistances of the boundaries, and also the design parameters of the subsurface irrigation system such as drain depth, the spacing between drains, drain conductance, drain material, and drain pressure heads (Siyal and Skaggs, 2009; Naglic et al., 2014; Saefuddin et al., 2019 Cai et al., 2017; Obnosov and Kacimov, 2018).

The larger the relaxation time of the subsurface moisture distribution, the higher the water efficiency of the irrigation system, and the lower the total solute mass injected into the soil, as effluent fed into the subsurface requires more time to be discharged towards the environs. Hence, a larger relaxation time allows the target groundwater level to be maintained with less irrigation water input. For example, if a low conductivity substratum underlies the irrigation drains, then the relaxation time of the system is decreased (Mohammad et al., 2014), and smaller irrigation fluxes (and less effluent injection) are sufficient to maintain the groundwater level at a specified height (Obnosov and Kacimov, 2018).

Amongst the pressure head timeseries illustrated in Figure 3.12a and Figure 3.12b, the simulations with large relaxation times are those that have large fluctuations in pressure head over time, in response to transient variability in atmospheric fluxes and irrigation fluxes. Scenarios with smaller relaxation times have nearly constant pressure heads, because the irrigation fluxes respond instantly to changes in pressure heads caused by changes in atmospheric fluxes, and the pressure heads in turn respond instantly to changes in irrigation fluxes. Simulations with large relaxation times tend to have high resistance to flow, thus they are scenarios with small aquifer conductivities and high boundary resistances. Figure 3.12c shows that all simulations with different drain conductivities have similar pressure head timeseries, thus drain conductivity does not significantly affect the relaxation time. Hence, the relaxation time can also be understood as the irrigation and drainage system's effective response time to perturbations in the atmospheric fluxes.

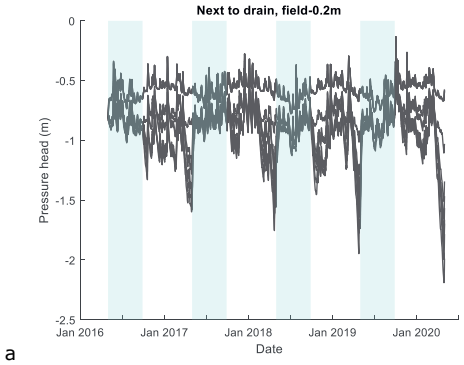

a

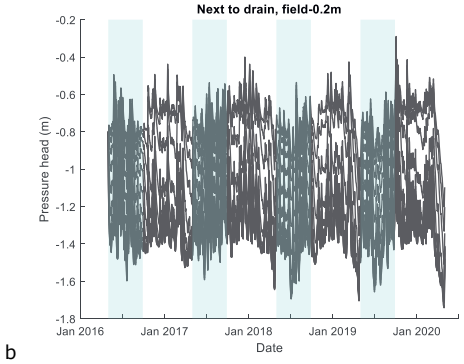

b

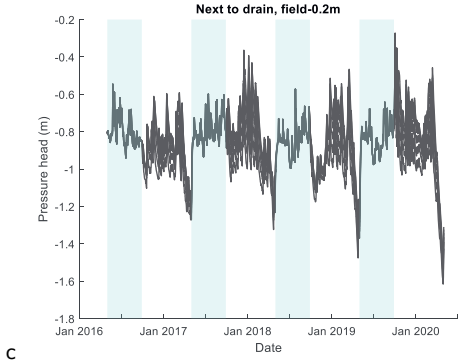

c

Figure 3.12: Pressure heads over time in the root zone for the sensitivity analysis simulations with (a) varying aquifer conductivity, and (b) varying right boundary conductivity, and (c) varying irrigation drain conductivity. Each line represents an individual simulation within the sensitivity analysis, and many lines may overlap, as in Figure 12c.

It is also evident that parameters that affect the relaxation times more significantly are the same parameters that affect solute mass balances more significantly (as discussed in section 3.3), and vice-versa. Hence it can be deduced that the hydrogeological parameters affect groundwater mobility and solute fate most strongly amongst the physical parameters for the same fundamental reason: they strongly determine the relaxation time of the subsurface moisture distribution. Furthermore, this also suggests that pressure head timeseries, which are easier to measure than solute concentrations and

mass balances and provide an indication of the relaxation time, may serve as a proxy variable for gauging the sensitivity of solute fate to changes in system parameters.

3.4.3 Solute breakthrough curves

Solute breakthrough curves are complementary to solute mass balances in assessing environmental risk, as elevated solute concentrations may have adverse consequences on water potability (EC, 2006) and water quality scores (e.g. Alexakis, 2020). Solute breakthrough curves in the root zone are sensitive to the atmospheric fluxes, and also to the regional head gradient. The breakthrough curves at observation points very close to the drains depend heavily on the irrigation and drainage fluxes and are thus most sensitive to parameters that directly affect the water balance (i.e. atmospheric fluxes, and the regional head gradient). Breakthrough curves elsewhere in the saturated zone are highly sensitive to parameters that affect regional flow, such as the regional head gradient and aquifer conductivity, but not to the atmospheric fluxes. Root zone soil properties do not significantly affect breakthrough curves anywhere in the domain, not even in the root zone, except when soil properties cross some threshold of low conductivity and poor water retention (e.g. hydrophobicity), in which case breakthrough curves in the root zone and in the saturated zone differ significantly from simulations with other soils.

Generally, the breakthrough curves at observation points directly above and below drains (Figure 3.4) were more greatly affected by changes in parameters than those midway between drains (Figure 3.5). This is because breakthrough curves at points closer to drains would be more greatly affected by differences in irrigation or drainage fluxes caused by said differences in other parameters. By the time the effluent plume reaches the observation points midway between drains, the solutes would have had ample time to undergo hydrodynamic dispersion, which smooths out spatial differences in concentration, thereby reducing the variability in breakthrough curves across simulations with different parameter values.

While mild soil heterogeneity had little impact on solute mass balance outcomes on average, it had a large effect on solute breakthrough curves in both the saturated zone and root zone. Naturally, variation in breakthrough curves across heterogeneous realizations is greater for strong heterogeneity than for mild heterogeneity.

The relatively large influence of the regional head gradient and soil heterogeneity on breakthrough curves may hinder the characterization of effluent transport, since regional flow may be transient and soil heterogeneity is difficult to fully characterize. This has relatively minor consequences on solute transport in the saturated zone in an idealized two-dimensional domain: the general transport direction is always clear because the upstream and downstream directions are unmistakable except if the regional head gradient reverses. However, in real three-dimensional soils, there is an additional degree of freedom in movement, and regional flow vectors may rotate across the cardinal directions over time as regional climates change. Hence, effluent transport directions may be misjudged unless observed at sufficiently frequent temporal and spatial intervals. Accordingly, it may be useful to monitor soil water EC or temperature to continuously track the transport of effluent.

Comparing the breakthrough curves also reveal that tracer concentrations in the root zone are much larger directly above drains (Figure 3.4) for all scenarios than midway between drains (Figure 3.5). This was also observed for the base model chapter 2. Thus, crop solute uptake is always spatially heterogeneous, even in homogeneous soils. Thus, it is important to take this into account when

determining the placement of crops in the field, if attempting to minimize possible ecotoxicological consequences.

3.5. Conclusions

In this study of a subirrigation system that uses marginal water for irrigation, we perform a sensitivity analyses on a numerical model, with realistic parameter ranges that reflect real-world possibilities and uncertainties. Thirty years of weather data, and random spatial heterogeneity in soil hydraulic parameters, were also simulated to characterize the impact of temporal and spatial heterogeneity in the system. Important outcomes we considered include breakthrough curves, solute concentrations, and the mass balances of the irrigated solutes, such as the root solute uptake and the solute mass drained by the drainage system, and the amount and direction of solute discharge in the saturated zone.

Altogether, the fate of solutes in the effluent is primarily determined by factors that are primarily determined by the geography (i.e. effluent type, CEC content of the effluent, soil properties, and hydrogeological properties) of the agricultural plot. Factors that may be engineered (i.e. irrigation parameters) only minimally affect the hazards of subirrigation with treated wastewater. Since the availability of effluent in agricultural areas with more favourable soil and aquifer properties is limited by the cost efficiency of transporting effluent and by the geography of human settlement (Narain-Ford et al., 2021), the placement of treatment plants and agricultural zones is therefore an important factor in the implementation of subirrigation systems. Hence, overcoming barriers towards wider adoption of deep subirrigation systems may ultimately be an urban planning challenge.

Chapter 4

Dispersion and Recovery of Solutes and Heat under Cyclic Radial Advection

Based on:

Tang, D. W. S., & van der Zee, S. E. A. T. M. (2021). Dispersion and Recovery of Solutes and Heat under Cyclic Radial Advection. Journal of Hydrology, 126713.

Abstract

For cyclic injection-extraction wells with various radial flow geometries, we study the transport and recovery of solute and heat. We derive analytical approximations for the recovery efficiency in closed-form elementary functions. The recovery efficiency increases as injection-extraction flow rates increase, dispersion decreases, and spatial dimensionality decreases. In most scenarios, recovery increases as cycle periods increase, but we show numerically and analytically that it varies non-monotonically with cycle period in three-dimensional flow fields, due to competing effects between diffusion and mechanical dispersion. This illustrates essential differences between the spreading mechanisms, and reveals that for a single well it may be impossible to optimize recovery of both solute and heat simultaneously. Whether retardation increases or decreases recovery thus depends on aquifer geometry and the dominant dispersion process. As the dominant dispersion process heavily determines the sensitivity of the recovery efficiency to other parameters, we introduce the dimensionless kinetic dispersion factor S_T, to distinguish whether diffusion or mechanical dispersion dominates. We also introduce the geometric dispersion factor G, which is derived from our full solution for the recovery efficiency and improves upon the concept of the area-to-volume ratio (A/V), often used in analysing well problems. Unlike A/V, G accounts for spatio-temporal interactions between dispersion and flow field geometry, and can be applied to determine recovery efficiencies across a wider range of scenarios. It is found that A/V is a special case of G, describing the recovery efficiency only when mechanical dispersion with linear velocity dependence is the sole mechanism of spreading.

4.1 Introduction

Wells in geological porous media are used in cyclic injection-extraction processes, otherwise named push-pull processes, in many applications. These include aquifer thermal energy storage (ATES) (Lee, 2010), aquifer storage and recovery (ASR) (Lowry & Anderson, 2006), subsurface irrigation with excess moisture drainage (Narain-Ford et al., 2020), hydraulic fracturing (Penny et al., 1983), air sparging (van Dijke & van der Zee, 1998), aquifer characterization (Istok et al., 1997; Haggerty et al., 1998; Schroth et al., 2000; Gouze et al., 2008; Anderson, 2005), the treatment of drinking water production aquifers (Van Halem et al., 2011), and gasoline spill remediation (van Dijke and van der Zee, 1998). Natural forces also drive oscillatory environmental flows: coastal aquifers experience oscillatory flows due to tidal, seasonal and glacial cycles, resulting in the oscillatory transport of salinity (Pool et al., 2016) across freshwater lenses. Another example of oscillatory environmental flow is barometric pumping: subsurface gases and vapors are periodically drawn upwards and forced downwards due to seasonal variations in atmospheric pressure (Stauffer et al., 2019; Nilson et al., 1991; Scotter & Raats., 1968). Oscillatory flows also result from a combination of human and natural factors. For example, soils in semi-arid regions receive sodium ions from capillary rise in the dry season, which are subsequently flushed downwards by infiltrating rain and irrigation (van de Craats et al., 2020; van der Zee et al., 2014).

In many of these oscillatory flow problems, an interface separates two bodies of water of different quality, a classical example being the freshwater lens. With aquifer storage systems, the interface separates the injected freshwater or hot water from background groundwater. A chemical or thermal gradient, which undergoes transport due to advection and hydrodynamic dispersion, is responsible for the difference in water quality across the interface. In light of the wide variety of applications, especially regarding water, environmental, and energy sustainability, fundamental research into the general behavior of solute and heat transport under oscillatory conditions has recently received a significant amount of engagement (e.g. Laemmel et al., 2019; Stauffer et al., 2019; van Duijn & van der Zee., 2018; Dey & Sekhar., 2016; Pauw et al., 2016; Sanz-Prat et al., 2016; Cirkel et al., 2015; Eeman et al., 2015; Wang & Chen., 2015; Lu et al., 2011). Amongst the various oscillatory flow scenarios, managed aquifer recharge systems such as ASR and ATES are unique in that they are concerned with not only the spreading of solutes and heat in the subsurface, but also the recovery of freshwater or heat.

In this study, we characterize the performance of aquifer storage systems. A key performance metric of an injection-extraction system is the recovery efficiency of injected solutes or heat, which is the proportion of injected solute mass or thermal energy that can be recovered during the extraction phase. Solutes and heat spread around the injected water front due to hydrodynamic dispersion processes, that are partly advection velocity-dependent, such as mechanical pore-scale dispersion, and partly velocity-independent, such as molecular and thermal diffusion. The types of dispersion process that occur, the relative strengths of the dispersion processes, the strength of dispersion relative to advection, and a number of other factors such as flow field geometry and injection rate determine the recovery efficiency. We employ analytical methods to derive simple solutions for the recovery efficiency as a function of these parameters, and discuss the implications of well design, well operational parameters, and aquifer characteristics on the recovery efficiency.

4.2 Literature Review

Many prior analytical characterizations of injection-extraction systems make use of exact solutions (e.g. Yang et al., 2010; Yates, 1990; Chen, 1987; Veling, 2012; Aichi & Akitaya, 2018), and are valid for specific scenarios. For example, they might apply only to specific flow field geometries, or omit either mechanical dispersion or molecular diffusion. Some, giving non-closed form functions that require numerical integration, may be somewhat less transparent for directly comparing different geometrical or dispersion properties. Furthermore, no exact analytical solutions are available for some scenarios such as

wells modelled as point sources. Quite a number of analytical solutions are available, including studies with closed-form analytical solutions (e.g. Pophillat et al., 2020a; Gelhar and Collins, 1971), but they currently describe only the spatial distribution of concentration and temperature, but not the recovery efficiency. A large body of literature on direct numerical simulations of the recovery efficiency exists, (e.g. Doughty et al., 1982; Sommer et al., 2013; Sommer et al., 2015; van Lopik et al., 2016; Bloemendal and Hartog, 2018; Pophillat et al., 2020a; Pophillat et al., 2020b). However, such numerical studies are computationally intensive and specific to certain combinations of parameter values and aquifer geometry, which makes their findings difficult to generalize. To overcome these limitations, we turn to analytical approximations to describe the recovery efficiency with elementary mathematical functions. Such closed-form analytical approximations allow for straightforward sensitivity analysis, rapid evaluation of a vast parameter space, and identification of suitable regions within parameter space for further in-depth investigation with more exact methods. They also give more insight in synergistic and antagonistic effects of different parameters, and they are fast to evaluate.

The area-to-volume ratio (A/V) is a popular approximate method for estimating the recovery efficiency of radial transport systems (e.g. Sommer et al., 2015; Schout et al., 2014; Novo et al., 2010; Forkel & Daniels., 1995). It is based on a simple principle: in three spatial dimensions "the volume of a storage unit increases as the cube of the characteristic dimension (i.e. storage radius), and its area for heat loss increases as the square, so increasing the size reduces the loss-to-capacity ratio" (Duffie and Beckman, 2013). Similar considerations apply to problems of any number of spatial dimensions. However, the A/V is a purely geometric argument that does not consider other factors within the system, such as those previously described. These other aspects of the system also interact with flow field geometry in determining the recovery efficiency, thus the validity of the A/V ratio in characterizing recovery efficiency hinges upon these other factors. For instance, the evolution of the A/V ratio with time depends on the flow field geometry and injection rate at the well, and so does the Peclet number (Kim et al., 2010). While the A/V ratio might decrease over time as the storage radius increases and indicate a larger recovery efficiency, the magnitude of dispersion relative to advection might in some cases increase with the storage radius thereby suggesting a smaller recovery efficiency. Therefore, the A/V ratio as an indicator of recovery efficiency ignores aspects of complexity that are instrumental to the problem.

Gelhar and Collins' (1971) classical model of concentration profiles around injection wells remains instrumental today in characterizing aquifer-well systems (Pophillat et al., 2020a). Furthermore, Gelhar and Collins' model for the concentration profiles continues to be applied and modified in recent years (e.g. Shi et al., 2020; Guimerà, 2007; Schroth and Istok, 2005). Hence, we derive approximate solutions for the recovery efficiency, taking into account the interactions between flow field geometry, hydrodynamic dispersion, and the recovery efficiency, that are ignored with the A/V ratio, by extending the model of Gelhar and Collins (1971), and validating our analytical results with numerical models. For notational convenience and brevity, we proceed with solute transport terminology. Under the assumption that density differences induced by chemical and thermal gradients are negligible, the analysis is mathematically analogous and fully applicable to heat transport (Lee, 1998).

4.3 Methods

In homogeneous aquifers with negligible background flow, flow fields around wells can be described as radially axisymmetric flow around a point source. Radial flow in one, two, and three dimensions implies a linear, disk-shaped, and spherical flow field, respectively. These three radial geometries correspond respectively to $d = 1, 2, 3$ in the mathematical construct of a d-dimensional sphere. The radially axisymmetric advection-dispersion equation (ADE) describing conservative solute and heat transport in any number of dimensions is (Gelhar & Collins, 1971)

$$\frac{\partial c}{\partial t} = \alpha v \frac{\partial^2 c}{\partial r^2} - v\frac{\partial c}{\partial r} + D_m\left(\frac{\partial^2 c}{\partial r^2} - \frac{1}{v}\frac{\partial v}{\partial r}\frac{\partial c}{\partial r}\right), \tag{4.1}$$

where r is the radial positional coordinate, c is the dimensionless concentration of the solute, t is time, v is the flow velocity, α is the longitudinal mechanical dispersivity, and D_m is the molecular (or thermal) diffusion coefficient. Chemical and thermal retardation is implicitly considered, as it implies only a linear re-scaling of time.

The pore water velocity $v(r)$, and therefore also the mechanical dispersion, is position-dependent for $d > 1$ in view of mass continuity, where d denotes dimensionality. For d-dimensional axisymmetric radial flow,

$$v(r,d) = \frac{A_d}{r^{d-1}}, \tag{4.2}$$

$$A_d = \frac{Q}{\theta}\left[\frac{2\pi^{\frac{d}{2}}}{\Gamma\left(\frac{d}{2}\right)}\right]^{-1}, \tag{4.3}$$

where θ is the porosity, Q is the injection or extraction rate, A_d is the d-dependent shape constant, where the term in square brackets is the surface area of a d-dimensional sphere of unit radius, and Γ is the gamma function. Essentially, (4.2) and (4.3) force mass continuity by requiring that the rate of volumetric expansion (contraction) of the body of injected water is equal to the injection (extraction) rate.

In practice, for injection/extraction in groundwater aquifers, the $d = 2$ situation of a fully penetrating well seems to be quite common. The confining layers below and on top of the aquifer may affect the flow pattern somewhat if they are not completely impermeable. For leaky aquifers or wells that do not penetrate fully, a $d = 3$ point injection may be a more appropriate limiting case. The one-dimensional $d = 1$ case reflects an infinite row of fully penetrating wells, in which case the flow of injected water occurs rectilinearly along one dimension (e.g. Molinari and Peaudecerf, 1977; Sauty, 1977). A graphic illustration of these flow field geometries is presented in Figure 4.1. Note that although Figure 4.1 illustrates 3D rectangular and cylindrical flow fields for the 1D and 2D cases respectively for the sake of visualization, these cases are identical to 1D line and 2D disk flow fields under the assumption that no dispersion or flow occurs into the confining layers.

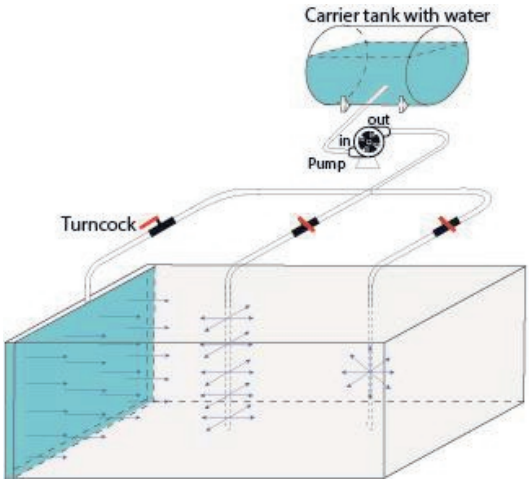

Figure 4.1: Conceptual image of (left) 1D, (middle) 2D, and (right) 3D radial flow in a horizontal aquifer.

Substituting the hydrodynamic dispersion coefficient

$$D(r) = D_m + \alpha v(r), \tag{4.4}$$

into the ADE (4.1) allows us to rewrite the ADE in a simpler form:

$$\frac{\partial c}{\partial t} = D(r)\frac{\partial^2 c}{\partial r^2} + \left[(d-1)\frac{D_m}{r} - v(r)\right]\frac{\partial c}{\partial r}. \tag{4.5}$$

In the base model scenario, at the well, a duration T of injection rate Q alternates with the same duration T of extraction rate $-Q$, in a step-cyclic manner in a d-dimensional infinite domain. We henceforth refer to this base scenario as the standard cycle. The standard cycle consists of equal volumes of injected and extracted water during each phase, $V_{in} = V_{ex}$. Later, we also investigate the effects of varying the ratio of extraction to injection volume. The flow field achieves steady-state instantaneously upon switching between injection or extraction. The well injects a total mass $M = c_0 QT$ of solute, and recovers $M_r(i)$, over the i-th injection period. Therefore, the recoverable proportion F_r of solute over the i-th injection-extraction cycle is

$$F_r(i) = \frac{M_r(i)}{M}. \tag{4.6}$$

The cumulative solute recovery efficiency after n cycles, F_c, is

$$F_c(n) = \frac{1}{n}\sum_{i=1}^{n}\frac{M_r(i)}{M} = \frac{1}{n}\sum_{i=1}^{n}F_r(i). \tag{4.7}$$

The initial and boundary conditions that describe this problem are

$$c(r,0) = 0, \tag{4.8}$$

$$c(0,t)_{in} = c_0, \tag{4.9}$$

$$\frac{\partial c}{\partial r}(0,t)_{ex} = 0, \tag{4.10}$$

where subscripts in and ex refer to the injection and extraction phases respectively. For analytical tractability, we disregard heterogeneity and interactions with the overlying or underlying low hydraulic

conductivity layers and flow driven by density gradients, and comment on these simplifications at the end. We also disregard storage periods, where the injection and extraction phases are separated by a period where neither occurs.

Numerical simulations were performed using MODFLOW-2005 (Harbaugh, 2005) and MT3DMS (Langevin & Guo, 2006), for flow and solute transport, respectively. For the computation of the flow field, the initial hydraulic head in the entire domain was set to a uniform value. The boundaries of the numerical domain are set as uniform constant-head boundaries, which imply an absence of background flow. The geometry of the numerical domains are identical to that of the flow field being modelled (i.e. line-, disc-, and sphere-shaped domains for 1D, 2D, and 3D, respectively). The solute boundary condition at the edge of the domain is

$$\frac{\partial c}{\partial r} = 0, \tag{4.11}$$

to preserve the continuity of $c(r)$ and minimize dispersive spreading caused by the boundary. To minimize the influence of numerical edge effects on the transport of water and solutes in a semi-infinite domain $0 \leq r < \infty$, we placed the boundary sufficiently distant from the source, as checked in pilot simulations. Parameter values used in examples validated with numerical simulations are, unless otherwise specified, $Q = 2^d$, $T = 16$, $\alpha = 0.1$, $D_m = 0.1$, $n = 50$. A summary of the parameters and variables referred to in this chapter is provided in Table 4.1.

Table 4.1: List of variables. The symbols L, T and M under units represent units of length, time and mass respectively.

Symbol	Units	Description
A_d	$[L^dT^{-1}]$	Shape constant
b	Varies	Placeholder in equation 22
c	$[ML^{-d}]$	Solute concentration
c_0	$[ML^{-d}]$	Injected solute concentration
c_{crit}	$[ML^{-d}]$	Critical solute concentration
d	$[-]$	Dimensionality
D	$[L^2T^{-1}]$	Hydrodynamic dispersion coefficient
D_m	$[L^2T^{-1}]$	Molecular diffusion coefficient
F_c	$[-]$	Cumulative recovery efficiency
F_{eff}	$[-]$	Effective recovery efficiency
F_r	$[-]$	Recovery efficiency
G	$[L^{xd}T^{y-x}]$	Geometric dispersion factor
i	$[-]$	i-th cycle
m	[M]	Solute mass lost by the end of the injection phase
m_c	[M]	Solute mass lost by the end of a cycle
M	[M]	Injected solute mass
M_r	[M]	Recovered solute mass
n	$[-]$	Number of cycles
Q	$[L^dT^{-1}]$	Injection rate
r	[L]	Radial coordinate
r'	[L]	Hydraulic front position
r_m	[L]	Storage radius
S_T	$[-]$	Kinetic dispersion factor
t	[T]	Time
T	[T]	Injection duration
T_m	[T]	Injection duration that optimizes F_r in 3D flow fields
v	$[LT^{-1}]$	Flow velocity
V	$[L^d]$	Volume of a d-dimensional sphere
V_{in}	$[L^d]$	Injected water volume
V_{ex}	$[L^d]$	Extracted water volume
x	$[-]$	Exponent for computing F_r and G
y	$[-]$	Exponent for computing F_r and G
z	$[-]$	Exponent for computing F_r
α	[L]	Mechanical dispersivity
Δ	$[-]$	Placeholder in equation 35
ζ	Varies	Placeholder in equation 35
η	$[-]$	Exponent of power-law mechanical dispersion
θ	$[-]$	Saturation
ω	$[-]$	Sub-function for the calculation of concentration profiles

4.4 Theory

4.4.1 Frontal Spreading

The volume of injected water at time t is $V_{in}(t) = Qt$, and the position of the injected water front (i.e. hydraulic front), is given by

$$r' = (dA_d t)^{\frac{1}{d}}, \qquad (t \leq T)$$

$$r' = \left(dA_d(2T - t)\right)^{\frac{1}{d}}. \qquad (t > T)$$

(4.12)

where the expression takes on a different form for $t > T$ as injection switches to extraction.

Gelhar and Collins (1971) showed the expression for $c(r,t)$ to be

$$c(r, r'(t)) = \frac{1}{2} c_0 \operatorname{erfc}\left[\frac{r^d - r'^d}{dA_d\sqrt{4\alpha\omega}}\right], \tag{4.13}$$

$$\omega = \int_0^{r'} \frac{v(r) + D_m/\alpha}{v^3(r)} dr\,. \tag{4.14}$$

The solution for the concentration during the injection phase $t \le T$, found by substituting (4.2), (4.12) and (4.14) into (4.13), is

$$c(r,t) = \frac{1}{2} c_0 \operatorname{erfc}\left[\frac{\left(r^d - (dA_d t)\right)}{\sqrt{4d^2\alpha(dA_d t)^{\frac{2d-1}{d}}}} \sqrt{\frac{(3d-2)(2d-1)\alpha A_d}{(3d-2)\alpha A_d + (2d-1)D_m(dA_d t)^{\frac{d-1}{d}}}}\right]. \tag{4.15}$$

Expansions of (4.15) for specific scenarios are given in Table 4.2.

Table 4.2: Table of functions describing some limiting cases of transport.

Limiting scenario	Shape constant A_d	Concentration profile $c(r,t)$	Flow exponent x	Period exponent y	Area-to-volume ratio A/V	Geometric dispersion factor $G = Q^x T^y$
1D $D = \alpha\|v\|$	$A_1 = \frac{Q}{2\theta}$	$\frac{1}{2}c_0 \operatorname{erfc}\left[\frac{(r-A_1 t)}{\sqrt{4\alpha A_1 t}}\right]$	$-\frac{1}{2}$	$-\frac{1}{2}$	$2\theta(QT)^{-1}$	$Q^{-1/2}T^{-1/2}$
1D $D = D_m$		$\frac{1}{2}c_0 \operatorname{erfc}\left[\frac{(r-A_1 t)}{\sqrt{4D_m t}}\right]$	-1			$Q^{-1}T^{-1/2}$
1D $D = \alpha\|v^2\|$		$\frac{1}{2}c_0 \operatorname{erfc}\left[\frac{(r-A_1 t)}{\sqrt{4\alpha A_1^2 t}}\right]$	0			$T^{-1/2}$
2D $D = \alpha\|v\|$	$A_2 = \frac{Q}{2\pi\theta}$	$\frac{1}{2}c_0 \operatorname{erfc}\left[\frac{(r^2-2A_2 t)}{(2A_2 t)^{3/4}}\sqrt{\frac{3}{16\alpha}}\right]$	$-\frac{1}{4}$	$-\frac{1}{4}$	$2\sqrt{\pi\theta}(QT)^{-1/2}$	$Q^{-1/4}T^{-1/4}$
2D $D = D_m$		$\frac{1}{2}c_0 \operatorname{erfc}\left[\frac{(r^2-2A_2 t)}{4A_2 t}\sqrt{\frac{A_2}{D_m}}\right]$	$-\frac{1}{2}$	0		$Q^{-1/2}$
2D $D = \alpha\|v^2\|$		$\frac{1}{2}c_0 \operatorname{erfc}\left[\frac{(r^2-(2A_2 t))}{\sqrt{16\alpha A_2^2 t}}\right]$	0	$-\frac{1}{2}$		$T^{-1/2}$
3D $D = \alpha\|v\|$	$A_3 = \frac{Q}{4\pi\theta}$	$\frac{1}{2}c_0 \operatorname{erfc}\left[\frac{(r^3-3A_3 t)}{(3A_3 t)^{5/6}}\sqrt{\frac{5}{36\alpha}}\right]$	$-\frac{1}{6}$	$-\frac{1}{6}$	$3\left(\frac{4\pi\theta}{3}\right)^{\frac{1}{3}}(QT)^{-1/3}$	$Q^{-1/6}T^{-1/6}$
3D $D = D_m$		$\frac{1}{2}c_0 \operatorname{erfc}\left[\frac{(r^3-3A_3 t)}{(3A_3 t)^{7/6}}\sqrt{\frac{7A_3}{36D_m}}\right]$	$-\frac{1}{3}$	$\frac{1}{6}$		$Q^{-1/3}T^{1/6}$
3D $D = \alpha\|v^2\|$		$\frac{1}{2}c_0 \operatorname{erfc}\left[\frac{(r^3-(3A_3 t))}{\sqrt{36\alpha A_3^2 t}}\right]$	0	$-\frac{1}{2}$		$T^{-1/2}$

4.4.2 Recovery efficiency

The dispersion processes ensure that all solute mass or thermal energy that has escaped beyond the hydraulic front is irrecoverable in a standard cycle. Let m be this irrecoverable solute mass or thermal energy, at the time when the front is at r'. To quantify m outside r' during the injection phase $t \leq T$, we integrate the concentration (4.15) beyond the hydraulic front, as follows:

$$m(t) = \int_{V(r')}^{V(r=\infty)} c(r,t)\, dV = \int_{r'}^{\infty} c(r,t)\frac{dV(r)}{dr}dr, \tag{4.16}$$

where $V(r)$ is the volume of a d-dimensional sphere of radius r. Integrating over r the area of a d-dimensional sphere (see Equation 4.3) gives

$$V(r) = \frac{2\pi^{\frac{d}{2}}}{d\cdot\Gamma\left(\frac{d}{2}\right)}r^d \tag{4.17}$$

Substituting $t = T$ into (4.16) yields the total solute mass lost at the end of the injection phase:

$$m(t=T) = \sqrt{\frac{1}{(3d-2)(2d-1)\pi}}(A_d)^{-\frac{3}{2}}Qc_0\sqrt{(3d-2)\alpha(A_d)^{\frac{3d-1}{d}}(Td)^{\frac{2d-1}{d}} + (2d-1)D_m(A_d)^{\frac{3d-2}{d}}(Td)^{\frac{3d-2}{d}}} \tag{4.18}$$

Let the storage radius

$$r_m = r'(T) = (dA_d T)^{\frac{1}{d}} \tag{4.19}$$

be the furthest position of the hydraulic front attained during a cycle. Recall that the flow field is modelled as a sequence of successive steady states. Since ω is a path integral over the travel history of

the hydraulic front, and since the indefinite integral in ω during the extraction phase is negative of that during the injection phase (Gelhar and Collins, 1971), ω for the complete cycle is:

$$\omega = \int_0^{r_m} \frac{v(r) + D_m/\alpha}{v(r)^3} dr - \int_{r_m}^0 \frac{v(r) + D_m/\alpha}{v(r)^3} dr = 2\int_0^{r_m} \frac{v(r) + D_m/\alpha}{v(r)^3} dr\,. \tag{4.20}$$

Repeating the steps from (4.13) to (4.18), and using (4.20) for ω, yields the total solute mass that disperses out of the hydraulic front by the end of a complete cycle, $m_c = \sqrt{2}m$.

The recovery efficiency over a cycle, which is the ratio of mass not lost to dispersion, to the total solute or thermal mass injected M, is $F_r(Q,T) = 1 - \frac{m_c}{M}$, which yields

$$F_r(Q,T) = 1 - \left[\sqrt{\frac{2}{(3d-2)(2d-1)\pi}}(A_d)^{-\frac{3}{2}}T^{-1}\sqrt{(3d-2)\alpha(A_d)^{\frac{3d-1}{d}}(Td)^{\frac{2d-1}{d}} + (2d-1)D_m(A_d)^{\frac{3d-2}{d}}(Td)^{\frac{3d-2}{d}}}\right]. \tag{4.21}$$

Expansions of (4.21) for specific scenarios are presented in Table 4.3.

Table 4.3: Expansions of F_r and S_T for various scenarios.

Scenario	Single cycle recovery efficiency $F_r(Q,T)$	Kinetic dispersion factor S_T
d-dimensions $D = D_m + \alpha\|v\|$	$1 - \left[\sqrt{\frac{2}{(3d-2)(2d-1)\pi}}(A_d)^{-\frac{3}{2}}T^{-1}\sqrt{(3d-2)\alpha(A_d)^{\frac{3d-1}{d}}(Td)^{\frac{2d-1}{d}} + (2d-1)D_m(A_d)^{\frac{3d-2}{d}}(Td)^{\frac{3d-2}{d}}}\right]$	$\frac{(3d-2)\alpha v}{(2d-1)D_m}$
1D $D = D_m + \alpha\|v\|$	$1 - \left[\sqrt{\frac{2}{\pi}}\left(\frac{2\theta}{Q}\right)^{\frac{3}{2}}\sqrt{\alpha\left(\frac{Q}{2\theta}\right)^{2}T^{-1} + D_m\frac{Q}{2\theta}T^{-1}}\right]$	$\frac{Q\alpha}{2\theta D_m}$
2D $D = D_m + \alpha\|v\|$	$1 - \left[\sqrt{\frac{2}{12\pi}}\left(\frac{2\pi\theta}{Q}\right)^{\frac{3}{2}}\sqrt{2\alpha\left(\frac{Q}{\pi\theta}\right)^{\frac{5}{2}}T^{-1/2} + 3D_m\left(\frac{Q}{\pi\theta}\right)^{2}}\right]$	$\frac{4\alpha}{3D_m}\left(\frac{Q}{4\pi\theta T}\right)^{\frac{1}{2}}$
3D $D = D_m + \alpha\|v\|$	$1 - \left[\sqrt{\frac{2}{35\pi}}\left(\frac{4\pi\theta}{Q}\right)^{\frac{3}{2}}\sqrt{\frac{7}{3}\alpha\left(\frac{3Q}{4\pi\theta}\right)^{\frac{8}{3}}T^{-1/3} + 5D_m\left(\frac{3Q}{4\pi\theta}\right)^{\frac{7}{3}}T^{1/3}}\right]$	$\frac{7\alpha}{5D_m}\left(\frac{Q}{36\pi\theta T^2}\right)^{\frac{1}{3}}$
d-dimensions $D = D_m + \alpha\|v^2\|$	$1 - \left[\sqrt{\frac{2}{(3d-2)\pi}}(A_d)^{-\frac{3}{2}}T^{-1}\sqrt{(3d-2)\alpha(A_d)^3T + D_m(A_d)^{\frac{3d-2}{d}}(Td)^{\frac{3d-2}{d}}}\right]$	$\frac{(3d-2)\alpha v^2}{(d)D_m}$
1D $D = D_m + \alpha\|v^2\|$	$1 - \left[\sqrt{\frac{2}{\pi}}\left(\frac{2\theta}{Q}\right)^{\frac{3}{2}}\sqrt{\alpha\left(\frac{Q}{2\theta}\right)^{3}T^{-1} + D_m\frac{Q}{2\theta}T^{-1}}\right]$	$\frac{Q^2\alpha}{4\theta^2 D_m}$
2D $D = D_m + \alpha\|v^2\|$	$1 - \left[\sqrt{\frac{2}{8\pi}}\left(\frac{2\pi\theta}{Q}\right)^{\frac{3}{2}}\sqrt{\alpha\left(\frac{Q}{\pi\theta}\right)^{3}T^{-1} + 4D_m\left(\frac{Q}{\pi\theta}\right)^{2}}\right]$	$\frac{\alpha}{D_m}\left(\frac{Q}{4\pi\theta T}\right)$
3D $D = D_m + \alpha\|v^2\|$	$1 - \left[\sqrt{\frac{2}{21\pi}}\left(\frac{4\pi\theta}{Q}\right)^{\frac{3}{2}}\sqrt{\frac{7}{9}\alpha\left(\frac{3Q}{4\pi\theta}\right)^{3}T^{-1} + 3D_m\left(\frac{3Q}{4\pi\theta}\right)^{\frac{7}{3}}T^{1/3}}\right]$	$\frac{7\alpha}{3D_m}\left(\frac{Q}{36\pi\theta T^2}\right)^{\frac{2}{3}}$
d-dimensions $D = D_m + \alpha\|v^\eta\|$	$1 - \left[\frac{\sqrt{\frac{2}{(3d-2)(3d-2+\eta-\eta d)\pi}}(A_d)^{-\frac{3}{2}}T^{-1}\cdot}{\sqrt{(3d-2)\alpha(A_d)^{\frac{3d-2+\eta}{d}}(Td)^{\frac{3d-2+\eta-\eta d}{d}} + (3d-2+\eta-\eta d)D_m(A_d)^{\frac{3d-2}{d}}(Td)^{\frac{3d-2}{d}}}}\right]$	$\frac{(3d-2)\alpha v^\eta}{(3d-2+\eta-\eta d)D_m}$

We plotted (4.21) together with the numerical results for the recovery efficiency of the first cycle in Figure 4.2a and 4.2b. The solutions agree excellently with the numerical results for all cases, but deviate moderately for 3D flow fields when molecular diffusion dominates at larger T. In this case, (4.21) is not a proper expression for F_r, because expression (4.21) becomes negative at large T,, which is physically impossible. This deviation occurs because the approximation (4.15) is appropriate only when the scale of transport due to hydrodynamic dispersion is not larger than that of advection (Gelhar and Collins, 1971). In 3D, advective transport scales with $r' \propto t^{1/3}$ (see Equation 4.12), and thus so does mechanical dispersion. In contrast, displacement due to molecular diffusion scale with $t^{1/2}$ regardless of dimensionality (Woess, 2000). Therefore, (4.15) and (4.21) are accurate in all modelled scenarios except in 3D if molecular diffusion is dominant.

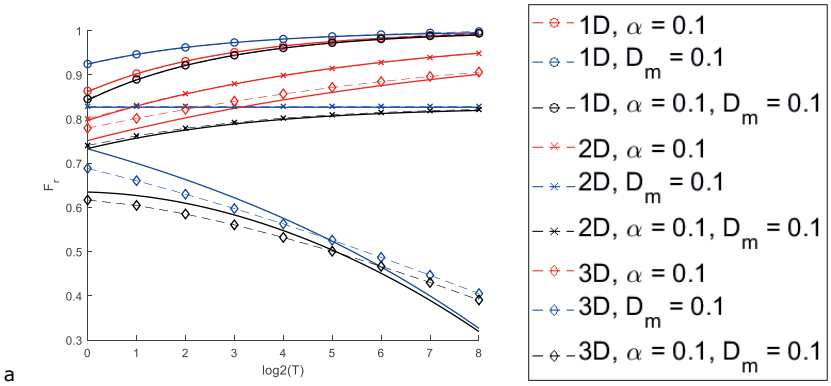

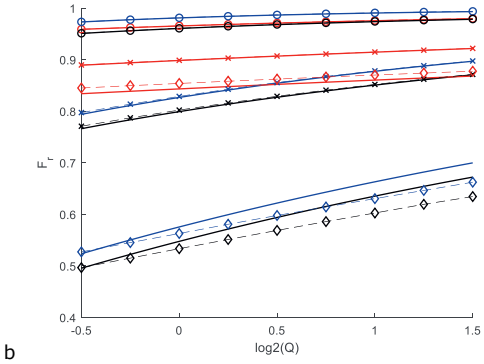

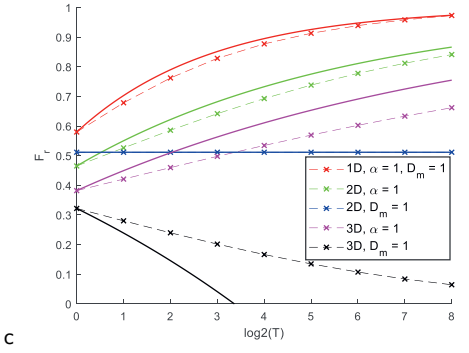

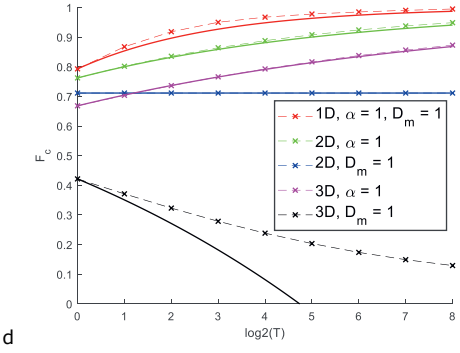

Figure 4.2: Dashed lines with markers are numerical results, while solid lines are analytical solutions. (a) First cycle $F_r(T)$ using (21). (b) First cycle $F_r(Q)$ using (21). (c) First cycle $F_r(T)$ extrapolated using (24), (d) $F_c(T)$ after 50 cycles extrapolated using (24). Extrapolations use $T_0 = 1$ as reference.

Several important characteristics of the system are revealed in (4.21): F_r increases monotonically as Q increases, and as D decreases. Remarkably, if $\alpha \neq 0$ and $D_m \neq 0$, in 1D and 2D F_r increases monotonically as T increases, but varies non-monotonically in 3D with a maximum. These observations can be explained in further detail, by considering the following scenarios, which we will refer to as limiting scenarios.

Notice that the rightmost root term (4.21) contains the sum of a mechanical dispersive and a diffusive component. In limiting cases where one hydrodynamic dispersion process completely dominates (i.e. either $D = \alpha|v|$ or $D = D_m$), then (4.21) simplifies to

$$F_r(Q,T) = 1 - \left[b\sqrt{\alpha}|Q^x|T^y\right], \tag{4.22a}$$

$$x = -\frac{1}{2d}, \tag{4.22b}$$

$$y = -\frac{1}{2d}, \tag{4.22c}$$

for $D = \alpha|v|$, and

$$F_r(Q,T) = 1 - \left[b\sqrt{D_m}|Q^x|T^y\right], \tag{4.23a}$$

$$x = -\frac{2}{2d}, \tag{4.23b}$$

$$y = \frac{d-2}{2d}, \tag{4.23c}$$

for $D = D_m$, where all terms in (4.21) not explicitly written in (4.22a) and (4.23a) are lumped into b for brevity. Essentially, b is a function of dimensionality, and the identity (but not magnitude) of the dominant dispersion process. Values of x and y in scenarios of all spatial dimensions are included in Table 4.2. In all limiting cases, $1 - F_r \propto \sqrt{\alpha}$ or $1 - F_r \propto \sqrt{D_m}$, regardless of dimensionality. Note however that when both α and D_m are non-zero, the relationship $1 - F_r \propto \sqrt{\alpha Q + D_m}$ does not hold. As follows from the above equations, the period exponent y and flow exponent x are crucial in determining how both concentration profile and dispersive loss are affected by T and Q. In the limiting cases described by (4.22 – 4.23), $F_r(d = 2, D = D_m)$ is independent of T, and $F_r(d = 3, D = D_m)$ decreases as T increases. In all other limiting cases, F_r increases as T increases and as Q increases. The fact that $F_r(d = 3, D = D_m)$ decreases as T increases, whereas $F_r(d = 3, D = \alpha|v|)$ increases as T increases, explains why $F_r(d = 3, D = \alpha|v| + D_m)$ varies non-monotonically with T. Many problems in practice can be reduced to such limiting cases. For example, thermal diffusion typically dominates heat transport (Anderson, 2005; Vandenbohede et al., 2009), while mechanical dispersion typically dominates solute transport (Anderson, 1984).

Direct estimation with (4.21) is inaccurate if the hydrodynamic dispersion coefficient is sufficiently large to result in a single cycle F_r smaller than 0.7. The reason is that in scenarios with smaller F_r, the scale of dispersive transport becomes large relative to advection. Nevertheless, in practice aquifer storage systems typically have recovery efficiencies of 0.7 or higher (Drijver et al., 2012) except for systems with very large concentration or thermal gradients where density effects play a significant role in transport (Schout et al., 2016), thus (4.21) remains applicable to real systems. (4.21) is also inaccurate in predicting the cumulative recovery efficiency F_c if the number of cycles is larger than 1. In these two cases, it is possible to gain insight on $F_r(Q,T)$ and the cumulative recovery efficiency $F_c(Q,T)$ by extrapolation, even if α and D_m are unknown, provided it is a limiting case where either mechanical dispersion or molecular diffusion completely dominates. If $F_r(Q_0,T_0)$ or $F_c(Q_0,T_0)$ of some reference injection rate Q_0 and injection period T_0 is known, then the recovery efficiency for any Q,T can be approximated using

$$F_r(Q,T) = 1 - [1 - F_r(Q_0,T_0)]\left(\frac{Q}{Q_0}\right)^x\left(\frac{T}{T_0}\right)^y. \tag{4.24a}$$

$$F_c(Q,T) = 1 - [1 - F_c(Q_0,T_0)]\left(\frac{Q}{Q_0}\right)^x\left(\frac{T}{T_0}\right)^y. \tag{4.24b}$$

Figure 4.2c shows a good agreement for the single cycle recovery efficiency F_r, and Figure 4.2d for the cumulative recovery efficiency F_c after 50 cycles. A comparison of Figure 4.2c and Figure 4.2d suggests that the accuracy of the extrapolation improves as the number of elapsed cycles increases. Here too, the solution is inaccurate in 3D scenarios where molecular diffusion dominate, but (4.24) nevertheless reveals the qualitatively valid outcome that F_r decreases as T increases.

A retardation factor representing linear adsorption implies a linear re-scaling of time. Thus, for a fixed injection duration T, an increase in the retardation factor implies a decrease in recovery for scenarios where $y < 0$, and vice versa. This means that the linear retardation of diffusion-dominated transport hinders recovery in 1D flow fields, has no effect in 2D flow fields, and enhances recovery in 3D flow fields.

4.4.3 Multiple cycles

Consider a scenario in which the total operational duration of the injection-extraction well is prescribed, whereas the total number of cycles N is a variable. Assume that one standard cycle operated with an injection duration of T_0 results in a total solute mass loss of $m_c(T = T_0, N = 1) = m_{0,0}$. In the low frequency multiple cycle scenario ($T = nT_0, N = 1$), where $n > 1$ is an arbitrary integer, the total solute mass loss is $m_{n,0} = n^y m_{0,0}$. The high frequency multiple cycle case is ($T = T_0, N = n$), and has an identical total duration as the low frequency multiple cycle case. We approach the high frequency case by first assuming that $m_{0,n} = (n)^z m_{0,0}$, where z is a constant. Then, the upper bound of the cycle exponent z can be inferred by assuming that $c(r) = 0$ at the onset of each new cycle, whereupon $m_{0,n} = nm_{0,0}$ exactly, and $z = 1$. If this assumption is omitted, then $m_{0,n} < (n)^z m_{0,0}$, thus we can conclude $z < 1$.

A lower bound for z is found if after the first injection phase, the boundary condition at the well is $\left(\frac{\partial c}{\partial r}(0,t) = 0\right)$ instead of $(c(0,t) = c_0)$, so that previously extracted water is re-injected, without mixing in the well. In this case, multiplying the number of cycles by n implies that ω is also multiplied by n, which yields $m_{0,n} = \sqrt{n} m_{0,0}$, or $z = 1/2$. Under the original boundary condition $(c(0,t) = c_0)$, new solute is injected into the system, therefore $z > 1/2$ necessarily.

In summary, we have found for the cycle exponent that $\frac{1}{2} < z \leq 1$. Using $m_{0,n} = n^z m_{0,0}$, we obtain the recovery efficiency of the n-th cycle

$$F_r(h) = 1 - \frac{m_{0,0} n^z}{M_{0,0} n} = 1 - \left(1 - F_{r,0}\right) n^{z-1}, \tag{4.25}$$

where $F_{r,0}$ is the recovery efficiency of the first cycle. Numerical results using empirically fitted z agree excellently with (4.25) (Figure 4.3), and fitted z values fall within the bounds predicted $\frac{1}{2} \leq z \leq 1$. Figure 4.3 also shows that although the fitted value of z increases slightly with the number of cycles, the difference is small even when data from 5 and 50 cycles is compared. This shows the added value that only a minimal amount of data is required to empirically calibrate z.

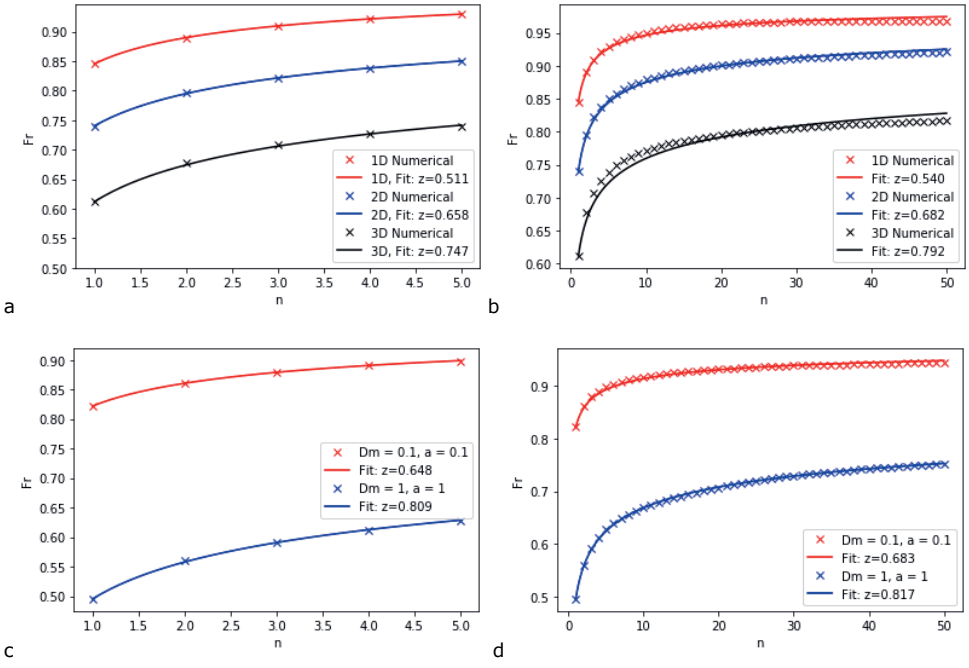

Figure 4.3: Recovery efficiency F_r as a function of the n-th cycle, fitted to (25) after (a,c) 5 cycles and (b,d) 50 cycles, showing the effect of (a,b) spatial dimensionality and (c,d) dispersion parameters in a 2D scenario.

The manner by which the upper and lower bounds for the cycle exponent z have been derived, suggest that z can be interpreted as a measure of how much the recovery efficiency of a cycle is affected by all preceding cycles. The larger the value of z, the smaller this memory effect. Figure 4.3 a,b illustrates this, showing that z increases as the spatial dimensionality increases. This occurs because in each subsequent cycle, the ambient chemical gradient enveloping the new injection water front dissipates more rapidly when the spatial dimensionality is large, thus weakening the memory effect. Similarly, Figure 4.3 c,d shows that a larger dispersion coefficient $D = D_m + \alpha v$ leads to faster dissipation of ambient solute, resulting in a larger z. Comparing all the scenarios shown in Figure 4.3 reveals that z is inversely related to F_r of the first cycle; this is logical in that a complete recovery implies no memory effect, and vice-versa.

Combining (4.24) and (4.25), $F_r(Q,T,n)$ can be extrapolated from a reference operation with known $F_r(Q_0,T_0,n_0)$, by using

$$F_r(Q,T,n) = 1 - [1 - F_r(Q_0,T_0,n_0)]\left(\frac{Q}{Q_0}\right)^x \left(\frac{T}{T_0}\right)^y \left(\frac{n}{n_0}\right)^{z-1}. \tag{4.26}$$

From (4.26), we can deduce how cycle frequency affects dispersive losses. If $y > z-1$, then high frequency operations under a prescribed total time result in larger F_r, and vice-versa. Since $z > 1/2$, it means that in 1D where $y = 1/2$, more dispersive losses occur for high than for low frequencies (Figure 4.4a). Since $z \leq 1$, it follows that for $y \geq 1$, more dispersive losses occur in low than for high frequencies. Therefore, for $D = D_m$ in 2D $(y = 1)$ (Figure 4.4b) and 3D $(y = 7/6)$ (Figure 4.4c), F_c decreases as T increases in the case of a fixed total time. This is in contrast with the case of $D = D_m$ for a fixed T, where F_c is independent of T in 2D, and decreases as T increases in 3D. If $y \approx z-1$, then recovery is roughly

independent of frequency; this is most likely to occur in general in 2D, where $-\frac{1}{4} \leq y \leq 0$ and $-\frac{1}{2} \leq z-1 \leq 0$, and the ranges of y and $z-1$ overlap closely (e.g. curves for $D=\alpha|v|$ in Figure 4.4b).

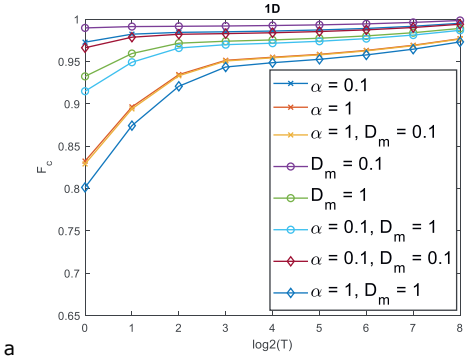

a

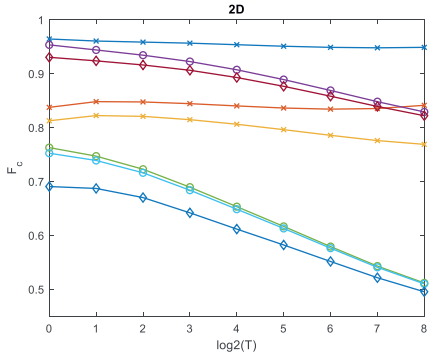

b

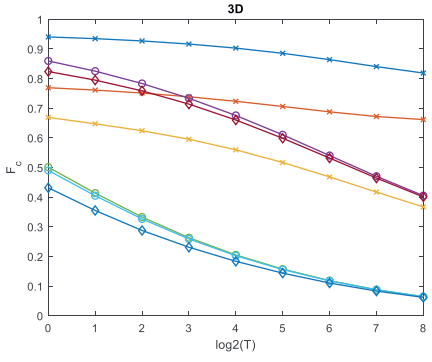

c

Figure 4.4: Numerical results for the variation of the cumulative recovery efficiency F_c against cycle period for fixed total time with $2nT = 512$ after 50 cycles, in a (a) 1D, (b) 2D, and (c) 3D homogeneous medium.

4.4.4 Kinetic dispersion factor

In $d = 1$, the velocity and hence hydrodynamic dispersion coefficient is the same everywhere. For $d > 1$, since $R \propto T^{1/d}$, the cycle period influences the relative lengths of time for which dispersive loss is primarily controlled by either mechanical dispersion or molecular diffusion. The relative contribution from mechanical dispersion $\alpha|v|$ to the dispersion coefficient $D = D_m + \alpha|v|$ decreases with R and $T^{1/d}$ as distance increases, because $|v|$ decreases with distance. Therefore, in $d > 1$, the dominant process of spreading of solutes around the plume front increasingly shifts towards molecular diffusion, with distance from the well. Field evidence has shown that thermal breakthrough curves are highly sensitive to mechanical dispersivity at early times of the injection phase, due to the large $v(R)$ associated with small plume volumes (Vandenbohede et al., 2011). This means that some ATES systems are controlled by mechanical disperson (Lin et al., 2019) although heat transport is predominantly controlled by thermal diffusion in uniform flow fields. Hence, it is important to be able to determine the relative strengths of diffusion and mechanical dispersion as a function of well operational parameters.

Dispersive losses attributable to $\alpha|v|$, relative to D_m, can be obtained by taking the ratio of their contributions to F_r in (4.21), and yields

$$\sqrt{S_T} = \sqrt{\frac{(3d-2)\alpha(A_d)^{\frac{3d-1}{d}}(Td)^{\frac{2d-1}{d}}}{(2d-1)D_m(A_d)^{\frac{3d-2}{d}}(Td)^{\frac{3d-2}{d}}}}. \tag{4.27}$$

where we introduce the dimensionless kinetic dispersion factor S_T. Writing this in terms of $v(R)$ yields

$$S_T = \frac{(3d-2)\alpha v(R)}{(2d-1)D_m}. \tag{4.28}$$

which is a weighted form of the ratio $\frac{\alpha v(R)}{D_m}$ of the components of $D(r) = D_m + \alpha v(R)$. The unweighted ratio omits the contribution of the term $(d-1)\frac{D_m}{r}\frac{\partial c}{\partial r}$ to the ADE (4.5). In 1D, $(d-1)\frac{D_m}{r}\frac{\partial c}{\partial r}$ vanishes and the weighted ratio becomes equal to the unweighted ratio. As spatial dimensionality increases, so does S_T, which suggests that the effects of velocity-dependent and velocity-independent dispersion are increasingly different in higher dimensional spaces. Expansions of S_T are presented in Table 4.3. Concepts similar to S_T have been used in prior studies to determine relative contributions of the dispersion processes in radial flow. Hoopes and Harleman (1967) obtained a weighted ratio, $\frac{4\alpha v(R)}{3D_m}$, which is (4.28) with $d = 2$ specifically, while Bloemendal and Hartog (2018) applied the unweighted ratio $\alpha v(R)/D_m$ to a two-dimensional radial problem, which underestimates the contribution of mechanical dispersion.

In 3D scenarios, $F_r(T)$ increases monotonically for $D = \alpha|v|$, yet decreases monotonically for $D = D_m$. Thus, a logical reason for the non-monotonicity of $F_r(T)$ in 3D (Figure 4.5a) is that the relative strengths of $\alpha|v|$ and D_m at the hydraulic front change with T. Solving $\frac{\partial F_r(T)}{\partial T} = 0$ in (4.21) yields $S_T = 1$; this agrees with the numerical results for F_r (Figure 4.5b). Therefore, the optimum period T_m that corresponds to the maximum $F_r(T)$ can be found by solving substituting $T = T_m$, $d = 3$, and $S_T = 1$ in (4.27), and solving for T_m:

$$T_m = \sqrt{\left(\frac{7\alpha}{5D_m}\right)^3 \frac{Q}{36\pi\theta}}. \tag{4.29}$$

(4.29) agrees excellently with numerical results for the first cycle (Figure 4.6). Empirically, we observe that F_c after 50 cycles also peaks close to $S_T = 1$ (Figure 4.5c). However, the presence of ambient solute in the aquifer causes (4.29) to overestimate T_m for multiple cycles (Figure 4.6), as only the first cycle

recovery efficiency was considered in deriving (4.29). Nevertheless, Figure 4.6 shows that the proportional relationship $T_m \propto \left(\frac{\alpha}{D_m}\right)^{3/2}$ remains valid even after 50 cycles.

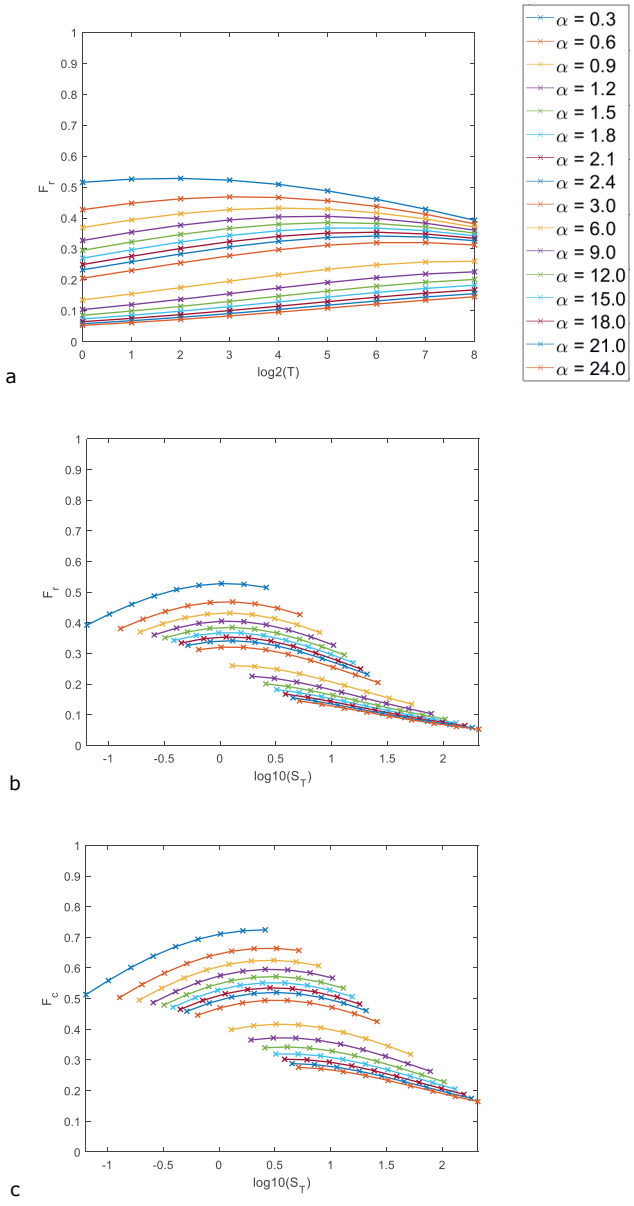

Figure 4.5: The relationship between (a) T and F_r for the first cycle, (b) S_T and F_r for the first cycle, and (c) S_T and F_c after 50 cycles, for 3D injection-extraction from a point source; $D_m = 0.1$.

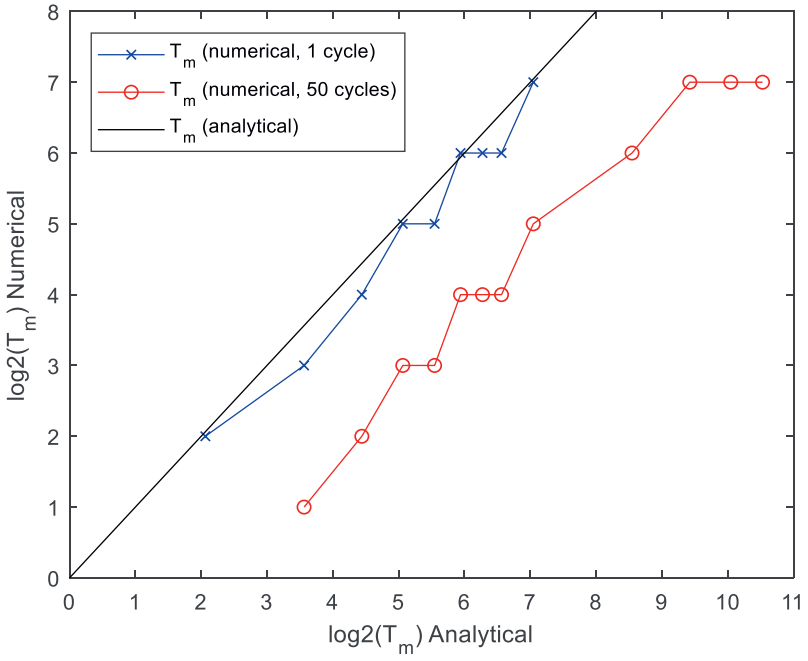

Figure 4.6: The numerically obtained and analytically approximated (Eq. 35) optimum cycle period T_m, corresponding to (crosses) maximum F_r for the first 1 cycle, and (circles) maximum F_c after 50 cycles.

4.4.5 Geometric dispersion factor

Recall that $A_d \propto Q$. The area-to-volume ratio (A/V), which was previously discussed in the introduction, is

$$\frac{A}{V} = \frac{d}{(dA_d T)^{\frac{1}{d}}} \propto (QT)^{-\frac{1}{d}}, \tag{4.30}$$

which suggests that either Q or T should be maximized, to minimize losses through the surface area.

While A/V is identical for any combination of Q and T that yield identical QT, the recovery efficiency can significantly differ for different combinations of Q and T. Doughty et al (1982) found that when the total solute mass injected $c_0 QT$ was kept constant, in a system with $D = D_m$, the recovery efficiency was higher under large Q small T operation, than under small Q large T operation. Bloemendal and Hartog (2018) investigated heat storage in a system with a 2D flow field. They concluded from sensitivity analyses of Q that $1 - F_r \propto A/V$ approximately when thermal diffusion dominates, which agrees superficially with our findings for 2D flow fields that $1 - F_r \propto Q^{-\frac{1}{2}} T^0$ (Equation 4.23), because $A/V \propto (QT)^{-\frac{1}{2}}$. Since T was not tested, framing the solution in terms of A/V might lead to ambiguity in interpretation. The principle behind A/V does not consider that the rate of velocity dependent and independent dispersive loss depend differently on plume area and volume, and flow field dimensionality.

The recovery efficiency can be expressed as a function of Q and T in the limiting cases previously discussed where a single dispersion process dominates, namely $1 - F_r \propto Q^x T^y$ (4.22 – 4.23), which is

similar in form to $A/V \propto (QT)^{-\frac{1}{d}}$. Therefore, as an alternative to A/V, we propose the geometric dispersion factor G:

$$G = Q^x T^y, \tag{4.31}$$

The curves in Figure 4.2a and Figure 4.2b for scenarios with a single dominant dispersion process illustrate the dependence of G on T and Q respectively. Unlike A/V, the exponents of Q and T in G are not necessarily identical. Essentially, G generalizes A/V, by considering spatio-temporal (as opposed to solely spatial) interactions between plume geometry and hydrodynamic dispersion. Table 4.2 shows that G is a function of A/V, namely $G \propto \sqrt{A/V}$, only when the velocity-independent dispersion process is omitted. Hence, G should replace A/V in the characterization of aquifer-well systems, as it provides deeper insight into how recovery varies with well operation parameters.

4.4.6 Production and recovery

By substituting (4.12) into (4.13), and using the form of ω appropriate for the extraction phase (Gelhar and Collins, 1971),

$$\omega = \int_0^{r_m} \frac{v(r) + D_m/\alpha}{v(r)^3} dr + \int_{r_m}^{r'} \frac{v(r) + D_m/\alpha}{-v(r)^3} dr \tag{4.32}$$

the production concentration or temperature at the well during the extraction phase $c(r = 0, t > T)$ is found to be

$$c = \frac{1}{2} c_0 \operatorname{erfc}\left[\frac{-[2T - t]}{\sqrt{4d^2\alpha}} \sqrt{\frac{(3d-2)(2d-1)\alpha A_d}{(3d-2)\alpha A_d (dA_d)^{\frac{-1}{d}} \left\{ 2T^{\frac{2d-1}{d}} - [2T-t]^{\frac{2d-1}{d}} \right\} + (2d-1) D_m (dA_d)^{\frac{d-2}{d}} \left\{ 2T^{\frac{3d-2}{d}} - [2T-t]^{\frac{3d-2}{d}} \right\}}} \right] \tag{4.33}$$

In order to analyze the production concentration and recovery efficiency in non-standard cycles where $\frac{V_{ex}}{V_{in}} \neq 1$ we seek to express (4.33) as a function of $V_{in} = QT$ and $V_{ex} = Q \cdot (t - T)$, where Q in (4.33) originates from A_d. This yields, for limiting case where $D = \alpha v$,

$$c(r = 0, t > T) = \frac{1}{2} c_0 \operatorname{erfc}\left[\left(\frac{V_{ex}}{V_{in}} - 1 \right) \left[\frac{V_{in} \Gamma\left(\frac{d}{2}\right) d}{2\theta \pi^{\frac{d}{2}}} \right]^{\frac{1}{2d}} \sqrt{\frac{(2d-1)}{4d^2\alpha \left[2 - \left| 1 - \frac{V_{ex}}{V_{in}} \right|^{\frac{d-1}{d}} \left(1 - \frac{V_{ex}}{V_{in}} \right) \right]}} \right]. \tag{4.34a}$$

where the absolute function ensures that $c(r = 0, t > T)$ remains real and continuous for $V_{ex} \geq V_{in}$. For the opposite limiting case, when $D = D_m$,

$$c(r = 0, t > T) = \frac{1}{2} c_0 \operatorname{erfc}\left[\left(\frac{V_{ex}}{V_{in}} - 1 \right) \left[\frac{V_{in} \Gamma\left(\frac{d}{2}\right) d}{2\theta \pi^{\frac{d}{2}}} \right]^{\frac{2-d}{2d}} \sqrt{\frac{(3d-2) A_d}{4d^2 D_m \left\{ 2 - \left| 1 - \frac{V_{ex}}{V_{in}} \right|^{\frac{2d-2}{d}} \left(1 - \frac{V_{ex}}{V_{in}} \right) \right\}}} \right]. \tag{4.34b}$$

We can rewrite the production concentrations of the two limiting cases (4.34) in the form

$$c\left(r=0,\frac{V_{ex}}{V_{in}}\right)=\frac{1}{2}c_0\,\mathrm{erfc}\left[\zeta\frac{\left(\frac{V_{ex}}{V_{in}}-1\right)}{\sqrt{\left\{2-\left|1-\frac{V_{ex}}{V_{in}}\right|^{\Delta}\left(1-\frac{V_{ex}}{V_{in}}\right)\right\}}}\right], \tag{4.35}$$

where the exponent Δ ranges from $0\leq\Delta\leq\frac{4}{3}$ depending on the spatial dimensionality and dominant hydrodynamic dispersion process, and the other terms are lumped into the constant ζ for readability. Figure 4.7a shows that for a fixed value of ζ, the influence of varying the exponent Δ on the production concentration is negligible. Therefore, $\frac{V_{ex}}{V_{in}}$ is effectively the only independent variable in (4.35) if ζ is fixed. Physically, this implies that at any given production concentration, the marginal effect on the production concentration of increasing $\frac{V_{ex}}{V_{in}}$ is almost independent of flow field dimensionality and the dominant hydrodynamic dispersion process. Therefore, the recovery efficiency as a function of $\frac{V_{ex}}{V_{in}}$ can be obtained by numerically integrating (4.35) with respect to $\frac{V_{ex}}{V_{in}}$, the outcomes of which for $\Delta=\frac{1}{2}$ are shown in Figure 4.7b.

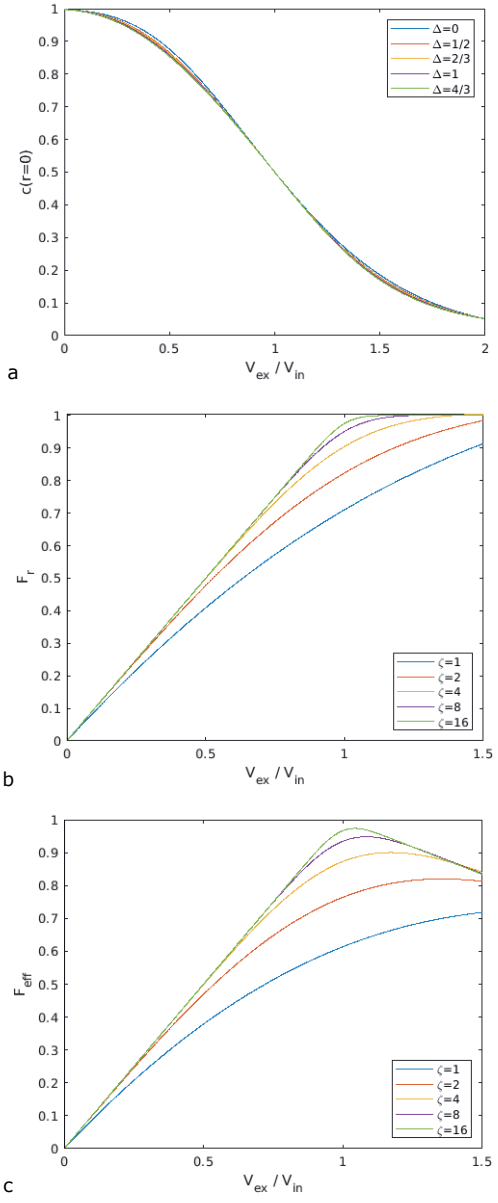

Figure 4.7: (a) Production concentration $c(r=0)$ against the extraction ratio $\frac{V_{ex}}{V_{in}}$ when $\zeta = 2$. (b) Recovery efficiency F_r against $\frac{V_{ex}}{V_{in}}$, for $\Delta = \frac{1}{2}$. (c) Effective recovery efficiency F_{eff} against $\frac{V_{ex}}{V_{in}}$ for $c_{crit} = \frac{1}{4}c_0$.

The concavity of the curves in Figure 4.7b implies that the marginal benefit to F_r of increasing $\frac{V_{ex}}{V_{in}}$, has diminishing returns in all cases. Where ζ is small (e.g. 3D scenarios, or scenarios with large D), F_r of a symmetric cycle $\frac{V_{ex}}{V_{in}} = 1$ is small. In these cases, using a longer extraction period $\frac{V_{ex}}{V_{in}} > 1$ can increase F_r significantly (Figure 4.7b), because there remains relatively large amounts of solute mass deposited

immediately outside the hydraulic front. However, where ζ is large, the marginal benefit to F_r is small when $\frac{V_{ex}}{V_{in}}$ is increased beyond 1. This agrees with Sauty et al's (1982) conclusion that symmetric cycles yield an optimum balance between cost (V_{ex}) and benefit (F_r).

In some applications, the recovered hot water in ATES is too cold for heating, or in ASR is of marginal quality for drinking or irrigation, if the production concentration or temperature falls below a critical value c_{crit}. Hence, we may define the effective recovery efficiency as

$$F_{eff} = \frac{\int [c(r=0) - c_{crit}] dV_{ex}}{(c_0 - c_{crit}) V_{in}}. \tag{4.36}$$

An example F_{eff} as a function of $\frac{V_{ex}}{V_{in}}$, solved numerically, is presented in Figure 4.7c, with $\Delta = \frac{1}{2}$ and $c_{crit} = \frac{1}{4}c_0$. If $\frac{V_{ex}}{V_{in}} = 1$, then F_{eff} is simply equal to $\frac{F_r - (c_{crit}/c_0)}{1-(c_{crit}/c_0)}$. Once $c(r=0, t>T) < c_{crit}$, extraction should cease, because the remaining water is unusable and the marginal benefit of increasing $\frac{V_{ex}}{V_{in}}$ becomes negative. Extraction of additional water beyond this point will degrade the quality of the earlier extracted water, if they mix. The marginal benefit to F_{eff}, of increasing $\frac{V_{ex}}{V_{in}}$, becomes smaller for larger c_{crit}, because $[c(r=0) - c_{crit}]$ monotonically decreases as c_{crit} increases. These diminishing returns can become negative returns if c_{crit} is non-zero, as illustrated in Figure 4.7c.

4.4.7 Generalizations

Since all derived expressions (i.e. F_r, S_T, G) can be written as functions of d, the preceding analyses can be generalized to non-integer dimensions. Non-integer dimensions are primarily used to describe porous media with fractal pore-scale geometry. Dispersive transport in fractal geometry is a distinct aspect of research into pore-scale connectivity and percolation (Bouchard & Georgess, 1990), fractured porous media (Sahimi, 2011), and multi-phase transport (Hunt et al., 2014). Figure 4.8a shows that if all other parameters are kept constant, the recovery efficiency mostly decreases monotonically as dimensionality increases. Interestingly however, in the range of small d and small Q, $F_r(d)$ is non-monotonic, with a maximum. Whether this non-monotonicity, and non-integer dimensional radial flow in general, describe meaningful physical phenomena, or are mathematical artefacts, remains to be investigated. Figure 4.8b shows that curves of $F_r(d)$ for different T intersect at some point at $d > 2$. This implies that $F_r(T)$ can be non-monotonic in any $d > 2$; amongst all model parameters, such behavior is unique to T. In Section 4.4.2, we discussed $d = 3$, a specific instance of this.

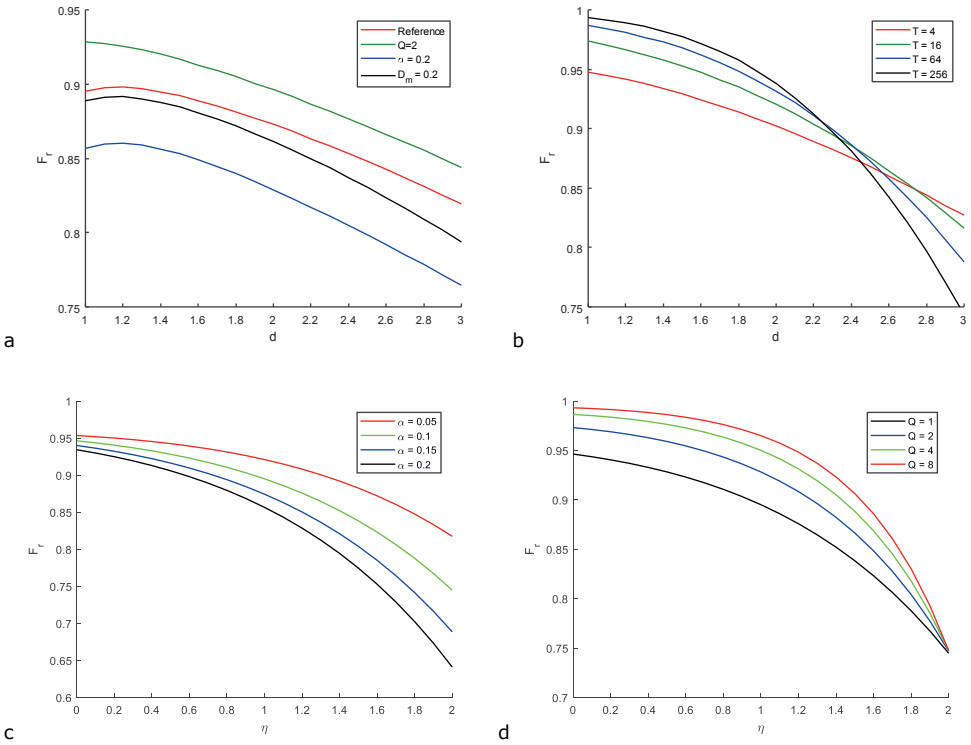

Figure 4.8: Recovery as a function of d when (a) Q, α, D_m is varied, and (b) T is varied. Recovery as a function of η, when (c) α is varied, and (d) Q is varied. Unless otherwise specified, $\eta = 1$, $d = 1$, $T = 1$, $Q = 1$, $\alpha = 0.1$, $D_m = 0.1$.

Analyses under other definitions of hydrodynamic dispersion are also possible, using the methods we have presented. For example, power-law mechanical dispersion $\alpha|v^\eta|$, with $0 \le \eta \le 2$ not necessarily an integer. Molecular diffusion corresponds to $\eta = 0$, and standard mechanical dispersion to $\eta = 1$. Other suggested values of η include η~1.2 for Peclet numbers $5 < Pe < 300$ (Sahimi., 1993), η~1.25 when large spatial variances exist in the pore-scale velocity field, (Salles et al., 1993), and $\eta = 2$ in media with solute particle traps (Bouchaud & Georges., 1990), Taylor dispersion (Taylor., 1953), or large tortuosities or low saturations (de Gennes, 1983). Salles et al (1993) also found that η varies continuously with porosity.

The generalized radially axisymmetric ADE for $D = D_m + \alpha|v^\eta|$ is (see Appendix A for derivation)

$$\frac{\partial c}{\partial t} = D(r)\frac{\partial^2 c}{\partial r^2} + \left[\frac{(d-1)}{r}[D_m - (\eta-1)\alpha v^\eta] - v(r)\right]\frac{\partial c}{\partial r}. \tag{4.37}$$

Then, applying the same steps as in Section 4.3 and Section 4.4.1, with $\omega = \int_0^{r'} \frac{v^\eta(r) + D_m/\alpha}{v^3(r)} dr$, results in

$$c(r,t) = \frac{1}{2}c_0 \operatorname{erfc}\left[\frac{\left(r^d - (dA_d t)\right)}{\sqrt{4d^2\alpha(dA_d t)^{\frac{2d-1}{d}}}}\sqrt{\frac{(3d-2)(3d-2+\eta-\eta d)\alpha A_d}{(3d-2)\alpha A_d^\eta (dA_d t)^{\frac{\eta+d-1-\eta d}{d}} + (3d-2+\eta-\eta d)D_m (dA_d t)^{\frac{d-1}{d}}}}\right]. \tag{4.38}$$

If $\eta = 2, D_m = 0$ is substituted into (4.38), the solutions for $c(r,t)$ in 1D, 2D and 3D found by Philip (1994) are recovered (see Table 4.2), with two differences. Philip's exact solutions include an additional term that vanishes for large Q or t, and Philip imposed Robin boundary conditions at the well, whereas we use Dirichlet boundary conditions. Differences in outcomes originating from different boundary conditions also vanish rapidly as t (Philip, 1994; Chen, 1987) or Q (Aichi & Akitaya, 2018) increases.

The generalized exponents in the geometric dispersion factor $G = Q^x T^y$ are

$$x = [\eta - 2]\left(\frac{1}{2d}\right), \tag{4.39}$$

$$y = \frac{(d-1)[1-\eta]-1}{2d}. \tag{4.40}$$

Full expansions of $F_r(\eta = 2)$ and $F_r(d,\eta)$ and the corresponding kinetic dispersion factors, derived from (4.38) in the same manner as in Section 4.4.1 and Section 4.4.2, are available in Table 4.3. Figure 4.8c and 4.8d illustrate the behavior of $F_r(\eta)$ when α and Q respectively are varied. Remarkably, when $\eta = 2$ and $D = \alpha|v^\eta|$, $1 - F_r \propto T^{-1/2}$ regardless of spatial dimensionality, and recovery is independent of the injection rate. Comparing (4.39) and (4.40) reveals an additional limitation of the area-to-volume ratio: F_r is a function of A/V (i.e. $x = y$) only when $D = \alpha|v|$, and never for $D = \alpha|v^\eta|$ with any $\eta \neq 1$. Furthermore, when $D = \alpha|v^\eta|$ with $d = \frac{2-\eta}{1-\eta}$, then $1 - F_r \propto Q^{\frac{\eta-2}{2d}}$, and recovery is independent of the injection period. In Section 4.2, we discussed a specific instance of this, namely $d = 2,\ \eta = 0$.

4.5 Discussion

Our more general results agree with specific scenarios discussed in the literature. Several numerical studies (e.g. Bakker, 2010; Lu et al., 2011; Chen, 2014; Barker et al., 2016; Majumdar et al., 2021) showed that in 2D and with $D_m = 0$, the recovery efficiency can be increased by increasing the injection period, or the injection rate, which agrees with the exponents we found for the geometric dispersion factor G. The fact that the recovery efficiency increases as Q or T increases for $d = 2$ has also been observed in practice (e.g. Bloemendal and Hartog, 2018; Kastner et al., 2017). Bakker (2010) modelled an ASR system in a 2D cylindrical flow field in a homogeneous medium, and investigated how varying the injection and storage duration affected the recovery efficiency of freshwater. They demonstrated that the recovery efficiency increases sub-linearly with the number of cycles. The sub-linear increase of the recovery efficiency with cycle number was also observed in practice (Bakr et al., 2013; Kastner et al., 2017) and in other numerical studies (Sommer et al., 2013; Zeghici et al., 2015; Lu et al., 2011; Majumdar et al., 2021). These findings in the literature agree with the bounds we derived for the cycle exponent, $\frac{1}{2} \leq z \leq 1$.

It is possible for a single well to function both as an ATES (heat storage) and ASR (freshwater storage in a brackish aquifer) system simultaneously (Miotlinski and Dillon, 2015). Given that, as previously elaborated, heat spreading is primarily controlled by thermal conduction while solute spreading depends mostly on mechanical dispersion, the optimal operational parameters of the well for recovering heat and solutes will differ. When spreading occurs in three dimensions, increasing T might increase the recovery efficiency of freshwater, but decrease that of heat. Therefore, it is impossible to optimize for the recovery efficiency for both heat and solutes simultaneously.

Single well push-pull tracer tests are often used to determine various hydrogeological properties of aquifers, such as porosity (Hall et al., 1991), in-situ microbial activity (Istok et al., 1997), fracture geometry (Klepikova et al., 2016), and geochemical reaction rates (Haggerty et al., 1998), by

interpreting breakthrough data at the well during the extraction phase (Schroth et al., 2000). Equations (4.33) and (4.35) may be used to interpret data from push-pull tests using the methodology of Schroth and Istok (2005). Schroth and Istok's results pertain only to solute transport in 2D and 3D radial flow fields with a more limited model of dispersion, defined as $D = \alpha|v|$, whereas our results apply to a wider range of dispersion models, and also in the presence of multiple coexisting dispersion mechanisms (e.g. $D = D_m + \alpha|v|$).

In this study, to enable an analytical approach, we omitted several aspects. These include heterogeneity in aquifer physical properties, background regional flow, diffusion of heat and solute into confining layers, density driven convection. Nevertheless, these omissions do not negatively affect the ability of simple approximate analyses like that discussed in this study from accurately predicting the behavior of well-aquifer systems under a wide range of realistic conditions (Pophillat et al., 2020a). The assumption of homogeneity has been found to be appropriate for aquifers where the log-conductivity field is autocorrelated and has a variance smaller than 0.25 (Wang et al., 2018). In some systems, the injection and extraction regimes are separated by a stand still storage phase, thus some adaptation may be needed if the velocity-independent component of hydrodynamic dispersion is significant and if the storage phase is long. With low or no regional groundwater flow, the storage period reduces the recovery efficiency by only around 0.5 percentage points per month (Majumdar et al., 2021), and thus has minimal impact. All of these omitted factors would cause a decrease in the recovery efficiency, if they were accounted for. Therefore, our analysis forms a theoretical upper bound of the recovery efficiency of some real applications.

Witt et al (2021) presented injection-extraction experiments of density driven flow with several fully-penetrating and partially-penetrating well configurations, where freshwater was injected into a laboratory-scale brackish aquifer. Experimentally, doubling the injection-extraction rate and halving the injection-extraction duration (maintaining the total volume) led to an increase in recovery efficiency. For three well shapes that create 2D radial flow fields, the recovery efficiency increases they observed were from 0.39 to 0.55, 0.40 to 0.61, and 0.55 to 0.69. They calibrated the hydrogeological parameters based on experimental data, yielding $D_m = 8.8 \cdot 10^{-8} m/min$ and $\alpha = 7 \cdot 10^{-3} m$. With injection rates around $2 \cdot 10^{-6} m^3/min$ to $5 \cdot 10^{-6} m^3/min$, and injection durations of around 60 minutes, we obtain $S_T = 28$. This value suggests that mechanical dispersion dominates over molecular diffusion. However, they also noted that density driven convection dominated over hydrodynamic mixing in the transport of the salinity gradient. Hence the effect of hydrodynamic dispersion was weaker than that of density driven convection. When we insert their hydrogeological parameters into our equation (4.26), and set $x = -1/2$, $y = 0$ to account for velocity-independent spreading in 2D, the calculated increases in recovery efficiency would be from 0.39 to 0.57, 0.40 to 0.58, and 0.55 to 0.69, which agrees almost exactly with their experimental results. Our power-law relationship between number of cycles and recovery efficiency also agrees well with their results, which show diminishing marginal returns as the number of cycles increases (compare our Figure 4.3 with Witt et al's Figure 9). The agreement between our results for spreading under molecular diffusion, and their results for density driven convection, suggests that the effects of density driven convection on recovery efficiencies, might be similar to the effects of molecular diffusion in some idealized problems. This is possibly because density driven convection is a form of velocity-independent spreading (at these low viscosities) that results in a radial plume shape (i.e. conical shape, see Witt et al's Figure 2h).

The modelled flow field geometries often arise as small or large time limiting cases in other flow field geometries. For example, a point source in a typical vertically confined aquifer generates a 3D spherical solute plume at small times, and a 2D spherical solute plume (i.e. cylindrical) at large times when the size of the plume has grown large (e.g. Schroth and Istok, 2005). From field data, Bloemendal and Hartog (2018) found that when the outlet screen height of a fully penetrating well in a confined aquifer is

reduced, the recovery efficiency of heat decreases. This is because the flow field of a non-fully-penetrating well is three-dimensional at small times, and that losses are larger when spatial dimensionality d increases (see Equation 4.21). For space-use efficiency, often multiple wells are spatially distributed in a single large aquifer, such as with zonation patterns (e.g. Sommer et al., 2015). In such implementations, the dimensionality of the flow field essentially depends on whether the neighboring wells mutually interfere (Kandelous et al., 2011), thus a transitional time scale also exists for such systems.

During transitional regimes when solute plumes transition from, for example, a 3D to 2D geometry, the dispersive behavior is bounded by the solutions for 2D and 3D systems. This is because the radial velocity of the plume front, which affects the plume size, surface area, and mechanical dispersion, is bounded from above by the 2D solution, and from below by the 3D solution. Consequently, it appears plausible that a mathematical description of dispersion and recovery during transitional times can be obtained by setting $2 < d < 3$ in the analysis, and is a topic for further research. If and only if $d > 2$, the recovery efficiency varies non-monotonically with well parameters, and retardation may increase the recovery efficiency instead of decreasing it. Hence, systems that undergo transitional regimes experience profound differences in parameter sensitivity across the small, transitional, and large time scales.

4.6 Conclusions

In our analysis, we approximated solute and heat transport, towards the recovery efficiency of injected solute and heat in 1D, 2D, and 3D homogeneous aquifers under cyclic radial flow. These new analytical solutions are broadly applicable in sensitivity analyses, as they comprise simple closed-form expressions. These expressions enable to determine the effect on the recovery efficiency of varying the: (i) mechanical dispersion and diffusion parameters, (ii) aquifer hydrogeological parameters, (iii) injection and extraction duration, (iv) injection and extraction rate, (v) flow field geometry, (vi) number of operating cycles and (vii) extraction volume relative to injection volume. Hence, a first-order assessment of aquifer-well systems can be conducted with minimal computational demand, e.g. to pave the way for further focussed evaluations with numerical modelling or exact analyses, by enabling the identification of interesting regions in parameter space. As discussed, our solutions are in broad agreement with various analytical, experimental, and numerical modelling studies in the literature.

Key factors that determine the recovery efficiency are the flow field geometry, and whether mechanical dispersion or diffusion dominates. Whereas in 1D and 2D flow fields, recovery efficiency is a non-decreasing function of the injection-extraction duration and rate, in 3D flow fields, it increases with the duration of the cycle when velocity-dependent mechanical dispersion dominates, but decreases if velocity-independent diffusion dominates. Consequently, if velocity-dependent and independent dispersion are of comparable magnitude in 3D spreading, recovery varies with cycle duration non-monotonically, peaking at a maximum. Therefore, as solute and heat injection/extraction are dominated by different dispersion processes, it may be impossible to optimize for the recovery efficiency of both simultaneously. Another consequence is that that when diffusion dominates over mechanical dispersion, chemical or thermal retardation leads to decreased recovery in 1D and 2D flow fields, but increased recovery in 3D flow fields. We generalized this to non-integer dimensional flow fields, and for mechanical dispersion processes that have an arbitrary power-law dependence on advection velocity.

As the sensitivity of the recovery efficiency to parameters is highly dependent on the dominant dispersion process, we introduce the kinetic dispersion factor, for identifying the dominant dispersion process. We also introduce the geometric dispersion factor, a simplified form of our full solution for recovery efficiency, that applies if the spreading of solutes or heat may be described by a single

dispersion process. We show that the classical Area-to-Volume ratio is a special case of the geometric dispersion factor that characterizes the recovery efficiency only in the specific scenario where mechanical dispersion with linear velocity dependence is the sole mechanism of spreading.

Appendix A: Derivation of the Advection-Dispersion Equation for Nonlinear Mechanical Dispersion

To derive the ADE for the generalized power-law dispersion case $D(r) = D_m + \alpha v^{\eta}(r)$, we begin from a modified form of Equation 3 and Equation 4 of Gelhar and Collins (1971):

$$\frac{\partial c}{\partial t} + v\frac{\partial c}{\partial r} = \frac{\alpha}{h_2 h_3}\frac{\partial}{\partial r}\left[h_2 h_3 v^{\eta}\frac{\partial c}{\partial r}\right] + \frac{D_m}{h_2 h_3}\frac{\partial}{\partial r}\left[h_2 h_3 \frac{\partial c}{\partial r}\right], \quad (A1)$$

$$\frac{1}{h_2 h_3}\frac{\partial}{\partial r}[h_2 h_3 v] = 0, \quad (A2)$$

where h_2 and h_3 are scale factors of the curvilinear coordinates orthogonal to the primary coordinate r, and the condition (A2) implies the incompressibility of water.

Rewriting (A1) in the following form

$$\frac{\partial c}{\partial t} + v\frac{\partial c}{\partial r} = \frac{\alpha}{h_2 h_3}\frac{\partial}{\partial r}\left[h_2 h_3 v v^{\eta-1}\frac{\partial c}{\partial r}\right] + \frac{D_m}{h_2 h_3}\frac{\partial}{\partial r}\left[h_2 h_3 v \frac{1}{v}\frac{\partial c}{\partial r}\right] \quad (A3)$$

and substituting (A2) into (A3) yields

$$\frac{\partial c}{\partial t} + v\frac{\partial c}{\partial r} = \alpha v\frac{\partial}{\partial r}\left[v^{\eta-1}\frac{\partial c}{\partial r}\right] + D_m v\frac{\partial}{\partial r}\left[\frac{1}{v}\frac{\partial c}{\partial r}\right], \quad (A4)$$

which can be fully expanded to

$$\frac{\partial c}{\partial t} + v\frac{\partial c}{\partial r} = \alpha(\eta-1)v\frac{\partial c}{\partial r}\frac{\partial v}{\partial r}v^{\eta-2} + \alpha v^{\eta}\frac{\partial^2 c}{\partial r^2} + D_m v\left[\frac{1}{v}\frac{\partial^2 c}{\partial r^2} - \frac{1}{v^2}\frac{\partial v}{\partial r}\frac{\partial c}{\partial r}\right], \quad (A5)$$

Substituting the following into (A5) (see Section 3),

$$v(r,d) = \frac{A_d}{r^{d-1}},$$

$$\frac{\partial v}{\partial r} = (1-d)\frac{A_d}{r^d} = (1-d)\frac{v}{r},$$

yields the general ADE (37):

$$\frac{\partial c}{\partial t} = D(r)\frac{\partial^2 c}{\partial r^2} + \left[\frac{(d-1)}{r}[D_m - (\eta-1)\alpha v^{\eta}] - v(r)\right]\frac{\partial c}{\partial r}. \quad (A6)$$

Setting $\eta = 1$ recovers the specific case described in (5), where $D(r) = D_m + \alpha v(r)$.

Chapter 5

Macrodispersion and Recovery of Solutes and Heat in Heterogeneous Aquifers

Based on:

Tang, D. W. S., & Van Der Zee, S. E. A. T. M. (2022). Macrodispersion and Recovery of Solutes and Heat in Heterogeneous Aquifers. Water Resources Research, 58(2), e2021WR030920.

Abstract

The recovery efficiency of aquifer storage systems with radial flow fields are studied for heterogeneous aquifers. Macrodispersion, arising from spatially heterogeneous hydraulic conductivity, is modelled as a scale-dependent mechanical dispersion process. Approximate solutions for the recovery efficiency as a function of local dispersion and macrodispersion parameters, the injection-extraction rate Q and duration T, and storage cycle count, are derived and validated against numerical simulations. If macrodispersion dominates and the macrodispersion coefficient scales linearly with distance, the recovery efficiency is independent of both Q,T. For sublinear and superlinear scalings, recovery increases and decreases respectively if Q,T increases. However, if local dispersion dominates, increasing Q,T always increases recovery. As macrodispersion becomes increasingly dominant with scale, the recovery efficiency may be a non-monotonic function of Q,T – with a maximum. In homogeneous aquifers, non-monotonicity does not occur for 1D and 2D radial flow, but occurs for 3D radial flow fields only as a function of T, not Q. These methods may also be used for fitting local dispersion and macrodispersion parameters with push-pull tests using recovery data, with advantages in scope of applicability and ease of data acquisition and interpretation, compared to existing push-pull test methods, which fit to breakthrough curves and do not consider macrodispersion. Furthermore, characterizing macrodispersion with push-pull tests may be advantageous over methods that use observation wells, as observation well placement may be challenging in highly heterogeneous aquifers. The results show that the macrodispersion parameters are not innate aquifer hydraulic properties, as their values vary with flow field geometry.

5.1. Introduction

Wells in groundwater aquifers are used in cyclic injection-extraction processes, otherwise named push-pull processes, in a variety of applications related to the storage of water of some particular quality (Dillon et al., 2019). Examples include fresh water supplies that are of drinking or irrigation quality, and hot or cold water to be used for indoor heating or cooling. Water that is stored in an open environment, such as within a dam or reservoir, will interact with the atmosphere and surface runoff, thereby gradually diminishing its thermal quality through heat exchange, and its chemical quality through contamination with environmental aerosols, soluble gases, and runoff of marginal quality. This has led to a pressing need for research into efficient means of large capacity seasonal thermal (Rad & Fung, 2016) and freshwater (Misssimer et al., 1992) storage, amongst which geological storage exhibits the most immediate economic potential and technological feasibility (Xu et al., 2014; Misssimer et al., 2012). Confined groundwater aquifers, which permit minimal interaction between groundwater and the external environment (e.g. the vadose zone and the atmosphere), are increasingly being used as geological storage vessels for water. Aquifer Thermal Energy Storage (ATES) (Fleuchaus et al., 2018) and Aquifer Storage and Recovery (ASR) (Pyne, 2017) are two aquifer storage technologies currently in widespread usage for the storage of heat and freshwater, respectively.

A crucial performance metric of an aquifer storage system is the recovery efficiency of the injected solutes or thermal gradient, which is the fraction of injected solutes or heat that can be recovered at the end of a storage cycle. During the injection and extraction phases, solutes and/or heat spread around the injected water front due to hydrodynamic dispersion processes. Local hydrodynamic dispersion, which governs the rate of dispersive losses, comprises the flow velocity-dependent mechanical dispersion, and the flow velocity-independent molecular or thermal diffusion (for solutes and heat, respectively). For storage systems in homogeneous aquifers, the dependence of the recovery efficiency on hydrodynamic dispersion parameters, well operational parameters, and flow field geometry were analyzed in chapter 4. In heterogeneous aquifers, with a spatially heterogeneous distribution of the hydraulic conductivity, an additional mechanism of dispersion has to be considered, namely macrodispersion.

Heterogeneity creates preferential flow paths that bypasses some of the surrounding aquifer, leading to a larger interface between injected and ambient water, which increases the area-to-volume ratio (A/V) of the injected plume. As dispersive losses occur through the surface of the injected plume that comes into direct contact of ambient water, the surface area of the injected body of water affects the magnitude of spreading due to local dispersion (Kitanidis, 1994). In homogeneous aquifers, a larger injected volume corresponds to a smaller A/V. Accordingly, in most cases dispersive losses decrease as the injected volume increases (chapter 4). In heterogeneous aquifers, where flow fields are nonuniform, a larger injected volume might increase the number and the extent of the preferential flow channels, thereby increasing A/V. Spatially nonuniform solute advection, caused by the heterogeneous flow field, is described in the literature as macrodispersion. Macrodispersion increases A/V, which thereby enhances local dispersion, resulting in increased plume spreading.

Prior studies characterized solute and heat spreading in random autocorrelated heterogeneous aquifers with solute mass moments and ensemble statistics (e.g. Dagan, 1988; Indelman and Dagan, 1999; Indelman, 2004). Deterministic mathematical analyses of concentration distributions in heterogeneous aquifers are seldom possible, except for the simplest heterogeneity structures such as one-dimensional flow in layered aquifers (e.g. Lauwerier 1955; van Duijn and van der Zee, 1986; Leij et al, 1991; Jury and Utermann, 1992; Zhan et al, 2009). Despite these difficulties in characterizing the concentration distributions, the recovery efficiency may be more easily characterized, as it is related to the concentration profile's zeroth spatial moment.

In the existing literature, no general analysis of the effects of heterogeneity on recovery efficiency is available. Studies employing numerical simulations have reported that heterogeneity results in significantly greater dispersive losses in ASR systems (e.g. Maliva et al., 2019; Maliva et al., 2006; Guo et al, 2015) and ATES systems (e.g. Winterleitner et al., 2018; Visser et al., 2015; Possemiers et al., 2015; Sommer et al., 2013; Ferguson, 2007). However, numerical simulations are computationally intensive, especially for heterogeneous aquifers, and their output is highly situation-specific and not easily generalized. Our aim is thus a general analysis of the recovery efficiency as affected by aquifer heterogeneity. In section 5.2, the problem is defined in detail, and our methods and approach are presented. In section 5.3, we develop an general analytical expression that relates the recovery efficiency of aquifer storage systems to the parameters related to dispersion, aquifer properties, flow field geometry, and well operation. In section 5.4.1 to 5.4.3, the expression is verified with numerical simulations, and the relationships between the simulation parameters and the fitted macrodispersion parameters are verified against existing literature. In section 5.4.4, we discuss the application of the methods introduced in this paper to push-pull tests. In section 5.4.5, we derive and verify the relationship between the number of storage cycles and F_r.

5.2. Methods

5.2.1 Problem statement

We use solute transport terminology, but note that the analysis is mathematically analogous and fully applicable to heat transport (Lee., 1998): molecular diffusion in solute transport is equivalent to thermal diffusion in heat transport, while mechanical dispersion applies similarly to both heat and solute transport. Linear chemical and thermal retardation, that occur when solutes adsorb onto the pore matrix, and when the heat capacity of the solid and liquid phases differ, respectively, are implicitly considered as both can be captured through a linear rescaling of time.

Consider the geometry of flow fields originating from wells in homogeneous aquifers with negligible background flow. The flow fields investigated in this study are the d-dimensional spheres. A commonly studied conceptualization of ASR and ATES is that of a fully penetrating well in a confined aquifer, corresponding to a cylindrical flow field. Since the well is fully penetrating, the cylindrical flow field is equivalent to a disc-shaped field, which is a 2D sphere. Figure 5.1 illustrates that other radially axisymmetric macroscopic flow field configurations are possible in a 3D space: unidirectional planar flow is a 1D radial flow field, while spherical flow from a point source is a 3D radial flow field.

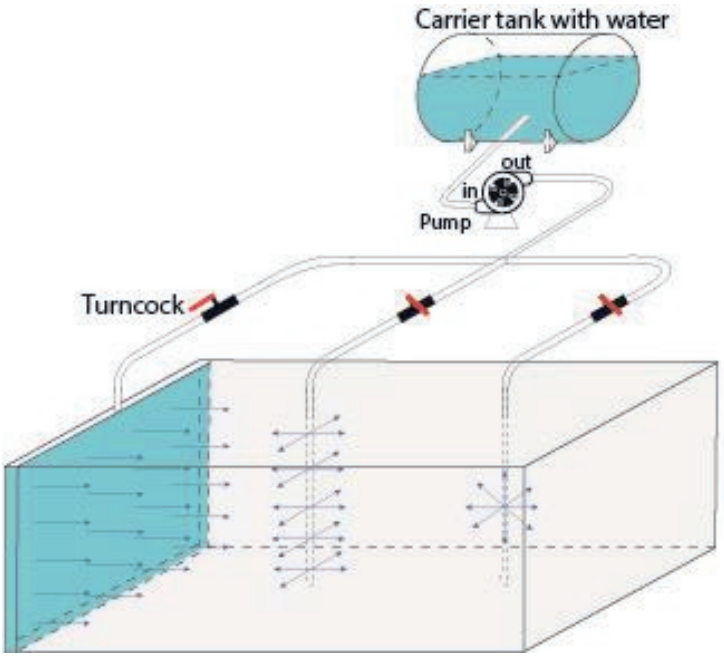

Figure 5.1: Conceptual image of (left) 1D, (middle) 2D, and (right) 3D radial flow in a horizontal aquifer.

In heterogeneous aquifers, flow around wells can be described as radially axisymmetric flow around a point source, perturbed by velocity field fluctuations at a smaller spatial scale (Neuweiler et al., 2001). The flow velocity $\tilde{v}(r_1, \dots, r_d)$ in a d-dimensional heterogeneous flow field can therefore be approximated as the sum of the macroscopically-averaged axisymmetric velocity $v(r)$ and a spatially dependent fluctuation $v_\epsilon(r_1, \dots, r_d)$ (Indelman, 2001; Dagan, 1988):

$$\tilde{v}(r_1, \dots, r_d) = v(r) + v_\epsilon(r_1, \dots, r_d), \tag{5.1}$$

where $r = \sqrt{\sum_{i=1}^{d} r_i^2}$ is the radial position and the $r_1, \dots, r_d$ are the Cartesian coordinates. For small-scale fluctuations with zero mean, the macroscopic flow field is radially-aligned, and the macroscopically-averaged axisymmetric velocity obeys

$$v(r) = \frac{A_d}{r^{d-1}}, \tag{5.2}$$

$$A_d = \frac{Q}{\theta}\left[\frac{2\pi^{\frac{d}{2}}}{\Gamma\left(\frac{d}{2}\right)}\right]^{-1}, \tag{5.3}$$

$$\Gamma(\xi) \equiv \int_0^\infty \gamma^{\xi-1} \exp(-\gamma)\, d\gamma$$

where Q is the injection rate, θ is the porosity of the aquifer, $\Gamma(\xi)$ is the gamma function, and ξ, γ are arbitrary variables. d is the spatial dimensionality of the macroscopically-averaged radial flow field (e.g. $d = 1$ for planar, $d = 2$ for disc, and $d = 3$ for spherical flow). A_d is shape coefficient of the injected water front, whose component within square brackets is the surface area of a d-dimensional sphere of unit radius.

The governing advection-dispersion equation (ADE) that describes the transport of solutes and heat in homogeneous soils is (chapter 4)

$$\frac{\partial c}{\partial t} = D(r)\frac{\partial^2 c}{\partial r^2} + \left[(d-1)\frac{D_m}{r} - v(r)\right]\frac{\partial c}{\partial r}, \tag{5.4}$$

$$D(r) = D_h(r) = D_m + \alpha v(r) \tag{5.5}$$

where D is the dispersion coefficient, D_m is the molecular diffusion coefficient, α is the longitudinal mechanical dispersivity constant, and D_h is the hydrodynamic dispersion coefficient. Since no transverse dispersion occurs under radial flow in homogeneous aquifers (Gelhar and Collins, 1971), we assume that the effects of transverse mechanical dispersion in heterogeneous aquifers are captured through macrodispersion, which will be introduced later. Lessoff and Indelman (2004) found that varying the transverse dispersivity has only a minor impact on overall dispersion. Hence, in the numerical simulations that follow, the transverse mechanical dispersivity constant α_T is set as equal to α to maximize computational efficiency.

We consider a problem in which at the well, a duration T of injection rate Q alternates with the same duration T of extraction rate $-Q$, in a step-cyclic manner in a d-dimensional infinite domain. Assume that the flow field immediately achieves steady-state as the injection switches to extraction or vice versa. The injected volume $V_{in} = QT$ and extracted volume $V_{ex} = QT$ are equal. The water injected by the well contains a solute at some dimensionless reference concentration $c = c_0$, while the ambient water surrounding the well initially contains solute at $c = 0$. The well injects a total mass $M = c_0 QT = c_0 V_{in}$ of solute, and extracts V_{ex} of water, recovering M_r of solute. The recovery efficiency F_r of solute is

$$F_r = \frac{M_r}{M}. \tag{5.6}$$

5.2.2 Numerical model

The problem described above is solved with MODFLOW-2005 (Harbaugh, 2005) and MT3DMS (Langevin & Guo, 2006) for flow and solute transport, respectively. The finite difference flow calculations were performed using the pre-conjugated gradient (PCG) package of MODFLOW in block-centered numerical grids. Solute transport in MT3D was solved with the third-order ULTIMATE TVD scheme. A uniform head initial condition was imposed across the numerical domain, and an imposed head boundary condition (magnitude equal to the initial condition) was imposed at the edges of the domain, to simulate the absence of background flow. Imposed flux boundary conditions were used at the well, with the flux uniformly distributed along the well screen, during both the injection and extraction phases. The initial and boundary conditions that describe solute transport are

$$\begin{aligned} c(r,0) &= 0, \\ c(0,t)_{in} &= c_0, \\ \frac{\partial c}{\partial r}(0,t)_{ex} &= 0, \\ \frac{\partial c}{\partial r}(r_{max},t) &= 0, \end{aligned} \tag{5.7}$$

where subscripts in and ex refer to the injection and extraction phases respectively and r_{max} is the r-coordinate at the edge of the numerical domain. The zero-gradient boundary condition at the well during the extraction phase implies that the concentration immediately inside the wellbore is equal to that immediately outside, and reflects the assumption that mixing within the wellbore is negligible.

The radial flow fields and aquifer geometries considered in the numerical simulations are planar flow ($d = 1$) in a two-dimensional domain and in a three-dimensional domain, and cylindrical flow fields ($d = 2$) in a three-dimensional domain. Solute transport in these flow fields with three types of heterogeneity structures were modelled: a) spatially autocorrelated heterogeneity with exponential covariance; b) white noise heterogeneity; and c) layer stratification. In the two-dimensional simulations, a 256x256 numerical grid with horizontal and vertical dimensions $L_x = 75,\ L_y = 50$ was used. In the three-dimensional simulations, a 128x128x64 numerical grid was used, with $L_x = 75,\ L_y = 50,\ L_z = 10$. Grid cells along the edges of the square (two-dimensional) and cubic (three-dimensional) numerical grids were de-activated so that the active area of the numerical grid resembled a circle (two-dimensional) or sphere (three-dimensional) as closely as possible, to prevent edge effects caused by simulating radial flow in square or cubic domains. For cylindrical flow fields ($d = 2$), the well is fully penetrating along the z-axis. In both 2D and 3D models with planar flow ($d = 1$), the macroscopic flow direction is along the x-axis. Dispersion into confining layers of the aquifer is not explicitly considered in this study, because such scenarios are essentially specific cases of aquifer stratification with high conductivity variances: one can consider high conductivity layers to be aquifer layers, and low conductivity layers to be confining layers.

For the non-autocorrelated (white noise) fields, the log-conductivities were independently drawn at each cell. In the stratified aquifers, 16 layers were generated; the hydraulic conductivity is heterogeneous only along the y-axis for 2D simulations and z-axis for 3D simulations, with no autocorrelation between layers. As such, this model of stratification represents a limiting case of autocorrelated heterogeneity in which the correlation length ρ is infinite within the strata and zero across the strata. For the exponentially autocorrelated fields $\mathrm{Cov}(r) = \sigma_k^2 \exp(-\rho)$, the simulated autocorrelation lengths along each axis are $\rho_i = L_i/10$, where i refers to the index of each spatial dimension, to ensure non-trivial structures of heterogeneity within the confines of the numerical grid. No assumption of ergodicity is made, as in practice, for managed aquifer recharge applications such as ATES and ASR, the storage radius of the system may be even smaller than a single integral scale of heterogeneity (e.g. Sommer et al, 2013). For example, in the Netherlands, where most presently operating ATES systems worldwide are located, the storage radius of wells never exceeds 100m, with most being under 50m (Bloemendal and Hartog, 2018). Real aquifers reported in many studies in the literature (e.g. Sommer et al (2013), Vereecken et al (2000), and Fernandez-Garcia et al (2005)) have horizontal correlation lengths of between 2.5m to 100m. This means that many aquifer storage systems in practice may not sample a sufficient volume of the aquifer they are located in to approach ergodic conditions. Therefore, our choice of a numerical domain with 10 integral scales appears to be a good middle-of-the-road choice to show that non-ergodicity does not preclude the applicability of our findings. The exponentially autocorrelated conductivity fields were generated using the RandomFields R package (Schlather et al., 2015). The natural logarithms of the hydraulic conductivity at each cell was drawn from a normal distribution with mean 1 and four different standard deviations $\sigma_k = \{0.5, 1, 1.5, 2\}$. The modelled values of σ_k are field-realistic values that are spread around those of three experimentally studied aquifers, Cape Cod ($0.37 \leq \sigma_k \leq 0.49$), Borden ($0.49 \leq \sigma_k \leq 0.54$), and MADE ($1.64 \leq \sigma_k \leq 2.12$) (Fernàndez-Garcia et al., 2005).

5.3. Theory

5.3.1 Scale-dependent macrodispersion

We define the scale-dependent macrodispersion coefficient as $D_k = \beta r^{\lambda d} v$ (e.g. Dagan, 1988), where β is the macrodispersivity constant and λ is a positional scaling exponent. Such macrodispersion scaling (i.e. $\log D_k \propto \log r$) is frequently reported in the literature (e.g. Wheatcraft and Tyler, 1988; Zech et al, 2015). By the principle of conservation of mass, due to the assumed incompressibility of water, the macroscopically-averaged radial position r' of the injected hydraulic front is related to the injection rate $Q \propto A_d$ by

$$r'(t) = (A_d td)^{\frac{1}{d}}. \tag{5.8}$$

Thus, the macrodispersion coefficient at r' is

$$D_k(r') = \beta(A_d td)^{\lambda} v(r'). \tag{5.9}$$

We account for macrodispersion in the dispersion coefficent D by adding the macrodispersion coefficient D_k to the hydrodynamic dispersion coefficient D_h:

$$D(r) = D_h(r) + D_k(r) = D_m + \left[\alpha + \beta r^{\lambda d}\right] v(r). \tag{5.10}$$

Adding the macrodispersion coefficient to the hydrodynamic dispersion coefficient, and using the macroscopically-averaged velocity $v(r)$ to model velocity-dependent dispersion terms, is sufficient to successfully describe macroscopic spatial moments of plume spreading (Dagan, 1988). The ability to additively combine the local dispersion and macrodispersion terms into an overall dispersion term stems from the observation that in typical situations where the heterogeneity autocorrelation scale is larger than α, the macrodispersion term and the local dispersion term are independent (Gelhar, 1986).

5.3.2 Recovery efficiency under scale-dependent macrodispersion in planar flow fields

The recovery efficiency in a planar flow field in a homogeneous aquifer subject to only scale-independent mechanical dispersion (i.e. $D = \alpha v$) is (chapter 4)

$$F_r = 1 - \sqrt{\left(\frac{4\alpha\theta}{\pi QT}\right)}. \tag{5.11}$$

Here, the recovery efficiency increases as Q, T increases.

In the case of Equation (5.4) subject to $D_m = 0$, $\alpha = 0$, and $\lambda = 1$, in a planar flow field, under purely scale-dependent dispersion $D = \beta r^{\lambda} v$, the exact solution for the concentration profile under continuous injection is (Pang and Hunt, 2001)

$$c(r,t) = c_0 \int_0^t \frac{1}{\tau\Gamma\left(\frac{1}{\beta}\right)} \left(\frac{r\theta}{\beta Q\tau}\right)^{\frac{1}{\beta}} \exp\left(-\frac{r\theta}{\beta Q\tau}\right) d\tau \tag{5.12}$$

which yields

$$c(r,t) = \frac{c_0}{\Gamma\left(\frac{1}{\beta}\right)} \Gamma\left(\frac{1}{\beta}, \frac{r\theta}{\beta Qt}\right) \tag{5.13}$$

$$\Gamma(\xi,\chi) \equiv \int_{\chi}^{\infty} \gamma^{\xi-1} \exp(-\gamma)\, d\gamma \tag{5.14}$$

where $\Gamma(,)$ is the upper incomplete gamma function and ξ, τ, χ, γ are arbitrary variables. The mass of solute (i.e. the zeroth spatial moment) M_l outside the hydraulic front during the injection phase can be found by integrating the concentration profile from the front to infinity and multiplying by the porosity θ:

$$M_l(t) = \frac{c_0\theta}{\Gamma\left(\frac{1}{\beta}\right)} \int_{\frac{Qt}{\theta}}^{\infty} \Gamma\left(\frac{1}{\beta}, \frac{r\theta}{\beta Qt}\right) dr = \frac{c_0 Qt}{\Gamma\left(\frac{1}{\beta}\right)} \left[\beta\Gamma\left(1 + \frac{1}{\beta}, \frac{1}{\beta}\right) - \Gamma\left(\frac{1}{\beta}, \frac{1}{\beta}\right)\right] \tag{5.15}$$

The recovery efficiency of a complete injection-extraction cycle is then approximately given by the following expression from chapter 4:

$$F_r = \frac{c_0 QT - \sqrt{2}\, M_l(T)}{c_0 QT} = 1 - \frac{\sqrt{2}}{\Gamma\left(\frac{1}{\beta}\right)}\left[\beta\Gamma\left(1+\frac{1}{\beta},\frac{1}{\beta}\right) - \Gamma\left(\frac{1}{\beta},\frac{1}{\beta}\right)\right] \tag{5.16}$$

which is accurate only when dispersion is not too strong relative to advection (i.e. when $F_r \geq 0.7$), because it uses a boundary layer solution to the ADE.

Remarkably, in contrast to the position-independent mechanical dispersion (5.11), the recovery efficiency is independent of the porosity θ and the well operational parameters Q, T if the dispersion coefficient D increases linearly with distance from the source, i.e. $\lambda = 1$. In summary, the recovery efficiency is independent of Q, T for $\lambda = 1$, and the recovery efficiency increases as Q, T increases if $\lambda = 0$ as implied by Equation 5.11. Accordingly, assuming that the function mapping Q, T to the recovery efficiency is continuous, the recovery efficiency should decrease as Q, T increases if $\lambda > 1$. With multiple coexisting dispersion processes (e.g. $D = D_m + \alpha v$), whether the recovery efficiency increases or decreases as Q, T increase should then depend on whichever process dominates. This is because mechanical dispersion is velocity-dependent, whereas molecular diffusion is not, thus the r-dependence of flow velocity in radial flow fields causes the relative contribution of mechanical dispersion and molecular diffusion to solute losses to change with Q, T. For example, in three-dimensional radial flow in a homogeneous aquifer, F_r increases as T increases if mechanical dispersion dominates, but the opposite occurs if molecular diffusion dominates (chapter 4). Unfortunately, the solution to the ADE for values of λ other than 0 or 1 (Guerrero and Skaggs, 2010), or for higher dimensional flow field geometries (Hunt, 1998), are too complex to obtain a closed-form solution for the recovery efficiency. Therefore, we seek to obtain an approximate solution for the recovery efficiency that applies to a wide range of scenarios.

5.3.3 Approximate general solution for recovery efficiency

An approximation by Gelhar and Collins (1971) states that the radial concentration profile $c(r)$ in d-dimensional flow in a homogeneous aquifer is

$$c(r, r') = \frac{1}{2} c_0 \operatorname{erfc}\left[\frac{r^d - r'^d}{dA_d\sqrt{4\omega}}\right], \tag{5.17}$$

$$\omega = \int_0^{r'} \frac{D_h}{v^3(r)}\, dr = \int_0^{r'} \frac{\alpha v(r) + D_m}{v^3(r)}\, dr \tag{5.18}$$

The approximation is accurate when the average hydraulic front radius $r'(t)$ is significantly larger than the width of the dispersed zone, i.e. $r' \gg v(r')\sqrt{\omega}$, or equivalently, $r'^d \gg A_d\sqrt{\omega}$.

It was previously shown that in radial flow fields, the first spatial moment obtained from the solution of the radial ADE (5.4) is able to characterize the first spatial moment of solute concentration in heterogeneous aquifers, when the macrodispersion coefficient is substituted for the hydrodynamic dispersion coefficient (Adams and Gelhar, 1992). Since the first spatial moment of concentration essentially quantifies the total mass of solutes within a certain volume of space, this allows us to approximate the recovery efficiency, by first substituting D (5.10) for D_h in (5.18), and also expressing r' using (5.8), which yields

$$\omega = \int_0^{r'} \frac{D}{v^3(r)}\, dr = \int_0^{r'} \frac{D_m + \alpha v(r) + \beta r^{\lambda d} v(r)}{v^3(r)}\, dr \tag{5.19}$$

$$c(r,t) = \frac{1}{2} c_0 \operatorname{erfc}\left[\frac{\left(r^d - (A_d td)\right)}{\sqrt{4d^2\alpha(A_d td)^{\frac{2d-1}{d}}}\sqrt{\alpha A_d\left(\frac{\alpha A_d}{2d-1} + \frac{D_m(A_d td)^{\frac{d-1}{d}}}{3d-2} + \frac{\beta(A_d td)^{\lambda} A_d}{\lambda d + 2d - 1}\right)^{-1}}}\right]. \tag{5.20}$$

for the macroscopically averaged radial concentration profile of a heterogeneous aquifer.

The storage radius R is the maximum extent of the hydraulic front achieved during a cycle, and can be found by substituting the injection duration T into (5.8), which yields $R = (A_d T d)^{\frac{1}{d}}$. The mass of solute M_l dispersed beyond the stored volume may be obtained by spatially integrating (5.20) beyond the storage volume:

$$M_l(T) = \int_{V(R)}^{V(r=\infty)} c(r,T)\, dV = \int_R^\infty c(r,T) \frac{dV(r)}{dr} dr, \tag{5.21}$$

$$V(r) = \frac{2\pi^{\frac{d}{2}}}{d \cdot \Gamma\left(\frac{d}{2}\right)} r^d \tag{5.22}$$

where $V(r)$ is the volume of a d-dimensional sphere of radius r. With $F_r = \frac{c_0 QT - \sqrt{2}\, M_l(T)}{c_0 QT}$ (chapter 4), applicable when $F_r \geq 0.7$, F_r may computed as

$$F_r(Q,T) = 1 - \left[\sqrt{\frac{2}{\pi}} (A_d)^{-\frac{3}{2}} T^{-1} \sqrt{\frac{\alpha A_d (A_d T d)^{\frac{2d-1}{d}}}{2d-1} + \frac{D_m (A_d T d)^{\frac{3d-2}{d}}}{3d-2} + \frac{\beta (A_d T d)^{\lambda} A_d (A_d T d)^{\frac{2d-1}{d}}}{\lambda d + 2d - 1}} \right]. \tag{5.23}$$

In the case of $D_m = 0$, $\alpha = 0$, $d = 1$, and $\lambda = 1$, as previously discussed in section 5.3.2, the recovery efficiency (5.23) becomes

$$F_r(Q,T) = 1 - \sqrt{\frac{\beta}{\pi}} \tag{5.24}$$

which is independent of $A_d(\theta, Q)$ and T, in agreement with (5.16). Comparing F_r obtained from the approximate concentration profile (5.24) to that obtained from the exact profile (5.16) reveals that the two approaches of calculating F_r are effectively identical for low (macro)dispersion and high recovery scenarios (regions of low β in Figure 5.2).

The implications of (5.16) and (5.24) that the recovery efficiency in this case is independent of Q and T is extremely remarkable, therefore we numerically solved this problem (equation 5.4 and equation 5.10 with $d = 1$, $D_m = 0$, $\alpha = 0$, and $\lambda = 1$) with the *pdepe* routine of MATLAB for the purpose of additional verification. The F_r obtained with equation (5.24) agrees exactly with those numerically obtained for $\beta \leq 0.01$. More importantly, the numerical results confirm that varying Q and T does not affect the recovery efficiency at all for $\beta \leq 0.01$. As β increases beyond 0.01, (5.16) and (5.24) begin to underestimate the numerical result, to a larger extent as β becomes larger (i.e. the smaller F_r becomes) due to the use of boundary layer approximations in the derivations, though the relative underestimation remains well below 10% at $\beta \sim 0.1$ (Figure 5.2). Laboratory and field evidence suggests that in practice β is mostly on the order of 0.001 to 0.01 (discussed further in Section 5.4.3), with 0.1 being a soft upper bound. Therefore, equation (5.16) and (5.24) are essentially accurate for most situations of practical relevance. Figure 5.2 also shows that for larger β, varying Q and T affects the numerically computed recovery efficiency slightly. Simulations with various combinations of Q and T reveal that as the storage volume $V_{in} = QT$ increases, (5.16) underestimates the numerically computed recovery efficiency to a larger but still reasonable extent. In summary, the results show that (5.16) is always larger than (5.24), and that (5.16) and (5.24) closely approximate the numerical results for $\beta < 0.1$. Furthermore, (5.16) and (5.24) lower bound the numerically computed recovery efficiency for cases with atypically large β or V_{in}.

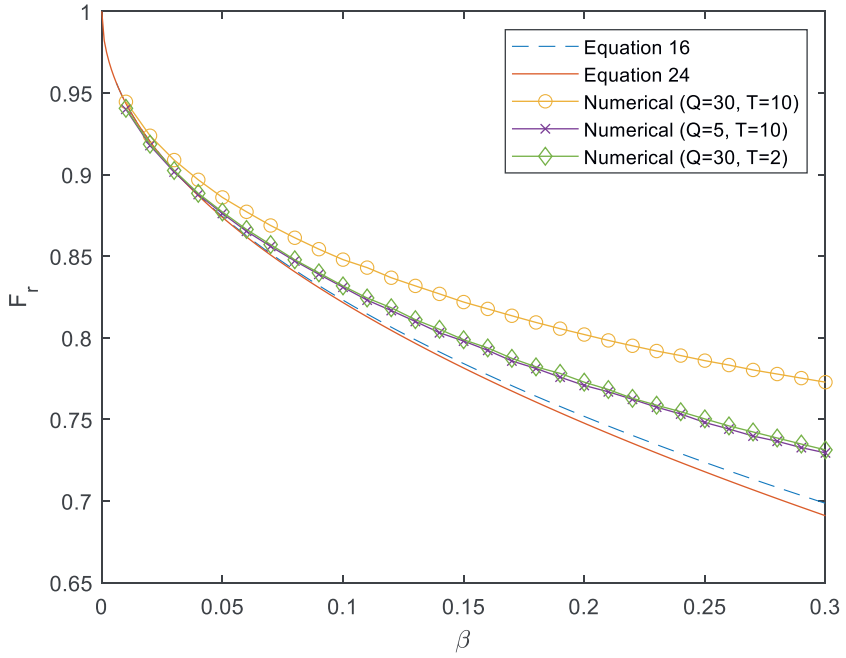

Figure 5.2: Recovery efficiency F_r as a function of the macrodispersivity constant β, computed with Equation 5.16, Equation 5.24, and the results from the numerical simulations of the corresponding ADE with various values of the parameters Q and T.

From (5.23) it follows that if $D_m = 0$, $\alpha = 0$, and $\lambda d > 1$, then the recovery efficiency (5.23) decreases as Q, T increases whereas the opposite is true if $\lambda d < 1$, in agreement with our hypothesis in section 5.3.2. Furthermore, from (5.23) it can be deduced that if $D = \beta r^{\lambda d} v$, then for all combinations of $\lambda d = 1$ the recovery efficiency is independent of Q, T, and the scenario analyzed above ($\lambda = 1, d = 1$) is only one of many possibilities. Equation (5.23) is also reducible to the solution for the recovery efficiency in homogeneous aquifers (chapter 4), by setting $\beta = 0$. Thus, (5.23) captures the complexity relating F_r to the two empirical macrodispersion parameters β and λ, which have to be fitted from observational data and are somehow related to the aquifer properties σ_k and ρ.

5.3.4 Relation between aquifer structure and macrodispersion parameters

Both in 3D and 2D domains, when $\sigma_k^2 < 2$, solute moments can be effectively described with only two parameters, namely σ_k and ρ, and other characteristics of the structure of heterogeneity are mostly inconsequential (Jankovic et al., 2017; Di Dato et al., 2019; Zinn and Harvey, 2003). Therefore, here we relate σ_k and ρ to the macrodispersion parameters β and λ.

The macrodispersivity constant β is related to the heterogeneity of the aquifer, but is not simple to derive from the statistics of the conductivity distribution (Fernàndez-Garcia et al., 2005), and its validity in representing true mixing is often disregarded. Expressions have been derived for β (Dagan, 1988), including expressions specifically concerning cylindrical flow (Attinger et al., 2001; Neuweiler et al., 2001; Indelman and Dagan, 1999; Indelman, 2004) and spherical flow (Indelman and Dagan, 1999).

Mostly, these expressions pertain to the two limiting cases $R \gg \rho$ and $R \ll \rho$ of autocorrelated heterogeneity. In these cited studies, the macrodispersion coefficient is shown to be proportional to the flow velocity and the variance of the log-conductivity:

$$D_k \propto \beta v \propto \sigma_k^2 v. \tag{5.25}$$

Accordingly, β decreases to zero if the aquifer is homogeneous ($\sigma_k = 0$), and no macrodispersion occurs.

For autocorrelated structures, preferential flow paths may be more persistent than under the absence of autocorrelation, and this affects λ, which describes the positional scaling of the macrodispersion. Therefore, λ is a function of the autocorrelation length ρ, which encodes how disordered or connected the structure of the aquifer heterogeneity is (Bianchi & Pedretti, 2017; Trinchero et al, 2008). In aquifers with longer autocorrelation ranges or less disorder, such as perfectly stratified aquifers, λ should be larger, as preferential flow channels form and persist over a larger spatial expanse. In aquifers with preferential flow channels, the amount of ambient water that the solute-rich injected water encounters increases significantly as the volume injected increases, because the surface area of the plume expands (Figure 5.3a, 5.3b), allowing more solutes to disperse into relatively immobile channels (Guven et al., 1985). Furthermore, as stratification represents the extreme case of infinite ρ along the direction of flow, λd is expected to be larger in stratified than in exponentially autocorrelated aquifers.

In contrast, non-autocorrelated heterogeneity gives rise to some degree of 'surface roughness' at the hydraulic front without persistent preferential flow (Figure 5.3c), with a relatively small surface area of interaction with the ambient water. Setting $\lambda = 0$ in (5.23) reduces the macrodispersion term to a scale-independent mechanical dispersion term. Since macrodispersion under non-autocorrelated heterogeneity gives rise to apparently radially axisymmetric concentration fronts which are macroscopically similar to those created by mechanical dispersion in homogeneous aquifers aside from some jaggedness at the circumference, it is to be expected that λ is small or close to zero under non-autocorrelated heterogeneity, and that λ increases as ρ increases. The observation that the plume spreading arising from non-autocorrelated heterogeneity behaves similarly as from local mechanical dispersion has also been made previously (Luther and Haitjema 1988).

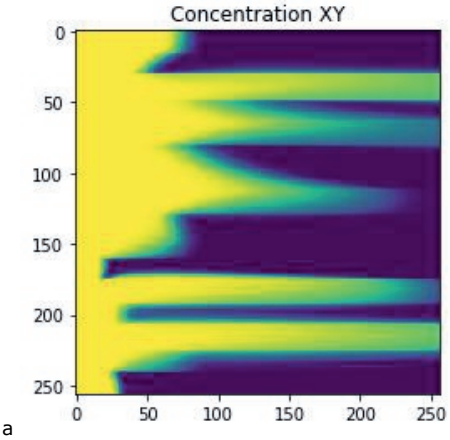

a

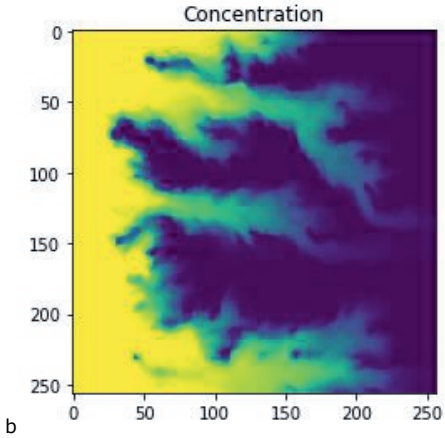

b

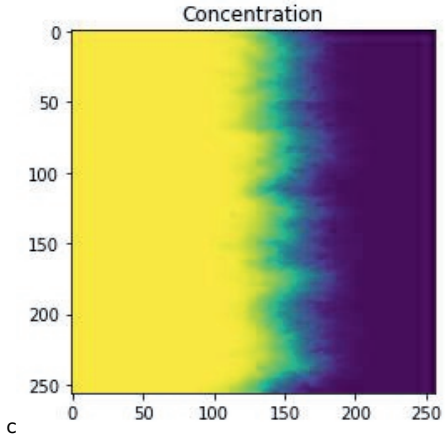

c

Figure 5.3: Examples of 2D cross sections of the concentration profile in a heterogeneous aquifer with (a) stratified (b) exponentially autocorrelated, and (c) non-autocorrelated heterogeneity for planar flow.

5.4. Results and discussion

5.4.1 Recovery efficiency

The relationship between F_r and T are illustrated in Figures 5.4 and 5.5, and the fitted macrodispersion parameters (β_0, λ) are listed in Table 5.1, where the reported β_0 is the β of the scenario with $\sigma_k = 0.5$. Fitting of (β_0, λ) in each individual scenario (e.g. Figure 5.4a for planar flow in a non-autocorrelated heterogeneous 2D domain) was accomplished by substituting $\beta = \beta_0 \frac{\sigma_k^2}{0.5^2}$ into (5.23) and minimizing the total RMSE of all four sets of analytical and numerical curves corresponding to all four values of σ_k. In other words, $\sum_{i=1}^{4} RMSE(\sigma_k^2 = 0.5 \cdot i)$ is minimized to fit (β_0, λ), under the condition that $\beta = \beta_0 \frac{\sigma_k^2}{0.5^2}$. The following discussion, and the good agreement between the analytical and numerical outcomes, also apply to the relationship between F_r and Q (not shown).

Table 5.1: Macrodispersion parameters fitted to the numerical data for the case of $\sigma_k = 0.5$.

	Planar flow field (2D grid) $d = 1$ $D_k \propto R^{\lambda}$	Planar flow field (3D grid) $d = 1$ $D_k \propto R^{\lambda}$	Cylindrical flow field (3D grid) $d = 2$ $D_k \propto R^{2\lambda}$
No autocorrelation $\lvert\rho\rvert = 0$	$\beta = 0.002$, $\lambda = 0.39$ $D_k \propto R^{0.39}$	$\beta = 0.005$, $\lambda = 0.1$ $D_k \propto R^{0.1}$	$\beta = 0.001$, $\lambda = 0.32$ $D_k \propto R^{0.64}$
Exponential covariance $0 < \lvert\rho\rvert < \infty$	$\beta = 0.004$, $\lambda = 1.17$ $D_k \propto R^{1.17}$	$\beta = 0.007$, $\lambda = 1.14$ $D_k \propto R^{1.14}$	$\beta = 0.004$, $\lambda = 0.49$ $D_k \propto R^{0.98}$
Layer stratification $\lvert\rho\rvert = \infty$	$\beta = 0.004$, $\lambda = 1.44$ $D_k \propto R^{1.44}$		$\beta = 0.004$, $\lambda = 0.59$ $D_k \propto R^{1.18}$

Figure 4 and Figure 5 show that equation (5.23) characterizes well the numerical recovery efficiency of an injection-extraction system, and its sensitivity to the parameters Q, T, σ_k, d. Recall the approximate theoretical relationship $\beta \propto \sigma_k^2$ that was previously discussed. In non-autocorrelated aquifers, $\beta \propto \sigma_k^2$ is remarkably accurate (Figure 5.4a, 5.4b, 5.5a). Figure 5.4 and Figure 5.5 also shows that $\beta \propto \sigma_k^2$ is valid but sometimes slightly underpredicts F_r (i.e. slightly overpredicts β) for stratified and exponentially autocorrelated heterogeneity, in agreement with Sommer et al (2013) and Gelhar and Axness (1983). Despite the slight overprediction with $\beta \propto \sigma_k^2$, the relative errors $\left|\frac{Numerical - Predicted}{Numerical}\right|$ in Figure 5.4 and Figure 5.5 do not exceed 10% even though T and σ_k^2 are varied over an order of magnitude.

In some cases the recovery efficiency varies non-monotonically with injection duration, and attains a maximum. For a fixed value of λ, the value of T at which the maximum point is located becomes smaller as β increases, as can be seen in Figure 5.4e and Figure 5.5c. While non-monotonicity in the recovery efficiency is only possible under 3D spherical flow in homogeneous aquifers (Equation 5.23; also see chapter 4), and only for $F_r(T)$ but not $F_r(Q)$, we show here that it is possible in 1D and 2D radial flow in heterogeneous aquifers for both $F_r(T)$ and $F_r(Q)$ due to the positional scaling of macrodispersion.

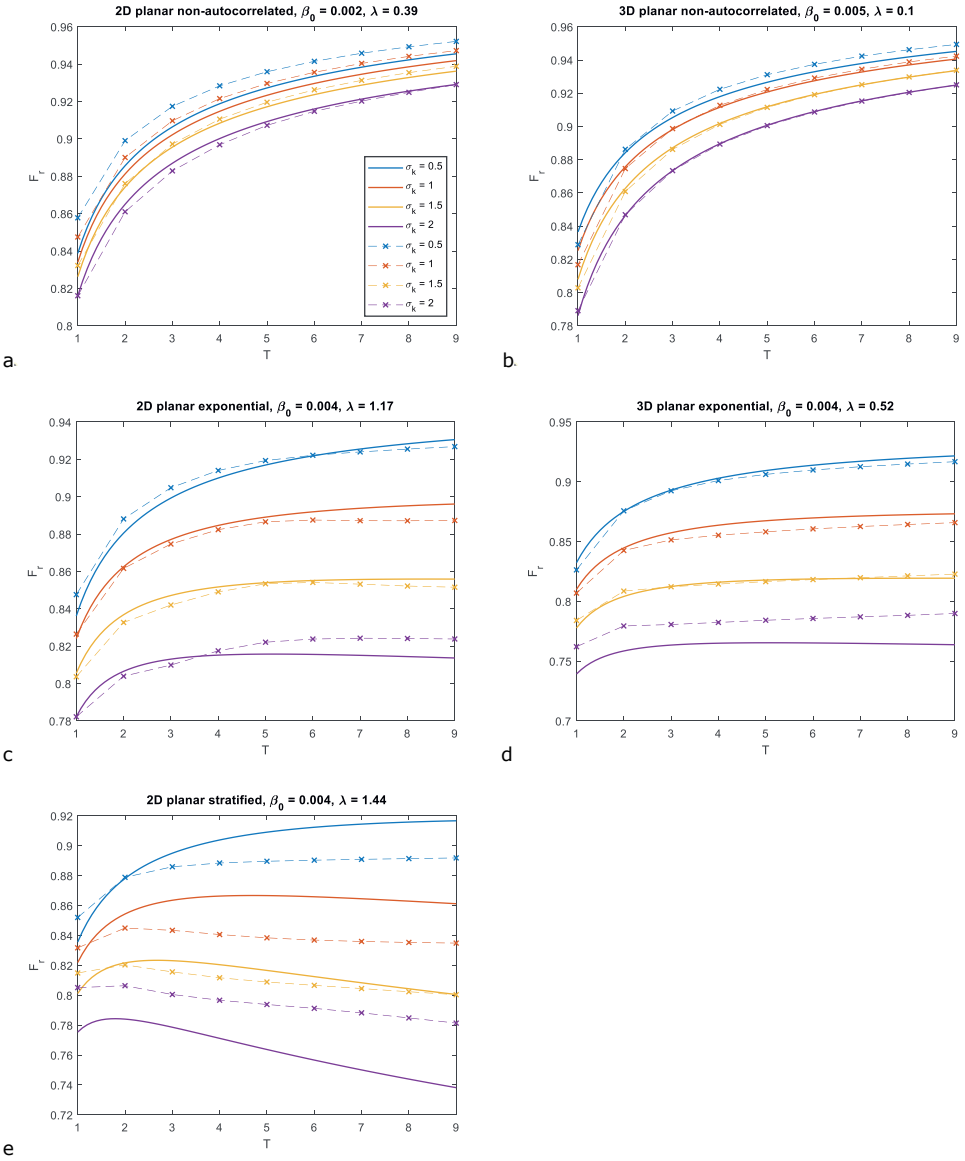

Figure 5.4: Numerical (crossed lines) results and approximate analytical (Equation 5.23, solid lines) solutions of the recovery efficiency against time for planar flow in a (top) non-autocorrelated heterogeneous conductivity field, (middle) exponentially autocorrelated in a (left) 2D and (right) 3D domain, and also for a (bottom) stratified aquifer. In these simulations, $\alpha = 0.1$, $D_m = 0$, and $Q = 2$. Analytical curves for $\sigma_k > 0.5$ are estimated from curves for $\sigma_k = 0.5$ using the relation $\beta \propto \sigma_k^2$.

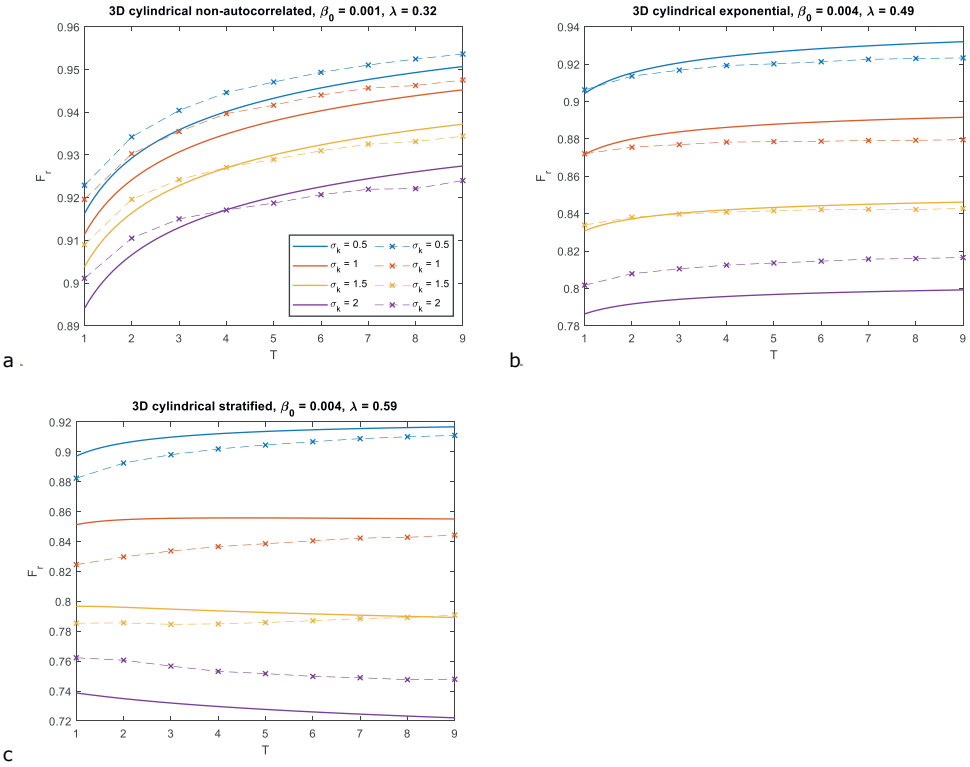

Figure 5.5: Numerical (crossed lines) results and approximate analytical (Equation 5.23, solid lines) solutions of the recovery efficiency against time for cylindrical flow in a (a) non-autocorrelated heterogeneous conductivity field, (b) exponentially autocorrelated, and (c) stratified aquifer in a 3D domain. In these simulations, $\alpha = 0.1$, $D_m = 0$, and $Q = 200$. Analytical curves for $\sigma_k > 0.5$ are estimated from curves for $\sigma_k = 0.5$ using the relation $\beta \propto \sigma_k^2$.

Macrodispersion is weak compared to local dispersion at small plume travel distances (Molz et al., 1983), thus the recovery efficiency increases with Q,T (see equation 5.11). In contrast, when macrodispersion dominates the spreading at large travel distances, the effects of local dispersion may be disregarded (Zhang and Neuman, 1996) and the recovery efficiency may decrease as Q,T increases for some combinations of β,d,λ. Depending on the values of β,d,λ, the dominance of macrodispersion over local dispersion increases with the distance from the inlet. Therefore, in scenarios where local dispersion dominates at small distances from the inlet, the recovery efficiency maximizes at some intermediate storage volume. The Q,T corresponding to maximum recovery can be found by equating the derivative of (5.23) to zero.

The area-to-volume ratio A/V under the assumption of aquifer homogeneity, which is the area-to-volume ratio of a uniform d-dimensional sphere calculated as $H = \frac{d}{(dA_dT)^{\frac{1}{d}}}$ (chapter 4), is a popular metric for the estimation of the recovery efficiency of radial transport systems. Note that H is not the actual area-to-volume ratio that takes into account heterogeneous flow paths. In homogeneous aquifers, an increase in the injected volume necessarily leads to a decrease in the actual A/V (which is identical to H) for geometrical reasons. Many studies therefore suggest that an increased injected volume leads to an increase in the recovery efficiency (e.g. Bloemendal and Hartog, 2018; Sommer et al., 2015; Schout et

al., 2014; Novo et al., 2010; Forkel & Daniels., 1995). In aquifers with heterogeneous hydraulic conductivity and scale-dependent macrodispersion, this rule might no longer apply, as increasing V_{in} would necessarily decrease H but possibly lead to an increase in the actual A/V, due to the large interfaces that may develop between fast and slow flow zones. Accordingly, we found that increasing V_{in} beyond some threshold will decrease the recovery efficiency if $\lambda d > 1$, even in scenarios where the recovery efficiency would have increased monotonically as V_{in} increased if the aquifer were to be homogeneous.

5.4.2 Effects of heterogeneity structure and flow field geometry on macrodispersion parameters

The fitted λ values support the hypotheses presented in Section 5.3.4: λ is smallest under non-autocorrelated heterogeneity, intermediate under exponentially autocorrelated heterogeneity, and largest under layer stratification. Indeed, λ is smallest under non-autocorrelated heterogeneity for all tested scenarios. Preferential flow paths in stratified aquifers do not collide or fuse, therefore allowing preferential flow paths the greatest extent of persistence. Thus, the positional scaling of macrodispersion λ is larger in stratified than in heterogeneous aquifers with a finite autocorrelation length (Indelman and Dagan, 1999). Furthermore, the macrodispersion coefficient D_k appears to converge towards some asymptotic value at large advective scales in practice (Zech et al, 2015), which agrees with our observation that λ is small or close to zero for non-autocorrelated heterogeneous aquifers, where the advective scale is much larger than the correlation scale of heterogeneity.

For planar flow in exponentially autocorrelated aquifers, if the storage radius R is heavily increased such that $R \gg \rho$, the system will eventually approach the limiting behavior of small λ associated with non-autocorrelated aquifers. Thus, λ is a decreasing function of R when ρ is neither infinite (stratified aquifer) nor zero (non-autocorrelated aquifer). However, at least within the parameter ranges investigated in this study, we observe the following. As seen in Figure 5.4c, 5.4d, and 5.5b even when R is varied by one order of magnitude, modelling the recovery efficiency with a constant λ yields a good fit with the numerical simulations. This means that any variation of λ with R is a higher-order effect that may be neglected in the design of aquifer storage systems. For stratified aquifers (i.e. infinite ρ) with flow parallel to the layers, the macrodispersion coefficient D_k never converges to an asymptotic value (Matheron and De Marsily, 1980). Thus, D_k grows unboundedly with R in stratified aquifers, and λ never converges to zero.

The results listed in Table 5.1 agree with the mathematical analyses of Indelman and Dagan (1999). In all simulated heterogeneous aquifers, β is larger under planar than cylindrical flow having otherwise identical circumstances. The scale-dependence of macrodispersion is larger for planar than for cylindrical flow in stratified and exponentially autocorrelated aquifers. Table 5.1 shows that for non-autocorrelated heterogeneity, λd is larger under cylindrical flow than planar flow. This agrees with Indelman (2004), who showed that when $R \gg \rho$, as is the case for non-autocorrelated heterogeneity, the macrodispersion coefficient D_k grows slowly with distance for cylindrical flow but not for planar flow, although we found that λ is small but not exactly zero under planar flow. In summary, for identical heterogeneous aquifers, imposing a different flow field results in different fitted macrodispersion parameters β, λ. Therefore, the macrodispersion parameters β, λ are emergent properties that arise from the dynamic interactions between flow field geometry and aquifer properties σ_k, ρ. In contrast, the static properties σ_k, ρ are intrinsic to the structure of aquifer heterogeneity. Hence, the presence of additional factors affecting the flow field, such as background flow, multiple interacting wells, or an unconfined upper boundary, can be expected to alter β, λ.

5.4.3 Validation of fitted macrodispersion parameters

Laboratory experiments by Pang and Hunt (2001) suggest that β is around 0.005. Review studies have shown that β fitted to field tracer tests mostly range between 0.001 to 0.1 (Gelhar, 1986; Gelhar et al., 1992), though a more recent evaluation shows that β clusters around 0.01 and below (Zech et al., 2015). The β fitted to the simulation results (Table 5.1) range between 0.001 to 0.008 for $\sigma_k = 0.5$, leading accordingly to a range between 0.016 to 0.128 for $\sigma_k = 2$ based on $\beta \propto \sigma_k^2$. Therefore, the range of β explored in this study covers the entire range of β encountered in practice. Recall that $D_k = \beta(A_d td)^\lambda v \propto r'^{\lambda d}$. Table 5.1 shows that λd is different for different flow field geometries, and that for the simulated scenarios, λd lies within the range 1.04 to 1.4 (excluding non-autocorrelated aquifers). Zech et al's (2015) review, and Pickens and Grisak's (1981) numerical study, suggests that λ appears to vary across different geological formations and is thus non-universal. Various studies and reviews of field, laboratory, and numerical studies (Arya, 1988; Schulze-Makuch, 2005; Neumann, 1990) have found a range of 0.755 to 1.46 for λd in heterogeneous aquifers, which agrees well with the range of λd we found.

The review studies referenced in the previous paragraph obtained β and λd by fitting a regression line between observed longitudinal dispersivity values and aquifer scale from an extensive database of numerical and experimental breakthrough curves. The agreement between the range of β and λd we find and the range found in the cited studies indicate that the β and λd we fit to recovery data, and the β and λd those studies have obtained, correspond to the same physical process. Furthermore, our findings that $\beta \propto \sigma_k^2$ approximately, which as previously discussed agrees with the literature, also emphasize that the macrodispersion described by our model of recovery efficiency corresponds mathematically and physically to the macrodispersion phenomenon observed in breakthrough curves. These agreements thus validate the methodology that we have developed for predicting and interpreting the effects of aquifer heterogeneity and macrodispersion on recovery efficiency.

For the Cape Cod experiment, Fernàndez-Garcia et al (2005) report $0.14 \leq \sigma_k^2 \leq 0.24$, $\lambda = 1$, and $45m \leq r' \leq 54m$. Based on our findings for planar flow in an exponentially autocorrelated aquifer that $\beta = 0.004$ when $\sigma_k = 0.5$, and using the relationship $\beta \propto \sigma_k^2$, we estimate that the macrodispersion coefficient $\beta r'^\lambda$ lies between 0.1m and 0.21m. Field evidence suggests a value of 0.96m for $\beta r'^\lambda$ (Garabedian et al., 1991). In contrast, Hess et al (1992) estimated $\beta r'^\lambda$ in Cape Cod to be between 0.35m to 0.78m based on the significantly more exact and complex methodology of Gelhar and Axness (1983). For the Borden experiment, also using data reported by Fernàndez-Garcia et al (2005), we estimate $\beta r'^\lambda$ to be 0.18m to 0.42m, whereas the field observed $\beta r'^\lambda$ is 0.45m to 0.49m, and the estimate based on Gelhar and Axness' method is 0.61m (Sudicky, 1986).

Although our model is somewhat less accurate for the Cape Cod experiment than for the Borden experiment, our model nevertheless provides reasonable estimates for both considering the similarly large margins of error of Gelhar and Axness' (1983) more exact and complex method. Other complex methods of estimating $\beta r'^\lambda$, such as those of Attinger et al (2001), Gelhar (1993), and Chang and Yeh (2012), also result in similarly large or even larger margins of error, even when compared against numerical simulation data (Sommer et al., 2013) that preclude the influence of measurement errors. We thus emphasize that our easily evaluable model provides utility for the characterization of macrodispersion despite being approximate.

5.4.4 Push-pull tests

Aquifer characterization by parameter inversion from single source injection-extraction cycles is known as the push-pull test method, and has thus far been successfully employed to determine a variety of

aquifer properties (Ptak et al., 2004), such as the porosity (Hall et al., 1991), in-situ microbial activity (Istok et al., 1997), fracture geometry (Klepikova et al., 2016), and geochemical reaction rates (Haggerty et al., 1998). The currently established methodology for obtaining field-scale data on dispersion and macrodispersion parameters is to measure breakthrough curves downstream of a solute source (Gelhar et al., 1992). For intentional solute introduction (with a cylindrical flow field), at least two wells are required, one for the injection and another downstream for the observations (e.g. Ptak and Teutsch, 1994). Rows of recharge wells can be lined up against rows of pumping wells to simulate forced planar flow (Molinari and Peaudecerf, 1977; Sauty, 1977). Furthermore, in heterogeneous aquifers, choosing suitable locations to place injection and observation wells is challenging due to possible bypass flow, and the scale-dependence of macrodispersion may require more wells to resolve. Gelhar and Collins' (1971) original model based on equation (5.17), which does not account for macrodispersion, has been widely used to interpret the results of push-pull tests (e.g. Schroth & Istok, 2005; Schroth et al., 2000; Wang et al., 2018). For push-pull tests in aquifers with significant heterogeneity and macrodispersion, performing parameter estimation with such local-scale dispersion models will result in significant inaccuracy (Schroth et al., 2000). Our methods, which extend Gelhar and Collins' model to explicitly consider scale-dependent macrodispersion, may therefore be more appropriate for interpreting the results of push-pull tests in heterogeneous aquifers.

Our findings that it is possible to fit these macrodispersion parameters with recovery data suggest the possibility of performing tracer tests with recovery data, in addition to solely breakthrough curve data. If Equation (5.23) is employed to estimate dispersion parameters, only a single well is required for cylindrical flow, and only a single row is required for planar flow, halving the number of required wells. While such 'single-source' methods do not solve all difficulties related to aquifer characterization, such as an inability to resolve changes in the structure of heterogeneity across space, it can simplify the problem. If regional flow is negligible, the streamlines during the extraction phase are identical to those of the injection phase, but reversed. This ensures that the experiment is less sensitive to well placement, reducing the technical complexity and reducing the minimum aquifer size necessary to simulate a (semi-)infinite domain.

Though using breakthrough curves in push-pull tests imply more flexibility in characterizing observational data, in practice the shape of the breakthrough curve is often fixed a-priori by researchers (e.g. Davis et al., 2002; Schroth et al., 2000; Snodgrass and Kitanidis, 1998). With only dispersivity to be fitted for a designated flow geometry, breakthrough curves lose this advantage over recovery efficiency. While measuring the total mass of solutes in the recovered water to calculate the recovery efficiency is straightforward, the measurement of concentrations, especially flux-averaged concentrations (Bloem et al., 2008), to construct breakthrough curves is more complicated, prone to measurement errors (Novakowski, 1992; Moench, 1989; Palmer, 1988), and often involves uncertainty regarding field-appropriate boundary conditions (Parker and van Genuchten, 1984; Kreft and Zuber, 1978; Ellsworth et al., 1996). For push-pull tests with planar flow fields (Molinari and Peaudecerf, 1977; Sauty, 1977), using the recovery efficiency instead of breakthrough curves allows the challenging task of temporally synchronizing breakthrough curves recorded by a row of observation wells to be avoided. Breakthrough curve data is also vulnerable to random errors and limited measurement precision, whereas those would be smoothed out in recovery data, as it is essentially the cumulative breakthrough curve. This suggests that using the recovery efficiency data of single-source setups may be an attractive method of characterizing aquifers.

The main limitation of using the recovery efficiency in a push-pull test is that to resolve β and λ, one has to obtain F_r a function of Q or T. Thus, multiple cycles with varying Q or T are required, but the plumes of the second and subsequent cycles will interact with the residual solutes from the previous cycles, convoluting the data. Methods to deal with this disadvantage is a potential avenue for further research,

although simply waiting between each cycle to allow the concentration or temperature to return to background levels is a possible solution. An alternative is to take into account the effects of multiple consecutive cycles in the calculations when estimating the macrodispersion parameters. In addition, as the numerical scenarios simulated were meant to represent typical ATES and ASR applications, in which the storage radius may not be large enough to sample the aquifer heterogeneity under ergodic conditions, we emphasize that the macrodispersion parameters obtained from push-pull tests with the described method characterize only the local macrodispersion. The applicability of this method in obtaining ergodic macrodispersion parameters may perhaps be clarified through stochastic testing.

5.4.5 Multiple storage cycles

In scenarios with multiple cycles, the recovery efficiency of the n-th cycle in homogeneous aquifers is given in chapter 4 as:

$$F_r(n) = 1 - \left(1 - F_{r,0}\right)n^{z-1}, \tag{5.26}$$

where $F_{r,0}$ is the recovery efficiency of the first cycle, and z is a constant with analytical bounds $\frac{1}{2} < z \leq 1$. In this study, our numerical results show that this relation applies also to heterogeneous aquifers. Figure 5.6a shows that z increases as hydrodynamic dispersion increases, but does not depend on whether a 2D or 3D aquifer is simulated, assuming the conductivity distribution and flow field geometry are identical. Figure 5.6b shows that when comparing scenarios with similar $F_{r,0}$ but different flow field geometries, z is not sensitive to the flow field geometry. Results show that z increases when σ_k increases if macrodispersion is dominant (i.e. large T) (Figure 5.6c), but not for small T where macrodispersion is weak (Figure 5.6d). Figure 5.6e and Figure 6f show that z increases as the correlation length of heterogeneity increases (i.e. z is larger in stratified than in exponentially autocorrelated aquifers) for planar and cylindrical flow, respectively. Altogether, the various plots in Figure 5.6 show that (5.26) excellently describes the recovery efficiency under multiple cycles.

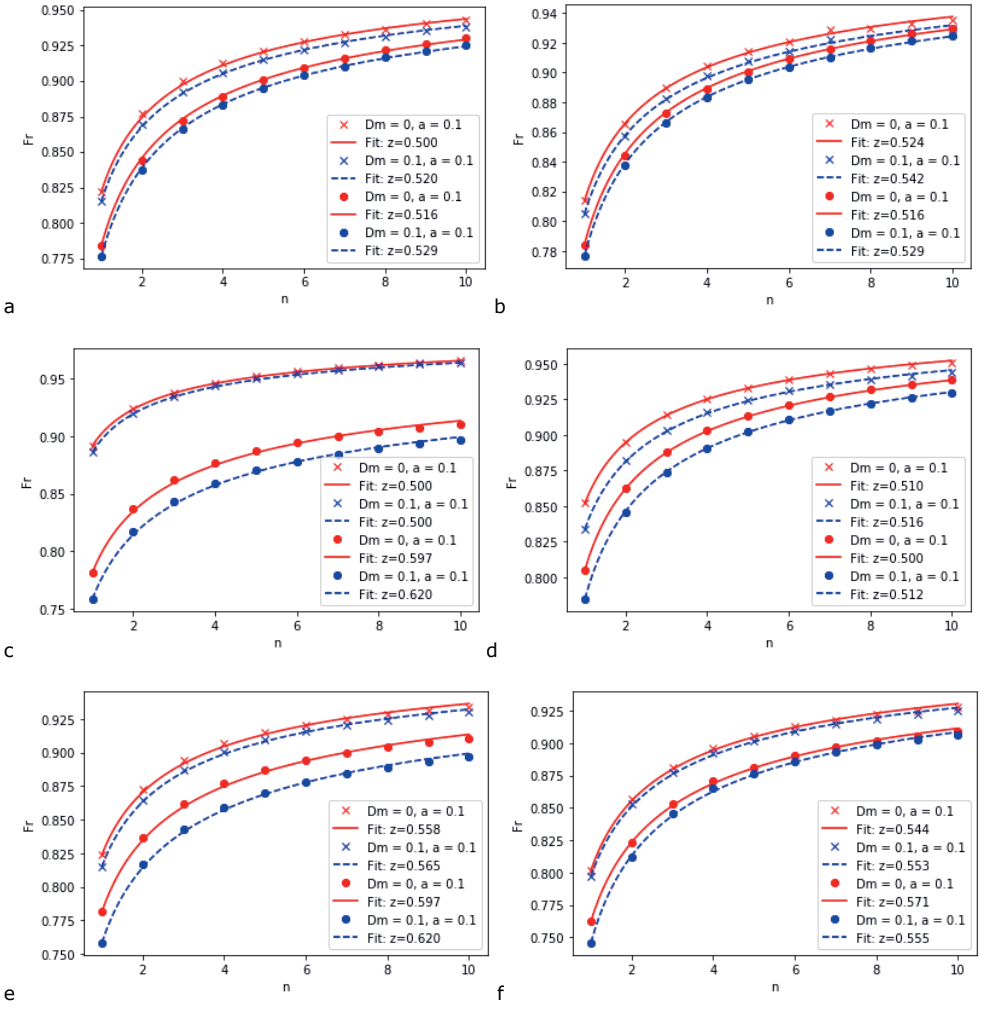

Figure 5.6: Recovery efficiency F_r of the n-th cycle, with z fitted to (26) after 10 cycles, for

(a) planar flow in 2D (**x**) and 3D (**o**) with exponentially autocorrelated heterogeneity, $T = 5$

(b) cylindrical (**x**) and planar (**o**) flow in 3D with exponentially autocorrelated heterogeneity, $T = 5$

(c) planar flow in 2D with stratification, $\sigma_k = 0.5$ (**x**) and $\sigma_k = 2$ (**o**), $T = 9$

(d) planar flow in 2D with stratification, $\sigma_k = 0.5$ (**x**) and $\sigma_k = 2$ (**o**), $T = 1$.

(e) planar flow in 2D with exponentially autocorrelated (**x**) and stratified (**o**) heterogeneity, $T = 9$

(f) cylindrical flow in 3D with exponentially autocorrelated (**x**) and stratified (**o**) heterogeneity, $T = 1$

Parameter values are $\sigma_k = 2$, $Q = 2$ for planar flow, $Q = 200$ for cylindrical flow, unless otherwise stated.

Even when additional complexity such as dispersion to confining layers, multiple wells in a densely packed configuration, storage periods without flow, density-driven flow, and regional flow are present, the general form of Equation (5.26) agrees with experimental data (see Figure 7 of Bakr et al (2013) and

Figure 10b of Kastner et al (2017)), and numerical studies (see Figure 4 of Sommer et al (2013) and Figure 5 of Zeghici et al., 2015). In particular, the heat or solute mass lost per cycle decreases rapidly, and the recovery efficiency increases sub-linearly with an apparent power-law relation, as the number of cycles increases.

The exponent z has to be empirically fitted and has a clear physical meaning, as z is a measure of how much the recovery efficiency of a cycle is affected by all the preceding cycles. The solutes left behind in the aquifer after each cycle decreases the concentration gradient between injected and ambient water in subsequent cycles, thus decreasing mixing, and increasing the recovery efficiency with each new cycles. If $z = 1$, then the recovery efficiency of every cycle is identical, meaning that solutes dissipate away from the hydraulic front infinitely quickly. Hence, the larger z is, the smaller this memory effect, and it is thus physically necessary that $z \leq 1$. In the numerical results (Figure 5.6), z increases as dispersion increases because in each subsequent cycle, the ambient chemical gradient enveloping the new injection water front dissipates more rapidly, which implies weakening the memory effect. It can also be observed in Figure 5.6 that in general, z is larger when $F_{r,0}$ is smaller, and vice-versa, though there does not appear to be a unique relationship between z and $F_{r,0}$. In our simulations, highly efficient systems with $0.75 < F_{r,0} < 1$, which are of most interest for actual implementation of aquifer storage systems, correspond to $0.5 < z < 0.65$. Additional numerical simulations (not shown) suggest that z increases towards $z \approx 0.8$ as $F_{r,0} \approx 0.5$, then $z \approx 1$ as $F_{r,0} \approx 0$. This suggests the potential for future research to possibly uncover simple analytical or empirical relationships between $F_{r,0}$ and z.

Ward et al (2008) found that if stratified aquifers are simplified and modelled as homogeneous aquifers using the harmonic mean conductivity, the recovery efficiency of the simplified model converges to that of the actual stratified aquifer after 10 cycles. Figure 5.6 indeed reveals that after 10 cycles, the recovery efficiency of all the simulated scenarios converge to approximately 0.9 regardless of the heterogeneity structure and flow field geometry. After 10 cycles, the local dispersion parameters α, D_m become more important than structural and geometrical factors in determining F_r. This can be explained by the fact that the large surface area of solute plumes associated with stratified and autocorrelated heterogeneity become inconsequential after many cycles, as the ambient water's concentration between preferential flow channels gradually equilibrates with that of the injected water. Note, however, that Ward et al simulated only one combination of well operational parameters. As we have shown, the sensitivity of the recovery efficiency to Q, T may be directionally opposite between aquifers with and without scale-dependent macrodispersion. Hence, the simplification of stratified aquifers to a homogeneous one using a harmonic mean conductivity, or analogously the simplification of exponentially autocorrelated aquifers using a geometric mean conductivity (Zinn and Harvey, 2003), should not be applied to studies where the effect of varying the injection front position is to be investigated.

5.4.6 Limitations

A limitation of our methods is that the model of the local mechanical dispersion coefficient used in the numerical simulations is $\alpha v(r)$, but that used in the analytical solution is $\alpha\langle v(r)\rangle$, where $\langle v(r)\rangle$ refers to the ensemble arithmetic mean velocity. When the spatial variance in flow velocity is small (weak heterogeneity), $\alpha\langle v(r)\rangle$ approximates $\alpha v(r)$, but the difference between the two models increases as the spatial variance in flow velocity increases (e.g. aquifers with strong heterogeneity and/or stratification). This may partly explain why the curve fitting under the imposed condition that $\beta \propto \sigma_k^2$ leads to the largest error for the stratified aquifers, because as σ_k increases the analytical model becomes insufficient to account for the effects of heterogeneity on local mechanical dispersion. This error appears to become large only for $\sigma_k \gg 1$ (Boso et al., 2013; Jankovic et al., 2006). An analysis of the numerical results shows that the fit between the analytical and numerical curves, and the theoretical relationship $\beta \propto \sigma_k^2$, are both stronger in stratified aquifers when scenarios with $\sigma_k > 1$ are excluded from the fitting. Nevertheless, the

results of Jankovic et al (2006) suggest that even in aquifers with $\sigma_k \gg 1$, applying an appropriate mean (i.e. fitted in the case of this study) β and average velocity $\langle v(r) \rangle$ to (5.23) will accurately account for over 95% of the transported solute mass.

Another limitation of our study is that we were unable to account for the magnitude of transverse dispersion in the mathematical analysis. Nevertheless, the recovery curves of numerical scenarios with both extremes of transverse dispersion magnitude: relatively small (non-autocorrelated heterogeneity) and relatively large (stratified aquifers), were successfully fitted to equation (5.24). Furthermore, the extrapolated macrodispersion parameter values presented in section 5.4.3 were reasonable. Therefore, we do not expect the omission of transverse dispersion from the mathematical analysis to invalidate our findings, at least under the common assumption that the transverse mechanical dispersivity is not larger than the longitudinal mechanical dispersivity. We reiterate that the purpose of this study is to argue that it is possible to fit the macrodispersivity parameters from recovery data using our methods, and not to find the parameter values corresponding to the heterogeneous conductivity distribution we simulated or to the field experiments discussed in this section using the most accurate possible method. In real-life cases, the intrinsic conductivity distribution and autocorrelation is seldom known, after all, thus it is arguably more important to understand the effects of macrodispersion on the recovery efficiency of aquifer storage systems, than to mathematically relate one abstract notion (conductivity distribution) to another (dispersion parameters).

5.5. Conclusion

The methods of chapter 4 are extended to calculate the recovery efficiency of an injection-extraction well under scale-dependent dispersion, such as macrodispersion in a heterogeneous aquifer. An effective dispersion constant D is constructed by adding a scale-dependent macrodispersion coefficient $D_k = \beta r^{\lambda d} v$ to the local hydrodynamic dispersion coefficient $D_h = \alpha v + D_m$. This general approach is able to characterize the recovery efficiency of aquifer storage systems and how they respond to variations in well operational parameters, number of recovery cycles, dispersion and macrodispersion parameters, aquifer heterogeneity structure, and flow field geometry.

Remarkably, if macrodispersion dominates and $\lambda d = 1$, the recovery efficiency becomes independent of both Q and T. As Q, T increases, if $\lambda d < 1$ then F_r increases, and if $\lambda d > 1$ then F_r decreases. Hence, linear scaling marks an important threshold in the effects of macrodispersion on recovery. Since macrodispersion becomes stronger with displacement, whereas pore-scale dispersion is either scale-independent (molecular diffusion) or weakens with displacement (mechanical dispersion), the recovery efficiency may be a non-monotonic function of the operational parameters T and Q in heterogeneous aquifers in 1D and 2D radial flow. In contrast, in homogeneous aquifers, non-monotonicity of the recovery efficiency occurs only for $F_r(T)$ under 3D radial flow, and never for $F_r(Q)$.

The macrodispersion parameters β and λ may be fitted from recovery efficiency data, and are parameters that are not intrinsic to the hydrogeological structure and properties of the subsurface, as they depend also on the geometry of the flow field. The expression $\beta \propto \sigma_k^2$, derived in several prior theoretical studies, agrees quite well with the values fitted to our numerical simulations. In aquifers where the heterogeneity has a longer autocorrelation range, such as perfectly stratified aquifers, λ tends to be larger.

Using the recovery efficiency as observational data in single-well tracer tests has several advantages over the classical downstream sampling of breakthrough curves. The necessary data is easier to measure

and interpret, less vulnerable to erratic data caused by fluctuations in environmental conditions, less affected by bypass flow, necessitates fewer well installations, and can be performed in smaller aquifers. As far as we are aware, transport data from single well push-pull dispersivity tests have thus far been fitted only to local-scale mechanical dispersion models, and not to macrodispersion models in particular. Single well push-pull tests based on the recovery efficiency instead of the breakthrough curve have also not yet been attempted. The findings of this paper suggest that these two endeavours are possible, especially in combination, due to their mutual complementarity.

Our methods for interpreting single well push-pull tests in heterogeneous aquifers readily reveal key insights that are complex to uncover with classical methods involving breakthrough curve fitting. Under planar or cylindrical flow, if and only if the recovery efficiency is a non-monotonic function of the injection rate, duration, or volume, then the macrodispersion coefficient of the tested system increases superlinearly with distance from the well, implying the presence of well-connected high conductivity flow paths in the aquifer. The possible universality of macrodispersion scaling, as well as whether it is linear, sublinear, or superlinear with distance, remains a longstanding unresolved topic of ongoing research. While we did not fully resolve this question, we have introduced for the first time important practical implications for aquifer storage systems and push-pull tests that arise at the threshold separating sublinear, linear, and superlinear macrodispersion scaling.

Chapter 6

Soil Contaminant Transport and Mixing-limited Biodegradation

Based on:

Tang, D. W. S., French, H. K., Leijnse, A., Bartholomeus, R. P., Van Der Zee, S. E. A. T. M. Soil Contaminant Transport and Mixing-limited Biodegradation. *Under review in Water Resources Research.*

Abstract

Aerobic biodegradation is an important mechanism of organic contaminant removal by dissipation from soils. We simulate nonlinear multicomponent biodegradation and transport of contaminants in heterogeneous soils under various transient infiltration conditions. These processes, and their interactions, introduce spatio-temporally complex behaviour that affect contaminant travel times, the extent of reactant mixing, solute and microbial biomass distributions in the soil, and biodegradation outcomes. We find that multicomponent biodegradation is predominantly limited by the extent of reactant mixing when infiltration rates are small, contaminant concentrations are high, and electron acceptors (e.g. oxygen) are abundant in the soil. Otherwise, biodegradation is mostly limited by the reaction rate. Soil heterogeneity and transient flow affect the biodegraded contaminant fraction more substantially for mixing-limited than for rate-limited biodegradation. Furthermore, the combined effects of soil heterogeneity and transient flow appear additive for rate-limited but not for mixing-limited biodegradation. Under transient flow, preferential flow zone switching reduces the spatiotemporal heterogeneity of biomass and contaminant concentrations, which accordingly also reduces biodegradation variability across random realizations of macroscopically similar heterogeneous soils. Therefore, interactions between transient flow and soil heterogeneity give rise to important higher-order effects on contaminant fate in the unsaturated zone that cannot yet be reproduced with simpler models. However, using a modified form of the Damköhler number, we were able to compute lower and upper bounds of the contaminant biodegraded fractions of the simulated scenarios, that apply when $Da < O(1)$ and $Da > O(1)$ respectively.

6.1. Introduction and literature review

Contaminants that enter the unsaturated zone at the soil surface will contaminate groundwater (Kass et al., 2005) if not transformed on the way down. For organic contaminants, aerobic biodegradation is an important mechanism of transformation (Mulligan & Yong, 2004; Singh, 2008). Essential for aerobic biodegradation is the necessity that an electron acceptor such as oxygen is simultaneously present with the contaminant and the biodegrading micro-organisms. Hence, a multicomponent description of transformation necessitates reactant mixing. However, soils are not well-mixed (Li et al., 2006; Acharya et al., 2005), thus applying multicomponent interactions at the bulk porous medium scale neglects spatial interactions that ultimately determine the fate of contaminants. For biodegradation, this has been recognized by Janssen et al. (2006), using insights from Keijzer et al. (2000). Assuming that multicomponent Monod biodegradation kinetics (e.g. Blum et al., 2009) apply at the continuum scale, mixing of the various reactants is a major factor. Accordingly, mixing-controlled biodegradation in aquifers has been widely studied, though the literature largely concerns fully saturated aquifers and steady-state flow (e.g. Puyguiraud et al., 2020; Rolle & Le Borgne, 2019; Valocchi et al., 2019; Benson et al., 2017; Ding et al., 2013; Freitas et al., 2011; Dentz et al., 2011b; Bauer et al., 2009; Cirpka & Valocchi (2007); Seeboonruang and Ginn, 2006; Janssen et al., 2006; Ham et al., 2004).

In the vadose zone, transient flow is more distinct, due to atmospheric forcing and because soil saturation and hydraulic properties dependent on the infiltration rate. This leads to fluid pressure waves that can travel as much as three orders of magnitude faster than a non-retarded solute front (Rasmussen et al., 2000). The pressure wave velocity, or *celerity*, differs from the *shock-front velocity* (Beven & Germann, 2013). If fast flow follows slow flow (a wetting front), as investigated by Warrick et al. (1971), the pressure wave which is always faster than the wetting front (McDonnell & Beven, 2014) compresses the envelope of water ahead of the wetting front into a smaller band with larger saturation. When slow flow follows fast flow, a negative pressure wave causes the envelope of water to expand. Therefore, transient flow dynamically alters the separation of 'old' and 'new' water in the vadose zone, which may be expected to influence the mixing process. Kuntz and Grathwohl (2009) found that steady-state models are sufficient in characterizing biodegradation in the vadose zone except under extreme infiltration events. However, they modelled monocomponent decay kinetics, which has a mixing-independent reaction rate. With mixing-dependent multicomponent biodegradation, it is plausible that greater differences will emerge between steady-state and transient flow situations.

A factor that affects mixing and therefore biodegradation is spatial variability of the flow domain. This has been investigated by Cirpka and Valocchi (2007), Janssen et al. (2006), Schotanus et al. (2013), and Loschko et al. (2018). Cirpka and Valocchi (2007) analytically considered transversal mixing for homogeneous steady flow, and suggested that extending the model to transient and heterogeneous flow most likely requires a numerical approach. Schotanus et al. (2013) investigated first-order biodegradation in the vadose zone under transient flow and heterogeneous conditions both in the field and with numerical simulations, and found that transient flow affects the spatial distribution of solutes. In groundwater aquifers, it has been recognised that soil heterogeneity leads to increased mixing between contaminants entering aquifers and background groundwater (e.g. Rolle et al., 2009). Spatial heterogeneity in hydraulic conductivity leads to bypass flow, which was demonstrated by Gouet-Kaplan et al (2012) with laboratory column experiments. This can increase water transport velocities and decrease contaminant residence times and biodegradation. These studies considered either the saturated zone, where heterogeneity and transient flow have different implications, or mixing-independent biodegradation, and are thus not fully applicable to multicomponent biodegradation in the unsaturated zone.

For the unsaturated zone, soil heterogeneity is typically modelled with heterogeneity in the scaling parameter of the hydraulic conductivity and retention function. Heterogeneity complicates the spatial flow variability, as was shown for steady flow by Roth (1995): the zones of preferential flow and stagnant water that establish under small mean flow rates reverse position under large mean flow rates. Thus, under transient flow conditions in the unsaturated zone, preferential flow and relatively stagnant zones will vary spatiotemporally, which dynamically changes the spatial distribution of reactants and enhances mixing. Figure 6.1, which illustrates a pilot numerical simulation involving two tracers infiltrating one after the other, shows that transient flow in a heterogeneous soil enables the two plumes to come in contact and mix. This mixing effect depends on soil heterogeneity, the already mentioned Warrick-type compression/expansion effect (Warrick et al., 1971), and the shifting pattern of preferential and stagnant zones; the last two of which are absent under water-saturated conditions. Therefore, this effect occurs only in the unsaturated zone, and requires the presence of both transient flow and soil heterogeneity.

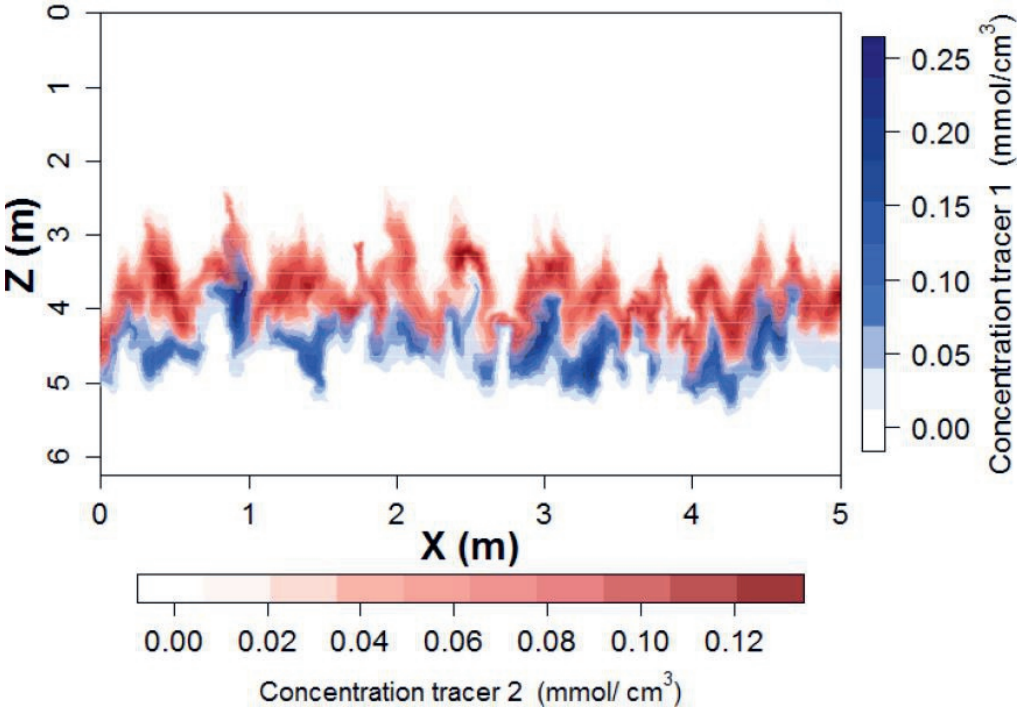

Figure 6.1: Pilot simulation of tracer plumes in a heterogeneous soil, which illustrates the how the transport of contaminant (blue) and oxygen (red) plumes in the single-transition transient flow scenarios studied would appear without biodegradation. The blue plume infiltrated first under a low infiltration rate of 0.036mm/h, and the red plume subsequently infiltrated under a high infiltration rate of 11mm/h.

It is clear that the piling up of various complexities (heterogeneity, transient flow, multicomponent degradation kinetics) allows for synergistic and antagonistic interactions; trends tend to become less clear. Nevertheless, multicomponent biodegradation may only proceed when all of the reactants involved in the reaction are present at the same place and time. Therefore, multicomponent biodegradation in soils may be limited by two overarching factors to varying extents: the rate of the reaction, and the rate of mixing (e.g. Hesse et al., 2009 and Battiato et al., 2009), relative to the soil residence time. The extents of these limitations affect the sensitivity of biodegradation outcomes to other model parameters (e.g. Song and Seagren, 2008 for saturated porous media). If the rate constant or the biomass

concentration is very low, or if the flow rate is very high, then contaminants are likely to leach because the reaction is rate-limited: there is insufficient time for the contaminants to biodegrade in the soil column. If the various reactants bypass each other in the soil, then biodegradation is limited by incomplete mixing. Perfectly rate-limited multicomponent biodegradation would display behavior akin to monocomponent biodegradation, of which first-order decay kinetics has been widely studied. However, the extent of rate-limitation and mixing-limitation are not mutually exclusive (Bauer et al., 2008; Luo et al., 2008). This is because reactant concentrations, the biodegradation rate, and the rate of dispersion and mixing are mutually dependent.

To address the effects of heterogeneity on multicomponent mixing-limited biodegradation analytically, complexity needs to be reduced. Such analyses have mostly been performed for saturated zone problems, and typically exploit some form of homogenization by dimensional reduction. For example, with quasi-one-dimensional stochastic-convective concepts, mechanisms such as transverse dispersion are neglected (Sanz-Prat et al., 2015; Sanz-Prat et al., 2016; Luo & Cirpka, 2008; Ding et al., 2013), though they may sometimes be important (Zhou et al., 2019; Zhou et al., 2020). The use of descriptive statistics, such as using average or 'effective' parameters to homogenize or upscale the problem (Dentz et al., 2011b), may be difficult to parameterize (Schäfer et al., 2020) and uncertain when extrapolated (Luo & Cirpka, 2011; Lu et al., 2018). Assuming constant parameters (e.g. van der Zee and Boesten (1991)) ignores feedbacks and is thus inappropriate for mixing-limited biodegradation. However, such simplifications may be less applicable in the unsaturated zone, as preferential flow switching makes transverse dispersion important. Furthermore, the continuous response of soil hydraulic properties to transient flow may make analyses involving constant or averaged parameters even more difficult to parameterize and generalize, while rendering binary models of heterogeneity (mobile-immobile domains: e.g. Willmann et al., (2010); Lu et al (2018)) physically unsuitable. Therefore, as a first step we approach the problem with numerical models that do not employ such simplifying methods.

Our objective is to address the combination of nonlinear multicomponent biodegradation (Monod kinetics), two-dimensional spatial variability of soil hydraulic conductivity, and transient flow, which has received little attention so far in the literature as far as we are aware. We use numerical models to investigate scenarios across categorical groups: in heterogeneous soils versus homogeneous soils, under transient flow versus steady-state flow, and for rate-limited versus mixing-limited multicomponent biodegradation scenarios. We postulate that scenarios within each category are somewhat consistent in how they respond to changes in some other parameters. Hence, a qualitative understanding of each category of scenarios is possible. The results of this general analysis may also guide the identification of important and unimportant parameters and complexities in subsequent studies, allowing the complex problem to be simplified if certain conditions are fulfilled.

Transient flow conditions can be very diverse. We emphasize two types of transient flow scenarios. The first involves a single flow rate transition, where slow infiltration of contaminant-carrying water is followed by a sudden and fast influx of contaminant-free water. This modelled situation is typical for infiltration under snow melt conditions where the infiltration rate greatly exceeds that of the preceding autumn (French et al., 2001), other situations with distinct seasonality as in Monsoonal climates, or a large rainfall season following a dryer season during which a field is irrigated with marginal water. Additionally, scenarios with daily precipitation timeseries are also studied, to obtain insights that reflect shorter-term highly variable weather.

6.2. Methods

The numerical simulations in this study concern Monod biodegradation of solutes in water that infiltrates into two-dimensional heterogeneous soils. The simulations were performed with HYDRUS2D (Simunek et al., 2012b) and PHREEQC (Parkhurst & Appelo, 2013) in the HP2 biogeochemical reactive transport package (Simunek et al., 2012a). The soil-hydraulic van Genuchten-Mualem functions are used to characterize the soil-water retention and the unsaturated hydraulic conductivity functions of soil. Scenarios with homogeneous soils were modelled with HP1 (Simunek et al., 2013). With Monod biodegradation, the reaction rate depends on the concentration of contaminant, an electron acceptor, and biomass. With biomass, in this paper we refer to microbial biomass that participates in, and is produced by aerobic transformation of the contaminant (and not to soil organic matter).

Aerobic biodegradation is modelled with Monod kinetics as described by Barry (2002). Although various chemical species such as oxygen, nitrate, and manganese can act as the electron acceptor, this is with varying levels of preference (Schotanus et al., 2014), and depends on the redox potential of the soil. We focus on dissolved oxygen as the electron acceptor. The reaction rates of the modelled reactants are

$$\frac{dC}{dt} = -\mu \frac{A}{k_A + A} \frac{C}{k_{A,C} + C} B \tag{6.1}$$

$$\frac{dA}{dt} = FX_C \tag{6.2}$$

while eliminated contaminant is converted to biomass at the following rate

$$\frac{dB}{dt} = GX_C \tag{6.3}$$

Here, A, C, and B $[mol/L$ water] are the electron acceptor (oxygen), contaminant, and biomass concentrations respectively. μ $[s^{-1}]$ is the maximum biomass growth rate, k_A $[mol/L$ water] is the half-saturation constant of the electron acceptor, $k_{A,C}$ $[mol/L$ water] is the inhibition parameter for the redox reaction between the electron acceptor and contaminant, F is the stoichiometric ratio of the oxygen in the biodegradation reaction relative to the contaminant, and G is the dimensionless yield ratio for biomass growth. Following Holden and Fierer (2005) and Grösbacher et al (2018), we omit biomass movement from the model. We also assume a uniform initial biomass concentration in the entire model domain.

As the simulations involve multicomponent dispersion and biodegradation, computational demand was large, so we reduced the domain to 100cm wide and 100cm deep. We discretized the domain with a finite element mesh of 101x101 evenly spaced nodes. This provided a balance between model resolution and computational speed. Random scaling of soil hydraulic parameters in heterogeneous soils is generated in HYDRUS2D, using exponentially autocorrelated Miller-Miller similitude (Miller and Miller, 1956). We considered 12 realizations of the heterogeneous scaling factor field, in addition to the homogeneous case. Unless stated otherwise, results reported for heterogeneous soils refer to averaged outcomes.

We simulate various biogeochemical scenarios, to investigate how they interact with the combination of complex processes we model. Table 6.1 lists the scenarios, which are simulated for all unique permutations, and the soil hydraulic parameter values used in the simulations. The soil type is loamy sand in the entire domain, and the associated soil hydraulic parameters are obtained from Carsel and Parish (1988). Parameters describing the biodegradation reaction are inspired by realistic values for propylene glycol – an antifreeze fluid used widely in climates that experience snowmelt infiltration (Schotanus et al., 2014). The outcomes analyzed are the biodegraded fraction F_d and the spatial

distribution of biomass growth $B(x,z)$. Since the biomass is immobile, $B(x,z)$ is a cumulative snapshot of where contaminant is biodegraded and reaction byproducts are formed. In turn, this contains spatial information about the mixing process.

Table 6.1: List of parameters and modelled scenarios. The infiltration regimes L(ow), M(edium), H(igh), and E(xtremely high) correspond to infiltration rates I $1x10^{-6}$, $1.09x10^{-5}$, $1x10^{-4}$, and $1x10^{-3}$ cms^{-1} respectively.

Infiltration regime $I(t)$	**Explanation**
LH	Transient flow, slow to fast
LE	Transient flow, slow to very fast
MM	Steady-state flow
MH	Transient flow, medium slow to fast
ME	Transient flow, medium slow to very fast

Biochemical scenario	**Differences relative to reference scenario**
1	Reference scenario (Monod kinetics, initially anoxic soil $A_I = 0$)
2	Initially oxic soil, initial soil oxygen concentration = $2C_0$

Monod scenario	**Explanation**
A	B_0 = 8.75E-7 mol/cm^3 and μ = 6e-7s^{-1}. Same initial reaction rate as scenario B; biomass grows slow.
B	B_0 = 8.75E-8 mol/cm^3 and μ = 6e-6s^{-1}. Same initial reaction rate as scenario A; biomass grows fast.
C	B_0 = 8.75E-7 mol/cm^3 and μ = 6e-6s^{-1}.

Contaminant input concentration C_0	**Explanation**
2.5E-7 mol/cm^3	$C_0 \ll K_{A,C}$. The reaction begins in the first-order regime of the Monod rate curve.
2.5E-6 mol/cm^3	$C_0 \sim K_{A,C}$. The reaction begins in the transition regime of the Monod rate curve.
2.5E-5 mol/cm^3	$C_0 \gg K_{A,C}$. The reaction begins in the zeroth-order regime of the Monod rate curve.

Parameter	**Explanation**	**Value**
θ_r	Residual soil water content	0.057
θ_s	Saturated soil water content	0.41
K_s^*	Reference saturated hydraulic conductivity	4.05E-3 cm/s
$\langle \log_{10} \lambda \rangle$	Mean of log(scaling factor)	0
$\sigma(\log_{10} \lambda)$	Standard deviation of log(scaling factor)	0.75
l_x	Horizontal autocorrelation length	20 cm
l_z	Vertical autocorrelation length	5 cm
α_v	Van Genuchten-Mualem parameter	0.124 cm^{-1}
n	Van Genuchten-Mualem parameter	2.28
L	Van Genuchten-Mualem parameter	0.5
α_L	Longitudinal dispersivity	1 cm
α_T	Transverse dispersivity	0.1 cm
$D_{e,C}$	Diffusion coefficient (contaminant)	1.00E-5 cm^2/s
$D_{e,A}$	Diffusion coefficient (oxygen)	2.29E-5 cm^2/s
k_A	Oxygen half-saturation constant	5E-8 mol/cm^3
$k_{A,C}$	Inhibition parameter	1.25E-6 mol/cm^3
F	$A:C$ stoichiometric coefficient	4
G	Biomass yield ratio	0.5

Simulating different combinations of μ and B_0 allows us to keep the initial biodegradation rate constant across multiple scenarios, while changing the relative rate of biomass growth, to elucidate the influence of biomass growth on the system. We also varied the contaminant concentration while keeping the oxygen:contaminant ratio constant. This enables us to compare the impact of starting at the almost linear (low concentration) or at the plateau part of the nonlinear Monod rate curve. We also compare scenarios with initially oxic and initially anoxic soils, as these scenarios are affected differently by mixing.

The initial condition for flow is steady-state with the initial infiltration rate at the upper boundary. Simulations begin with the soil containing a spatially uniform distribution of biomass (active in biodegradation) and oxygen. A 2.5cm band of contaminated water (uncorrected for porosity and saturation) infiltrates the soil uniformly at the surface, containing sufficient dissolved oxygen to biodegrade half of the contaminant according to the stoichiometric ratio. Therefore, the absolute maximum possible biodegraded contaminant fraction is 0.5 in the complete absence of mixing. All subsequent infiltrated water is contaminant-free water containing dissolved oxygen, at the same concentration as initially present in the contaminant band. Additional simulations with first-order biodegradation with a constant decay rate 6e-7s^{-1}, and where biomass growth is tracked but not factored into the decay rate, are presented for comparison where appropriate, but excluded from the data analyses.

A free drainage and boundary condition for water flow is used at the bottom of the domain, signifying that the water table is sufficiently deep that it does not affect hydraulic heads in the simulated domain. A prescribed flux boundary is used at the top of the domain. In the single-transition flow scenarios, at transition the infiltration rate changes instantaneously to a new value, occurring approximately when the center of the contaminant plume is at a depth of 35 cm. To elucidate the effect of changing preferential flow zones, the infiltration rate transitions we simulate are increases of multiple orders of magnitude.

Additionally, to investigate the effect of real weather patterns, which represent more realistic conditions and include periods of slower flow following faster flow, we repeated the simulations with two months of daily precipitation data (Volkel, the Netherlands) for May 1 to June 30 2016, a period of large weather variability. In these simulations, the infiltrating water contains contaminants and oxygen only during the first four weeks, and only oxygen during the remainder of the period. These simulations with daily precipitation data, were compared against simulations using averaged precipitation rates, wherein the two aforementioned periods were averaged separately (Figure 6.2) to ensure identical contaminant mass inflows. The precipitation timeseries were chosen such that the contaminant plume peak exits a homogeneous soil at similar times under daily and averaged precipitation rates, allowing the effects of transient flow and soil heterogeneity to be studied independently of expected contaminant residence times. Due to the large computational times required, Monod scenario B was excluded from these simulations.

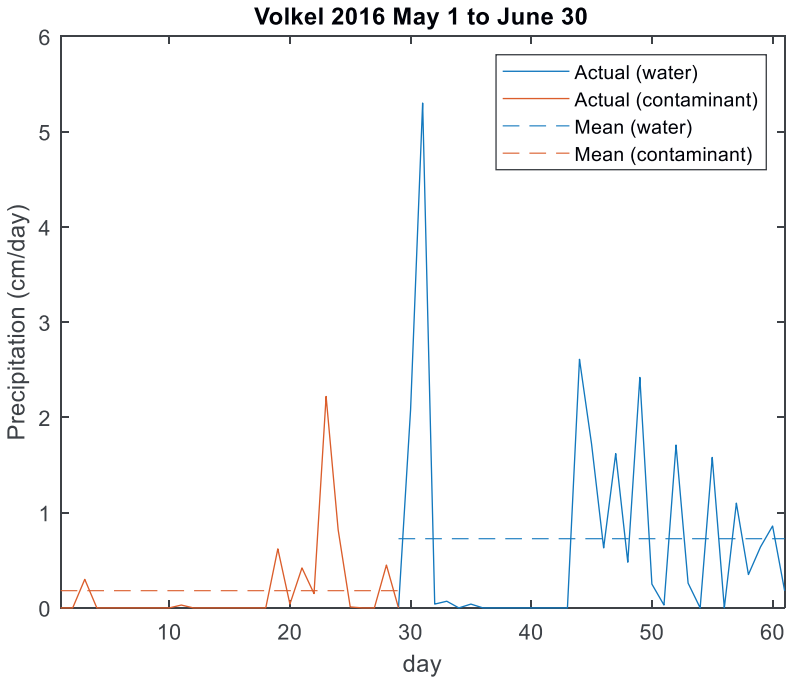

Figure 6.2: Daily precipitation data (solid lines) for Volkel, the Netherlands, from May 1 to June 30 2016 (solid lines). The red lines represent the period when infiltrating water contains contaminants, and the blue lines the period with no contaminants. The dashed horizontal lines are the averaged precipitation rates of these two periods, used in the simplified simulations.

6.3. Results and discussion

6.3.1 Flow and transport

In sections 6.3.1 – 6.3.4, we discuss how flow, transport and biodegradation outcomes vary across the modelled scenarios under single-transition transient flow. Results for real precipitation timeseries are presented in section 6.3.5. Implications of the findings are discussed in section 6.3.6.

The locations of preferential flow zones, and the extent to which they conduct water faster than the average, depend upon the infiltration rate (Figure 6.3). As shown in Figure 6.3, the switching of the preferential flow channels occurs at an infiltration rate between regime H ($1x10^{-4}$ cms^{-1}) and E ($1x10^{-3}$ cms^{-1}). As the infiltration rate increases from L to H, preferential flow weakens, because the flow finger becomes wider and the preferential flow velocity decreases from $20I$ to $3I$. When the infiltration rate increases further to E, the preferential and stagnant flow zones switch. Thus, the extent of differentiation between preferential and stagnant flow zones is the largest, and the extent of solute plume deformation relative to a homogeneous soil is largest, for low infiltration rates, in agreement with Ursino et al. (2001), and Schotanus et al (2012) and (2013).

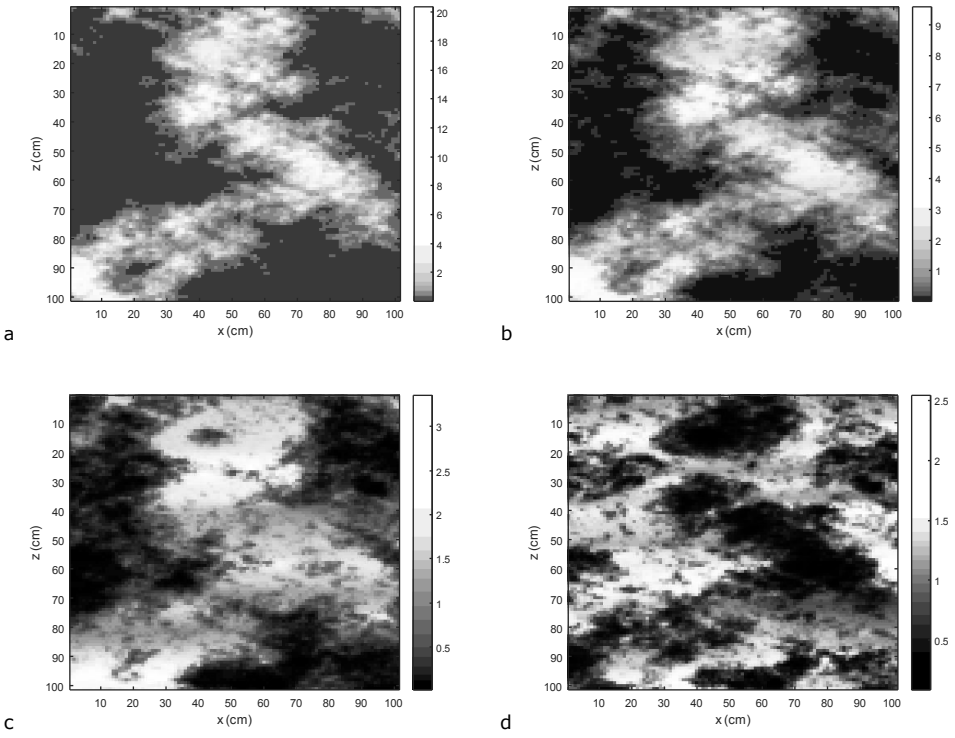

Figure 6.3: Maps of the vertical component of flow velocity divided by infiltration rate, for (a-d) infiltration rates L, M, H, E respectively at steady-state.

For 83 out of the 90 Monod biodegradation scenarios, the breakthrough time of the contaminant peak was earlier in the heterogeneous scenarios than in the homogeneous scenarios, and the similar in the remaining 7 scenarios. In steady-state scenarios in particular, the peak travel time is on average 14% smaller, and up to 21% smaller in heterogeneous soils, suggesting that the persistent preferential flow in heterogeneous soils are able to quickly channel much of the contaminant plume to the bottom of the soil column. This confirms that heterogeneity reduces the mean travel time under steady-state flow (Birkholzer and Tsang, 1997), by focusing the transport of solutes within preferential flow channels. For all transient flow scenarios, any reduction in peak travel time due to heterogeneity is less than 2 percent. Furthermore, very little solute mass remains trapped in stagnant flow zones in transient flow scenarios (Figure 6.1) – preferential flow zone switching in heterogeneous soils causes each part of the solute plume to spend some time in a preferential flow zone and some time in a stagnant flow zone. In other words, the spatio-temporal heterogeneity of solute transport in heterogeneous soils is relatively small under transient flow. Therefore, we emphasize that heterogeneity mostly decreases leaching times, and in a few scenarios results in little change to leaching times. Hence, if more biodegradation occurs in a heterogeneous soil than in a homogeneous soil, then it must be attributable to enhanced mixing and not prolonged degradation exposure or contaminants being trapped in stagnant flow zones (under transient flow).

6.3.2 Effect of biochemical parameters on biodegraded fractions

The complete list of F_d of all the simulated scenarios (averaged from the twelve heterogeneous realizations) is given in the supplementary material. Comparing F_d data of all scenarios shows that

overall F_d depends much more significantly on the infiltration rates and biogeochemical parameters, such as soil oxygen concentration (biochemical scenario 1 vs 2), relative initial biomass growth rate (Monod scenarios A vs B), and initial contaminant concentration (low vs mid vs high), than on soil heterogeneity.

For most scenarios, the biodegraded fraction depended significantly on initial soil oxygen concentration, but was quite insensitive to the relative initial biomass growth rate. When oxygen availability is the limiting factor, a larger biomass growth rate only shifts the biodegradation to shallower soil, but does not increase total biodegradation. The reverse, a significant effect of biomass growth but not of initial oxygen concentration, occurs only for the scenarios with a medium (M) pre-transition infiltration rate and large reactant concentrations in the infiltrating contaminant plume. This reveals a bottleneck behavior based on either biomass or oxygen as a limiting reagent: each scenario is sensitive to either initial oxygen concentration or biomass growth rate, but never both or neither.

When varying C_0 in Monod biodegradation scenarios, the highest degraded fraction occurs for $C_0 \sim K_{A,C}$, so F_d varies non-monotonically with C_0; this can be analytically proven for a perfectly mixed reaction (Appendix 6A). Amongst the scenarios we simulated, F_d varies non-monotonoically with C_0 for 53% of Monod scenarios. The non-monotonicity is not observed in all simulated scenarios, because the assumption of perfect mixing does not hold. This emphasises the importance of mixing in determining the fate of contaminants in our scenarios.

We attempted to investigate whether an easily observable modified form of the Damköhler number Da (Appendix 6B), may be used to characterize biodegradation outcomes. In the idealized case that biodegradation is first-order, soils are homogeneous, and no dispersion occurs, F_d and Da are related exactly through the relationship $F_d = 1 - \exp(-Da)$. A scatterplot of F_d against Da for all simulated scenarios (Figure 6.4) shows that this theoretical relationship does not describe the studied scenarios well. However, we note that the pivot point where underprediction of F_d with $F_d = 1 - \exp(-Da)$ switches to overprediction occurs at around $Da \sim 1$. At $Da \sim 1$, the idealized reaction rate and transport rate are of similar orders of magnitude.

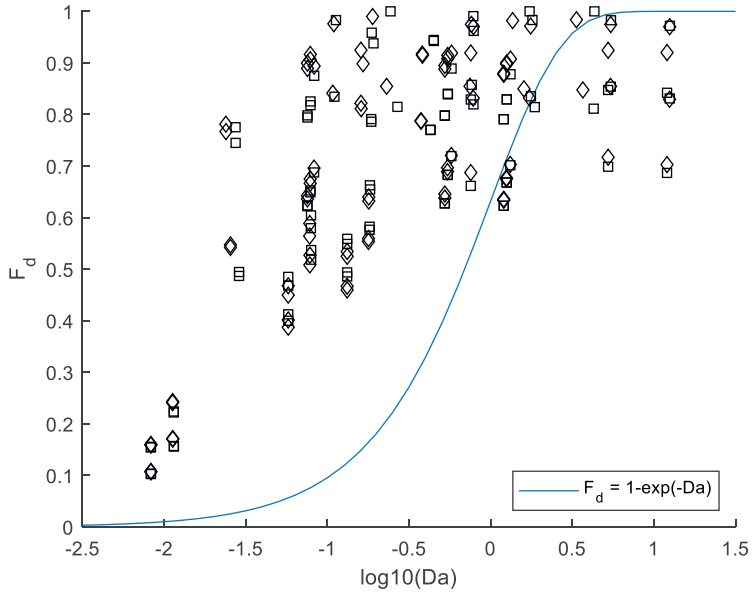

Figure 6.4: Scatter plot of F_d against log10(Da) for all scenarios; squares are homogeneous scenarios and diamonds are averages of heterogeneous scenarios.

Consider that the relative contaminant depletion rate $\frac{1}{C}\frac{dC}{dt}$ may only increase due to biomass growth, and decreases due to all other processes (reactant dilution and depletion). The fact that $F_d = 1 - \exp(-Da)$ underpredicts F_d at $Da < O(1)$ suggests that for these scenarios, the influence of biomass growth in increasing F_d is greater than the influence of reactant depletion and dilution in decreasing F_d. When Da is small and the (initial) reaction rate is low, biomass growth strongly influences F_d, because the reaction rate is more sensitive to increases in the biomass density. When Da is large and the reaction rate is high, F_d in the simulated scenarios is lower than predicted because of imperfect mixing, which suggests that as the extent of rate-limitation decreases, F_d becomes more controlled by mixing-limitation. Ultimately, the wide scatter and weak fit of the data with $F_d = 1 - \exp(-Da)$ suggests that the complexities neglected in the calculation of Da render it of minimal use in predicting overall biodegradation outcomes. However, $F_d = 1 - \exp(-Da)$ appears to be a soft lower bound for $Da < O(1)$ and soft upper bound for $Da > O(1)$, that requires further research to ascertain.

6.3.3 Role of mixing in biodegraded fraction outcomes

Since soil heterogeneity increases dispersion and mixing (Birkholzer & Tsang, 1997; Moreno & Tsang, 1994; Rolle et al., 2009; Valocchi et al., 2019; Cirpka et al., 2011; Luo et al., 2008; Willingham et al., 2010; Werth & Cirpka, 2006), and since we have found that soil heterogeneity causes decreased residence times in most scenarios, and never significantly increasing it, it follows that if F_d is increased by soil heterogeneity then the scenario is most likely mixing-limited.

Out of 90 Monod scenarios, 59 were mixing-limited as F_d was larger in heterogeneous soils than in homogeneous soils. Scenarios are found to be mixing-limited if one or more of the following three criteria

are fulfilled. 1) The initial infiltration rate is low (regime L), which makes biodegradation less limited by reaction rate. 2) The incoming contaminant concentration is large ($C_0 \gg K_{A,C}$). This is because even as the contaminant plume grows due to dispersion, the reaction rate per unit soil volume does not decrease much, because it is in the zeroth-order (plateau) region of the Monod rate curve. Therefore, its biodegradation potential is limited by how fast the contaminant plume can spread and mix. The observations that a large C_0 and transport dominated by diffusion (i.e. low advection velocity) leads to enhanced biodegradation under spatially heterogeneous concentrations has also been made by Hubert et al (2020), for reactions in a bulk fluid. 3) The soil is initially oxic and the initial infiltration rate is low. Then, the reaction is less rate-limited, as oxygen is abundant outside of the contaminant plume in this case, hence biodegradation is more sensitive to how much mixing occurs.

These factors that contribute to the mixing-limitation score suggest that rate-limited biodegradation is more limited by the rate of consumption of oxygen initially present in the contaminant plume, while mixing-limited biodegradation is limited by the extent of spreading and mixing with oxygen external to the contaminant plume. For each of the above three criteria, we give a score (0,1) which we sum. We call this sum the mixing-limitation score, and it reflects the extent that mixing is the dominant limiting factor. For a score of 0, biodegradation is limited predominantly by the reaction rate, whereas a score of 3 indicates strong mixing-limitation.

There are 36, 30, 18 and 6 scenarios with a mixing-limitation score of 0, 1, 2 and 3, respectively. The scenarios with a score of at least 1 overwhelmingly have F_d larger in heterogeneous soils than in homogeneous soils (Figure 6.5a). The mean increase in F_d, compared to homogeneous soils, increased with the mixing-limitation score, and were -2%, 3%, 6% and 10% respectively. Since the increase in F_d increases with mixing-limitation score, we have identified the right factors that contribute to mixing-limitation. Furthermore, the higher the mixing-limitation score, the less likely that heterogeneity decreases F_d of a scenario. The small average effect of heterogeneity on F_d for scenarios with a mixing-limitation score of 0 agrees with Mohamed et al (2006), who found that soil heterogeneity is inconsequential for Monod F_d, in scenarios where the contaminant and electron acceptors are already perfectly mixed upon entry into the soil (i.e. not mixing limited).

The Damköhler number also reveals interesting nuances in the results of the F_d ratio. Figure 6.5b does not show a clear relation between the F_d ratio (heterogeneous F_d/ homogeneous F_d) and Da, except for the black-colored points, which represent scenarios with a mixing-limitation score of 0. For these points, a positive relationship is discernible in Figure 6.5b. This suggests that the F_d ratio increases for rate-limited scenarios when Da increases (i.e. when the extent of rate-limitation decreases). This implies that as rate-limitation becomes less and mixing-limitation more dominant, soil heterogeneity becomes more likely to increase F_d, even for mixing score 0. In other words, for scenarios that do not fulfil the discrete mixing-limitation criteria, a large Da may nevertheless signify increased likelihood of mixing-limitation. Hence, the two causes of limitation are not mutually exclusive, in agreement with Bauer et al. (2008), but may only be compared in terms of which is more dominant.

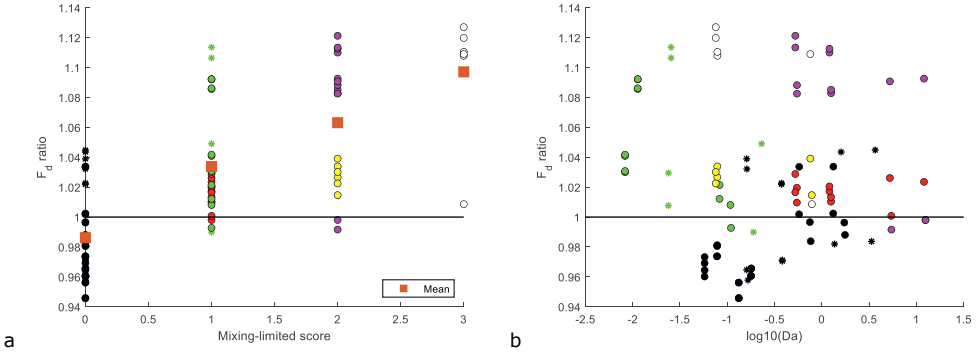

Figure 6.5: Scatter plot of how the F_d ratio, $F_d(heterogeneous)/F_d(homogeneous)$ varies with a) mixing-limitation score and b) Da. A ratio larger than 1 implies that the heterogeneous average F_d is larger than the homogeneous case, and vice versa. Solid and asterisk symbols refer to transient and steady flow respectively. The colors represent their respective combinations of mixing criteria 1, 2, and 3 respectively (see section 6.3.3). Red = (1); Green = (2); Magenta = (1,3); Yellow = (1,2); White = (1,2,3); Black = rate-limited scenario.

6.3.4 Spatial distribution of biomass

The resulting spatial distribution of biomass determine where and to what extent future influxes of contaminant will be biodegraded in the soil, and how the infiltration rate and its variability affect biodegradation. Under highly variable infiltration rates, contaminant infiltration paths during subsequent influxes may bypass established biomass hotspots if biomass is heterogeneously distributed in the soil. Furthermore, the spatial distribution of biomass also reveals the distribution of reaction byproducts, which may be toxic or ecotoxic for some contaminants.

The simulations for the lowest initial infiltration rate (LH, LE) show that almost all of the biodegradation occurs in the uppermost layers. Thus, $\langle B(z) \rangle$ decays monotonically with depth for these scenarios, similar to experimentally observed $\langle B(z) \rangle$ (Biro et al., 2014) for first-order biodegradation. Figure 6.6a (steady-state) and Figure 6.6b (transient flow) illustrate simulated $\langle B(z) \rangle$ for first-order biodegradation. Unlike first-order biodegradation, however, for Monod kinetics a maximum in biomass population density $\langle B(z) \rangle$ might occur at some distance beneath the surface (Figure 6.6c with steady-state flow, Figure 6.6d with transient flow) for larger initial infiltration rates, regardless of steady-state or transient flow. We refer to this distance as the maximum biomass depth d_{max}.

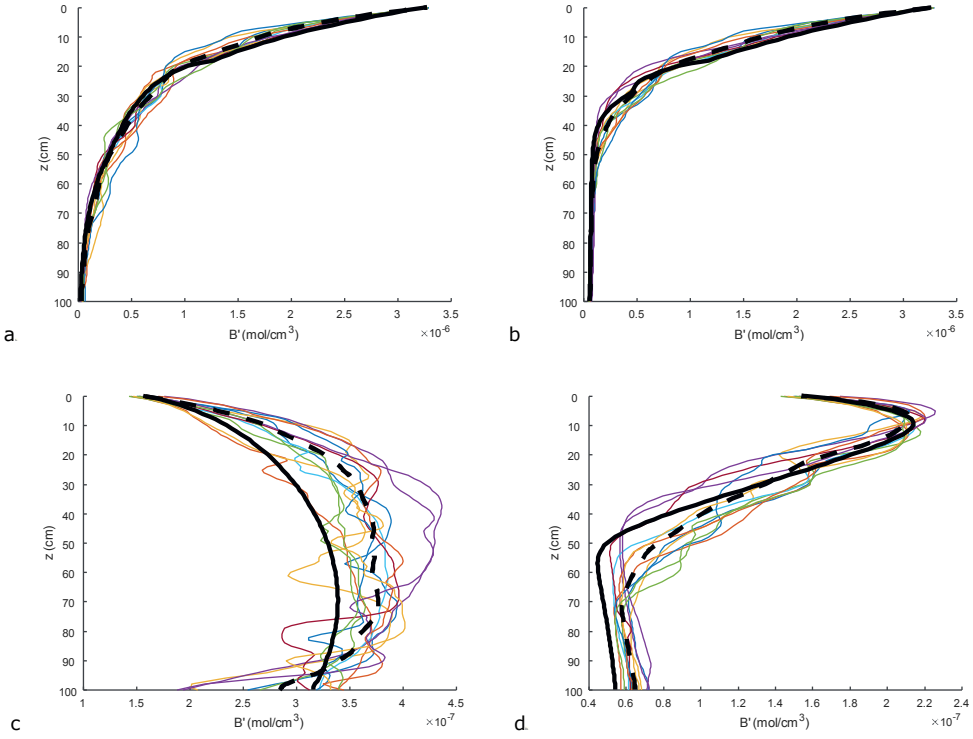

Figure 6.6: Depth against biomass growth $B' = B - B_0$. The bold solid line is for homogeneous soils, the bold dashed line is for the heterogeneous average, and the thin solid lines are for individual realizations in heterogeneous soils. (a,b) First-order biodegradation, steady-state MM and transient MH infiltration respectively. (c,d) Monod scenario B1 and $C_0 \gg K_{A,C}$, with steady-state MM and transient MH infiltration respectively.

The presence of a non-monotonic biomass profile with depth was also not correlated to Da, because the vertical distribution of biomass is controlled more significantly by the initial reaction and infiltration rates, than the average reaction and infiltration rates.

In the scenarios where $\langle B(z) \rangle$ does not monotonically decrease with depth, the reason is that dispersion causes the contaminant and oxygen plumes to grow as the plume travels downwards. Meanwhile, the initial decrease in reaction rate due to dispersion and biodegradation is small. Hence, the biomass at d_{max} has greater total exposure time to the reaction, as compared to the top of the soil, due to the larger plume encountered. The biomass at d_{max} also encounters more backwards dispersion than the biomass at the topsoil. If the larger total exposure time outweighs the slow decrease in reaction rate, then soil at d_{max} will experience more total reaction than upstream soil. Therefore, Monod biodegradation activity is often largest at some depth beneath the soil surface, especially when reactants require time and distance to mix. On the other hand, first-order biodegradation activity is always at a maximum at the soil surface, as it is not mixing-dependent. Under field and experimental conditions, both monotonically decreasing and non-monotonically varying biomass densities have been observed (Hickman & Novak, 1989; Soulas and Lagacherie, 2001).

The vertical distribution of the biomass population varies significantly in shape between each heterogeneous realization, and the heterogeneous average (Figure 6.6). However, the heterogeneous average $B(z)$ is similar to the homogeneous $B(z)$ in shape, and heterogeneity does not alter d_{max} significantly on average. Although the shape of the average $B(z)$ curve is similar in heterogeneous and homogeneous soils, the $B(z)$ curves in heterogeneous soils are somewhat larger because more biodegradation occurred there. Figure 6.6 also shows that the variance in $B(z)$ across heterogeneous realizations is significantly larger for Monod biodegradation than first-order biodegradation, due to differences in mixing across each realization.

The horizontal coefficient of variation of biomass ($\eta_B = \sigma_B/\langle B \rangle$), where σ_B is the standard deviation of $B(z)$ in the horizontal direction calculated across all heterogeneous realizations, quantifies how unevenly biomass is distributed across a horizontal layer of soil. Such uneven distributions of biomass have previously been observed in groundwater aquifers (e.g. Vroblesky and Chapelle, 1994), in addition to hotspots of the associated biodegradation reaction products (Jobelius et al., 2011). For steady-state flow, Figure 6.7a shows that η_B tends to increase with depth; more for first-order biodegradation than for multicomponent biodegradation. This is because first-order biodegradation occurs primarily in the preferential flow zones under steady-state flow. In contrast, Monod biodegradation mostly occurs in tandem with reactant mixing, and as a result is less concentrated in preferential flow zones.

For transient flow scenarios (Figure 6.7b), since the time of the flow rate transition is fixed across all 12 realizations, the maximum in η_B located in shallower soil corresponds to the plume's vertical position at the time of flow transition. This maximum in η_B occurs because the vertical location of the plume is different in the 12 heterogeneous realizations at the time of the transition. However, η_B decreases at depths traversed by the plume after the onset of transient flow, as the horizontal distribution of the reaction becomes spread more uniformly, due to preferential flow switching. Therefore, after a flow transition, the vertical displacement of the contaminant plume becomes controlled by the cumulative infiltration and less sensitive to heterogeneity, in agreement with French et al's (1999) findings for conservative solutes.

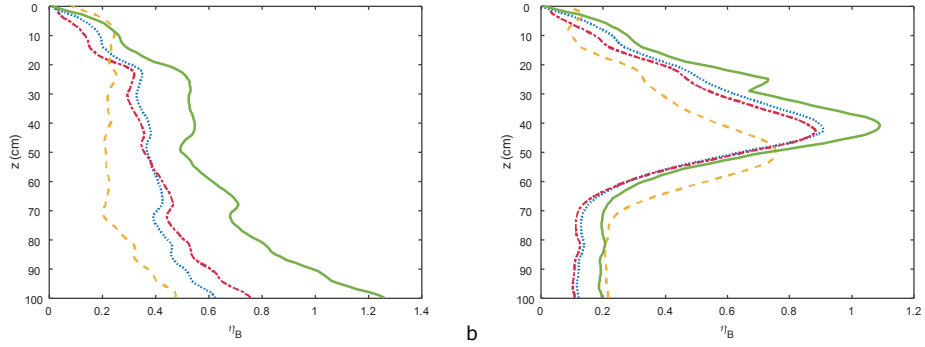

Figure 6.7: Depth against horizontal coefficient of variance of biomass η_B at the end of the simulation for Monod scenario B2. The dashed, dotted, and dash-dotted lines are for Monod biodegradation with $C_0 \gg K_{A,C}$, $C_0 \ll K_{A,C}$, and $C_0 \sim K_{A,C}$ respectively. The solid line represents a first-order biodegradation scenario. (a) Steady-state infiltration MM. (b) Transient infiltration MH.

6.3.5 Real precipitation timeseries

Outcomes of F_d in the comparison of scenarios with daily (transient) and averaged (steady-state) real precipitation timeseries are presented in Table 6.2. This data is consistent with the results of the single-transition scenarios, which show that soil heterogeneity increased F_d for most scenarios. Henceforth, we refer to simplified scenarios which simulate homogeneous soils under mean precipitation rates as the base case.

Table 6.2: Biodegraded fractions and CV of Volkel scenarios. CV refers to the coefficient of variance of F_d across heterogeneous realizations.

	Actual Daily Infiltration Rates			**Mean (single-transition) Infiltration Rates**		
Rate-limited Scenarios	**Homogeneous Soil F_d**	**Heterogeneous Soil F_d (Average)**	**CV**	**Homogeneous Soil F_d**	**Heterogeneous Soil F_d (Average)**	**CV**
$C_0 \ll K_{A,C}$						
A1	0.674	0.719	0.023	0.658	0.700	0.032
A2	0.830	0.887	0.030	0.801	0.880	0.040
C1	0.690	0.749	0.025	0.673	0.739	0.030
C2	0.876	0.960	0.024	0.832	0.945	0.029
$C_0 \sim K_{A,C}$						
A1	0.680	0.729	0.024	0.664	0.711	0.043
A2	0.841	0.896	0.031	0.813	0.903	0.059
Mixing-limited Scenarios						
C1	0.692	0.752	0.025	0.845	0.743	0.032
C2	0.879	0.965	0.023	0.983	0.950	0.030
$C_0 \gg K_{A,C}$						
A1	0.547	0.560	0.054	0.597	0.640	0.101
A2	0.565	0.583	0.036	0.693	0.717	0.164
C1	0.707	0.750	0.026	0.965	0.740	0.032
C2	0.891	0.961	0.025	1.000	0.948	0.030

For scenarios that are more rate-limited, F_d under daily precipitation rates are slightly higher than under mean rates. This suggests that transient flow is of relatively limited consequence to rate-limited biodegradation, which agrees with the findings of Kuntz and Grathwohl (2009) for first-order biodegradation. For all rate-limited scenarios here, soil heterogeneity slightly increases F_d. Comparing F_d in the base case, against scenarios with one or both types of spatio-temporal heterogeneity, suggests that the effects of soil heterogeneity and daily precipitation rates are somewhat additive. This implies that under rate-limited biodegradation, the effects of soil heterogeneity and transient flow on F_d may be mostly independent of each other.

For scenarios that are more mixing-limited, Table 6.2 reveals that compared to the base case, adding transient flow in isolation greatly decreases F_d in all cases. Adding soil heterogeneity alone to the base case may either increase or decrease F_d. However, adding soil heterogeneity to scenarios with daily infiltration rates always increases F_d. Therefore, for mixing-limited biodegradation, the effects of spatial heterogeneity and temporal heterogeneity in flow rates clearly interact non-additively, and may counteract each other to some extent. The fact that the coefficient of variance of F_d across heterogeneous soil realizations is smaller under transient flow (Table 6.2) also attests to this, in agreement with Schotanus et al (2012) and our aforementioned findings that transient flow reduced the spatial heterogeneity in biomass growth and the temporal heterogeneity in contaminant leaching to groundwater.

Compared to the base case, the greatest relative difference (decrease) in F_d occurs when transient flow (but not soil heterogeneity) is introduced to mixing-limited scenarios. This is because under transient flow, the contaminant plume receives oxygen due to mechanical dispersion mostly on days with substantial rainfall, during which established biomass is quickly bypassed. On days with low rainfall, the contaminant plume moves minimally allowing consumption by biomass, but because the scenario is mixing-limited the oxygen supply is limited by the lack of mechanical dispersion. This stop-and-go transport of contaminant leads to less mixing-limited biodegradation because oxygen and biomass availability tend to occur at different points in time and space. Furthermore, the magnitude of reactant mixing has a relationship of diminishing returns with respect to concentration gradients. Therefore, separate periods of dispersion and biodegradation under the highly variable daily precipitation rates lead to less mixing, compared to continuous mixing and depletion of oxygen under steady-state flow.

When soil heterogeneity is introduced to the above transient flow case, the decrease in F_d caused by the stop-and-go effect is weaker because mixing is more evenly distributed across space and time, because preferential flow channels always exist somewhere, allowing significant flow and mechanical dispersion to occur at any moment regardless of the infiltration rate. It has already been emphasized in the literature (e.g. Schirmer et al., 2001) that more highly variable flow rates also lead to larger transversal interfaces between 'old' and 'new' water, and hence larger areas where mixing may occur (Bauer et al., 2008). This further emphasizes the importance of transverse dispersion in the unsaturated zone, and that spatial heterogeneity and transient flow have mutually interacting and compensating effects for mixing-limited biodegradation.

6.3.6 Implications

The complexity of multicomponent biodegradation in steady-state saturated zone transport is already quite large, as current complexity reducing approaches are mostly accurate for specific conditions that assume reactants are well-mixed to some extent. For example, quasi-steady-state chemical conditions (Schäfer et al., 2020), reaction rates dependent on averaged concentrations (Massoudieh & Dentz, 2020), predominantly rate-limited conditions (Wright et al., 2021), (near-)instantaneous kinetics (Loschko et al., 2019), or large time asymptotic behavior (Wright et al., 2017). Unsaturated zone solute leaching occurs on a much shorter length and time scale than saturated zone transport. Here transient flow profoundly alters F_d, variance in F_d across realizations, and the spatial distribution of biomass growth, which shows that transient changes in soil hydraulic properties play an important role in determining the location and extent of mixing. These observations, in addition to the wide scatter in the relationship between F_d and Da, and the importance of transverse dispersion, suggest that current complexity reducing methods may be less applicable in the unsaturated zone. In particular, physical and chemical heterogeneity cannot be separately homogenized or upscaled (Dentz et al., 2011a). Since transient flow in unsaturated soils also gives rise to continuously changing physical conditions, and not only chemical conditions, the complexity of the heterogeneous problem greatly increases. The difficulty of coupling these processes is exacerbated in real three-dimensional soils, where twisting and helical streamlines are present (Cirpka et al., 2015; Chiogna et al., 2015).

Many recent developments on solute transport in heterogeneous aquifers have characterized spreading as a stochastic Markov process (Aquino & Le Borgne, 2021; Sherman et al., 2020; Dentz et al., 2020; Kang et al., 2020; Comolli & Dentz, 2017; Kang et al., 2015). Homogenization and upscaling of mixing-limited reactions is challenging even for steady-state flow in fully saturated aquifers, because the characterization of chemical reactions is non-Markovian: the system state at every moment depends on every step in its history (Dentz et al., 2011b). For the unsaturated zone, we found that interactions between transient flow and heterogeneity appear additive for rate-limited scenarios, but not for mixing-

limited scenarios. This highlights the influence of the nonlinear relationships between infiltration rate, soil water retention, hydraulic conductivity, and extent of preferential flow, on mixing. With such nonlinearity, homogenization and upscaling becomes even more challenging, as the characterization of flow and water retention also becomes non-Markovian and depends on the exact sequence of infiltration events. For example, whether fast flow follows slow flow or vice-versa determines the evolution of the contaminant plume's spreading and dilution, which affect the concentration gradients that control dispersive mixing and the spatial distribution of biomass growth. The stop-and-go effect we introduced is another example. Thus, for general analytical characterizations to be possible, it is necessary to first develop methods to simultaneously upscale continuously changing physical and chemical heterogeneity, and take into account coupled non-Markovian behavior in both the physical and chemical aspects of the problem. Accordingly, a possible starting approach is to assume that physical and chemical heterogeneity are correlated, as has been studied recently for saturated zone transport (Zhou et al., 2019; Mohamed et al., 2010; Jang et al., 2017; Chaudhuri & Sekhar., 2007; Loschko et al., 2018; Loschko et al., 2019), though it is unclear to what extent this assumption is valid.

6.4. Conclusion

We addressed the combination of biodegradation with multicomponent Monod kinetics, spatially autocorrelated heterogeneous soil physical properties, and transient flow, and investigated how the biodegradation of contaminants in unsaturated soil is affected by these factors. Growth of immobile biomass is used to track the cumulative history of biodegradation. We demonstrated that models with and without these complexities may result in significantly different predictions of biodegraded contaminant mass, biomass growth, and spatial distributions of contaminants, biomass, and reaction byproducts. This may be important in practice, if prior events affect subsequent ones. For microbial transformations, with lag phases and priming effects, the spatiotemporal variability of microbial activity will have implications on degradation (Biro et al, 2014).

In soil contamination scenarios, multicomponent biodegradation may be limited by the extent of mixing between reactants. Soil heterogeneity has been shown to increase mixing in the literature, and found to decrease mean contaminant residence times in our scenarios. Therefore, we determined which of the simulated scenarios are limited by reactant mixing by observing which resulted in more biodegradation under soil heterogeneity. We find that multicomponent Monod biodegradation is more likely mixing-limited when (i) the infiltration rate is small, (ii) the contaminant concentration is large, and (iii) the soil is abundant in electron acceptors such as oxygen prior to infiltration. For scenarios that do not satisfy the above criteria, a large Damköhler number may also signify increased mixing-limitation, because it reduces the extent of rate-limitation. In mixing-limited cases, mixing between contaminants and reactants is more likely to be a bottleneck for biodegradation, than residence time.

We find that the influence of the additional complexities (soil heterogeneity and transient flow) on biodegraded fractions is significantly greater for mixing-limited scenarios than for rate-limited scenarios. Furthermore, the effects of soil heterogeneity and transient flow appear to be additive for rate-limited biodegradation but not for mixing-limited scenarios. If both soil heterogeneity and transient flow are present, it is important to simulate both simultaneously, especially for mixing-limited scenarios, as coupled and interaction effects would not be accounted for otherwise. These higher-order interactions between heterogeneity and transient flow make Monod biodegradation difficult to characterize, especially under mixing-limited conditions.

Reduced complexity models of mixing-limited biodegradation, widely developed for saturated zone transport, do not appear generally applicable to the unsaturated zone. Fortunately, the highly

heterogeneous spatial distribution of biomass and reaction byproducts that would occur in heterogeneous soils under steady-state flow is less prominent under transient flow. Therefore, transient flow reduces the variation in outcomes across heterogeneous realizations, which may alleviate the computationally intensive task of using full-complexity models to characterize multicomponent biodegradation in heterogeneous soils under transient flow. Using the peak breakthrough time and initial reaction rate, we defined a modified form of the Damköhler number, which systematically underpredicted biodegradation for $Da < O(1)$, and systematically overpredicted biodegradation for $Da > O(1)$, using the relationship $F_d = 1 - \exp(-Da)$. Additional research may reveal whether this equation may be generally used to compute lower and upper bounds of F_d for similar biodegradation problems, thereby enabling rough predictions of the biodegraded fraction when computationally intensive simulations are not possible.

Appendix 6A: Input concentration dependence of perfectly mixed Monod biodegradation

Consider two generic perfectly mixed Monod biodegradation scenarios with $C_0 = C_1$ and $C_0 = C_2$, where $C_1 < C_2$ and $C_1, C_2 \ll K_{A,C}$. This reaction behaves similarly to first-order decay with growing rate constant. To illustrate, we omit oxygen concentration dependence and absorb the biomass term into the rate constant $\mu'(t) = \mu B(t)$, so that $\frac{\partial C}{\partial t} \approx -\mu BC = -\mu'(t)C$. Since $C_1 < C_2$, it follows that $\left(\frac{\partial B}{\partial t}\right)_1 < \left(\frac{\partial B}{\partial t}\right)_2$, $B_1(t) < B_2(t)$ and $\mu_1'(t) < \mu_2'(t)$ for all $t > 0$, ultimately resulting in $F_{d,1} < F_{d,2}$. Now instead consider the cases $C_0 = C_3$ and $C_0 = C_4$, where $C_3 < C_4$ and $C_3, C_4 \gg K_{A,C}$. For all small t (i.e. while the reaction remains zeroth-order), $B_1(t) \approx B_2(t)$ and $\left(\frac{\partial C}{\partial t}\right)_3 \approx \left(\frac{\partial C}{\partial t}\right)_4$. Therefore, $\frac{d}{dt}\left(\frac{C}{C_0}\right)_3 > \frac{d}{dt}\left(\frac{C}{C_0}\right)_4$ and $F_{d,3} > F_{d,4}$. Therefore, F_d for Monod kinetics varies non-monotonically with C_0, maximizing approximately when $C_0 \sim K_{A,C}$.

Appendix 6B: Damköhler number

The Damköhler number, which specifies the dimensionless ratio of the reaction rate over the characteristic transport (advection) rate of the system, and is widely used in describing and characterizing biodegradation in hydrogeological systems (e.g. Kuntz and Grathwold, 2009), especially for first-order biodegradation. The Damköhler number describes how much the biodegradation is limited by reaction rate, relative to the transport velocity.

Since the total biodegradation in the soil profile is the result that we seek to characterize, and since computing the true Damköhler number of each scenario requires prior knowledge of biodegradation outcomes, it would be circular reasoning to use the true Damköhler number to estimate the biodegradation outcomes of scenarios. Therefore, we instead introduce a modified version of the Damköhler number, that may be more easily determined in field and laboratory situations, and possibly be used to estimate or characterize biodegradation outcomes such as F_d, which is more difficult to measure. We define this modified Damköhler number as $Da = \frac{t_{peak}}{C_0}\left(\frac{dC}{dt}\right)_{t=0}$, where t_{peak} is the time at which the peak of the contaminant plume exits the soil column, and $\left(\frac{dC}{dt}\right)_{t=0}$ is easily calculated from equation (6.1).

Chapter 7

Synthesis

7.1 General discussion

Subsurface irrigation and drainage with treated wastewater is an emerging technology that may play a significant role in the alleviation of freshwater scarcity and environmental pollution. It falls under the umbrella of technologies referred to as managed aquifer recharge (MAR), which generally refer to systems that store water for a period of time while retaining or improving its quality, whilst achieving other goals such as agricultural irrigation or the reduction of coastal seawater intrusion. In the most commonly implemented MAR systems, such as aquifer storage and recovery (ASR) and aquifer thermal energy storage (ATES), the recovery efficiency of the injected freshwater and heat, respectively, is the key performance metric of the system. For subsurface irrigation and drainage with treated wastewater, the goal is to ensure that the phreatic groundwater level is maintained at a sufficiently high level so that crops receive enough moisture from capillary rise. This has to be done while ensuring that the contaminants of emerging concern (CECs) contained within the treated wastewater are not taken up by the crops, and do not spread in an untransformed state to deeper groundwater aquifers or surface water bodies.

Two processes that occur under subsurface irrigation and drainage with treated wastewater can eliminate the irrigated CECs from the subsurface, before they spread to the environment. The first process is transformation into nontoxic or less toxic substances, of which biodegradation by soil microorganisms plays an important role. The second process is drainage by the drainage system outside of the crop season, or on very wet days during the crop season. Although all CECs are susceptible to transformation to some extent, given that they are not elemental contaminants such as lead, the biodegradation rate of a CEC may strongly depend on the extent of mixing of the CEC with the substances and microorganisms required for biodegradation to occur, and on the identity of the CEC. Firstly, this implies that the spatial distribution of the CECs, microorganisms, and other substances such as electron acceptors that are required for the biodegradation to occur, are important in determining the fate of CECs irrigated into the soil by the subsurface irrigation system. Secondly, in practice, some CECs may be much more biodegradable than others in the soil. This means that for CECs which biodegrade very slowly or not at all, recovery with the drainage system is the only way to prevent the substances from spreading untransformed into the wider environment, where they pose a toxic and ecotoxic hazard. Therefore, the ability of a subsurface irrigation and drainage system to recover irrigated solutes is also an important metric of its performance, just as with other MAR systems such as ASR and ATES.

In this thesis, the various factors affecting the environmental impact and crop contamination risks of subsurface irrigation with treated wastewater were studied, with a particular focus on the two aforementioned processes that contribute towards removing the irrigated CECs from the subsurface – CEC biodegradation, and CEC recovery by drainage. Hence, as discussed in the introduction, the three main objectives of this thesis were to 1) study the subsurface irrigation and drainage system and perform sensitivity analyses using numerical models, with the aid of field experimental data (Chapters 2 and 3), 2) understand the effects of various hydrogeological and operational parameters on the recovery efficiency of a generic MAR system (Chapters 4 and 5), and 3) investigate how biodegradation processes that involve multicomponent reactions are affected by spatio-temporal heterogeneity in the transport processes that occur in the subsurface (Chapter 6). Figure 7.1 graphically illustrates how the various chapters of this thesis relate to each other and to the subject of this thesis. All of these objectives were primarily fulfilled through numerical modelling of the respective problems. Analytical models were used where the problems could be sufficiently simplified (Chapters 2, 4 and 5), in order to obtain results that are widely and easily applicable without the need for intensive computation.

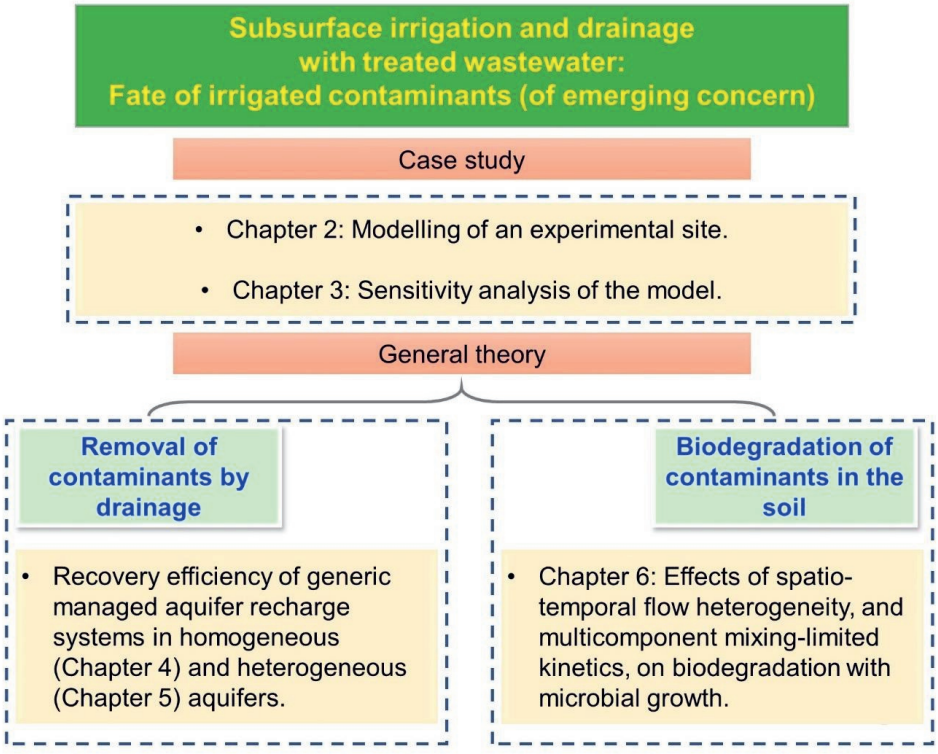

Figure 7.1: An overview of the content of each main chapter of this thesis, that illustrates of how they relate to each other and to the subject of the thesis.

7.2 Subsurface irrigation and the fate of irrigated contaminants

The subsurface irrigation and drainage system, and the use of treated wastewater as a source of irrigation water in this system, was introduced in Chapter 2. The introduced system is new to the scientific literature, and significantly different from subsurface irrigation systems that have been used in the past, such as subsurface drip irrigation. With subsurface drip irrigation and other subsurface irrigation systems that precede the introduced system, water is irrigated directly into the root zone, making the water immediately accessible to the crop roots. However, if treated wastewater is to be used as a source of irrigation water, then it is necessary to irrigate deeper in the subsurface in order to avoid directly exposing the crops to CECs. Situating the irrigation pipes at around the natural level of the groundwater table allows both the soil between the water table and the root zone, and the background groundwater, to act as buffers of the CECs. Although the distance between the irrigation pipes and the root zone causes the introduced system to possibly have a lower water use efficiency than the subsurface irrigation systems that irrigate directly into the root zone, it also allows treated wastewater to be used safely as long as the irrigated CECs do not spread to the root zone.

The results of Chapter 2 indicate that crop contamination with CECs is not expected to be a significant problem associated with using treated wastewater at the experimental site of the subsurface irrigation and drainage system studied. In any case, regardless of the extent of root zone contamination by CECs within a single crop season, the annual precipitation excess implies that CEC concentrations in the root zone would reset to background levels by the start of the following year's crop season. Furthermore,

CECs would not contaminate the root zone uniformly – if they reach the root zone, they are taken up in significant quantities only by crop roots that are situated directly above the irrigation drains. Further research into the effects of drain spacing on crop contamination, capillary flux, and aquifer contamination, along with research on the optimal drain spacing, may shed more light into this issue. Similarly, a balance has to be struck between a shallow positioning of the drains, which increases the risk of crop contamination, or a deeper positioning, which increases the risk of deeper groundwater contamination; this is also a possible direction for future research.

Biodegradable CECs that are not extremely mobile and persistent would be mostly biodegraded before being transported towards deeper aquifers, or surface water bodies located more than several hundred meters from the agricultural plot. Although non-biodegradable contaminants may be recovered from the subsurface through the drainage system, since most drainage occurs outside the crop season, most of the contaminants would have been transported away from the vicinity of the drains, and very little would be recovered. The only means of CEC removal from the subsurface without adverse environmental effects is thus the transformation and biodegradation of the CECs. Accordingly, it is expected that non-biodegradable contaminants would eventually spread to the wider environment. It is therefore important that the only treated wastewater with relatively low concentrations of non-biodegradable contaminants are used in the subsurface irrigation and drainage system.

In Chapter 3, a sensitivity analysis is performed on the numerical model developed in Chapter 2. The sensitivity analysis covers a wide range of parameters relevant to the spreading of the irrigated CECs, while the fate of the CECs was measured through their mass balances. It was found that the geochemical parameters exhibited the greatest influence on the fate of the CECs, due to the exponential nature of decay-type biodegradation kinetics. The adsorption coefficient strongly affected whether the CECs accumulated near the drains, or contaminated the aquifer further afield. This is followed by the hydrogeological parameters, especially the hydrogeological parameters that affect the groundwater flux to a larger extent. This is because groundwater flow makes up a majority of the total water mass balance of the subsurface, and also because the capillary rise flux comprises only a small fraction of the total irrigation flux. The optimal hydrogeological conditions are those in which little regional groundwater flow occurs, and where perturbations to the soil matric head due to factors such as rainfall or irrigation require a long time to dissipate. The irrigation parameters had the smallest impact on CEC fate, although they can be adjusted to increase or decrease the total amount of treated wastewater irrigated into the subsurface.

The geochemical and hydrogeological parameters are also much larger sources of uncertainty than the irrigation parameters, which can be directly controlled. The geochemical parameters are uncertain as they are dependent on a wide range of environmental factors, including soil composition, temperature, and pH, which means that the geochemical parameters that describe the behavior of any particular CEC may have a possible range across three orders of magnitude. The hydrogeological parameters are costly to measure, and some such as the regional groundwater flux may change over time, thereby bringing about uncertainty in the field. Therefore, it would be prudent to obtain a proper characterization of the environmental and hydrogeological parameters of a site before treated wastewater is used for irrigation there. Such an endeavour could be performed using the push-pull test methods discussed in Chapter 5.

For subsurface irrigation and drainage with treated wastewater, weak spatial heterogeneity in the soil hydraulic conductivity had little effect on the mean and median solute mass balance outcomes, but strong spatial heterogeneity led to significant changes. On average, strong spatial heterogeneity in the soil hydraulic conductivity meant that more irrigation was necessary to maintain target groundwater levels, which increased the irrigated CEC mass and decreased the drained CEC mass, thereby leading to

a larger net irrigated CEC mass. Accordingly, a heterogeneous conductivity field also increased the average CEC discharge to the wider environment. However, it appears to have little impact on average on the total root CEC uptake and on the mean direction of CEC discharge towards the wider environment. This implies that a heterogeneous conductivity field does not lead to significantly worse crop contamination outcomes, though the spatial distribution of the contaminated roots may differ from that arising in a homogeneous soil. Assuming that the biodegradation leads to multiple log-reductions in CEC mass by the time it reaches surface water or deeper aquifers, then the increase in net irrigated CEC mass caused by soil heterogeneity should not lead to a significantly higher absolute CEC mass in the wider environment.

The results of the sensitivity analysis suggest that optimizing the irrigation and drainage system is much less important than choosing a suitable type of treated wastewater that does not contain too persistent contaminants, and an agricultural site with the appropriate hydrogeological characteristics and climate. If spatial heterogeneity in the subsurface hydraulic conductivity is present, and if the scale of the agricultural plot is large enough that it covers a representative elementary volume of the heterogeneity field, then the fate of the irrigated CECs is determined mostly by the geometric mean conductivity rather than the specific details of the realized heterogeneity structure. Altogether, these findings imply that the wider adaptation of the introduced subsurface irrigation and drainage system is primarily a challenge in physical geography (hydrogeological characteristics) and human geography (marginal water resource type), not engineering.

7.3 Solute and heat recovery from groundwater aquifers

In the scientific literature, it is generally accepted that the recovery efficiency of a MAR system is positively related to the scale of the MAR system. In other words, the more water is stored in the aquifer, the larger the recovery efficiency tends to be. Hence, the area-to-volume ratio (A/V) of the stored water plume is often used as an indicator of the recovery efficiency of a MAR system: the smaller the ratio, the larger the recovery efficiency. The derived and numerically validated solutions for the recovery of a MAR system (Chapter 4) reveal that indeed, in most cases the recovery efficiency increases as A/V decreases, though the mathematical dependence differs for each combination of flow field geometry and dispersion process. However, two exceptional combinations break the above tendency. When molecular diffusion is the dominant dispersion process and the forced flow field is circular, then the recovery efficiency is independent of A/V. When molecular diffusion is the dominant dispersion process and the forced flow field is spherical, then the recovery efficiency decreases as A/V decreases. Furthermore, when both mechanical dispersion and molecular diffusion contribute significantly to spreading under spherical advection, the recovery efficiency varies non-monotonically with the storage volume, as the relative strength of the two dispersion processes varies with the injected plume's reach. Unless mechanical dispersion is the dominant mechanism of dispersion, the recovery efficiency would differ for a different injection-extraction flux and duration. These findings imply that the use of A/V as an indicator of the recovery efficiency is seldom justified.

The simple form of the analytical solution of the recovery efficiency also enabled the analytical quantification of how the recovery efficiency increases as the number of storage cycles increases, the derivation of the storage volume corresponding to the optimum recovery efficiency in the case that the recovery efficiency varies non-monotonically with the storage volume. The derived analytical solution reveals that the main reason that mechanical dispersion and molecular diffusion have different interactions with the other parameters in determining the recovery efficiency, is because the strength of the two dispersion processes have different velocity dependencies. The strength of mechanical dispersion varies linearly with the advection velocity, whereas that of molecular diffusion is independent of the advection velocity. Accordingly, the recovery efficiency in the case that the dominant dispersion process

has a constant non-linear velocity dependence was also analytically derived. Whether the recovery efficiency increases, decreases, or remains unchanged as the injection-extraction rate or duration increases, was found to be a continuous function of the dimensionality of the flow field and the exponent of the velocity dependence.

In Chapter 5, the analysis of Chapter 4 was extended to aquifers with heterogeneous conductivity fields. Aquifer heterogeneity gives rise to macrodispersion, which is a dispersion process whose strength is widely accepted to depend explicitly on the distance travelled by the stored solute or heat plume, in addition to its dependence on the advection velocity which under radial flow in two and three dimensions also varies with the travelled distance. Therefore, macrodispersion falls outside of the spectrum of dispersion processes covered by the analysis in Chapter 4.

It was found that if macrodispersion is the dominant dispersion process, and the explicit dependence of the macrodispersion strength on the plume's travelled distance is sublinear, linear, or superlinear, then as the stored volume increases the recovery efficiency increases, remains unchanged, and decreases respectively. The exponent of this explicit dependence appears to be much more dependent on the characteristics of the aquifer heterogeneity structure, such as its autocorrelation length, than on the strength of the heterogeneity. Stronger heterogeneity always implies a lower recovery efficiency, but does not appear to significantly alter the relationship between the recovery efficiency and the storage volume. Due to these characteristics of macrodispersion, it is possible for the recovery efficiency to vary non-monotonically with the storage volume in heterogeneous aquifers regardless of the dimensionality of the radial flow field, unlike in homogeneous aquifers where it is only possible under spherical flow. Since most aquifers are likely to be heterogeneous to some degree in reality, in practice this means that the recovery efficiency of a MAR system is a non-trivial optimization problem. Furthermore, since the dispersion of solute and heat in aquifers tend to have significantly different characteristics, this implies that multi-purpose MAR systems that attempt to store both freshwater and heat simultaneously cannot be simultaneously optimized for both. Despite the complexity of describing solute and heat dispersion and recovery under macrodispersion, it was found that the dependence of the recovery efficiency on the number of storage cycles in heterogeneous aquifers obey the same mathematical relationship as in homogeneous aquifers.

In Chapter 5, the possibility of using the analytical relations derived in Chapter 4 and Chapter 5 to interpret the data obtained from push-pull aquifer characterization tests is also discussed. It is argued that the use of the recovery efficiency for push-pull aquifer characterization is associated with several advantages over other widely used methods. With the proposed method, the required number of installed wells is smaller, as separate observation wells are not necessary. Furthermore, in heterogeneous aquifers, the tracer plume may bypass the observation wells, leading to erroneous conclusions. The use of recovery efficiency data, rather than breakthrough curve data, should allow for much easier data interpretation especially in heterogeneous aquifers. This is because breakthrough curves in heterogeneous aquifers fluctuate with time to a significantly larger extent than recovery efficiency data does.

7.4 Contaminant mixing and biodegradation

The focus of Chapter 6 is on the multicomponent biodegradation of contaminants in a heterogeneous soil subject to transient flow, which implies spatio-temporal heterogeneity in the solute transport processes that determine the fate of the contaminants. The biodegradation reaction depends on the Monod equation, in which the biodegradation rate depends on the concentration of the contaminant, the concentration of an electron acceptor such as oxygen, and the spatial density of the microorganisms

involved in the biodegradation process. As the microorganisms metabolize the contaminants, they grow in number, leading to an increase and spatial heterogeneity in the microbial biomass over time. Monod kinetics implies that the biodegradation rate is maximized when the three components of the reaction are well mixed. Due to soil heterogeneity, transient flow, and the higher-order transport phenomena that arise in the unsaturated zone under the interactions between soil heterogeneity and transient flow, the mixing process is significantly different than when either of these spatio-temporal complexities are absent. The higher-order phenomena referred to here is that when soil heterogeneity and transient flow are simultaneously present, the spatial distribution of fast flow and slow flow zones in the soil changes dynamically with time. As research on multicomponent biodegradation of contaminants with biomass growth in the unsaturated zone under soil heterogeneity and transient flow is scarce, the work in Chapter 6 attempts to fill this knowledge gap through numerical simulations, and to investigate under what circumstances it is possible to conceptually simplify this computationally intensive problem.

The results of the numerical simulations suggest that the complexity arising from the combination of processes simulated (multicomponent biodegradation, biomass growth, soil heterogeneity, and transient flow) cannot be easily simplified, as they interact with each other through a web of nonlinear feedback loops. Therefore, computationally intensive numerical simulations are necessary to predict the fate of contaminants in the soil. Under some circumstances, the fate of the contaminant appears to become slightly more predictable in a qualitative sense, but not in a quantitative manner. When soil heterogeneity and transient flow both occur, their effects on the biodegraded contaminant fraction appear to be somewhat additive on rate-limited scenarios but highly nonlinear and unpredictable on mixing-limited scenarios, sometimes cancelling each other out and sometimes amplifying each other. Predictions of extreme outcomes made by simpler models are likely to be too extreme, for both the biodegraded contaminant fraction and heterogeneity in the spatial distribution of contaminant leaching to the saturated zone. Regardless of the specific combination of processes present in a simulation, microbial biomass growth is always an important factor in the biodegradation of contaminants, as the biodegradation rate increases in the presence of a larger biomass density, even though the spatial distribution of the biomass may differ across scenarios.

7.5 Limitations

Chapter 4 and Chapter 5 are intended to provide highly generic and generalizable characterizations of MAR systems including ASR and ATES. Hence, unlike in the other chapters, some processes that have a large influence on solute and heat transport were omitted, even though they occur for some MAR systems in practice. Regional groundwater flow, which pushes the stored water away from the well and hence decreases the recovery efficiency, was omitted from Chapter 4 and Chapter 5. More sophisticated ASR and ATES systems attempt to resolve this in practice by positioning a separate extraction well downstream from the injection well (Bloemendal and Olsthoorn, 2018). In homogeneous aquifers, this strategy can effectively prevent irrecoverable solute losses to regional flow. In heterogeneous aquifers, however, it would be a challenging task to find a suitable location for the downstream extraction well, due to bypass flow. As preferential flow channels might be sparsely hydraulically connected to each other, such as in aquifers with stratified and autocorrelated heterogeneity, placing an extraction well in one channel might nevertheless lead to the loss of solutes transported through other channels. Furthermore, the decrease of recovery efficiency at large solute displacements, due to the positional scaling of macrodispersion, is exacerbated by regional flow. Therefore, the simultaneous occurrence of strong regional flow and strong heterogeneity may preclude the practical viability of ASR and ATES systems, but not that of a subsurface irrigation and drainage system, as discussed in Chapter 2 and Chapter 3, because here the primary goal is not the storage of water.

Another process omitted from Chapter 4 and Chapter 5 is the mutual interference between adjacent MAR wells, which is especially important in heterogeneous aquifers. In subsurface irrigation and drainage systems, the irrigation drains are intentionally placed close together so that the irrigated plumes overlap, in order for the raised groundwater level to be uniform, which enables spatially uniform capillary rise to the root zone. Hence, mutual interference between wells is a feature of subsurface irrigation and drainage systems, and is accounted for in the models presented in Chapter 2 and Chapter 3. For ASR and ATES systems, the existence of preferential flow channels in autocorrelated heterogeneous aquifers leads to an enlargement of the spatial thermal or chemical distribution (e.g. along the layers in stratified aquifers). Therefore, although for a single well system the spatial distribution is a smaller concern relative to the recovery efficiency, the spatial distribution becomes important when multiple wells are placed in proximity to each other, as each well might interfere with spreading and recovery at other wells (Sommer et al., 2015; Kandelous et al., 2011). This poses a problem when adjacent wells interfere destructively, such as when hot wells and cold wells of ATES systems are placed too close to each other, thereby producing lukewarm water that is useful for neither well (Sommer et al., 2015). Another example would be when the injection plume of ATES wells, which are sometimes not of potable quality, infringe upon the drawdown zone of adjacent drinking water wells (Possemiers et al., 2014) in densely populated regions. Hence, more research has to be accorded to spatial concentration distributions caused by macrodispersion when evaluating clusters of densely constructed systems, or systems where the assumption of an infinite aquifer breaks down. Currently, standard practice suggests that placing wells no closer than a straight-line distance of three storage radii apart is sufficient for minimizing interference risk in ATES systems with cylindrical flow fields in heterogeneous aquifers, at least in the Netherlands (Sommer et al., 2014). The same optimal spacing of three storage radii apart is also suggested for ATES systems that generate planar flow fields (Sommer et al., 2015).

The representation of the biogeochemical behavior of CECs used throughout this thesis may be much simpler than what occurs in reality. In Chapter 2 and Chapter 3, the contaminants were modelled as solutes subject to instantaneous linear adsorption and monocomponent decay-type biodegradation kinetics. In Chapter 6, the contaminants were modelled as solutes subject to multicomponent Monod biodegradation kinetics, but not to adsorption. Although the simple model of adsorption used in this thesis has enabled a clearer understanding of the relation between contaminant retardation and environmental outcomes, in practice the adsorption rate may neither be instantaneous or linear, leading to quantitative errors in the model predictions. Given that the solutes adsorb to soil pore surfaces, any spatial heterogeneity in the hydraulic conductivity of a soil should also be accompanied by spatial heterogeneity in the adsorption rate, as both are directly related to the local pore size distribution, but this was omitted from this thesis. The adsorption of contaminants may also be effectively irreversible, or cause changes to the structure and hydraulic properties of the soil (van de Craats et al., 2021) – although this is less likely to result from CECs, which are mostly organic contaminants present in trace quantities, treated wastewater may also contain other types of contaminants such as sodium.

Although the model of biodegradation used in Chapter 6 is more realistic than most existing models in the literature, it may still not be sufficiently complete. The adsorption coefficient and biodegradation rates of a contaminant may range across several orders of magnitude depending on a multitude of factors such as soil structure, soil texture, the presence and concentration of microorganisms that are able to metabolize the contaminant, and the presence of other substances in the soil (Nham et al., 2015). Certain contaminants may also biodegrade into product substances that are more toxic and ecotoxic than the parent compound, and it is likely that the product substance exhibits different biogeochemical and transport behavior in the soil due to its different molecular structure. An example of this the biodegradation of Glyphosate into AMPA in the soil (Silva et al., 2018), both of which are highly ecotoxic substances. The possible shortcomings listed in this paragraph stem partly from the fact that including these processes into the models would make them too computationally intensive and too scenario-specific to be generalizable, and partly from the fact that the behavior of CECs per definition are

not sufficiently well studied in the scientific literature to be rigorously described with models. Therefore, a necessary prerequisite to better understanding CEC transformation and transport in the soil and groundwater is additional research, especially field and laboratory studies, into the biogeochemical processes affecting CECs in the soil. Further research could be done to enable a more accurate parameterization of existing models of contaminant biodegradation and adsorption, or to develop new models that describe reality more precisely.

7.6 Implications and recommendations

In this thesis, the processes affecting the fate of CECs and the environmental outcomes of subsurface irrigation and drainage with treated wastewater were split up into mostly independent partitions that were then mostly analyzed separately. These partitions are 1) the subsurface irrigation and drainage system itself and the basic hydrogeological factors that affect the fate of irrigated solutes, 2) spatial heterogeneity in soil and aquifer physical properties, 3) the recovery efficiency and its relationship with the dispersion processes, and 4) contaminant biodegradation under more realistic conditions involving multicomponent kinetics, soil heterogeneity, and transient flow. Due to the complexity of these processes, it was necessary to analyze them separately.

A possible direction for future research would be to integrate the various aspects of the problem discussed above, and piece together the findings related to the individual partitions of processes. To some extent, such an attempt at integration can also be found in this thesis: the results of Chapters 3, 5, and 6 suggest that soil and aquifer heterogeneity in some cases lead to outcomes whose ensemble averages are similar, or different in a predictable manner, to the outcomes of similar MAR scenarios in homogeneous soils. The analysis of the effects of soil and aquifer heterogeneity on MAR systems and subsurface irrigation and drainage systems is thus one of the primary contributions of this thesis.

Another possible avenue for integration may be based on the results of Chapter 4 and Chapter 5, which provide analytical tools that apply throughout the various phases of implementing a MAR system: 1) the characterization and evaluation of an aquifer's suitability during the prospecting phase, 2) the prediction of the recovery efficiency of the first storage cycle, and 3) the long term performance of the MAR system and how it varies with the number of storage cycles. Although the generic model of MAR systems studied in Chapter 4 and Chapter 5 do not fully apply to subsurface irrigation and drainage systems, the theoretical and methodological findings provide a foundation on which to conduct further research and evaluation of such systems. For example, the push-pull test methodology introduced here (with modifications to make it suitable for a phreatic aquifer) may be used to investigate a prospective site's suitability for a subsurface irrigation and drainage system.

When irrigating the subsurface with treated wastewater, for persistent CECs that biodegrade very slowly, drainage is the only means of CEC removal from the subsurface short of discharge to the wider environment. The small contribution of drainage to the overall mass balance of the irrigated CECs, as found in Chapter 2 and Chapter 3, may not hold true for subsurface irrigation and drainage systems in all circumstances. In regions with a larger net precipitation shortage during the crop season, the irrigated water volume and CEC mass would be larger, which possibly but not necessarily increases the fraction of (non-biodegraded) CECs recoverable through drainage (Chapter 4 and Chapter 5). Furthermore, the recovered CEC fraction would also increase in a scenario with a smaller regional groundwater flux. Therefore, even marginal water containing a significant amount of persistent CECs may be used to feed subsurface irrigation and drainage systems, given favorable hydrogeological conditions.

The importance of biomass growth in determining the biodegradation and overall fate of contaminants in the soil, as found in Chapter 6, is encouraging for the long-term environmental sustainability of subsurface irrigation with treated wastewater. Assuming that the population of microorganisms that preferentially metabolize the irrigated CECs grows with the duration that the site is irrigated, and hence the number of crop seasons, the ability of the soil beneath an agricultural plot to act as a bioreactor of the irrigated marginal water should improve over time. This means that field experiments on the environmental consequences of new subsurface irrigation systems that use treated wastewater would yield results that underestimate the extent of CEC transformation within the soil in the long term. Furthermore, the analyses of Chapter 4 and Chapter 5 reveal that in most cases, the rate of dispersion at the irrigated plume front decreases as the size of the plume increases and as the number of irrigation cycles increases, which may facilitate a positive feedback loop of biomass growth and contaminant biodegradation in the soil surrounding each irrigation pipe. The discussion in this paragraph and the preceding one suggest that the environmental outcomes of subsurface irrigation with treated wastewater may improve as the system is used more intensively, whether in terms of irrigation volume or time. Considered together with the results of Chapter 2 and Chapter 3, which show that the crop and environmental contamination risks of the system are small at the experimental site and not too dissimilar regions, this discussion may be encouraging for the wider adoption of the system.

Given the large initial investment costs of installing MAR systems, it is important that the performance and cost effectiveness of MAR systems are well-understood. Subsurface irrigation and drainage with treated wastewater is possibly less complex and costly to implement due to its shallower placement in the phreatic zone, and due to its ability to utilize existing agricultural drainage systems. Nevertheless, it is similarly or even more important to understand how this system performs before implementation, due to the possible adverse effects on public health and the environment that may follow from the spreading of the irrigated contaminant substances. Through numerical modelling, this thesis has provided a fundamental backdrop for future research into the wider adaptability and environmental consequences of subsurface irrigation with marginal water such as treated wastewater, with a focus on the fate of the irrigated CECs. Further research into the fate of CECs irrigated into the subsurface should aim to provide a more comprehensive overview on the risks and benefits of the system, by using a wide range of approaches, such as field experiments and monitoring, numerical modelling, and laboratory investigations of CEC biodegradation in the soil.

Contemporary approaches towards obtaining water and nutrient resources may use engineered processes such as reverse osmosis and chemical fertilizer production, which are highly energy intensive (Gude, 2011; Wood and Cowie, 2004). With such engineered approaches, it is often necessary to trade one resource, such as energy, for another, such as water, possibly leading to no net gain in overall resource security and sustainability. The successful pilot of subsurface irrigation with treated wastewater may provide some inspiration for new ideas in the pursuit of sustainability. Rather than being an artificially engineered process, it essentially short-circuits the hydrological cycle and the nutrient cycle by returning water and nutrients from aboveground directly to the groundwater, bypassing the unsaturated zone. This provides the crops with additional water of acceptable quality, and possibly also nutrients contained within the treated wastewater, while simultaneously subjecting the CECs in the treated wastewater to in-situ biodegradation, all without adding any significant energy requirements to the disposal of the treated wastewater. Therefore, the future of sustainable resource management might lie in the manipulation and exploitation of natural cycles, rather than in the contemporary approach of obtaining resources through engineered processes.

7.7 Concluding remarks

A major bottleneck in efforts to promote the usage of treated wastewater in agriculture is that in many countries, such as across the EU countries, the concept currently either lies in a legislative black hole or is hindered by conservative and thus unjustifiably strict regulations (Paranychianakis et al., 2015). Hence, it is not immediately clear what can or cannot be done, especially with regards to subsurface irrigation, which has been much less explored. Furthermore, despite the benefits that subsurface irrigation and treated wastewater irrigation bring in combination, the normalization of this method in the legislative climate and public perspective might lead to abuse or reckless misuse, due to inadequate education or financial self-interest. Farmers might skirt regulations on the minimum quality of effluents, and this would be harder to uncover than in surface irrigation, because the manifestation of symptoms are dampened and delayed by the soil. As an example, raw wastewater has been used for irrigation in some developing nations for its low cost, where farmers were possibly either none the wiser about the harms that inevitably materialized (Jaramillo and Restrepo, 2017), or less concerned about public health than personal profit. Hence, it is important that supra-national or international regulations are formulated to ensure and enforce proper implementation (Paranychianakis et al., 2015). The novelty of the subject makes it unsurprising that lawmakers, for want of assurance and technical knowledge, are not actively engaged, and thus more technical research is necessary before it is possible to implement sound and justifiable regulatory policies.

Although the environmental consequences and crop contamination risks of subsurface irrigation with treated wastewater remains largely unknown from an empirical perspective, especially regarding long term implementation, the findings of this thesis paint a promising picture. As long as concentrations of highly persistent CECs in the treated wastewater are not excessive, then no long-term adverse crop or environmental damage from irrigating the treated wastewater are to be expected. Research on modifying or designing wastewater treatment plants, such that they more preferentially remove contaminants that are more persistent in the soil, would enhance the viability of subsurface irrigation with treated wastewater. If future research yields more positive results on the sustainability of the system, and if more efforts are undertaken to allay fears about the safety of intentionally adding treated wastewater into the food chain, then subsurface irrigation with treated wastewater would gain more widespread acceptance amongst policymakers and the general public. In addition to considering subsurface irrigation and drainage with treated wastewater as an agricultural technology that reduces freshwater consumption, one might also consider it to be a water treatment technology with minimal energy expenditure and a small carbon footprint. Therefore, in time, this new method of irrigation may become a new addition to the repertoire of tools at hand to combat the exacerbating global issues of freshwater scarcity, climate change, and environmental pollution, all of which are key issues in the sustainability of human society and the natural environment.

Literature Cited

Acharya, R. C., Van der Zee, S. E. A. T. M., & Leijnse, A. (2005). Transport modeling of nonlinearly adsorbing solutes in physically heterogeneous pore networks. Water resources research, 41(2).

Adams, E. E., & Gelhar, L. W. (1992). Field study of dispersion in a heterogeneous aquifer: 2. Spatial moments analysis. Water Resources Research, 28(12), 3293-3307.

Aichi, M., & Akitaya, K. (2018). Analytical solution for a radial advection-dispersion equation including both mechanical dispersion and molecular diffusion for a steady-state flow field in a horizontal aquifer caused by a constant rate injection from a well. Hydrological Research Letters, 12(3), 23-27.

Alcalde-Sanz, L., & Gawlik, B. M. (2017). Minimum quality requirements for water reuse in agricultural irrigation and aquifer recharge. Towards a legal instrument on water reuse at EU level.

Alcalá, F. J., & Custodio, E. (2008). Using the Cl/Br ratio as a tracer to identify the origin of salinity in aquifers in Spain and Portugal. Journal of Hydrology, 359(1-2), 189-207.

Alexakis, D. E. (2020). Meta-evaluation of water quality indices. application into groundwater resources. Water, 12(7), 1890.

Al-Nakshabandi, G.A., Saqqar, M.M., Shatanawi, M.R., Fayyad, M. and Al-Horani, H., 1997. Some environmental problems associated with the use of treated wastewater for irrigation in Jordan. Agricultural Water Management, 34(1), pp.81-94.

Amos, R.T., Mayer, K.U., Bekins, B.A., Delin, G.N. and Williams, R.L., 2005. Use of dissolved and vapor-phase gases to investigate methanogenic degradation of petroleum hydrocarbon contamination in the subsurface. Water Resources Research, 41(2).

Anderson, M. P. (1984). Movement of contaminants in groundwater: groundwater transport--advection and dispersion. Groundwater contamination, 37-45.

Anderson, M. P. (2005). Heat as a ground water tracer. Groundwater, 43(6), 951-968.

Aquino, T., & Le Borgne, T. (2021). The diffusing-velocity random walk: a spatial-Markov formulation of heterogeneous advection and diffusion. Journal of Fluid Mechanics, 910.

Arya, A., T. A. Hewett, R. G. Larson, and L. W. Lake (1988), Dispersion and reservoir heterogeneity, SPE Reservoir Eng., 3(01), 139–148, doi:10.2118/14364-PA

Assadian, N. W., Di Giovanni, G. D., Enciso, J., Iglesias, J., & Lindemann, W. (2005). The transport of waterborne solutes and bacteriophage in soil subirrigated with a wastewater blend. Agriculture, ecosystems & environment, 111(1-4), 279-291.

Attinger, S., Neuweiler, I., & Kinzelbach, W. (2001). Macrodispersion in a radially diverging flow field with finite Peclet numbers: 2. Homogenization theory approach. Water Resources Research, 37(3), 495-505.

Ayars, J.E., E.W. Christen, and J.W. Hornbuckle, Controlled drainage for improved water management in arid regions irrigatedagriculture. Agricultural Water Management, 2006. 86(1–2): p. 128-139.

Bakker, M. (2010). Radial Dupuit interface flow to assess the aquifer storage and recovery potential of saltwater aquifers. Hydrogeology Journal, 18(1), 107-115.

Bakker, M., Post, V., Langevin, C. D., Hughes, J. D., White, J. T., Starn, J. J., & Fienen, M. N. (2016). Scripting MODFLOW model development using Python and FloPy. Groundwater, 54(5), 733-739.

Bakr, M., van Oostrom, N., & Sommer, W. (2013). Efficiency of and interference among multiple Aquifer Thermal Energy Storage systems; A Dutch case study. Renewable Energy, 60, 53-62.

Barker, J. L., Hassan, M. M., Sultana, S., Ahmed, K. M., & Robinson, C. E. (2016). Numerical evaluation of community-scale aquifer storage, transfer and recovery technology: A case study from coastal Bangladesh. Journal of Hydrology, 540, 861-872.

Barry, D. A., Prommer, H., Miller, C. T., Engesgaard, P., Brun, A., & Zheng, C. (2002). Modelling the fate of oxidisable organic contaminants in groundwater. Advances in Water Resources, 25(8-12), 945-983.

Bartholomeus, R.P., B. Worm, M. Oosterhuis, G.A.P.H. Eertwegh, and K. Raat, Reuse of treated wastewater in agriculture? H2O WaterMatters, 2016. 1.

Bartholomeus, R.P., Stofberg, S.F., van den Eertwegh, G.A.P.H., Cirkel, D.G., 2017. Hergebruik restwater voor zoetwatervoorziening in het landelijk gebied: Monitoring sub-irrigatie met RWZI-effluent Haaksbergen - 2016. BTO 2017.062, KWR, Nieuwegein.
https://livelink.kwrwater.nl/livelink/livelink.exe/open/55459130

Bartholomeus, R.P., van den Eertwegh, G.A.P.H., Cirkel, D.G., 2016. Hergebruik restwater voor zoetwatervoorziening in het landelijk gebied: Monitoring sub-irrigatie met RWZI-effluent Haaksbergen. BTO 2016.050, KWR, Nieuwegein.

Battiato, I., Tartakovsky, D. M., Tartakovsky, A. M., & Scheibe, T. (2009). On breakdown of macroscopic models of mixing-controlled heterogeneous reactions in porous media. Advances in water resources, 32(11), 1664-1673.

Bauer, R. D., Maloszewski, P., Zhang, Y., Meckenstock, R. U., & Griebler, C. (2008). Mixing-controlled biodegradation in a toluene plume—results from two-dimensional laboratory experiments. Journal of Contaminant Hydrology, 96(1-4), 150-168.

Bauer, R. D., Rolle, M., Bauer, S., Eberhardt, C., Grathwohl, P., Kolditz, O., ... & Griebler, C. (2009). Enhanced biodegradation by hydraulic heterogeneities in petroleum hydrocarbon plumes. Journal of contaminant hydrology, 105(1-2), 56-68.

Beard, J. E., Bierkens, M. F., & Bartholomeus, R. P. (2019). Following the water: Characterising de facto wastewater reuse in agriculture in the Netherlands. Sustainability, 11(21), 5936.

Bellin, A., Salandin, P., & Rinaldo, A. (1992). Simulation of dispersion in heterogeneous porous formations: Statistics, first-order theories, convergence of computations. Water Resources Research, 28(9), 2211-2227.

Benson, D. A., Aquino, T., Bolster, D., Engdahl, N., Henri, C. V., & Fernandez-Garcia, D. (2017). A comparison of Eulerian and Lagrangian transport and non-linear reaction algorithms. Advances in Water Resources, 99, 15-37.

Bern, C. R., Breit, G. N., Healy, R. W., Zupancic, J. W., & Hammack, R. (2013a). Deep subsurface drip irrigation using coal-bed sodic water: Part I. Water and solute movement. Agricultural water management, 118, 122-134.

Bern, C. R., Breit, G. N., Healy, R. W., & Zupancic, J. W. (2013b). Deep subsurface drip irrigation using coal-bed sodic water: Part II. Geochemistry. Agricultural water management, 118, 135-149.

Bertelkamp, C., Verliefde, A.R.D., Reynisson, J., Singhal, N., Cabo, A.J., De Jonge, M. and van der Hoek, J.P., 2016. A predictive multi-linear regression model for organic micropollutants, based on a laboratory-scale column study simulating the river bank filtration process. Journal of hazardous materials, 304, pp.502-511.

Beven, K., & Germann, P. (2013). Macropores and water flow in soils revisited. Water Resources Research, 49(6), 3071-3092.

Bianchi, M., & Pedretti, D. (2017). Geological entropy and solute transport in heterogeneous porous media. Water Resources Research, 53(6), 4691-4708.

Birkholzer, J., & Tsang, C. F. (1997). Solute channeling in unsaturated heterogeneous porous media. Water resources research, 33(10), 2221-2238.

Biró, B., Toscano, G., Horváth, N., Matics, H., Domonkos, M., Scotti, R., Rao, M.A., Wejden, B., & French, H. K. (2014). Vertical and horizontal distributions of microbial abundances and enzymatic activities in propylene-glycol-affected soils. Environmental Science and Pollution Research, 21(15), 9095-9108.

Bloem, E., Vanderborght, J., & De Rooij, G. H. (2008). Leaching surfaces to characterize transport in a heterogeneous aquifer: Comparison between flux concentrations, resident concentrations, and flux concentrations estimated from temporal moment analysis. Water resources research, 44(10).

Bloemendal, M., & Hartog, N. (2018). Analysis of the impact of storage conditions on the thermal recovery efficiency of low-temperature ATES systems. Geothermics, 71, 306-319.

Bloemendal, M., & Olsthoorn, T. (2018). ATES systems in aquifers with high ambient groundwater flow velocity. Geothermics, 75, 81-92.

Blum, P., Hunkeler, D., Weede, M., Beyer, C., Grathwohl, P., & Morasch, B. (2009). Quantification of biodegradation for o-xylene and naphthalene using first order decay models, Michaelis–Menten kinetics and stable carbon isotopes. Journal of Contaminant Hydrology, 105(3-4), 118-130.

Bonaiti, G., & Borin, M. (2010). Efficiency of controlled drainage and subirrigation in reducing nitrogen losses from agricultural fields. Agricultural Water Management, 98(2), 343-352.

Borin, M., Bonaiti, G., & Giardini, L. (2001). Controlled drainage and wetlands to reduce agricultural pollution: a lysimetric study. Journal of environmental quality, 30(4), 1330-1340.

Borin, M., Bonaiti, G., & Giardini, L. (1998). First result on controlled drainage to reduce nitrate losses from agricultural sites. In Water and the environment: innovation issues in irrigation and drainage (pp. 35-42). E & FN Spon London.

Boso, F., Bellin, A., & Dumbser, M. (2013). Numerical simulations of solute transport in highly heterogeneous formations: A comparison of alternative numerical schemes. Advances in water resources, 52, 178-189.

Bouchaud, J. P., & Georges, A. (1990). Anomalous diffusion in disordered media: statistical mechanisms, models and physical applications. Physics reports, 195(4-5), 127-293.

Bouwer, H. (1991). Simple derivation of the retardation equation and application to preferential flow and macrodispersion. Groundwater, 29(1), 41-46.

Bridger, D. W., & Allen, D. M. (2014). Influence of geologic layering on heat transport and storage in an aquifer thermal energy storage system. Hydrogeology journal, 22(1), 233-250.

Cai, Y., Wu, P., Zhang, L., Zhu, D., Chen, J., Wu, S., & Zhao, X. (2017). Simulation of soil water movement under subsurface irrigation with porous ceramic emitter. Agricultural Water Management, 192, 244-256.

Cai, Y., Zhao, X., Wu, P., Zhang, L., Zhu, D., & Chen, J. (2019). Effect of soil texture on water movement of porous ceramic emitters: A simulation study. Water, 11(1), 22.

Carsel, R. F., & Parrish, R. S. (1988). Developing joint probability distributions of soil water retention characteristics. Water resources research, 24(5), 755-769.

Chaali, N., Comegna, A., Dragonetti, G., Todorovic, M., Albrizio, R., Hijazeen, D., ... & Coppola, A. (2013). Monitoring and modeling root-uptake salinity reduction factors of a tomato crop under non-uniform soil salinity distribution. Procedia Environmental Sciences, 19, 643-653.

Chang, C. M., & Yeh, H. D. (2012). Stochastic analysis of field-scale heat advection in heterogeneous aquifers. Hydrology and Earth System Sciences, 16(3), 641-648.

Chaudhuri, A., & Sekhar, M. (2007). Analysis of biodegradation in a 3-D heterogeneous porous medium using nonlinear stochastic finite element method. Advances in water resources, 30(3), 589-605.

Chen, C. S. (1987). Analytical solutions for radial dispersion with Cauchy boundary at injection well. Water Resources Research, 23(7), 1217-1224.

Chen, Y. (2014). Aquifer storage and recovery in saline aquifers (Doctoral dissertation, Georgia Institute of Technology).

Cheviron, B., & Coquet, Y. (2009). Sensitivity analysis of transient-MIM HYDRUS-1D: Case study related to pesticide fate in soils. Vadose Zone Journal, 8(4), 1064-1079.

Chiogna, G., Cirpka, O. A., Rolle, M., & Bellin, A. (2015). Helical flow in three-dimensional nonstationary anisotropic heterogeneous porous media. Water Resources Research, 51(1), 261-280.

Cirkel, D. G., Van der Zee, S. E. A. T. M., & Meeussen, J. C. L. (2015). Front spreading with nonlinear sorption for oscillating flow. Water Resources Research, 51(4), 2986-2993.

Cirpka, O. A., Chiogna, G., Rolle, M., & Bellin, A. (2015). Transverse mixing in three-dimensional nonstationary anisotropic heterogeneous porous media. Water Resources Research, 51(1), 241-260.

Cirpka, O. A., de Barros, F. P., Chiogna, G., Rolle, M., & Nowak, W. (2011). Stochastic flux-related analysis of transverse mixing in two-dimensional heterogeneous porous media. Water Resources Research, 47(6).

Cirpka, O. A., & Valocchi, A. J. (2007). Two-dimensional concentration distribution for mixing-controlled bioreactive transport in steady state. Advances in Water Resources, 30(6-7), 1668-1679. doi: 10.1016/j.advwatres.2006.05.022

Cole, B. E., & Silliman, S. E. (1997). Capture zones for passive wells in heterogeneous unconfined aquifers. Groundwater, 35(1), 92-98.

Comolli, A., & Dentz, M. (2017). Anomalous dispersion in correlated porous media: a coupled continuous time random walk approach. The European Physical Journal B, 90(9), 1-18.

Coppens, L.J., van Gils, J.A., Ter Laak, T.L., Raterman, B.W. and van Wezel, A.P., 2015. Towards spatially smart abatement of human pharmaceuticals in surface waters: Defining impact of sewage treatment plants on susceptible functions. Water research, 81, pp.356-365.

Cornelissen, P., van der Zee, S. E., & Leijnse, A. (2021). Framework for the Integrated Sustainability Assessment of Irrigation with Marginal Water. Water, 13(9), 1168.

Cox, M. H., Su, G. W., & Constantz, J. (2007). Heat, chloride, and specific conductance as ground water tracers near streams. Groundwater, 45(2), 187-195.

Dagan, G. (1988). Time-dependent macrodispersion for solute transport in anisotropic heterogeneous aquifers. Water Resources Research, 24(9), 1491-1500.

Dagan, G., & Cvetkovic, V. (1996). Reactive transport and immiscible flow in geological media. I. General theory. Proceedings of the Royal Society of London. Series A: Mathematical, Physical and Engineering Sciences, 452(1945), 285-301.

Dastorani, M.T., Heshmati, M. and Sadeghzadeh, M.A., 2010. Evaluation of the efficiency of surface and subsurface irrigation in dryland environments. Irrigation and drainage, 59(2), pp.129-137.

Davis, B. M., Istok, J. D., & Semprini, L. (2002). Push–pull partitioning tracer tests using radon-222 to quantify non-aqueous phase liquid contamination. Journal of contaminant hydrology, 58(1-2), 129-146.

Davis, S. N., Whittemore, D. O., & Fabryka-Martin, J. (1998). Uses of chloride/bromide ratios in studies of potable water. Groundwater, 36(2), 338-350.

De Gennes, P. G. (1983). Hydrodynamic dispersion in unsaturated porous media. Journal of Fluid Mechanics, 136, 189-200.

Dentz, M., Comolli, A., Hakoun, V., & Hidalgo, J. J. (2020). Transport upscaling in highly heterogeneous aquifers and the prediction of tracer dispersion at the MADE site. Geophysical Research Letters, 47(22), e2020GL088292.

Dentz, M., Gouze, P., & Carrera, J. (2011a). Effective non-local reaction kinetics for transport in physically and chemically heterogeneous media. Journal of contaminant hydrology, 120, 222-236.

Dentz, M., Le Borgne, T., Englert, A., & Bijeljic, B. (2011b). Mixing, spreading and reaction in heterogeneous media: A brief review. Journal of contaminant hydrology, 120, 1-17.

Devaux, I., Gerbaud, L., Planchon, C., Bontoux, J., & Glanddier, P. Y. (2001). Infectious risk associated with wastewater reuse: an epidemiological approach applied to the case of Clermont-Ferrand, France. Water Science and Technology, 43(12), 53-60.

Dey, B., & Sekhar, G. R. (2014). Mass transfer and species separation due to oscillatory flow in a Brinkman medium. International Journal of Engineering Science, 74, 35-54.

Di Dato, M., Bellin, A., & Fiori, A. (2019). Convergent radial transport in three-dimensional heterogeneous aquifers: The impact of the hydraulic conductivity structure. Advances in Water Resources, 131, 103381.

Dillon, P., Stuyfzand, P., Grischek, T., Lluria, M., Pyne, R. D. G., Jain, R. C., ... & Stefan, C. (2019). Sixty years of global progress in managed aquifer recharge. Hydrogeology journal, 27(1), 1-30.

Ding, D., Benson, D. A., Paster, A., & Bolster, D. (2013). Modeling bimolecular reactions and transport in porous media via particle tracking. Advances in Water Resources, 53, 56-65.

Dingemans, M. M., Smeets, P. W., Medema, G., Frijns, J., Raat, K. J., van Wezel, A. P., & Bartholomeus, R. P. (2020). Responsible Water Reuse Needs an Interdisciplinary Approach to Balance Risks and Benefits. Water, 12(5), 1264.

Dole, J. M., Cole, J. C., & von Broembsen, S. L. (1994). Growth of poinsettias, nutrient leaching, and water-use efficiency respond to irrigation methods. HortScience, 29(8), 858-864.

Doughty, C., Hellström, G., Tsang, C. F., & Claesson, J. (1982). A dimensionless parameter approach to the thermal behavior of an aquifer thermal energy storage system. Water Resources Research, 18(3), 571-587.

Drijver, B., van Aarssen, M., & Zwart, B. D. (2012). High-temperature aquifer thermal energy storage (HT-ATES): sustainable and multi-usable. Proceedings of the Innostock, 1-10.

Duffie, J. A., & Beckman, W. A. (2013). Solar engineering of thermal processes. John Wiley & Sons.

Durán-Álvarez, J. C., Prado-Pano, B., & Jiménez-Cisneros, B. (2012). Sorption and desorption of carbamazepine, naproxen and triclosan in a soil irrigated with raw wastewater: Estimation of the sorption parameters by considering the initial mass of the compounds in the soil. Chemosphere, 88(1), 84-90.

EC (European Community). (2006). Directive 2006/118/EC of the European Parliament and of the Council of 12 December 2006 on the protection of groundwater against pollution and deterioration. Off. J. Eur. Commun. 2006, 372, 19–31.

Eeman, S., De Louw, P. G., & Van der Zee, S. E. A. T. M. (2017). Cation exchange in a temporally fluctuating thin freshwater lens on top of saline groundwater. Hydrogeology journal, 25(1), 223-241.

Elliott, J., Deryng, D., Müller, C., Frieler, K., Konzmann, M., Gerten, D., ... & Wisser, D. (2014). Constraints and potentials of future irrigation water availability on agricultural production under climate change. Proceedings of the National Academy of Sciences, 111(9), 3239-3244.

Ellsworth, T. R., Shaouse, P. J., Jobes, J. A., Fargerlund, J., & Skaggs, T. H. (1996). Solute transport in unsaturated soil: Experimental design, parameter estimation, and model discrimination. Soil Science Society of America Journal, 60(2), 397-407.

Elrick, D. E., Mermoud, A., & Monnier, T. (1994). An analysis of solute accumulation during steady-state evaporation in an initially contaminated soil. Journal of Hydrology, 155(1-2), 27-38.

Ernst, L. F., & Feddes, R. A. (1979). Invloed van grondwateronttrekking voor beregening en drinkwater op de grondwaterstand (No. 1116). ICW.

Feddes, R.A., Kowalik, P.J., and Zaradny, H. 1978. Simulation of field water use and crop yield. John Wiley & Sons, New York.

Ferguson, G. (2007). Heterogeneity and thermal modeling of ground water. Groundwater, 45(4), 485-490.

Fernàndez-Garcia, D., Rajaram, H., & Illangasekare, T. H. (2005). Assessment of the predictive capabilities of stochastic theories in a three-dimensional laboratory test aquifer: Effective hydraulic conductivity and temporal moments of breakthrough curves. Water resources research, 41(4).

Fleuchaus, P., Godschalk, B., Stober, I., & Blum, P. (2018). Worldwide application of aquifer thermal energy storage–A review. Renewable and Sustainable Energy Reviews, 94, 861-876.

Forkel, C., & Daniels, H. (1995). Finite element simulation of circulation in large scale thermal energy storage basins. Advances in water resources, 18(3), 147-158.

Freitas, J. G., Mocanu, M. T., Zoby, J. L. G., Molson, J. W., & Barker, J. F. (2011). Migration and fate of ethanol-enhanced gasoline in groundwater: A modelling analysis of a field experiment. Journal of contaminant hydrology, 119(1-4), 25-43.

French, H. K., Van der Zee, S. E. A. T. M., & Leijnse, A. (1999). Differences in gravity-dominated unsaturated flow during autumn rains and snowmelt. Hydrological processes, 13(17), 2783-2800.

French, H. K., Van der Zee, S. E. A. T. M., & Leijnse, A. (2001). Transport and degradation of propyleneglycol and potassium acetate in the unsaturated zone. Journal of contaminant hydrology, 49(1-2), 23-48.

Fujimaki, H., Shimano, T., Inoue, M., & Nakane, K. (2006). Effect of a salt crust on evaporation from a bare saline soil. Vadose Zone Journal, 5(4), 1246-1256.

Gamerdinger, A. P., Achin, R. S., & Traxler, R. W. (1997). Approximating the impact of Sorption on biodegradation kinetics in soil-water systems. Soil Science Society of America Journal, 61(6), 1618-1626.

Gärdenäs, A. I., Hopmans, J. W., Hanson, B. R., & Šimůnek, J. (2005). Two-dimensional modeling of nitrate leaching for various fertigation scenarios under micro-irrigation. Agricultural water management, 74(3), 219-242.

Gelhar, L. W., & Collins, M. A. (1971). General analysis of longitudinal dispersion in nonuniform flow. Water Resources Research, 7(6), 1511-1521.

Gelhar, L. W. (1986). Stochastic subsurface hydrology from theory to applications. Water Resources Research, 22(9S), 135S-145S.

Gelhar, L. W., Welty, C., & Rehfeldt, K. R. (1992). A critical review of data on field-scale dispersion in aquifers. Water resources research, 28(7), 1955-1974.

Gelhar, L. W. (1993). Stochastic subsurface hydrology. Prentice-Hall.

Garabedian, S. P., LeBlanc, D. R., Gelhar, L. W., & Celia, M. A. (1991). Large-scale natural gradient tracer test in sand and gravel, Cape Cod, Massachusetts: 2. Analysis of spatial moments for a nonreactive tracer. Water Resources Research, 27(5), 911-924.

Ghezzehei, T. A., Kneafsey, T. J., & Su, G. W. (2007). Correspondence of the Gardner and van Genuchten–Mualem relative permeability function parameters. Water resources research, 43(10).

Gouet-Kaplan, M., Arye, G., & Berkowitz, B. (2012). Interplay between resident and infiltrating water: Estimates from transient water flow and solute transport. Journal of hydrology, 458, 40-50.

Gouze, P., Le Borgne, T., Leprovost, R., Lods, G., Poidras, T., & Pezard, P. (2008). Non-Fickian dispersion in porous media: 1. Multiscale measurements using single-well injection withdrawal tracer tests. Water Resources Research, 44(6).

Grassi, M., Kaykioglu, G., Belgiorno, V. and Lofrano, G., 2012. Removal of emerging contaminants from water and wastewater by adsorption process. In Emerging compounds removal from wastewater (pp. 15-37). Springer, Dordrecht.

Greskowiak, J., Hamann, E., Burke, V., & Massmann, G. (2017). The uncertainty of biodegradation rate constants of emerging organic compounds in soil and groundwater–A compilation of literature values for 82 substances. Water research, 126, 122-133.

Grösbacher, M., Eckert, D., Cirpka, O. A., & Griebler, C. (2018). Contaminant concentration versus flow velocity: drivers of biodegradation and microbial growth in groundwater model systems. Biodegradation, 29(3), 211-232.

Gude, V. G. (2011). Energy consumption and recovery in reverse osmosis. Desalination and water treatment, 36(1-3), 239-260.

Guerrero, J. P., & Skaggs, T. H. (2010). Analytical solution for one-dimensional advection–dispersion transport equation with distance-dependent coefficients. Journal of Hydrology, 390(1-2), 57-65.

Guimerà, J., Ortuño, F., Ruiz, E., Delos, A., & Pérez-Paricio, A. (2007). Influence of ground-source heat pumps on groundwater. In Conference Proceedings: European Geothermal Congress.

Guo, W., Coulibaly, K., & Maliva, R. G. (2015). Simulated effects of aquifer heterogeneity on ASR system performance. Environmental earth sciences, 73(12), 7803-7809.

Güven, O., Falta, R. W., Molz, F. J., & Melville, J. G. (1985). Analysis and interpretation of single-well tracer tests in stratified aquifers. Water Resources Research, 21(5), 676-684.

Haggerty, R., Schroth, M. H., & Istok, J. D. (1998). Simplified method of "push-pull" test data analysis for determining in situ reaction rate coefficients. Groundwater, 36(2), 314-324.

Hall, S. H., Luttrell, S. P., & Cronin, W. E. (1991). A method for estimating effective porosity and ground-water velocity. Groundwater, 29(2), 171-174.

Ham, P. A., Schotting, R. J., Prommer, H., & Davis, G. B. (2004). Effects of hydrodynamic dispersion on plume lengths for instantaneous bimolecular reactions. Advances in water resources, 27(8), 803-813.

Hamann, E., Stuyfzand, P.J., Greskowiak, J., Timmer, H. and Massmann, G., 2016. The fate of organic micropollutants during long-term/long-distance river bank filtration. Science of the Total Environment, 545, pp.629-640.

Hammel, K., Gross, J., Wessolek, G., & Roth, K. (1999). Two-dimensional simulation of bromide transport in a heterogeneous field soil with transient unsaturated flow. European journal of soil science, 50(4), 633-647.

Harbaugh, A. W. (2005). MODFLOW-2005, the US Geological Survey modular ground-water model: the ground-water flow process (pp. 6-A16). Reston, VA: US Department of the Interior, US Geological Survey.

Hartog, N., & Stuyfzand, P. J. (2017). Water quality considerations on the rise as the use of managed aquifer recharge systems widens.

Heidarpour, M., Mostafazadeh-Fard, B., Koupai, J. A., & Malekian, R. (2007). The effects of treated wastewater on soil chemical properties using subsurface and surface irrigation methods. Agricultural Water Management, 90(1-2), 87-94.

Heinen, M., Bakker, G., & Wösten, J. H. M. (2020). Waterretentie-en doorlatendheidskarakteristieken van boven-en ondergronden in Nederland: de Staringreeks: Update 2018 (No. 2978). Wageningen Environmental Research.

Hess, K. M., Wolf, S. H., & Celia, M. A. (1992). Large-scale natural gradient tracer test in sand and gravel, Cape Cod, Massachusetts: 3. Hydraulic conductivity variability and calculated macrodispersivities. Water Resources Research, 28(8), 2011-2027.

Hesse, F., Radu, F. A., Thullner, M., & Attinger, S. (2009). Upscaling of the advection–diffusion–reaction equation with Monod reaction. Advances in water resources, 32(8), 1336-1351.

Hickman, G. T., & Novak, J. T. (1989). Relationship between subsurface biodegradation rates and microbial density. Environmental science & technology, 23(5), 525-532.

Holden, P. A., & Fierer, N. (2005). Microbial processes in the vadose zone. Vadose Zone Journal, 4(1), 1-21.

Hoopes, J. A., & Harleman, D. R. (1967). Dispersion in radial flow from a recharge well. Journal of Geophysical Research, 72(14), 3595-3607.

Hopmans, J. W., & Stricker, J. N. M. (1989). Stochastic analysis of soil water regime in a watershed. Journal of Hydrology, 105(1-2), 57-84.

Hubert, A., Aquino, T., Tabuteau, H., Méheust, Y., & Le Borgne, T. (2020). Enhanced and non-monotonic effective kinetics of solute pulses under Michaelis–Menten reactions. Advances in Water Resources, 146, 103739.

Hunt, B. (1998). Contaminant source solutions with scale-dependent dispersivities. Journal of Hydrologic Engineering, 3(4), 268-275.

Hunt, A., Ewing, R., & Ghanbarian, B. (2014). Percolation theory for flow in porous media (Vol. 880). Springer.

Indelman, P., & Dagan, G. (1999). Solute transport in divergent radial flow through heterogeneous porous media. Journal of Fluid Mechanics, 384, 159-182.

Indelman, P. (2001). Steady-state source flow in heterogeneous porous media. Transport in porous media, 45(1), 105-127.

Indelman, P. (2004). On macrodispersion in uniform–radial divergent flow through weakly heterogeneous aquifers. Stochastic Environmental Research and Risk Assessment, 18(1), 16-21.

Indelman, P., Lessoff, S. C., & Dagan, G. (2006). Analytical solution to transport in three-dimensional heterogeneous well capture zones. Journal of contaminant hydrology, 87(1-2), 1-21.

Istok, J. D., Humphrey, M. D., Schroth, M. H., Hyman, M. R., & O'Reilly, K. T. (1997). Single-well,"push-pull" test for in situ determination of microbial activities. Groundwater, 35(4), 619-631.

Istok, J. D., Senko, J. M., Krumholz, L. R., Watson, D., Bogle, M. A., Peacock, A., ... & White, D. C. (2004). In situ bioreduction of technetium and uranium in a nitrate-contaminated aquifer. Environmental Science & Technology, 38(2), 468-475.

Jang, E., He, W., Savoy, H., Dietrich, P., Kolditz, O., Rubin, Y., ... & Kalbacher, T. (2017). Identifying the influential aquifer heterogeneity factor on nitrate reduction processes by numerical simulation. Advances in Water Resources, 99, 38-52.

Jankovic, I., Fiori, A., & Dagan, G. (2006). Modeling flow and transport in highly heterogeneous three-dimensional aquifers: Ergodicity, Gaussianity, and anomalous behavior—1. Conceptual issues and numerical simulations. Water Resour. Res, 42(6), W06D12.

Jankovic, I., Maghrebi, M., Fiori, A., & Dagan, G. (2017). When good statistical models of aquifer heterogeneity go right: The impact of aquifer permeability structures on 3D flow and transport. Advances in water resources, 100, 199-211.

Janssen, G. M., Cirpka, O. A., & Van der Zee, S. E. (2006). Stochastic analysis of nonlinear biodegradation in regimes controlled by both chromatographic and dispersive mixing. Water resources research, 42(1).

Jaramillo, M.F. and Restrepo, I., 2017. Wastewater Reuse in Agriculture: A Review about Its Limitations and Benefits. Sustainability, 9(10), p.1734.

Jenks, B.M., Roeth, F.W., Martin, A.R. and McCallister, D.L., 1998. Influence of surface and subsurface soil properties on atrazine sorption and degradation. Weed Science, pp.132-138.

Jobelius, C., Ruth, B., Griebler, C., Meckenstock, R. U., Hollender, J., Reineke, A., ... & Zwiener, C. (2011). Metabolites indicate hot spots of biodegradation and biogeochemical gradients in a high-resolution monitoring well. Environmental science & technology, 45(2), 474-481.

Jury, W. A., & Utermann, J. (1992). Solute transport through layered soil profiles: Zero and perfect travel time correlation models. Transport in porous media, 8(3), 277-297.

Kacimov, A. R., & Obnosov, Y. V. (2021). Infiltration-induced phreatic surface flow to periodic drains: Vedernikov–Engelund–Vasil'ev's legacy revisited. Applied Mathematical Modelling, 91, 989-1003.

Kandelous, M. M., Šimůnek, J., Van Genuchten, M. T., & Malek, K. (2011). Soil water content distributions between two emitters of a subsurface drip irrigation system. Soil Science Society of America Journal, 75(2), 488-497.

Kang, P. K., Le Borgne, T., Dentz, M., Bour, O., & Juanes, R. (2015). Impact of velocity correlation and distribution on transport in fractured media: Field evidence and theoretical model. Water Resources Research, 51(2), 940-959.

Kang, P. K., Hyman, J. D., Han, W. S., & Dentz, M. (2020). Anomalous Transport in Three-Dimensional Discrete Fracture Networks: Interplay Between Aperture Heterogeneity and Injection Modes. Water Resources Research, 56(11), e2020WR027378.

Kass, A., Gavrieli, I., Yechieli, Y., Vengosh, A., & Starinsky, A. (2005). The impact of freshwater and wastewater irrigation on the chemistry of shallow groundwater: a case study from the Israeli Coastal Aquifer. Journal of Hydrology, 300(1-4), 314-331.

Kastner, O., Norden, B., Klapperer, S., Park, S., Urpi, L., Cacace, M., & Blöcher, G. (2017). Thermal solar energy storage in Jurassic aquifers in Northeastern Germany: A simulation study. Renewable energy, 104, 290-306.

Keijzer, H., R.J. Schotting, and S.E.A.T.M. van der Zee, Semi-analytical traveling wave solution of one dimensional aquifer bioremediation, Comm. Nonlinear Analysis, 7, 1-20, 2000

Kim, J., Lee, Y., Yoon, W. S., Jeon, J. S., Koo, M. H., & Keehm, Y. (2010). Numerical modeling of aquifer thermal energy storage system. Energy, 35(12), 4955-4965.

Kitanidis, P. K. (1994). The concept of the dilution index. Water resources research, 30(7), 2011-2026.

Klepikova, M. V., Le Borgne, T., Bour, O., Dentz, M., Hochreutener, R., & Lavenant, N. (2016). Heat as a tracer for understanding transport processes in fractured media: Theory and field assessment from multiscale thermal push-pull tracer tests. Water Resources Research, 52(7), 5442-5457.

Klijn, F., J. ter Maat, E. Van Velzen, J. Hunink, N. Goorden, N. Kielen, W. Werkman, G. Baarse, V. Beumer, and J. Delsman,Zoetwatervoorziening in Nederland: Landelijke analyse knelpunten in de 21e eeuw. 2011, Deltares, pg 65.

Knapp, A.K., C. Beier, D.D. Briske, A.e.T. Classen, Y. Luo, M. Reichstein, M.D. Smith, S.D. Smith, J.E. Bell, P.A. Fay, J.L. Heisler, S.W.Leavitt, R. Sherry, B. Smith, and E. Weng, Consequences of more extreme precipitation regimes for terrestrial ecosystems.BioScience, 2008. 58(9): p. 811-821.

Kodešová, R., Kočárek, M., Klement, A., Golovko, O., Koba, O., Fér, M., ... & Grabic, R. (2016). An analysis of the dissipation of pharmaceuticals under thirteen different soil conditions. Science of the Total Environment, 544, 369-381.

Kreft, A., & Zuber, A. (1978). On the physical meaning of the dispersion equation and its solutions for different initial and boundary conditions. Chemical Engineering Science, 33(11), 1471-1480.

Kuntz, D., & Grathwohl, P. (2009). Comparison of steady-state and transient flow conditions on reactive transport of contaminants in the vadose soil zone. Journal of hydrology, 369(3-4), 225-233.

Laemmel, T., Mohr, M., Schack-Kirchner, H., Schindler, D., & Maier, M. (2019). 1D Air Pressure Fluctuations Cannot Fully Explain the Natural Pressure-Pumping Effect on Soil Gas Transport. Soil Science Society of America Journal, 83(4), 1044-1053.

LAGO (Werkgroep Landbouwkundige Aspecten), 1984. Landbouwkundige aspecten van grondwateronttrekking. CoGroWa, Utrecht, 154 pp.

Lamparter, A., Deurer, M., Bachmann, J., & Duijnisveld, W. H. (2006). Effect of subcritical hydrophobicity in a sandy soil on water infiltration and mobile water content. Journal of Plant Nutrition and Soil Science, 169(1), 38-46.

Langevin, C. D., & Guo, W. (2006). MODFLOW/MT3DMS–based simulation of variable-density ground water flow and transport. Groundwater, 44(3), 339-351.

Lauwerier, H. A. (1955). The transport of heat in an oil layer caused by the injection of hot fluid. Applied Scientific Research, Section A, 5(2-3), 145-150.

Laws, B.V., Dickenson, E.R., Johnson, T.A., Snyder, S.A. and Drewes, J.E., 2011. Attenuation of contaminants of emerging concern during surface-spreading aquifer recharge. Science of the Total Environment, 409(6), pp.1087-1094.

Lee, T. C. (1998). Applied mathematics in hydrogeology. Routledge.

Lee, K. S. (2010). A review on concepts, applications, and models of aquifer thermal energy storage systems. Energies, 3(6), 1320-1334.

Leij, F. J., van Genuchten, M. T., & Dane, J. H. (1991). Mathematical analysis of one-dimensional solute transport in a layered soil profile. Soil Science Society of America Journal, 55(4), 944-953.

Leray, S., Gauvain, A., & de Dreuzy, J. R. (2019). Residence time distributions in non-uniform aquifer recharge and thickness conditions–An analytical approach based on the assumption of Dupuit-Forchheimer. Journal of Hydrology, 574, 110-128.

Lessoff, S. C., & Indelman, P. (2004). Stochastic determination of three-dimensional capture zones for a fully penetrating well. Water resources research, 40(3).

Li, L., Peters, C. A., & Celia, M. A. (2006). Upscaling geochemical reaction rates using pore-scale network modeling. Advances in Water Resources, 29(9), 1351-1370.

Lin, Y. C., Hu, T. F., & Yeh, H. D. (2019). Analytical model for heat transfer accounting for both conduction and dispersion in aquifers with a Robin-type boundary condition at the injection well. Water Resources Research, 55(8), 7379-7399.

Liu, Y., Ao, C., Zeng, W., Srivastava, A. K., Gaiser, T., Wu, J., & Huang, J. (2021). Simulating water and salt transport in subsurface pipe drainage systems with HYDRUS-2D. Journal of Hydrology, 592, 125823.

Loos, R., Carvalho, R., António, D.C., Comero, S., Locoro, G., Tavazzi, S., Paracchini, B., Ghiani, M., Lettieri, T., Blaha, L. and Jarosova, B., 2013. EU-wide monitoring survey on emerging polar organic contaminants in wastewater treatment plant effluents. Water research, 47(17), pp.6475-6487.

Loos, R., Gawlik, B.M., Locoro, G., Rimaviciute, E., Contini, S. and Bidoglio, G., 2009. EU-wide survey of polar organic persistent pollutants in European river waters. Environmental Pollution, 157(2), pp.561-568.

Loschko, M., Wöhling, T., Rudolph, D. L., & Cirpka, O. A. (2018). Accounting for the Decreasing Reaction Potential of Heterogeneous Aquifers in a Stochastic Framework of Aquifer-Scale Reactive Transport. Water Resources Research, 54(1), 442-463. doi: doi:10.1002/2017WR021645

Loschko, M., Wöhling, T., Rudolph, D. L., & Cirpka, O. A. (2019). An Electron-Balance Based Approach to Predict the Decreasing Denitrification Potential of an Aquifer. Groundwater, 57(6), 925-939.

Lowry, C. S., & Anderson, M. P. (2006). An assessment of aquifer storage recovery using ground water flow models. Groundwater, 44(5), 661-667.

Lu, C., Du, P., Chen, Y., & Luo, J. (2011). Recovery efficiency of aquifer storage and recovery (ASR) with mass transfer limitation. Water Resources Research, 47(8).

Lu, C., Wang, Z., Zhao, Y., Rathore, S. S., Huo, J., Tang, Y., ... & Luo, J. (2018). A mobile-mobile transport model for simulating reactive transport in connected heterogeneous fields. Journal of Hydrology, 560, 97-108.

Lubello, C., Gori, R., Nicese, F. P., & Ferrini, F. (2004). Municipal-treated wastewater reuse for plant nurseries irrigation. Water research, 38(12), 2939-2947.

Luo, J., & Cirpka, O. A. (2008). Traveltime-based descriptions of transport and mixing in heterogeneous domains. Water Resources Research, 44(9).

Luo, J., & Cirpka, O. A. (2011). How well do mean breakthrough curves predict mixing-controlled reactive transport?. Water Resources Research, 47(2).

Luo, J., Dentz, M., Carrera, J., & Kitanidis, P. (2008). Effective reaction parameters for mixing controlled reactions in heterogeneous media. Water Resources Research, 44(2).

Luther, K. H., & Haitjema, H. M. (1998). Numerical experiments on the residence time distributions of heterogeneous groundwatersheds. Journal of Hydrology, 207(1-2), 1-17.

Majumdar, S., Miller, G. R., & Sheng, Z. (2021). Optimizing Multiwell Aquifer Storage and Recovery Systems for Energy Use and Recovery Efficiency. Groundwater.

Maliva, R. G., Guo, W., & Missimer, T. M. (2006). Aquifer storage and recovery: recent hydrogeological advances and system performance. Water environment research, 78(13), 2428-2435.

Maliva, R. G., Manahan, W. S., & Missimer, T. M. (2020). Aquifer storage and recovery using saline aquifers: Hydrogeological controls and opportunities. Groundwater, 58(1), 9-18.

Massoudieh, A., & Dentz, M. (2020). Upscaling non-linear reactive transport in correlated velocity fields. Advances in Water Resources, 143, 103680.

Matheron, G., & De Marsily, G. (1980). Is transport in porous media always diffusive? A counterexample. Water Resources Research, 16(5), 901-917.

Makkink, G. F. (1957). Testing the Penman formula by means of lysimeters. Journal of the Institution of Water Engineerrs, 11, 277-288.

McDonnell, J. J., & Beven, K. (2014). Debates—The future of hydrological sciences: A (common) path forward? A call to action aimed at understanding velocities, celerities and residence time distributions of the headwater hydrograph. Water Resources Research, 50(6), 5342-5350.

McLaughlin, D., & Ruan, F. (2001). Macrodispersivity and large-scale hydrogeologic variability. In Dispersion in Heterogeneous Geological Formations (pp. 133-154). Springer, Dordrecht.

Miller, E. E., & Miller, R. D. (1956). Physical theory for capillary flow phenomena. Journal of Applied Physics, 27(4), 324-332.

Miotliński, K., & Dillon, P. J. (2015). Relative recovery of thermal energy and fresh water in aquifer storage and recovery systems. Groundwater, 53(6), 877-884.

Moench, A. F. (1989). Convergent radial dispersion: A Laplace transform solution for aquifer tracer testing. Water Resources Research, 25(3), 439-447.

Moermond, C., C. Smit, R. van Leerdam, N. van der Aa, and M. Montforts, Geneesmiddelen en waterkwaliteit. RIVM briefrapport2016-0111, 2016.

Mohamed, M. M., Hatfield, K., & Hassan, A. E. (2006). Monte Carlo evaluation of microbial-mediated contaminant reactions in heterogeneous aquifers. Advances in water resources, 29(8), 1123-1139.

Mohamed, M., Hatfield, K., Hassan, A., & Klammler, H. (2010). Stochastic evaluation of subsurface contaminant discharges under physical, chemical, and biological heterogeneities. Advances in water resources, 33(7), 801-812.

Mohammad, M. J., & Mazahreh, N. (2003). Changes in soil fertility parameters in response to irrigation of forage crops with secondary treated wastewater. Communications in soil science and plant analysis, 34(9-10), 1281-1294.

Mohammad, N., Alazba, A. A., & Šimůnek, J. (2014). HYDRUS simulations of the effects of dual-drip subsurface irrigation and a physical barrier on water movement and solute transport in soils. Irrigation science, 32(2), 111-125.

Molinari, J., and P. Peaudeceff, Essais conjoints en laboratoire et sur le terrain en rue d'une approach simplefi6e de la pr6vision des propagations de substances miscibles dans les aquif•res r6els, paper presented at Symposium on Hydrodynamic Diffusion and Dispersion in Porous Media, Int. Assoc. for Hydraul. Res., Pavis, Italy, 1977.

Molinari, A., Pedretti, D., & Fallico, C. (2015). Analysis of convergent flow tracer tests in a heterogeneous sandy box with connected gravel channels. Water Resources Research, 51(7), 5640-5657.

Molz, F. J., Güven, O., & Melville, J. G. (1983). An examination of scale-dependent dispersion coefficients. Groundwater, 21(6), 715-725.

Moreno, L., & Tsang, C. F. (1994). Flow channeling in strongly heterogeneous porous media: A numerical study. Water Resources Research, 30(5), 1421-1430.

Moriasi, D. N., Arnold, J. G., Van Liew, M. W., Bingner, R. L., Harmel, R. D., & Veith, T. L. (2007). Model evaluation guidelines for systematic quantification of accuracy in watershed simulations. Transactions of the ASABE, 50(3), 885-900.

Moya, J. L., Primo-Millo, E., & Talón, M. (1999). Morphological factors determining salt tolerance in citrus seedlings: the shoot to root ratio modulates passive root uptake of chloride ions and their accumulation in leaves. Plant, Cell & Environment, 22(11), 1425-1433.

Mueller, T.C., Moorman, T.B. and Snipes, C.E., 1992. Effect of concentration, sorption, and microbial biomass on degradation of the herbicide fluometuron in surface and subsurface soils. Journal of agricultural and food chemistry, 40(12), pp.2517-2522.

Mulligan, C. N., & Yong, R. N. (2004). Natural attenuation of contaminated soils. Environment international, 30(4), 587-601.

Murrell, K. A., Teehan, P. D., & Dorman, F. L. (2021). Determination of contaminants of emerging concern and their transformation products in treated-wastewater irrigated soil and corn. Chemosphere, 281, 130735.

Naglič, B., Kechavarzi, C., Coulon, F., & Pintar, M. (2014). Numerical investigation of the influence of texture, surface drip emitter discharge rate and initial soil moisture condition on wetting pattern size. Irrigation science, 32(6), 421-436.

Narain-Ford, D. M., Bartholomeus, R. P., Dekker, S. C., & Wezel, A. P. V. (2020). Natural purification through soils: Risks and opportunities of sewage effluent reuse in sub-surface irrigation. Reviews of Environmental Contamination and Toxicology Volume 250, 85-117.

Narain-Ford, D. M., Bartholomeus, R. P., Raterman, B. W., van Zaanen, I., Ter Laak, T. L., van Wezel, A. P., & Dekker, S. C. (2021). Shifting the imbalance: Intentional reuse of Dutch sewage effluent in sub-surface irrigation. Science of the Total Environment, 752, 142214.

Neuman, S. P. (1990). Universal scaling of hydraulic conductivities and dispersivities in geologic media. Water resources research, 26(8), 1749-1758.

Neuweiler, I., Attinger, S., & Kinzelbach, W. (2001). Macrodispersion in a radially diverging flow field with finite Peclet numbers: 1. Perturbation theory approach. Water Resources Research, 37(3), 481-493.

Nham, H.T.T., Greskowiak, J., Nödler, K., Rahman, M.A., Spachos, T., Rusteberg, B., Massmann, G., Sauter, M. and Licha, T., 2015. Modeling the transport behavior of 16 emerging organic contaminants during soil aquifer treatment. Science of the Total Environment, 514, pp.450-458.

Nilson, R. H., Peterson, E. W., Lie, K. H., Burkhard, N. R., & Hearst, J. R. (1991). Atmospheric pumping: A mechanism causing vertical transport of contaminated gases through fractured permeable media. Journal of Geophysical Research: Solid Earth, 96(B13), 21933-21948.

Novakowski, K. S. (1992). An evaluation of boundary conditions for one-dimensional solute transport: 1. Mathematical development. Water Resources Research, 28(9), 2399-2410.

Novo, A. V., Bayon, J. R., Castro-Fresno, D., & Rodriguez-Hernandez, J. (2010). Review of seasonal heat storage in large basins: Water tanks and gravel–water pits. Applied Energy, 87(2), 390-397.

Obnosov, Y. V., & Kacimov, A. R. (2018). Steady Darcian Flow in Subsurface Irrigation of Topsoil Impeded by a Substratum: Kornev–Riesenkampf–Philip Legacies Revisited. Irrigation and Drainage, 67(3), 374-391.

Paranychianakis, N.V., Salgot, M., Snyder, S.A. and Angelakis, A.N., 2015. Water reuse in EU states: necessity for uniform criteria to mitigate human and environmental risks. Critical Reviews in Environmental Science and Technology, 45(13), pp.1409-1468.

Palmer, C. D. (1988). The effect of monitoring well storage on the shape of breakthrough curves—A theoretical study. Journal of Hydrology, 97(1-2), 45-57.

Parker, J. C., & Van Genuchten, M. T. (1984). Flux-averaged and volume-averaged concentrations in continuum approaches to solute transport. Water Resources Research, 20(7), 866-872.

Parkhurst, D., & Appelo, C. A. J. (2013). PHREEQC (Version 3)—A computer program for speciation, batch-reaction, one-dimensional transport, and inverse geochemical calculations. Water Resources Investigations Report, 99-4259.

Pang, L., & Hunt, B. (2001). Solutions and verification of a scale-dependent dispersion model. Journal of contaminant hydrology, 53(1-2), 21-39.

Pauw, P. S., van der Zee, S. E. A. T. M., Leijnse, A., & Essink, G. H. O. (2016). Saltwater upconing due to cyclic pumping by horizontal wells in freshwater lenses. Groundwater, 54(4), 521-531.

Pedersen, J.A., Soliman, M. and Suffet, I.H., 2005. Human pharmaceuticals, hormones, and personal care product ingredients in runoff from agricultural fields irrigated with treated wastewater. Journal of agricultural and food chemistry, 53(5), pp.1625-1632.

Pedretti, D., & Fiori, A. (2013). Travel time distributions under convergent radial flow in heterogeneous formations: Insight from the analytical solution of a stratified model. Advances in water resources, 60, 100-109.

Pellerin, B. A., Wollheim, W. M., Feng, X., & Vörösmarty, C. J. (2008). The application of electrical conductivity as a tracer for hydrograph separation in urban catchments. Hydrological Processes: An International Journal, 22(12), 1810-1818.

Peng, S., He, Y., Yang, S., & Xu, J. (2015). Effect of controlled irrigation and drainage on nitrogen leaching losses from paddy fields. Paddy and water environment, 13(4), 303-312.

Penny, G. S., Conway, M. W., & Briscoe, J. E. (1983, January). Enhanced load water-recovery technique improves stimulation results. In SPE Annual Technical Conference and Exhibition. Society of Petroleum Engineers.

Philip, J. R. (1994). Some exact solutions of convection-diffusion and diffusion equations. Water Resources Research, 30(12), 3545-3551.

Pickens, J. F., & Grisak, G. E. (1981). Modeling of scale-dependent dispersion in hydrogeologic systems. Water Resources Research, 17(6), 1701-1711.

Poeton, T. S., Stensel, H. D., & Strand, S. E. (1999). Biodegradation of polyaromatic hydrocarbons by marine bacteria: effect of solid phase on degradation kinetics. Water Research, 33(3), 868-880.

Pool, M., Dentz, M., & Post, V. E. (2016). Transient forcing effects on mixing of two fluids for a stable stratification. Water Resources Research, 52(9), 7178-7197.

Pophillat, W., Attard, G., Bayer, P., Hecht-Méndez, J., & Blum, P. (2020a). Analytical solutions for predicting thermal plumes of groundwater heat pump systems. Renewable Energy, 147, 2696-2707.

Pophillat, W., Bayer, P., Teyssier, E., Blum, P., & Attard, G. (2020b). Impact of groundwater heat pump systems on subsurface temperature under variable advection, conduction and dispersion. Geothermics, 83, 101721.

Possemiers, M., Huysmans, M., & Batelaan, O. (2014). Influence of Aquifer Thermal Energy Storage on groundwater quality: A review illustrated by seven case studies from Belgium. Journal of Hydrology: Regional Studies, 2, 20-34.

Possemiers, M., Huysmans, M., & Batelaan, O. (2015). Application of multiple-point geostatistics to simulate the effect of small-scale aquifer heterogeneity on the efficiency of aquifer thermal energy storage. Hydrogeology journal, 23(5), 971-981.

Pronk, G. J., Stofberg, S. F., Van Dooren, T. C. G. W., Dingemans, M. M. L., Frijns, J., Koeman-Stein, N. E., ... & Bartholomeus, R. P. (2021). Increasing water system robustness in The Netherlands: potential of cross-sectoral water reuse. Water Resources Management, 35(11), 3721-3735.

Ptak, T., & Teutsch, G. (1994). Forced and natural gradient tracer tests in a highly heterogeneous porous aquifer: Instrumentation and measurements. Journal of Hydrology, 159(1-4), 79-104.

Ptak, T., Piepenbrink, M., & Martac, E. (2004). Tracer tests for the investigation of heterogeneous porous media and stochastic modelling of flow and transport—a review of some recent developments. Journal of hydrology, 294(1-3), 122-163.

Puyguiraud, A., Perez, L. J., Hidalgo, J. J., & Dentz, M. (2020). Effective dispersion coefficients for the upscaling of pore-scale mixing and reaction. Advances in Water Resources, 146, 103782.

Pyne, R. D. (2017). Groundwater recharge and wells: a guide to aquifer storage recovery. Routledge.

Qadir, M., Wichelns, D., Raschid-Sally, L., McCornick, P. G., Drechsel, P., Bahri, A., & Minhas, P. S. (2010). The challenges of wastewater irrigation in developing countries. Agricultural water management, 97(4), 561-568.

Rad, F. M., & Fung, A. S. (2016). Solar community heating and cooling system with borehole thermal energy storage–Review of systems. Renewable and Sustainable Energy Reviews, 60, 1550-1561.

Rasmussen, T. C., Baldwin, R. H., Dowd, J. F., & Williams, A. G. (2000). Tracer vs. pressure wave velocities through unsaturated saprolite. Soil Science Society of America Journal, 64(1), 75-85.

Richardson, S. D., & Ternes, T. A. (2018). Water analysis: emerging contaminants and current issues. Analytical chemistry, 90(1), 398-428.

Rolle, M., Eberhardt, C., Chiogna, G., Cirpka, O. A., & Grathwohl, P. (2009). Enhancement of dilution and transverse reactive mixing in porous media: Experiments and model-based interpretation. Journal of contaminant hydrology, 110(3-4), 130-142.

Rolle, M., & Le Borgne, T. (2019). Mixing and reactive fronts in the subsurface. Reviews in Mineralogy and Geochemistry, 85(1), 111-142.

Röling, W.F. and Van Verseveld, H.W., 2002. Natural attenuation: what does the subsurface have in store?. Biodegradation, 13(1), pp.53-64.

Roth, K. (1995). Steady state flow in an unsaturated, two-dimensional, macroscopically homogeneous, Miller-similar medium. Water Resources Research, 31(9), 2127-2140.

Saefuddin, R., Saito, H., & Šimůnek, J. (2019). Experimental and numerical evaluation of a ring-shaped emitter for subsurface irrigation. Agricultural water management, 211, 111-122.

Sahimi, M. (2011). Flow and transport in porous media and fractured rock: from classical methods to modern approaches. John Wiley & Sons.

Sahimi, M. (1993). Flow phenomena in rocks: from continuum models to fractals, percolation, cellular automata, and simulated annealing. Reviews of modern physics, 65(4), 1393.

Salles, J., Thovert, J. F., Delannay, R., Prevors, L., Auriault, J. L., & Adler, P. M. (1993). Taylor dispersion in porous media. Determination of the dispersion tensor. Physics of Fluids A: Fluid Dynamics, 5(10), 2348-2376.

Salvucci, G. D., & Entekhabi, D. (1994). Equivalent steady soil moisture profile and the time compression approximation in water balance modeling. Water Resources Research, 30(10), 2737-2749.

Sanz-Prat, A., Lu, C., Finkel, M., & Cirpka, O. A. (2015). On the validity of travel-time based nonlinear bioreactive transport models in steady-state flow. Journal of contaminant hydrology, 175, 26-43.

Sanz-Prat, A., Lu, C., Amos, R. T., Finkel, M., Blowes, D. W., & Cirpka, O. A. (2016). Exposure-time based modeling of nonlinear reactive transport in porous media subject to physical and geochemical heterogeneity. Journal of contaminant hydrology, 192, 35-49.

Sauty, J.P., Contribution b. l'identification des parameters de dispersion dans les aquif•res par interpr6tation des exp6riences de tracage, dissertation, Univ. Sci. et Med. et Inst. Natl. Polytech. de Grenoble, Grenoble, France, 1977.

Sauty, J. P., Gringarten, A. C., Menjoz, A., & Landel, P. A. (1982). Sensible energy storage in aquifers: 1. Theoretical study. Water Resources Research, 18(2), 245-252.

Schäfer Rodrigues Silva, A., Guthke, A., Höge, M., Cirpka, O. A., & Nowak, W. (2020). Strategies for simplifying reactive transport models: A Bayesian model comparison. Water Resources Research, 56(11), e2020WR028100.

Schirmer, M., Durrant, G. C., Molson, J. W., & Frind, E. O. (2001). Influence of transient flow on contaminant biodegradation. Groundwater, 39(2), 276-282.

Schlather, M., Malinowski, A., Menck, P. J., Oesting, M., & Strokorb, K. (2015). Analysis, simulation and prediction of multivariate random fields with package RandomFields. Journal of Statistical Software, 63(8), 1-25.

Schotanus, D., van der Ploeg, M. J., & van der Zee, S. E. A. T. M. (2012). Quantifying heterogeneous transport of a tracer and a degradable contaminant in the field, with snowmelt and irrigation. Hydrology & Earth System Sciences, 16(8).

Schotanus, D., van der Ploeg, M. J., & Zee, S. V. D. (2013). Spatial distribution of solute leaching with snowmelt and irrigation: measurements and simulations. Hydrology and Earth System Sciences, 17(4), 1547-1560.

Schotanus, D., Meeussen, J. C. L., Lissner, H., van der Ploeg, M. J., Wehrer, M., Totsche, K. U., & van der Zee, S. E. A. T. M. (2014). Transport and degradation of propylene glycol in the vadose zone: model development and sensitivity analysis. Environmental Science and Pollution Research, 21(15), 9054-9066.

Schout, G., Drijver, B., Gutierrez-Neri, M., & Schotting, R. (2014). Analysis of recovery efficiency in high-temperature aquifer thermal energy storage: a Rayleigh-based method. Hydrogeology journal, 22(1), 281-291.

Schout, G., Drijver, B., & Schotting, R. J. (2016). The influence of the injection temperature on the recovery efficiency of high temperature aquifer thermal energy storage: Comment on Jeon et al., 2015. Energy, 103, 107-109.

Schroth, M. H., Istok, J. D., & Haggerty, R. (2000). In situ evaluation of solute retardation using single-well push–pull tests. Advances in Water Resources, 24(1), 105-117.

Schroth, M. H., & Istok, J. D. (2005). Approximate solution for solute transport during spherical-flow push-pull tests. Groundwater, 43(2), 280-284.

Schulze-Makuch, D. (2005). Longitudinal dispersivity data and implications for scaling behavior. Groundwater, 43(3), 443-456.

Scott, I. S., Huang, C. H., & Bowling, L. C. (2020). The use of electrical conductivity to develop temporally precise breakthrough curves in tracer injection experiments. Journal of Hydrology, 588, 124998.

Scotter, D. R., & Raats, P. A. C. (1968). Dispersion in porous mediums due to oscillating flow. Water Resources Research, 4(6), 1201-1206.

Scow, K. M., & Johnson, C. R. (1996). Effect of sorption on biodegradation of soil pollutants. Advances in agronomy, 58, 1-56.

Seeboonruang, U., & Ginn, T. R. (2006). Upscaling heterogeneity in aquifer reactivity via exposure-time concept: Forward model. Journal of contaminant hydrology, 84(3-4), 127-154.

Sherman, T., Engdahl, N. B., Porta, G., & Bolster, D. (2020). A review of spatial Markov models for predicting pre-asymptotic and anomalous transport in porous and fractured media. Journal of Contaminant Hydrology, 103734.

Shi, W., Wang, Q., & Zhan, H. (2020). New Simplified Models of Single-Well Push-Pull Tests With Mixing Effect. Water Resources Research, 56(8), e2019WR026802.

Silva, V., Montanarella, L., Jones, A., Fernández-Ugalde, O., Mol, H. G., Ritsema, C. J., & Geissen, V. (2018). Distribution of glyphosate and aminomethylphosphonic acid (AMPA) in agricultural topsoils of the European Union. Science of the Total Environment, 621, 1352-1359.

Šimůnek, J., & Hopmans, J. W. (2009). Modeling compensated root water and nutrient uptake. Ecological modelling, 220(4), 505-521.

Šimůnek, J., Jacques, D., Šejna, M., & van Genuchten, M. T. (2012a). The HP2 program for HYDRUS (2D/3D): A coupled code for simulating two-dimensional variably-saturated water flow, heat transport, and biogeochemistry in porous media, version 1.0. PC Progress, Prague, Czech Republic.

Šimůnek, J., M. Šejna, H. Saito, M. Sakai, and M. Th. van Genuchten. (2013) The Hydrus-1D Software Package for Simulating the Movement of Water, Heat, and Multiple Solutes in Variably Saturated Media, Version 4.17, HYDRUS Software Series 3, Department of Environmental Sciences, University of California Riverside, Riverside, California, USA, pp. 342.

Šimůnek, J., Van Genuchten, M. T., & Šejna, M. (2012b). The HYDRUS software package for simulating two-and three-dimensional movement of water, heat, and multiple solutes in variably-saturated media. Technical manual, version 2.

Šimůnek, J., Van Genuchten, M. T., & Šejna, M. (2016). Recent developments and applications of the HYDRUS computer software packages. Vadose Zone Journal, 15(7).

Singh, D. K. (2008). Biodegradation and bioremediation of pesticide in soil: concept, method and recent developments. Indian journal of microbiology, 48(1), 35-40.

Siyal, A. A., & Skaggs, T. H. (2009). Measured and simulated soil wetting patterns under porous clay pipe sub-surface irrigation. Agricultural water management, 96(6), 893-904.

Siyal, A. A., Van Genuchten, M. T., & Skaggs, T. H. (2013). Solute transport in a loamy soil under subsurface porous clay pipe irrigation. Agricultural Water Management, 121, 73-80.

Snodgrass, M. F., & Kitanidis, P. K. (1998). A method to infer in situ reaction rates from push-pull experiments. Ground Water, 36(4), 645-650.

Sommer, W. T., Doornenbal, P. J., Drijver, B. C., Van Gaans, P. F. M., Leusbrock, I., Grotenhuis, J. T. C., & Rijnaarts, H. H. M. (2014). Thermal performance and heat transport in aquifer thermal energy storage. Hydrogeology Journal, 22(1), 263-279.

Sommer, W., Valstar, J., van Gaans, P., Grotenhuis, T., & Rijnaarts, H. (2013). The impact of aquifer heterogeneity on the performance of aquifer thermal energy storage. Water Resources Research, 49(12), 8128-8138.

Sommer, W., Valstar, J., Leusbrock, I., Grotenhuis, T., & Rijnaarts, H. (2015). Optimization and spatial pattern of large-scale aquifer thermal energy storage. Applied energy, 137, 322-337.

Song, X., & Seagren, E. A. (2008). In situ bioremediation in heterogeneous porous media: Dispersion-limited scenario. Environmental science & technology, 42(16), 6131-6140.

Soulas, G., & Lagacherie, B. (2001). Modelling of microbial degradation of pesticides in soils. Biology and fertility of Soils, 33(6), 551-557.

Spurlock, F., Šimůnek, J., Johnson, B., & Tuli, A. (2013). Sensitivity analysis of soil fumigant transport and volatilization to the atmosphere. Vadose Zone Journal, 12(2), 1-12.

Stauffer, P. H., Rahn, T., Ortiz, J. P., Salazar, L. J., Boukhalfa, H., Behar, H. R., & Snyder, E. E. (2019). Evidence for High Rates of Gas Transport in the Deep Subsurface. Geophysical Research Letters, 46(7), 3773-3780.

Stofberg, S.F.Bartholomeus, R.P.Eertwegh, G.A.P.H. van denRaat, K.J. Hergebruik van gezuiverd restwater in de landbouw. Subirrigatie met RWZI effluent Haaksbergen 2015-2019. BTO 2021.026, KWR, Nieuwegein.

Sudicky, E. A. (1986). A natural gradient experiment on solute transport in a sand aquifer: Spatial variability of hydraulic conductivity and its role in the dispersion process. Water Resources Research, 22(13), 2069-2082.

Tang, D. W. S., & van der Zee, S. E. A. T. M. (2021). Dispersion and Recovery of Solutes and Heat under Cyclic Radial Advection. Journal of Hydrology, 126713.

Tang, D. W. S., & Van Der Zee, S. E. A. T. M. (2022). Macrodispersion and Recovery of Solutes and Heat in Heterogeneous Aquifers. Water Resources Research, 58(2), e2021WR030920.

Taylor, G. I. (1953). Dispersion of soluble matter in solvent flowing slowly through a tube. Proceedings of the Royal Society of London. Series A. Mathematical and Physical Sciences, 219(1137), 186-203.

Ternes, T.A., Bonerz, M., Herrmann, N., Teiser, B. and Andersen, H.R., 2007. Irrigation of treated wastewater in Braunschweig, Germany: an option to remove pharmaceuticals and musk fragrances. Chemosphere, 66(5), pp.894-904.

Thomas, J.M. and Ward, C.H., 1989. In situ biorestoration of organic contaminants in the subsurface. Environmental science & technology, 23(7), pp.760-766.

Toscano, G., Colarieti, M. L., Anton, A., Greco, G., & Biró, B. (2014). Natural and enhanced biodegradation of propylene glycol in airport soil. Environmental Science and Pollution Research, 21(15), 9028-9035.

Tratnyek, P.G. and Johnson, R.L., 2006. Nanotechnologies for environmental cleanup. Nano today, 1(2), pp.44-48.

Trinchero, P., Sánchez-Vila, X., & Fernàndez-Garcia, D. (2008). Point-to-point connectivity, an abstract concept or a key issue for risk assessment studies?. Advances in water resources, 31(12), 1742-1753.

Tsang, Y. W. (1995). Study of alternative tracer tests in characterizing transport in fractured rocks. Geophysical Research Letters, 22(11), 1421-1424.

Ursino, N., Gimmi, T., & Flühler, H. (2001). Dilution of non-reactive tracers in variably saturated sandy structures. Advances in water resources, 24(8), 877-885.

Valipour, M. and Singh, V.P., 2016. Global experiences on wastewater irrigation: challenges and prospects. In Balanced urban development: options and strategies for liveable cities (pp. 289-327). Springer, Cham.

Valocchi, A. J., Bolster, D., & Werth, C. J. (2019). Mixing-limited reactions in porous media. Transport in Porous Media, 130(1), 157-182.

Van de Craats, D., van der Zee, S. E., Sui, C., van Asten, P. J., Cornelissen, P., & Leijnse, A. (2020). Soil sodicity originating from marginal groundwater. Vadose Zone Journal, 19(1), e20010.

Van den Berg, F., Brus, D. J., Burgers, S. L. G. E., Heuvelink, G. B. M., Kroes, J. G., Stolte, J., ... & De Vries, F. (2008). Uncertainty and sensitivity analysis of GeoPEARL (No. 1330). Alterra.

Vandenbohede, A., Louwyck, A., & Lebbe, L. (2009). Conservative solute versus heat transport in porous media during push-pull tests. Transport in Porous Media, 76(2), 265-287.

Vandenbohede, A., Hermans, T., Nguyen, F., & Lebbe, L. (2011). Shallow heat injection and storage experiment: heat transport simulation and sensitivity analysis. Journal of hydrology, 409(1-2), 262-272.

Van Den Brink, C., Frapporti, G., Griffioen, J., & Zaadnoordijk, W. J. (2007). Statistical analysis of anthropogenic versus geochemical-controlled differences in groundwater composition in The Netherlands. Journal of Hydrology, 336(3-4), 470-480.

van der Zee, S. E. A. T. M., & Boesten, J. J. (1991). Effects of soil heterogeneity on pesticide leaching to groundwater. Water Resources Research, 27(12), 3051-3063.

Van der Zee, S. E. A. T. M., Shah, S. H. H., & Vervoort, R. W. (2014). Root zone salinity and sodicity under seasonal rainfall due to feedback of decreasing hydraulic conductivity. Water Resources Research, 50(12), 9432-9446.

Van Dijke, M. I. J., & Van Der Zee, S. E. A. T. M. (1998). Modeling of air sparging in a layered soil: Numerical and analytical approximations. Water resources research, 34(3), 341-353.

Van Duijn, C. J., & Van der Zee, S. E. A. T. M. (1986). Solute transport parallel to an interface separating two different porous materials. Water Resources Research, 22(13), 1779-1789.

van Duijn, C. J., & van der Zee, S. E. A. T. M. (2018). Large time behaviour of oscillatory nonlinear solute transport in porous media. Chemical Engineering Science, 183, 86-94.

Van Halem, D., De Vet, W., Verberk, J., Amy, G., & Van Dijk, H. (2011). Characterization of accumulated precipitates during subsurface iron removal. Applied geochemistry, 26(1), 116-124.

Van Lopik, J. H., Hartog, N., & Zaadnoordijk, W. J. (2016). The use of salinity contrast for density difference compensation to improve the thermal recovery efficiency in high-temperature aquifer thermal energy storage systems. Hydrogeology Journal, 24(5), 1255-1271.

Veling, E. J. M. (2012). Radial transport in a porous medium with Dirichlet, Neumann and Robin-type inhomogeneous boundary values and general initial data: analytical solution and evaluation. Journal of Engineering Mathematics, 75(1), 173-189.

Vereecken, H., Döring, U., Hardelauf, H., Jaekel, U., Hashagen, U., Neuendorf, O., ... & Seidemann, R. (2000). Analysis of solute transport in a heterogeneous aquifer: the Krauthausen field experiment. Journal of Contaminant Hydrology, 45(3-4), 329-358.

Vermue, E., K. Metselaar, and S. Van der Zee, Modelling of soil salinity and halophyte crop production. Environmental andexperimental botany, 2013. 92: p. 186-196.

Visser, P. W., Kooi, H., & Stuyfzand, P. J. (2015). The thermal impact of aquifer thermal energy storage (ATES) systems: a case study in the Netherlands, combining monitoring and modeling. Hydrogeology Journal, 23(3), 507-532.

Vroblesky, D. A., & Chapelle, F. H. (1994). Temporal and spatial changes of terminal electron-accepting processes in a petroleum hydrocarbon-contaminated aquifer and the significance for contaminant biodegradation. Water resources research, 30(5), 1561-1570.

Wang, P., & Chen, G. Q. (2015). Environmental dispersion in a tidal wetland with sorption by vegetation. Communications in Nonlinear Science and Numerical Simulation, 22(1-3), 348-366.

Wang, Q., Shi, W., Zhan, H., Gu, H., & Chen, K. (2018). Models of single-well push-pull test with mixing effect in the wellbore. Water Resources Research, 54(12), 10-155.

Ward, J. D., Simmons, C. T., & Dillon, P. J. (2008). Variable-density modelling of multiple-cycle aquifer storage and recovery (ASR): Importance of anisotropy and layered heterogeneity in brackish aquifers. Journal of Hydrology, 356(1-2), 93-105.

Warrick, A. W., Biggar, J. W., & Nielsen, D. R. (1971). Simultaneous solute and water transfer for an unsaturated soil. Water Resources Research, 7(5), 1216-1225.

Werth, C. J., Cirpka, O. A., & Grathwohl, P. (2006). Enhanced mixing and reaction through flow focusing in heterogeneous porous media. Water Resources Research, 42(12).

Wesseling, J. G., J. A. Elbers, P. Kabat, and B. J. van den Broek, SWATRE: instructions for input, Internal Note, Winand Staring Centre, Wageningen, the Netherlands, 1991.

Wheatcraft, S. W., & Tyler, S. W. (1988). An explanation of scale-dependent dispersivity in heterogeneous aquifers using concepts of fractal geometry. Water Resources Research, 24(4), 566-578.

Williams, C. F., Watson, J. E., & Nelson, S. D. (2014). Comparison of equilibrium and non-equilibrium distribution coefficients for the human drug carbamazepine in soil. Chemosphere, 95, 166-173.

Williams, C. F., Williams, C. F., & Adamsen, F. J. (2006). Sorption–desorption of carbamazepine from irrigated soils. Journal of environmental quality, 35(5), 1779-1783.

Williams, M., Ong, P. L., Williams, D. B., & Kookana, R. S. (2009). Estimating the sorption of pharmaceuticals based on their pharmacological distribution. Environmental toxicology and chemistry, 28(12), 2572-2579.

Willingham, T., Zhang, C., Werth, C. J., Valocchi, A. J., Oostrom, M., & Wietsma, T. W. (2010). Using dispersivity values to quantify the effects of pore-scale flow focusing on enhanced reaction along a transverse mixing zone. Advances in water resources, 33(4), 525-535.

Willmann, M., Carrera, J., Sanchez-Vila, X., Silva, O., & Dentz, M. (2010). Coupling of mass transfer and reactive transport for nonlinear reactions in heterogeneous media. Water resources research, 46(7).

Winterleitner, G., Schütz, F., Wenzlaff, C., & Huenges, E. (2018). The Impact of Reservoir Heterogeneities on High-Temperature Aquifer Thermal Energy Storage Systems. A Case Study from Northern Oman. Geothermics, 74, 150-162.

Witt, L., Müller, M. J., Gröschke, M., & Post, V. E. (2021). Experimental observations of aquifer storage and recovery in brackish aquifers using multiple partially penetrating wells. Hydrogeology Journal, 1-16.

Wright, E. E., Richter, D. H., & Bolster, D. (2017). Effects of incomplete mixing on reactive transport in flows through heterogeneous porous media. Physical Review Fluids, 2(11), 114501.

Wright, E. E., Sund, N. L., Richter, D. H., Porta, G. M., & Bolster, D. (2021). Upscaling bimolecular reactive transport in highly heterogeneous porous media with the LAgrangian Transport Eulerian Reaction Spatial (LATERS) Markov model. Stochastic Environmental Research and Risk Assessment, 1-19.

Woess, W. (2000). Random walks on infinite graphs and groups (Vol. 138). Cambridge university press.

Woo, S. H., Park, J. M., & Rittmann, B. E. (2001). Evaluation of the interaction between biodegradation and sorption of phenanthrene in soil-slurry systems. Biotechnology and bioengineering, 73(1), 12-24.

Wood, S. W., & Cowie, A. (2004). A review of greenhouse gas emission factors for fertiliser production.

Xu, J., Wang, R. Z., & Li, Y. (2014). A review of available technologies for seasonal thermal energy storage. Solar energy, 103, 610-638.

Yang, Y., Ok, Y. S., Kim, K. H., Kwon, E. E., & Tsang, Y. F. (2017). Occurrences and removal of pharmaceuticals and personal care products (PPCPs) in drinking water and water/sewage treatment plants: A review. Science of the Total Environment, 596, 303-320.

Yang, S. Y., Yeh, H. D., & Li, K. Y. (2010). Modelling transient temperature distribution for injecting hot water through a well to an aquifer thermal energy storage system. Geophysical Journal International, 183(1), 237-251.

Yates, S. R. (1990). An analytical solution for one-dimensional transport in heterogeneous porous media. Water Resources Research, 26(10), 2331-2338.

Zdeb, M., Papciak, D., & Zamorska, J. (2018). An assessment of the quality and use of rainwater as the basis for sustainable water management in suburban areas. In E3S Web of conferences (Vol. 45, p. 00111). EDP Sciences.

Zech, A., Attinger, S., Cvetkovic, V., Dagan, G., Dietrich, P., Fiori, A., ... & Teutsch, G. (2015). Is unique scaling of aquifer macrodispersivity supported by field data?. Water resources research, 51(9), 7662-7679.

Zeghici, R. M., Essink, G. H. O., Hartog, N., & Sommer, W. (2015). Integrated assessment of variable density–viscosity groundwater flow for a high temperature mono-well aquifer thermal energy storage (HT-ATES) system in a geothermal reservoir. Geothermics, 55, 58-68.

Zhan, H., Wen, Z., Huang, G., & Sun, D. (2009). Analytical solution of two-dimensional solute transport in an aquifer–aquitard system. Journal of contaminant hydrology, 107(3-4), 162-174.

Zhang, D., & Neuman, S. P. (1996). Effect of local dispersion on solute transport in randomly heterogeneous media. Water resources research, 32(9), 2715-2723.

Zhang, H., Xu, Y., & Kanyerere, T. (2020). A review of the managed aquifer recharge: Historical development, current situation and perspectives. Physics and Chemistry of the Earth, Parts A/B/C, 118, 102887.

Zhou, Z., Shi, L., Ye, M., & Zha, Y. (2019). Effects of Local Transverse Dispersion on Macro-scale Coefficients of Decaying Solute Transport in a Stratified Formation. Transport in Porous Media, 129(1), 53-74.

Zhou, Z., Shi, L., & Zha, Y. (2020). Effects of local transverse dispersion on macro-scale coefficients of oxygen-limited biodegradation in a stratified formation. Journal of contaminant hydrology, 228, 103580.

Zinn, B., & Harvey, C. F. (2003). When good statistical models of aquifer heterogeneity go bad: A comparison of flow, dispersion, and mass transfer in connected and multivariate Gaussian hydraulic conductivity fields. Water Resources Research, 39(3).

Summary

Water resource scarcity, food security, and environmental pollution are three major issues, that threaten the sustainability of the natural environment and the lives and livelihoods of people around the globe, especially the marginalized and those who live in developing regions. Despite increasing efforts by scientists and policymakers to resolve these issues, there is still no end in sight, partly because of the lack of conviction, and partly due to inability. With currently available technology, it is often necessary to make sacrifices regarding one of the issues in order to effect an improvement in another. For example, attempts to tackle food shortages by increasing agricultural production would necessitate the use of more water resources for irrigation, and agricultural chemicals for soil fertilization, which in turn may exacerbate water scarcity and environmental pollution, resulting in no net benefit to sustainability. It is therefore imperative that methods to resolve such issues that have minimal trade-offs are developed.

A new method of agricultural irrigation that has the potential to alleviate the above three issues is currently being tested at an experimental agricultural site in the Netherlands. This new method involves a newly developed subsurface irrigation and drainage system, irrigated with treated wastewater. To justify the use and development of this new method, Chapter 1 provides some historical context and a brief technical description of the method, along with an introductory discussion on its risks, benefits, shortcomings, and advantages in terms of environmental sustainability and crop contamination. Wastewater, including treated wastewater as no treatment technique can fully remove all impurities from wastewater without consuming large amounts of energy, contains residual biological and chemical substances. Some of these substances are known as contaminants of emerging concern (CECs), and are toxic or ecotoxic substances that are poorly understood in science due to reasons such as novelty or rarity. Hence, irrigating treated wastewater directly onto crops would contaminate the crops and the food supply.

Treated wastewater irrigation with minimal risks of crop exposure may be accomplished by subsurface irrigation through pipes buried in the phreatic zone, which is situated some distance beneath the root zone. Part of the agricultural water demand may thus be fulfilled by applying treated wastewater to the soil through these pipes, upon which they raise the water table and increase the capillary flux towards the root zone, thereby irrigating the crops without directly exposing them to the CECs in the treated wastewater. CECs transported upwards by the capillary flux would be at least partly biodegraded by microorganisms present in the soil, in addition to being diluted by the groundwater, and being adsorbed to the soil matrix. Therefore, the water that reaches the root zone through capillary rise should contain a much lower concentration of CECs than the irrigation water. On days with large precipitation fluxes, or outside of the annual crop season, the same pipes can be used to drain the soil, and remove a portion of any CECs that may remain. Nevertheless, there remains a risk that crops will be exposed to CECs, or that the CECs may be transported in the subsurface to deeper groundwater aquifers, which is a source of freshwater, or surface water at the end of the phreatic aquifer, whereupon the CECs would pollute the aboveground environment. An objective of this thesis is thus to evaluate the risks that irrigated CECs would contaminate crops or the wider environment in significant quantities, and this is the primarily concern of Chapter 2 and Chapter 3.

In Chapter 2, a model of subsurface irrigation and drainage with treated wastewater is constructed and validated against data from an experimental site in the Netherlands. CECs are modelled as solutes subject to monocomponent decay-type biodegradation kinetics and instantaneous adsorption. The results suggest that adverse outcomes of crop and environmental contamination are unlikely to occur unless the treated wastewater contains significant quantities of highly mobile and persistent CECs. Even if the root

zone is inadvertently contaminated following an extremely dry crop season that requires large irrigation volumes, CEC concentrations the root zone would reset to background levels by the following crop season, as the root zone would be flushed by rainfall in the period outside the crop season. The results also suggest that for the hydrogeological and climactic conditions at the experimental site, drainage plays a minor role in removing CECs from the subsurface, meaning that CEC biodegradation is the only effective means of preventing eventual environmental contamination. A sensitivity analysis of the system is conducted in Chapter 3, where the main conclusion is that the fate of irrigated CECs and the risks of crop and environmental contamination are primarily dependent on the biogeochemical behavior of the CECs and the hydrogeological conditions of the subsurface. Here, even if the hydrogeological characteristics of the subsurface are spatially heterogeneous, the mean hydrogeological characteristics have a larger influence than the heterogeneity. The specifics of the subsurface irrigation and drainage setup including factors such as the placement of the pipes, the flow resistance of the drains, and the irrigation pressure, contribute little to the fate of the CECs.

Subsurface irrigation and drainage with treated wastewater falls under an umbrella of environmental technologies known as managed aquifer recharge (MAR). MAR refers to the intentional recharge of groundwater aquifers either to achieve certain environmental objectives, or to store water of a certain quality for later extraction and use whilst ensuring that the water quality either improves or retains its quality over time. Subsurface irrigation and drainage with treated wastewater fulfils both purposes: the maintenance of relatively high phreatic groundwater levels to ensure that sufficient moisture is delivered to the root zone through capillary rise, and attenuation of the contaminants possibly contained within the treated wastewater. Other typical applications of MAR include aquifer storage and recovery (ASR) and aquifer thermal energy storage (ATES), which refers to the storage of freshwater and heat in groundwater aquifers, respectively, to be subsequently recovered when necessary. Accordingly, one of the key metrics of a MAR system's performance is the recovery efficiency, which is the fraction of injected freshwater or heat that may be recovered. In the case of subsurface irrigation and drainage with treated wastewater, the recovery efficiency is related to the ability of the system to recover the irrigated CECs, with the added complication that unlike freshwater and heat, CECs are also removed from the subsurface through biodegradation. Another objective of this thesis is thus to study the recovery efficiency of MAR systems through analytical and numerical modelling: Chapter 4 does this for spatially homogeneous aquifers, and Chapter 5 for spatially heterogeneous aquifers. For the sake of general applicability, the MAR systems modelled in these chapters are highly generic and may represent the various types of MAR systems to various degrees, rather than a specific study on the recovery of CECs by the subsurface irrigation and drainage system.

In Chapter 4, analytical relations between the operational parameters of an MAR system (injection-extraction rate and duration, number of storage cycles, geometry of flow field generated by the well) and its recovery efficiency in homogeneous aquifers are derived. These solutions depend on the dispersion characteristics of solutes and heat, namely on how the strength of the dispersion process(es) vary with the water flow velocity, which in turn varies with the storage volume and the flow field geometry. These analytical relations provide a more accurate and more generally applicable means of evaluating the recovery efficiency of MAR systems, compared to what was previously described in the literature. In Chapter 5, the work of Chapter 4 is extended to heterogeneous aquifers, where it is possible for the dispersion characteristics to vary not only with the water flow velocity, but also to depend directly on the storage radius of the MAR system, due to the occurrence of macrodispersion. Chapter 5 also discusses the possibility of using the recovery efficiency data of a testing well to assess the hydrogeological characteristics of an aquifer and evaluate its suitability for MAR applications. Hence, for example, this push-pull testing methodology may be used (with modifications to make it suitable for a phreatic aquifer) to prospect whether subsurface irrigation and drainage is a suitable means of soil moisture control at agricultural fields, and whether treated wastewater may be safely used for irrigation.

As mentioned above, the only mechanisms by which the irrigated CECs may be removed from the subsurface without contaminating crops or the wider environment is for them to either be drained away or to be biodegraded. Accordingly, Chapter 6 focusses on the in-situ biodegradation of contaminants in the subsurface. In the scientific literature, in-situ biodegradation of contaminants is often modelled as a monocomponent decay process with a constant decay rate. In practice, the kinetics of the biodegradation process is more likely to be a multicomponent reaction with a rate that depends on the concentrations of the CEC itself and the other substances that participate in the reaction. For this thesis, it is assumed that the reaction rate depends on the concentration of the CEC and an electron acceptor species such as oxygen, along with the spatial density of the microbial biomass, which grow as CECs are metabolized by the microorganisms. The multicomponent nature of the reaction implies that the extent of in-situ CEC biodegradation strongly depends on how well-mixed the various reactants are in the subsurface, which in turn strongly depends on the transport processes that affect these substances such as advection and dispersion. Two phenomena that affect the complexity of CEC transport are spatial heterogeneity of the soil physical properties, and transient flow. The presence of soil heterogeneity and transient flow leads to much more complex transport phenomena in the unsaturated zone than in the saturated zone, because here the distribution of water flow velocities is not only non-uniform in space but also dynamic in time. As the specific combination of multicomponent biodegradation with biomass growth, soil heterogeneity, and transient flow in the unsaturated zone has not been investigated in the literature, this combination is investigated in Chapter 6. The objective is to assess how soil heterogeneity and transient flow affect multicomponent biodegradation outcomes, while also investigating whether it is possible to simplify this problem, which is highly computationally intensive if numerically solved.

The results of Chapter 6 suggest that the complexity arising from the combination of processes simulated cannot be easily simplified, as they interact with each other through a web of nonlinear feedback loops. Therefore, computationally intensive numerical simulations are necessary to predict the fate of contaminants in the soil. Under some circumstances, the fate of the contaminant appears to become slightly more predictable in a qualitative sense, but not in a quantitative manner. When biodegradation is limited by reaction rate rather than by mixing, the problem appears to be more amenable to simpler models. Regardless of the specific combination of processes present in a simulation, predictions of extreme outcomes made by simpler models are likely to be too extreme, for both the biodegraded contaminant fraction and heterogeneity in the spatial distribution of contaminant leaching to the saturated zone. Furthermore, microbial biomass growth is always an important contributor to the overall biodegradation outcomes.

Altogether, the results of the work presented in this thesis suggest that treated wastewater irrigation with the introduced subsurface irrigation and drainage system is safe for crops and for the wider environment at the experimental site and in regions with similar hydrogeological and climactic conditions, as long as the treated wastewater does not contain excessive concentrations of highly mobile and persistent CECs. Although the drainage of CECs through the buried pipes contributes little to CEC removal from the soil at the experimental site, this may change under different hydrogeological conditions, such as if the regional groundwater flow velocity is slower. Extreme outcomes related to CEC spreading in the environment, as might be predicted by simpler models of CEC transport and transformation, are less likely to be observed when models accounting for more realistic conditions are used, suggesting that the tail risks of crop and environmental contamination would be overestimated by simpler models. The results also suggest that in many cases, but not all, crop and environmental contamination outcomes might improve on a relative basis as the irrigation volume and operational history of the system increases due to the nature of dispersion under radial advection and due to microbial adaptation, which is encouraging for wider adaptation. In conclusion, the introduced subsurface irrigation and drainage system is effective at safely fulfilling its purposes, as long as care is taken to

avoid irrigating the subsurface with water that contains contaminants that are highly persistent in the soil. Unlike some other approaches towards solving water and food scarcity, it does not consume excessive amounts of other non-renewable resources such as energy, making it more sustainable in the bigger picture.

Acknowledgements

My greatest appreciation goes to Sjoerd, my promotor, as he has made it possible for me to accomplish all that I have during this PhD. Throughout my PhD, Sjoerd had always encouraged me to work on my diverse interests, even if they did not completely fall under the scope of my PhD project. His support has allowed me to determine the direction of my work to a large extent, and has helped me better understand my strengths and weaknesses, and identify the subjects in science that can captivate me and capture my attention and curiosity. It was also with Sjoerd's encouragement and help that I have been able to take on as much teaching and student supervision as I have done during the course of my PhD, which has helped me discover the joys of teaching. Sjoerd's expertise and wisdom have been instrumental in the development of my own personal views on science. Our many enjoyable conversations together about science, academia, and life in general, have also given me a new perspective of life as a young scientist, and for that I am grateful.

I would like to thank my co-promotors, Ruud and Toon, for all the help and encouragement they have extended to me during my PhD, especially at the beginning of my PhD when I was quite clueless about everything. Toon, your knowledge of numerical modelling has been a great help to me. Ruud, your insight into the workings of the irrigation experiment has also been invaluable. I would also like to express a special gratitude to my promotion team as a whole, who trusted in my abilities and took me on for this PhD project, even though I hardly had any background in hydrology before starting my PhD. Thank you Coen, for all the help and advice that you have given me regarding my PhD, of which there are too many to list.

Thank you to all the teachers in SLM, and also in other groups, that I have worked with, and whose courses I have participated in: Jos, Klaas, Loes, Xiaomei, George, Lieke (HWM), and others. Your support has given me the opportunity to develop my teaching abilities through practice. On a similar note, thank you too to Huub and Nora at ETE for having the trust in me to take me on board the supervision team of their new PhD student, even at such an early stage of my academic career. I also sincerely thank Violette, who has involved me in some of the work being done on the microplastic and pesticide pollution part of the group, which has given me some familiarity with what others in the group are doing and has broadened my horizons beyond my research focus in hydrology. Xiaomei's mentorship on various aspects of life in academia has been indispensable for me, especially as I approach the end of my PhD. The other members of the RUST project have also been instrumental for the progress in my PhD: Dominique, Stefan, Annemarie, Ge, and others.

My life as a PhD student has also been enriched by the many people whom I have collaborated with in research outside of my PhD project: Xiaomei, Carlos, Yonghui, Jiaoyang. I have enjoyed the many discussions that we have had together. The same goes for my long-time officemates Yan, Pavan and Daniel, with whom I have had frequent interesting conversations not limited to science and work. The colleagues that I have especially bonded with during and after work have made my PhD life much more fulfilling: Xiaomei, Yan, Ke, Yanan. The never-ending ping pong games with them, and the other regulars Carlos, Nikola, Vera, and Jinfeng, have also made the daily grind in the office much more bearable. Finally, I would like to thank my family and distant friends, who have supported me from a distance. Every little bit counts, and I would not be who I am today without all of you.

About the author

Darrell Tang was born on September 15, 1990, in Singapore. After completing his secondary education, he decided to leave the confines of his 733km^2 island country to experience the world. He began studying mechanical engineering and the Japanese language at Waseda University in Tokyo, Japan, but left the program after a year and moved to the Netherlands to study liberal arts at the University of Amsterdam and the Vrije Universiteit Amsterdam. After obtaining a bachelor's degree cum laude with a major in physics and a minor in philosophy, he was looking forward to studying for a master's degree in either philosophy or linguistics, but ultimately chose to further his studies in the physical sciences due to mediocre career prospects in the humanities. He then obtained a master's degree cum laude in geophysics at Utrecht University, before starting a PhD in hydrology at the Soil Physics and Land Management group at Wageningen University under the Dutch Research Council (NWO) project 'Reuse of treated effluent for agriculture'. The aim of the project was to conserve freshwater resources by using treated wastewater for agriculture through innovative irrigation techniques. During the course of his PhD studies, he devoted time to collaborating with scientists working on other projects, teaching in bachelor's and master's courses, and supervising bachelor's and master's student theses, as he greatly enjoys communicating, exchanging, and debating ideas.

Publications

Tang, D. W. S., & van der Zee, S. E. A. T. M. (2022). Macrodispersion and Recovery of Solutes and Heat in Heterogeneous Aquifers. Water Resources Research, 58(2), e2021WR030920.

Tang, D. W. S., & van der Zee, S. E. A. T. M. (2021). Dispersion and Recovery of Solutes and Heat under Cyclic Radial Advection. Journal of Hydrology, 126713.

Yang, Y., Wu, J., Du, Y. L., Gao, C., **Tang, D. W. S.** & van der Ploeg, M. (2022). Effect on soil properties and crop yields to long-term application of superabsorbent polymer and manure. Frontiers in Environmental Science. In press.

Zhang, J., Ai, Z., Liu, H., **Tang, D. W. S.**, Yang, X., Wang, G., ... & Xue, S. (2022). Short-term N addition in a Pinus tabuliformis plantation: Microbial community composition and interactions show different linkages with ecological stoichiometry. Applied Soil Ecology, 174, 104422.

Urbina, C. A. F., van Dam, J. C., **Tang, D. W. S.**, Gooren, H., & Ritsema, C. J. (2021). Estimating macropore parameters for HYDRUS using a meta-model. European Journal of Soil Science, 72(5), 2006-2019.

Li, B., Huang, S., Wang, H., Liu, M., Xue, S., **Tang, D. W. S.**, ... & Yang, X. (2021). Effects of plastic particles on germination and growth of soybean (Glycine max): A pot experiment under field condition. Environmental Pollution, 272, 116418.

Yang, Y., Li, M., Wu, J., Pan, X., Gao, C., & **Tang, D. W. S.** (2021). Impact of Combining Long-Term Subsoiling and Organic Fertilizer on Soil Microbial Biomass Carbon and Nitrogen, Soil Enzyme Activity, and Water Use of Winter Wheat. Frontiers in Plant Science, 12, 788651-788651.

Yang, Y., Wu, J., Du, Y. L., Gao, C., Pan, X., **Tang, D. W. S.**, & van der Ploeg, M. (2021). Short-and long-term straw mulching and subsoiling affect soil water, photosynthesis, and water use of wheat and maize. Frontiers in Agronomy, 3, 708075

Yang, Y., Wu, J., Zhao, S., Gao, C., Pan, X., **Tang, D. W. S.**, & van der Ploeg, M. (2021). Effects of long-term super absorbent polymer and organic manure on soil structure and organic carbon distribution in different soil layers. Soil and Tillage Research, 206, 104781.

Urbina, C. A. F., van Dam, J. C., van den Berg, F., Ritsema, C. J., & **Tang, D. W. S.** (2020). Determination of the relative macroporosity and the effective aggregate width for different macropore geometries with disk infiltrometers. Vadose Zone Journal, 19(1).

Urbina, C. A. F., van den Berg, F., van Dam, J. C., **Tang, D. W. S.**, & Ritsema, C. J. (2020). Parameter sensitivity of SWAP–PEARL models for pesticide leaching in macroporous soils. Vadose Zone Journal, 19(1), e20075.

de Haro, S., Henke, J., & **Tang, D. W. S.** (2015). A. Cappelli, E. Castellani, F. Colomo and P. Di Vecchia (Eds.): The Birth of String Theory. Foundations of Physics, 45(6), 657-660.

Netherlands Research School for the
Socio-Economic and Natural Sciences of the Environment

D I P L O M A

for specialised PhD training

The Netherlands research school for the
Socio-Economic and Natural Sciences of the Environment
(SENSE) declares that

Darrell Tang

born on 15th September 1990 in Singapore, Singapore

has successfully fulfilled all requirements of the
educational PhD programme of SENSE.

Wageningen, 4th July 2022

Chair of the SENSE board

Prof. dr. Martin Wassen

The SENSE Director

Prof. Philipp Pattberg

The SENSE Research School has been accredited by the Royal Netherlands Academy of Arts and Sciences (KNAW)

KONINKLIJKE NEDERLANDSE
AKADEMIE VAN WETENSCHAPPEN

The SENSE Research School declares that **Darrell Tang** has successfully fulfilled all requirements of the educational PhD programme of SENSE with a work load of 43.4 EC, including the following activities:

SENSE PhD Courses

- Environmental research in context (2018)
- Research in context activity: 'Organization and lecturing in Ecohydrology MSc course' (2020)

Other PhD and Advanced MSc Courses

- Meta-Analysis, PE&RC and SENSE (2018)
- Ecological, Social and Socio-ecological Games, PE&RC, WASS and WIMEK (2018)
- Uncertainty Propagation in Spatial and Environmental Modelling, PE&RC (2018)
- Consumer-Resource Interactions, PE&RC (2018)
- Soil Ecology, PE&RC and WIMEK (2019)
- European Forest Management, PE&RC (2021)
- Teaching courses: International Classroom, Designing Courses, Giving Lectures, Start to Teach, Start to Supervise Theses, and Supervising Theses, Edu support WUR (2019-2021)

External training at a foreign research institute

- Training Event H (Environmental and Human Health Risk of Antibiotics), KWR Water Research Institute (2018)
- 2nd ANSWER Workshop 'Modelling and risk assessment tools towards sustainable wastewater reuse, KWR Water Research Institute (2018)
- Course on modelling with ORCHESTRA, WUR (2019)

Management and Didactic Skills Training

- Supervising two BSc students and one MSc student with thesis (2019-2022)
- Teaching in the MSc courses 'Advanced Hydrological Systems Analysis' (2018+2022), Water and Air Flow Numerical Techniques (2021-2022). 'Ecohydrology' (2021-2022), 'Interdisciplinary Topics for Earth and Environment' (2021) and 'Principles of Soil Processes' (2022)
- Teaching in the BSc courses 'Hydrogeology' (2018-2021), 'Subsurface Solute Transport (2019), 'Land Degradation and Remediation' (2019) and 'Soil Water Atmosphere Integration' (2018-2021)

Selection of Oral Presentations

- *Effects of Soil Heterogeneity and Transient Flow on Multicomponent Biodegradation*. Interpore, 31 May – 04 June 21, Online

SENSE coordinator PhD education

Dr. ir. Peter Vermeulen

The research described in this thesis was financially supported by Wageningen University and the Dutch Research Council (Nederlandse Organisatie voor Wetenschappelijk Onderzoek; NWO) through the project Re-USe of Treated effluent for agriculture (RUST) with project number ALWGK.2016.016.

Cover design by Yanan Huang

Printed by DigiForce